



Australian
National
University

THESES SIS/LIBRARY
R.G. MENZIES LIBRARY BUILDING NO:2
THE AUSTRALIAN NATIONAL UNIVERSITY
CANBERRA ACT 0200 AUSTRALIA

TELEPHONE: +61 2 6125 4631
FACSIMILE: +61 2 6125 4063
EMAIL: library.theses@anu.edu.au

USE OF THESES

This copy is supplied for purposes
of private study and research only.
Passages from the thesis may not be
copied or closely paraphrased without the
written consent of the author.

STUDIES IN THERMOLUMINESCENCE
DATING IN AUSTRALASIA

by

WILLIAM TERENCE BELL

A thesis submitted for the
degree of Doctor of Philosophy
at the Australian National University

Department of Physics
School of General Studies

February, 1978

Except as otherwise acknowledged or accredited
in the text, the contents of this thesis are
entirely my own work. No part of this work
has been submitted to any other university
or similar institution.

A handwritten signature in blue ink, appearing to read 'W.T. Bell'. The signature is stylized, with the first name 'W.' and the last name 'Bell' clearly legible, and a middle initial 'T.' that is more fluidly integrated into the script.

W.T. Bell
Canberra
February 1978

TABLE OF CONTENTS

	<u>Page</u>
List of Figures	viii
List of Tables	xii
Acknowledgements	xiv
Abstract	xvi
INTRODUCTION	1
PART I	
THEORETICAL ASPECTS OF THERMOLUMINESCENCE AND RADIATION DOSIMETRY	
CHAPTER I	KINETICS OF THERMOLUMINESCENCE AND APPLICATION TO AGE DETERMINATION
1.1	Introduction. 3
1.2	Basic Theory of Thermoluminescence. 4
1.3	First Order Kinetics. 6
1.4	Second Order Kinetics. 8
1.5	Applications of Theory to Experimental Studies. 12
1.6	Principles of Age Determination by the Thermoluminescence of Quartz. 14
1.7	Isothermal Stability of the Glow Curve Peaks of Quartz. 15
1.8	Supralinearity and Sensitivity Changes in Quartz. 18
1.9	'Additive' Procedure for Determining Archaeological Dose. 23
CHAPTER II	TL EQUIPMENT - SETTING UP AND CALIBRATION
2.1	Introduction. 28
2.2	Equipment. 28
2.3	Setting-up of the Photon Detector. 31
2.4	Pulse Pile-up and Non-linearity. 33
2.5	Alpha-Counting Equipment. 36

CHAPTER III	ALPHA PARTICLE DOSIMETRY	
3.1	The Attenuation of Radiation Through Interactions with Matter.	45
3.2	Inefficiency of Alpha Particles to induce Thermoluminescence.	46
3.3	The Attenuation and Range of Alpha Particles.	47
3.4	Absorbed Dose from Alpha Particles.	48
3.5	Effective Alpha Dose to Quartz Inclusions.	51
3.6	The Reduction of the Effective Alpha Dose by Etching in Hydrofluoric Acid.	55
3.7	Summary and Discussion of Results.	57
CHAPTER IV	BETA PARTICLE DOSIMETRY	
4.1	Introduction.	61
4.2	Various Models for Absorbed Dose Calculations.	61
4.3	The Attenuation of the Beta Dose in Spherical Geometry.	67
4.4	The Attenuation of the Beta Dose in Quartz Inclusions for the Natural Radioactive Series.	72
4.5	The Effect of Hydrofluoric Acid Etching on the Beta Dose Attenuation.	77
4.6	Summary and Discussion of Results.	78
CHAPTER V	GAMMA RAY DOSIMETRY	
5.1	The Passage of Ionizing Radiation Through Matter.	83
5.2	Attenuation, Scattering and Absorption of Gamma Radiation.	87
5.3	Gamma-Ray Buildup Factors.	89
5.4	Buildup Factors for an Overlying Layer.	92
5.6	The Energy-Size Dependence of the TL Response.	95

		<u>Page</u>
5.7	The Low Energy Photon Response of Quartz Grains in a Clay Matrix.	98
5.8	Summary and Discussion.	102
CHAPTER VI	RADIATION DOSE-RATE FROM THE NATURALLY-OCCURRING RADIOACTIVE SERIES	
6.1	Introduction.	104
6.2	Radiation Data.	105
6.3	Assessment of the Dose-Rate.	111
6.4	Summary of Results.	114
	PART II	
	APPLICATION OF THERMOLUMINESCENCE DATING TECHNIQUES TO THREE ARCHAEOLOGICAL SITES IN AUSTRALASIA	
CHAPTER VII	DATING OF ANCIENT FIREPLACES FROM LAKE MUNGO	
7.1	Introduction.	117
7.2	Archaeological Background of the Lake Mungo Site.	118
7.3	Aboriginal Fireplaces at Lake Mungo.	121
7.4	Previous Work and Preliminary Investigations.	122
7.5	Separation of Quartz Inclusions from the Clay Matrix.	124
7.6	The Effect of HF Etching on the Morphology of Quartz Inclusions.	128
7.7	TL Response of the Outer Layers of the Quartz Grains.	144
7.8	Measurement of the Archaeological Dose.	147
7.9	Saturation Tests of the Mungo Quartz.	153
7.10	Results of the Archaeological Dose Measurements.	155
7.11	Annual Dose-Rate Calculations.	169
7.12	Error Analysis and Age Determination.	179
7.13	Conclusion.	186

		<u>Page</u>
CHAPTER VIII	THE COMPARISON OF THERMOLUMINESCENCE AGES WITH RADIOCARBON AGES FOR THE MUNGO FIREPLACES	
8.1	Comparison of TL and Radiocarbon Ages.	188
8.2	The Radiocarbon Dating Method.	191
8.3	Variations in the Concentration of Atmospheric C-14.	193
8.4	Geomagnetic Field Variations as Recorded at Lake Mungo.	198
8.5	Sources of Error in Radiocarbon Dating.	201
8.6	The Lake Mungo Geomagnetic Excursion - Dipolar or Non-dipolar?	207
8.7	Conclusions.	210
CHAPTER IX	THERMOLUMINESCENCE DATING OF ABORIGINAL FIREPLACES FROM LAKE JINDABYNE	
9.1	Introduction.	213
9.2	Sample Preparation.	214
9.3	Archaeological Dose Measurements.	214
9.4	Dose-Rate Measurements.	216
9.5	Error Analysis.	218
9.6	Summary and Conclusions.	218
CHAPTER X	THERMOLUMINESCENCE DATING OF COOKING STONES FROM NEW GUINEA	
10.1	Introduction.	221
10.2	The Pre-dose Technique: Theory.	223
10.3	The Pre-dose Technique: Application.	226
10.4	Sample Preparation.	231
10.5	Archaeological Dose Measurements.	231
10.6	Dose-Rate Measurements.	237
10.7	Significance of the TL Ages.	237
10.8	Analysis of the Samples.	239
10.9	Summary and Conclusions.	242

CHAPTER XI	CONCLUSIONS AND SUGGESTIONS FOR FURTHER WORK	
	11.1 Conclusions.	244
	11.2 Suggestions for further work.	246
APPENDIX A	ALPHA SOURCE CALIBRATION	247
APPENDIX B	ALPHA-COUNTER CALIBRATION	251
APPENDIX C	BETA SOURCE CALIBRATION	253
APPENDIX D	BETA DOSE INFLUENCE FUNCTIONS	257
APPENDIX E	STATISTICAL FORMULAE	260
APPENDIX F	A POPULATION EXPANSION MODEL	261
BIBLIOGRAPHY		262

SUPPORTING PAPERS (available reprints in back pocket)

- Bell, W.T., 1976. The assessment of the radiation dose-rate for thermoluminescence dating, *Archaeometry*, 18(1), p107.
- Bell, W.T., 1976. Thermoluminescence dating of cooking stones from the Kuk Tea Research Station, New Guinea, *Arch. and Phys. Anthropol. in Oceania*, XI, No. 1, p51.
- Bell, W.T., 1976. Radiation dose-rate analysis for TL dating, *Proc. of the 1976 Symposium on Archaeometry and Archaeological Prospection*, Edinburgh.
- Bell, W.T., 1977. Thermoluminescence dating: revised dose-rate data, *Archaeometry*, 19(1), p99.
- Bell, W.T., 1978. Thermoluminescence dating for the Australian Archaeologist. In "Australian Archaeology: a Guide to Field and Laboratory Techniques", ed. G. Connah, 3rd edition, Australian Institute of Aboriginal Studies, Canberra (in press).
- Bell, W.T. and Zimmerman, D.W., 1978. The effect of HF etching on the morphology of quartz inclusions for thermoluminescence dating, *Archaeometry*, (in press).

LIST OF FIGURES

<u>FIGURES</u>		<u>Page</u>
<u>1.1</u>	Schematic representation of the thermoluminescence process.	5
<u>1.2a</u>	First order theoretical glow curves.	9
<u>1.2b</u>	Second order theoretical glow curves.	11
<u>1.3</u>	Glow curves constructed with maxima at the same temperature.	13
<u>1.4</u>	Low dose supralinearity of the TL growth curve of quartz.	19
<u>1.5</u>	Second glow-out growth curve parallel to the first.	21
<u>1.6</u>	Second glow-out growth curve not parallel to the first.	22
<u>1.7</u>	High dose saturation of the TL growth curve of quartz.	24
<u>1.8</u>	Pre-dose sensitivity enhancement of quartz.	25
<u>1.9</u>	The 'additive' procedure.	27
<u>2.1</u>	Diagrammatic representation of the thermoluminescence dating apparatus.	29
<u>2.2</u>	Spectral response of the EMI 9635 QB photomultiplier.	30
<u>2.3</u>	The thermoluminescence dating apparatus.	32
<u>2.4a</u>	"Betelight" output from the ratemeter versus discriminator threshold.	34
<u>2.4b</u>	Ratio of black-body to "Betelight" output versus threshold.	35
<u>2.5</u>	Non-linearity of the response of the TL apparatus at high photon count-rates.	37
<u>2.6</u>	The alpha-counting apparatus.	39
<u>2.7</u>	Diagrammatic representation of the alpha-counting apparatus.	40
<u>2.8</u>	The component parts of the alpha-counter sample holder.	41
<u>2.9</u>	Geometry used for alpha-counting activity calculations.	42

<u>FIGURES</u>		<u>Page</u>
<u>3.1</u>	The variation of the alpha particle geometrical function with penetration depth for the uranium and thorium series.	53
<u>3.2</u>	Geometry of a quartz grain with thickness d removed by etching in hydrofluoric acid.	56
<u>3.3</u>	The mean absorbed alpha dose in a quartz grain with a layer d removed by etching.	58
<u>4.1</u>	The "drunken man's path" of an electron in an absorber.	62
<u>4.2</u>	Energy dissipation of electrons in various media.	65
<u>4.3</u>	Energy dissipation of electrons of different initial energies.	66
<u>4.4</u>	Geometry used in the calculation of the beta dose attenuation.	70
<u>4.5</u>	Beta particle influence functions for the centre of a sphere.	71
<u>4.6a</u>	Mean absorbed beta dose in a quartz grain after etching for the uranium series.	79
<u>4.6b</u>	Mean absorbed beta dose in a quartz grain after etching for the thorium series.	80
<u>4.6c</u>	Mean absorbed beta dose in a quartz grain after etching for potassium-40.	81
<u>5.1</u>	Relative importance of the three types of gamma ray interactions.	86
<u>5.2</u>	Mass attenuation coefficients of quartz.	90
<u>5.3</u>	The variation of $B_{en}(\mu X)$ with X.	94
<u>5.4</u>	Fraction of the gamma dose experienced at a point distance X from an infinite plane interface.	97
<u>5.5</u>	The energy size dependence of the TL response of LiF.	99
<u>7.1</u>	The Willandra Lakes System.	119
<u>7.2</u>	Sample location relative to overlying Zanci layer.	126
<u>7.3</u>	The Franz magnetic separator.	127
<u>7.4</u>	Typical X-ray diffraction pattern from a Lake Mungo fireplace.	129
<u>7.5</u>	Optical photograph of quartz grains etched for 10 min.	131

<u>FIGURES</u>		<u>Page</u>
<u>7.6</u>	SEM photographs of individual unetched quartz grains.	132
<u>7.7</u>	SEM photographs of individual quartz grains etched for 100 min.	133
<u>7.8a</u>	SEM photographs of unetched quartz grains.	134
<u>7.8b</u>	SEM photographs of quartz grains etched for 10 min.	135
<u>7.8c</u>	SEM photographs of quartz grains etched for 40 min.	136
<u>7.8d</u>	SEM photographs of quartz grains etched for 100 min.	137
<u>7.9</u>	Isotropic and non-isotropic etching of quartz grains.	141
<u>7.10</u>	Dispenser for depositing quartz grains on aluminium discs.	149
<u>7.11a</u>	Aluminium disc resting on nichrome heating strip.	150
<u>7.11b</u>	Heat shield in position.	151
<u>7.11c</u>	Beta source holder in position.	152
<u>7.12</u>	Saturation curve for fireplace F9.	154
<u>7.13</u>	Actual TL glow curve for fireplace F6.	157
<u>7.14</u>	Actual TL glow curve for fireplace F7.	158
<u>7.15</u>	Actual TL glow curve for fireplace F8.	159
<u>7.16</u>	Actual TL glow curve for fireplace F9.	160
<u>7.17</u>	Actual TL glow curve for fireplace S7.	161
<u>7.18</u>	Plateau test for each of the Lake Mungo fireplaces.	163
<u>7.19</u>	Additive procedure for fireplace F7.	165
<u>8.1</u>	Production rate of carbon-14 as a function of the Earth's dipole moment.	196
<u>9.1</u>	Fireplace JH2 at Lake Jindabyne.	215
<u>10.1</u>	Houses unearthed at the Kuk Tea Research Station, Block A9g.	222
<u>10.2</u>	The trapping levels postulated to explain the pre-dose phenomenon.	224
<u>10.3</u>	Saturation of the pre-dose phenomenon.	228
<u>10.4a</u>	Saturation effects on the p-value determination.	229

<u>FIGURES</u>		<u>Page</u>
<u>10.4b</u>	Saturation effects on the q-value determination.	230
<u>10.5</u>	Typical X-ray diffraction pattern from the cooking stones.	232
<u>10.6a</u>	Glow curves from samples which exhibit a sensitivity increase.	234
<u>10.6b</u>	Glow curves from samples which do not exhibit a sensitivity increase.	235
<u>10.7</u>	Glow curves from a sample given a very large pre-dose.	240

LIST OF TABLES

<u>TABLE</u>		<u>Page</u>
<u>1.1</u>	Trapping paramaters based on first order kinetics.	17
<u>4.1</u>	Various models used to evaluate influence functions for electrons.	64
<u>4.2</u>	Influence functions for a spherical interface.	73
<u>4.3</u>	Average range of beta particles in quartz.	75
<u>5.1</u>	Contribution to total dose from gamma-rays within certain energy ranges.	96
<u>5.2</u>	The results of the X-ray fluorescence analysis for the Lake Mungo and the Lake Jindabyne fireplaces.	101
<u>6.1</u>	Reference sources for the uranium and thorium series.	106
<u>6.2</u>	Radiation data for the thorium-232 series.	108
<u>6.3</u>	Radiation data for the uranium-238 series.	109
<u>6.4</u>	Radiation data for the uranium-235 series.	110
<u>6.5</u>	Dose-rate for 1 ppm by weight of parent.	113
<u>6.6</u>	Dose-rate per alpha particle counted per cm^2 per ksec.	115
<u>7.1</u>	Values of Y, the isotropic/non-isotropic removal factor for a grain of diameter $D = 105$ microns.	142
<u>7.2</u>	Fraction of the alpha dose removed, in percent, by etching isotropically and non-isotropically (to give the same weight loss) for the uranium and thorium series.	143
<u>7.3</u>	Alpha efficiency factors for the different etching times.	146
<u>7.4</u>	Experimental data for fireplace F7.	164
<u>7.5</u>	Archaeological dose measurements for the Lake Mungo fireplaces.	167
<u>7.6</u>	Archaeological dose measurements at three different temperatures.	168
<u>7.7</u>	Sample location relative to the Zanci Unit and the fraction of the gamma dose experienced by the fireplaces.	174
<u>7.8</u>	Component parts of the annual dose-rates for the Lake Mungo fireplaces.	178

<u>TABLE</u>		<u>Page</u>
<u>7.9</u>	Fractional error components for the Mungo fireplaces.	183
<u>7.10</u>	Error terms for the Mungo fireplaces.	184
<u>7.11</u>	TL ages of the Lake Mungo fireplaces.	185
<u>8.1</u>	Radiocarbon ages of the Lake Mungo fireplaces.	189
<u>8.2</u>	Comparison of TL and radiocarbon ages.	190
<u>8.3</u>	Radiocarbon ages, virtual pole positions and dipole moments as recorded by the Mungo fireplaces.	200
<u>8.4</u>	Sources of error in radiocarbon dating.	202
<u>9.1</u>	The equivalent dose, supralinearity correction and archaeological dose of the Lake Jindabyne fireplaces.	217
<u>9.2</u>	Annual dose-rates, archaeological doses and TL ages of the Lake Jindabyne fireplaces.	219
<u>10.1</u>	The archaeological doses of the New Guinean cooking stones.	236
<u>10.2</u>	The archaeological dose, annual dose-rate and TL age of the New Guinean cooking stones.	238
<u>10.3</u>	Optical emission spectography results for the New Guinean cooking stones.	241

ACKNOWLEDGEMENTS

I should like to acknowledge the continuing advice and encouragement of my supervisor Dr. Allan Mortlock throughout the course of this work. I should also like to thank Mr. David Price for his expert technical assistance.

The etching experiments described in Chapter VII and the beta source calibration described in Appendix C were both carried out, in part, during the brief visit of Dr. David Zimmerman to this laboratory in September 1975. His expert knowledge and assistance are gratefully acknowledged.

The work of Chapter VI was very ably and constructively criticised by Dr. Martin Aitken who also had many of the calculations quoted in this Chapter checked for errors on my behalf.

Most of the relevant information on the archaeomagnetic and radiocarbon work on the Lake Mungo fireplaces was assimilated during many useful and stimulating discussions with Dr. Mike Barbetti. Dr. Mike McElhinny provided the samples from the fireplaces for dating and Mr. Henry Polach provided much valuable information on the radiocarbon dating of the sites. Dr. Isobel McBryde provided the samples from the Lake Jindabyne fireplaces and Professor Jack Golson the cooking stones from his archaeological sites in New Guinea.

All of the X-ray diffraction analysis was carried out by Mr. Jack Pennington of the Geology Department and Mr. Ross Freeman of the same Department carried out all of the trace element X-ray fluorescence and the majority of the major element analysis. Mr. Weldon Nance of the Research School of Earth Sciences carried out the optical emission spectrography.

David Pollard, Rosemary Bell, and Julie Howard assisted in the proof reading of this thesis which was neatly and efficiently typed by Mrs Maureen Powell and Mrs Moira Conn.

I was in receipt of an Australian National University Postgraduate Scholarship during the period of these studies.

ABSTRACT

This thesis is presented in two parts: Part I dealing with the theory of the thermoluminescence phenomenon and with the origins and effects of the natural radiation environment; and Part II dealing with three applications of the TL dating method to archaeological sites in Australia.

The first chapter describes the theories and mechanisms thought responsible for the thermoluminescence phenomenon. The application of these theories to the principles of age determination using quartz is explained and a review of the thermoluminescent properties of quartz itself is given. Nothing further has been added to knowledge already extant in these areas as the purpose of this chapter is to lay the foundation for the work found later in the thesis.

A full description of the setting up and calibration of the TL dating equipment, including the alpha counter, is given in the second chapter.

The third chapter deals with the passage of alpha particles through matter. The theory of Howarth (1965) is modified in this chapter so as to quantify the absorbed dose from alpha particles passing through a 105 micron quartz grain and to describe the alpha dose reduction due to HF etching. The results are significantly different from the "first order approximation" given by Fleming (1969, 1970).

In the fourth chapter the theoretical approach of Charlton (1970) for solving the problem of the energy dissipation of electrons passing through matter is discussed. This method is modified in this chapter to be applicable to a quartz grain irradiated by the natural radioactive series. The contribution from the internal conversion electrons is included in the dose attenuation factors. The assessment of the dose dilution resulting from etching the grains in HF is then given.

The fifth chapter describes qualitatively the interaction of gamma

radiation with matter. The concept of energy-absorption buildup factors is described and is used in the evaluation of the absorbed dose from an overlying clay layer. The dependence of the TL response on both the photon energy and the particle size is explained and a method for formulating a general solution of this problem is put forward. Specific solutions for the samples to be dated in Part II of this thesis are obtained.

Chapter six presents detailed radiation data concerning the naturally-occurring radioactive series. Tables giving the energy released during every transition of every radioisotope are given. These data are used to evaluate dose-rate conversion factors from ppm of the parent and from the alpha activity of the sample to mrad/yr. The information given in this chapter has been published.

The seventh chapter commences Part II of the thesis and it is concerned with the TL dating of ancient Aboriginal fireplaces from Lake Mungo in western New South Wales. The inclusion technique of TL dating is used but particular attention is paid to the assessment of the alpha particle contribution to the dose-rate because of the irregularity of the etching of quartz grains in HF acid. Other complicating factors which are also considered in detail are the saturation of the electron traps, the internal radioactivity of the quartz grains, and the gamma dose from an overlying stratigraphic layer of much higher radioactive content than the fireplaces themselves. The ages of the Mungo fireplaces range from 31,400 to 36,400 years which confirms the antiquity of the site as suggested previously by radiocarbon age determinations on charcoal from the fireplaces.

The radiocarbon ages are given in the eighth chapter and a small systematic discrepancy of between 10 and 15% appears to exist between them and the TL ages, with the TL ages being the older in each case. A full description of possible sources of error in the radiocarbon method is presented and one of these, the variations in the Earth's geomagnetic field, is put forward as a possible reason for the TL/C-14 age differences.

The ninth chapter describes a further application of the inclusion technique, as modified in the seventh chapter, to Aboriginal fireplaces from Lake Jindabyne in New South Wales. The ages of these fireplaces lie between 2000 and 3000 years.

In the tenth chapter the TL dating of cooking stones from New Guinea is described. Large uncertainties in the ages for these stones were encountered and an impurity analysis of the samples suggests that this is due to the high level of impurity diffusion into the quartz grains. The pre-dose technique of Fleming (1973) was used for this investigation and the results given in this chapter have been published.

INTRODUCTION

The long usage of the term 'thermoluminescence' since its early discovery has caused the retention of the name to describe the emission of visible light upon heating of certain materials. The more appropriate term 'thermostimulation' might equally well be applied to the phenomenon to conform with the modern explanation of thermoluminescence as the liberation by rise in temperature of trapped electrons, whose transitions result in the emission of light.

The first recorded observation of thermoluminescence was undoubtedly that of Sir Robert Boyle (1663) who noted the phenomenon when he held a diamond near a hot but non-luminous piece of iron and saw it glow. Elsholtz (1676) discovered a similar property in the mineral fluorspar which was described by Oldenburg (1676) as,

".... said to be of this nature that it collects its light not so much from the Sun-beams, or the illuminated air, as from the Fire itself; Seeing that if some of it be laid upon a Silver or Copper-plate, under which are put some live coals or a lighted taper, it will presently Shine ..."

It was not until relatively recently that Daniels et al. (1953) suggested the possibility of geological and archaeological age determination by thermoluminescence. Initial studies by Tite and Waine (1962) gave archaeological ages to within $\pm 20\%$ but this was based on a relative scale, it being necessary to calibrate the scale with similar material of known age. These studies were carried out at the Research Laboratory for Archaeology and the History of Art, Oxford which has since gone on to become one of the main centres for the development of the various absolute techniques of thermoluminescence dating.

Three of these absolute dating methods, (i) "the inclusion technique" first developed by Fleming in 1966, (ii) "the fine grain

technique" first developed by Zimmerman in 1967 and (iii) "the pre-dose technique" again developed by Fleming this time in 1973, have become the fundamental basis upon which the majority of the archaeological age determinations using thermoluminescence are carried out. Further details of these methods are given later in this thesis.

So we come to the work of this thesis itself which is essentially concerned with a review of the basic theoretical considerations involved in the dating techniques, resulting in a few cases in alteration of the previous data, and then the application of the theory to the age determination of three archaeological sites in Australasia. The relative success of these applications to the baked clay from Aboriginal fireplaces and to the cooking stones from New Guinean house sites is extremely encouraging and it is to be hoped that further work on similar materials will soon be undertaken.

PART I

THEORETICAL ASPECTS OF THERMOLUMINESCENCE
AND RADIATION DOSIMETRY

CHAPTER I - KINETICS OF THERMOLUMINESCENCE
AND APPLICATION TO AGE DETERMINATION

1.1 Introduction

Many naturally occurring minerals exhibit the phenomenon of radiothermoluminescence and various dating methods have been developed using certain of these.

The 'quartz inclusion technique' of Fleming (1966, 1970) is the method adopted for the dating work described in Part II of this thesis and as the name implies it is concerned with large crystalline inclusions of quartz (typically of the order of 100 μm) obtained from the sample by separation techniques described in later chapters.

The 'fine-grain technique' of Zimmerman (1967, 1971) utilises grains in the size range 1 to 8 μm separated from the sample by suspension in acetone. The separation is not mineral-specific so the thermoluminescence observed may come from several different minerals.

The 'feldspar inclusion technique' of Mejdahl (1969, 1972) uses grains in the size range 0.3 - 0.5 mm separated from the sample by sifting. The separated fraction will include quartz grains as well as feldspar but since the output from the former is usually an order of magnitude lower, the light observed will come mainly from the latter.

The 'radioactive inclusion technique' of Zimmerman (1971a) and Sutton and Zimmerman (1976) uses grains of zircon and apatite separated from the sample using heavy liquids. Because these grains are orders of magnitude more radioactive than the surrounding soil, almost all of the natural dose is from internal alpha particles so that no burial information is required.

In spite of the different methods involved in the above techniques, they all have in common the detection and measurement of the radio-

thermoluminescence (radiation-induced thermoluminescence) and then the assessment of the radiation levels which gave rise to it. As will be developed in later chapters, this latter problem is by far the more complex of the two but as a preface to that and the practical work of Part II, the rest of this chapter deals with the theory and physical properties of the thermoluminescence phenomenon itself.

1.2 Basic Theory of Thermoluminescence

The band structure of a perfect crystal lattice is such that electrons would fill all available states up to the valence band with an energy gap to the conduction band which would normally be empty of electrons. The presence of lattice imperfections, such as impurities and structural defects, modifies this band model by creating additional energy levels mostly in the gap between the conduction band and valence band which can be categorised as either electron traps (T) or hole traps. This latter category can be further subdivided into luminescent centres (L) and non-luminescent ('killer') centres.

The thermoluminescence process although far from being well understood can be represented as in Fig. 1.1. Before irradiation the luminescent centres (L) are full and the electron traps (T) empty. During irradiation electrons are ionized from their parent atoms into the conduction band where, because of the relatively long lifetime of the radiative dipole transition by which recombination with the parent atom might be achieved, the electrons can diffuse away from the parent site and become trapped at trapping centres T (Fig. 1.1a).

Holes created in the valence band diffuse in a similar manner and some become trapped at luminescent centres L. After irradiation, the length of time the electrons and holes remain trapped depends on the depth of the trap (Fig. 1.1b). For dating purposes, trap depths which

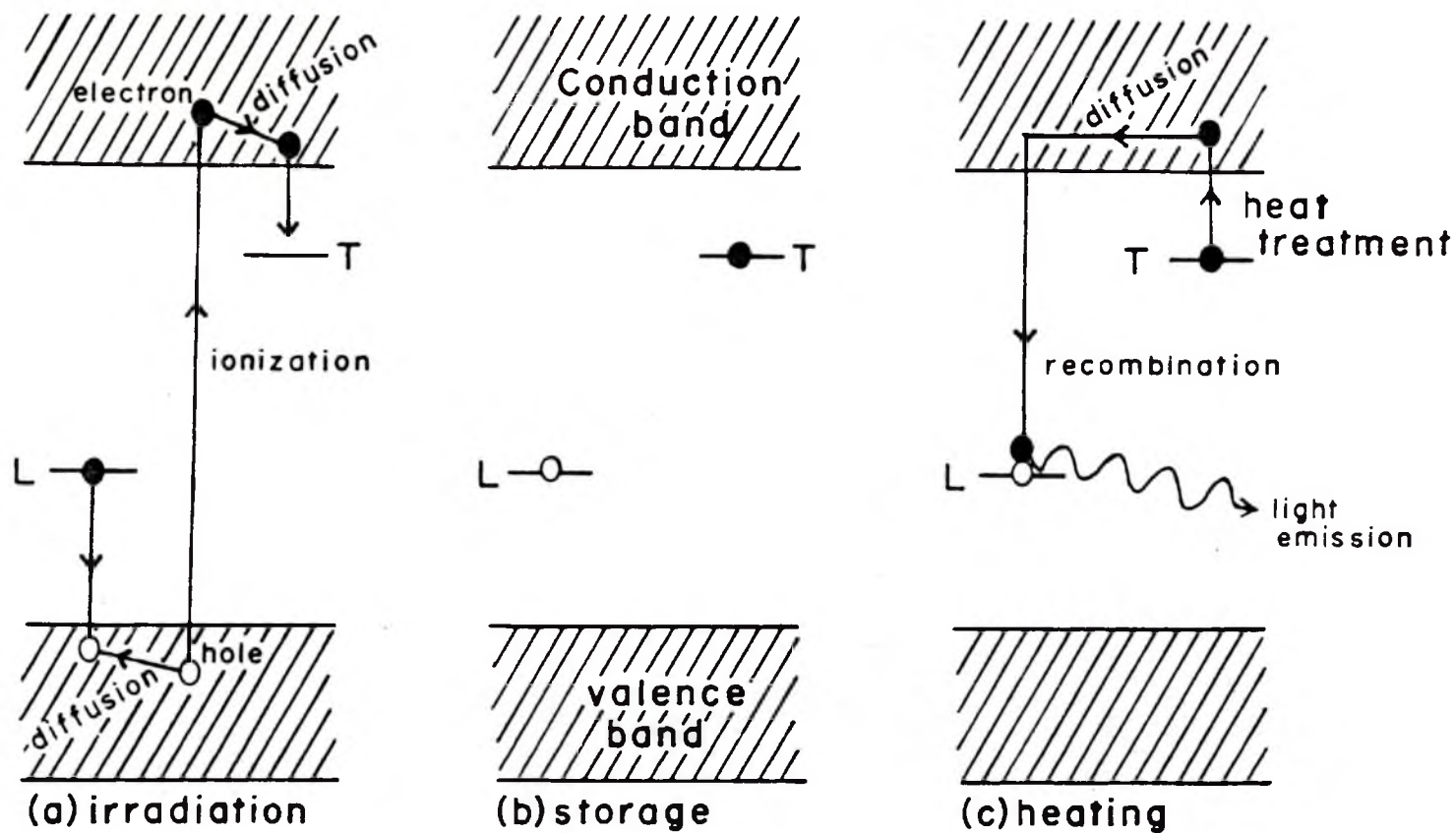


FIGURE 1.1: Schematic Representation of the Thermoluminescence Process.

allow negligible escape of charge carriers at ambient temperatures over archaeological periods are required. This is dealt with in Section 1.6.

When the crystal lattice is heated to a temperature sufficient to thermally excite electrons from their traps into the conduction band, they can then diffuse until they either become retrapped or recombine with a hole at a luminescent centre thus producing the thermo-luminescence which is observed (Fig. 1.1c). Recombination may also occur at non-luminescent centres where instead of the emission of visible light, energy is dissipated by lattice interactions.

Thus the thermoluminescence process is one of charging empty electron and hole trapping centres with their respective charge carriers; the storage of the charge carriers at these centres over extended periods of time and the eventual release and recombination of the carriers with the associated emission of thermoluminescence on heating. The kinetics which govern the release of electrons from traps and the shapes and positions of the peaks in the glow curve are exceedingly complex. The following sections are intended merely to provide a phenomenological formalism upon which the dating applications described in Part II of this work can be based.

1.3 First Order Kinetics

The first theoretical investigation of the thermoluminescence effect was carried out by Randall and Wilkins (1945). They used a 'monomolecular' model in which only a single electron trap and luminescent centre are considered and the probability of retrapping is neglected. If the traps are of depth E and at any instant in time, t , they contain n electrons then the thermoluminescence emission

intensity I is given by

$$I = -\frac{dn}{dt} = n s \exp(-E/kT) \quad (1.1)$$

where s is a frequency factor expressing the number of times the electron attempts to escape from the trap, k is Boltzmann's constant and T is the absolute temperature. This relation predicts that the number of electrons, initially n_0 at time $t = 0$, will decay exponentially at a fixed temperature according to

$$n = n_0 \exp(-t/\tau) \quad (1.2)$$

where τ is the mean lifetime of trapped electrons and is given by

$$\tau = s^{-1} \exp(E/kT) \quad (1.3)$$

If equation (1.1) is solved for a constant heating rate, $\beta = dT/dt$.

from an initial temperature T_i , then the variation of thermoluminescence intensity with temperature is given by

$$I(T) = n_0 s \exp(-E/kT) \exp \left[- \int_{T_i}^T \frac{s \cdot \exp(-E/kT)}{\beta} dT \right] \quad (1.4)$$

$I(T)$ will pass through a maximum value at a temperature T^* given implicitly by

$$\{dI(T)/dT\}_{T^*} = 0 \quad (1.5)$$

which results in

$$\frac{kT^{*2}}{\beta E} = s^{-1} \cdot \exp(E/kT^*) \quad (1.6)$$

The glow curve described by equation (1.4) is shown graphically in Fig. 1.2a, and has a peak at a temperature T^* , given by equation (1.6), which is dependent only on the trap depth E , frequency factor s and heating rate β . This first order (or monomolecular) theory deals essentially with the case of a single thermoluminescence peak. When more than one peak is present in a glow curve the above formalism must be applied to each peak separately thus implying that the trapping centres for each peak in the glow curve of a crystal are independent of one another. This is not necessarily a justifiable assumption and so it is essential to modify this theory for the case when an electron escaping from a trap has a finite probability of being retrapped.

1.4 Second Order Kinetics

Garlick and Gibson (1948) developed a second order (or bimolecular) formalism which allows an electron escaping from a trap an equal probability of either being retrapped or of recombining with an empty luminescence centre. Because the traps and centres are no longer independent, the probability of a electron released from a trap giving rise to luminescent emission is dependent not only on the number of electrons released but also on the number of empty luminescence centres and the number of empty traps at any one time, t .

If the total number of electron traps is N of which n are filled by electrons at any instant, then the number of empty traps is $(N - n)$ and the number of empty luminescence centres is n (those previously vacated by the trapped electrons). The probability, P , of an electron released from a trap recombining with a luminescence centre and not being retrapped is given by

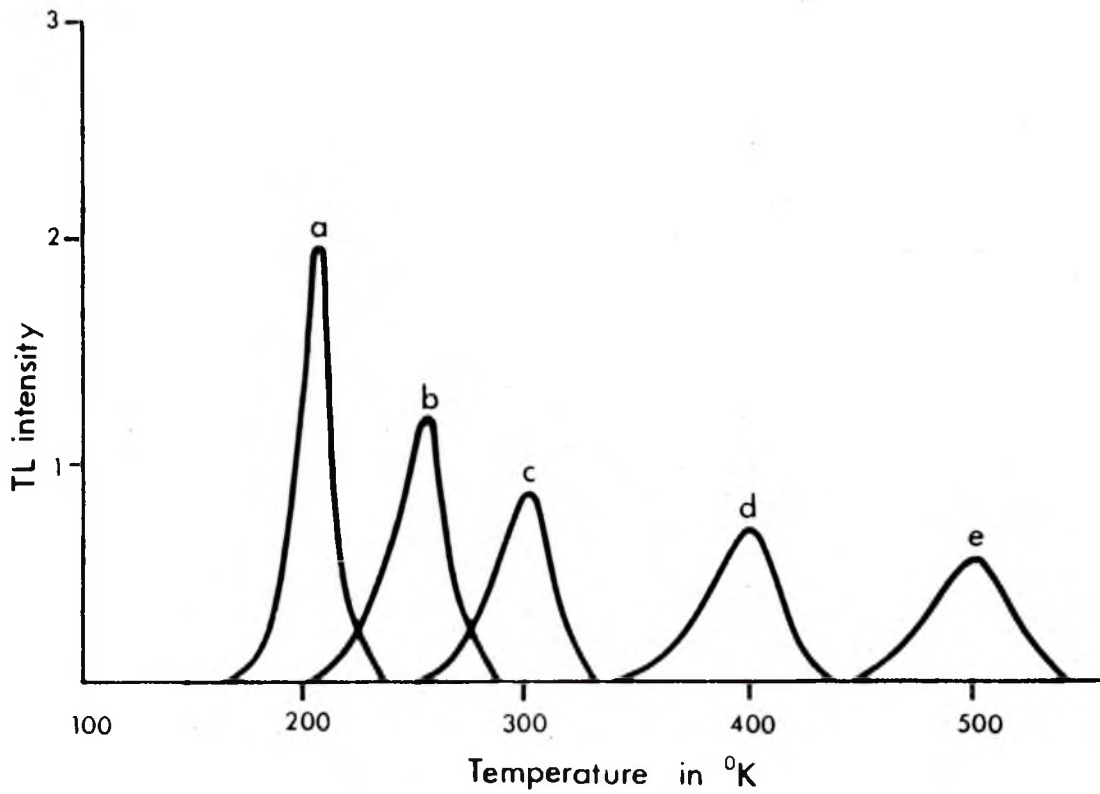


FIGURE 1.2a: First Order Theoretical Glow Curves. The heating rate is $2.5^{\circ}\text{C sec}^{-1}$.

(a)	$E = 0.4\text{eV}$	$s = 10^9 \text{ sec}^{-1}$
(b)	$E = 0.4\text{eV}$	$s = 10^7 \text{ sec}^{-1}$
(c)	$E = 0.6\text{eV}$	$s = 10^9 \text{ sec}^{-1}$
(d)	$E = 0.8\text{eV}$	$s = 10^9 \text{ sec}^{-1}$
(e)	$E = 0.4\text{eV}$	$s = 10^6 \text{ sec}^{-1}$

$$P = \frac{n}{(N - n) + n} = \frac{n}{N} \quad (1.7)$$

The intensity given by equation (1.1) for no retrapping must be modified by the probability of recombination, P , to give

$$I = -\frac{dn}{dt} = \frac{n^2}{N} s \cdot \exp(-E/kT) \quad (1.8)$$

This gives an isothermal decay of trap population which is no longer a simple exponential i.e.

$$n = \frac{n_o}{1 + (n_o/N) s \cdot t \cdot \exp(-E/kT)} \quad (1.9)$$

Solving equation (1.8) for a constant heating rate, β , gives the equation for a second order glow curve.

$$I(T) = \frac{n_o^2 \cdot s \cdot \exp(-E/kT)}{N \left[1 + \frac{n_o}{N} \int_{T_i}^T \frac{s \cdot \exp(-E/kT)}{\beta} dT \right]^2} \quad (1.10)$$

The maximum (or glow curve peak) occurs at a temperature T^* defined by equation (1.5) which results in the relation for T^* :

$$\frac{n_o \cdot s}{N\beta} = \left[\frac{2kT^{*2}}{E} \cdot \exp(-E/kT^*) - \int_{T_i}^{T^*} \exp(-E/kT) \cdot dT \right]^{-1} \quad (1.11)$$

The main features of the second order glow curve as described by equations (1.10) and (1.11) are shown graphically in Fig. 1.2b and the most significant difference between this and the first order glow curve is that the second order peak is a function of n_o the number of electrons initially trapped whereas the first order peak is not.

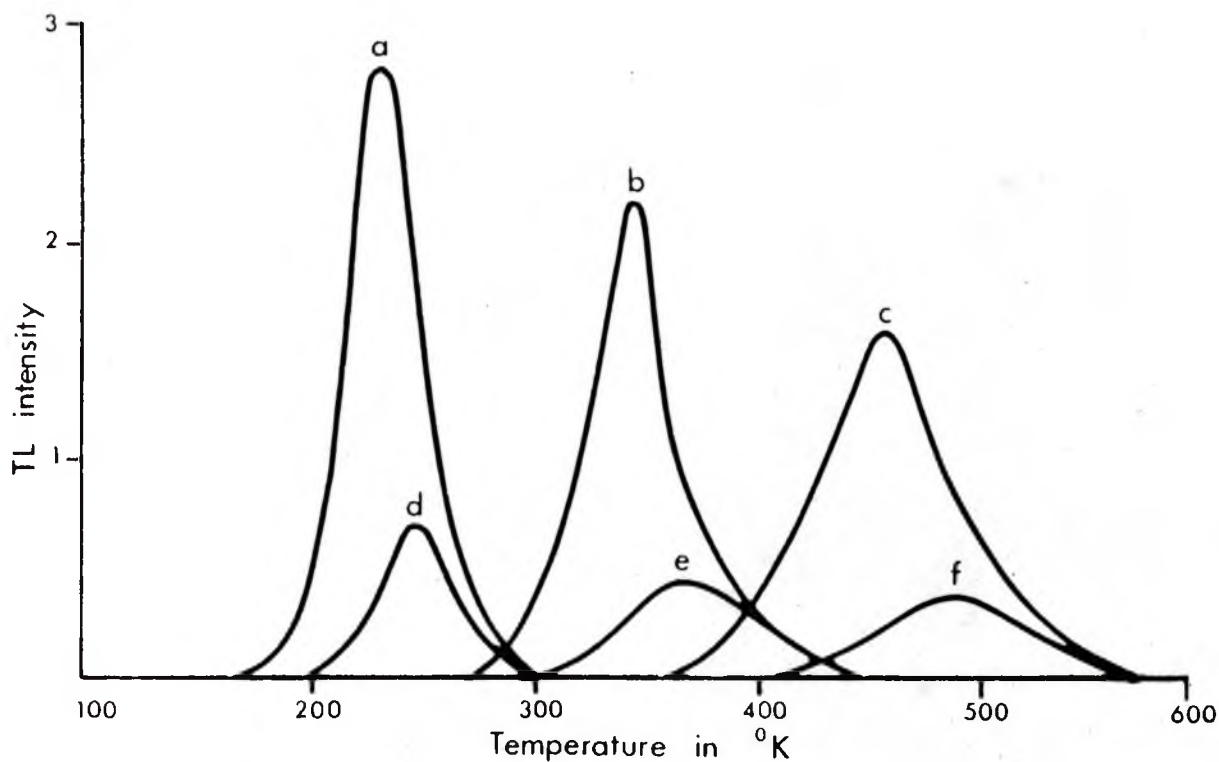


FIGURE 1.2b: Second Order Theoretical Glow Curves. The heating rate is $2.5^{\circ}\text{C sec}^{-1}$ and $s = 10^8 \text{ sec}^{-1}$. N is the total number of traps of depth E and n_0 is the number of these traps which are filled.

(a)	$E = 0.4\text{eV}$	$n_0 = N$
(b)	$E = 0.6\text{eV}$	$n_0 = N$
(c)	$E = 0.8\text{eV}$	$n_0 = N$
(d)	$E = 0.4\text{eV}$	$n_0 = 0.25N$
(e)	$E = 0.6\text{eV}$	$n_0 = 0.25N$
(f)	$E = 0.8\text{eV}$	$n_0 = 0.25N$

1.5 Applications of Theory to Experimental Studies

The application of the formalisms developed in Sections 1.3 and 1.4 to experimental results has so far proved rather unsatisfactory. For example, Hill and Schwed (1955), Bonfiglioli et al. (1959) and Halperin et al. (1960) have all studied the thermoluminescence of NaCl and yet they disagree as to the order of the kinetics involved and as to the value of the trap depth, E (also termed activation energy). The same situation occurred with research into the thermally stimulated current (TSC) of CdS. TSC is a directly analogous phenomena to thermoluminescence yet Dittfeld and Voigt (1963), Nicholas and Woods (1964) and Bube et al. (1966) all came to different conclusions regarding the trapping levels and electron kinetics.

Kelly and Braunlich (1970) put forward a phenomenological theory of thermoluminescence which led them to the conclusion that:

"It appears impossible to obtain relevant quantitative information on the trapping parameters by any method of evaluating experimental TL or TSC data unless the electron kinetics is known in detail. TL and TSC data may then provide a way to check experimental data obtained otherwise."

Kemmy et al. (1967) demonstrated one aspect of this by constructing a number of glow curves with maxima at the same temperature by simply using different values of E and s , keeping the other parameters constant, see Fig. 1.3.

It would appear that the state of the theory is still far from complete, but this does not rule out the usefulness of some experimental work based on even the more simple models described earlier in this chapter. A good deal of this work on quartz has been carried out by Fleming (1969) and the results obtained which are relevant to the

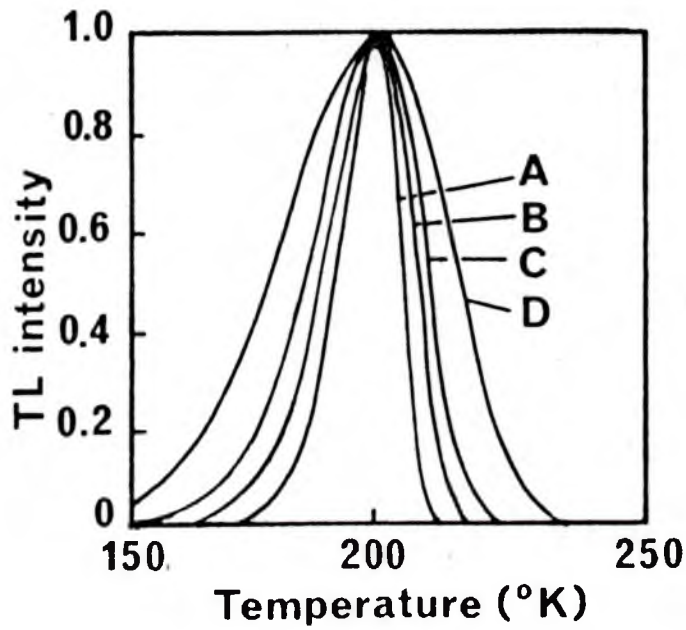


FIGURE 1.3: Glow Curves Constructed with
Maxima at the Same Temperature.

A	$E = 0.2\text{eV}$	$s = 6.37 \times 10^2 \text{sec}^{-1}$
B	$E = 0.3\text{eV}$	$s = 3.17 \times 10^5 \text{sec}^{-1}$
C	$E = 0.4\text{eV}$	$s = 1.40 \times 10^8 \text{sec}^{-1}$
D	$E = 0.6\text{eV}$	$s = 2.30 \times 10^{13} \text{sec}^{-1}$

applicability of quartz for thermoluminescence dating are presented in Sections 1.7 and 1.8.

1.6 Principles of Age Determination by the Thermoluminescence of Quartz

As mentioned in Section 1.1, there are several dating methods based on different naturally occurring minerals. The rest of this chapter is devoted to the properties of one of these minerals, quartz (or silicon dioxide, SiO_2).

Quartz has proven to be one of the most propitious minerals for dating purposes and it is perhaps somewhat fortuitous that it is also one of the more abundant. The 'quartz inclusion technique' developed by Fleming (1970) is the method which forms the basis of the practical work described in Part II of this thesis and a full description of the technique will be found there.

The principles of the technique are straightforward and are directly analogous to the situation described in Section 1.2 and Fig. 1.1. In ancient times some natural clay material was heated which caused electrons trapped at energy levels within the crystalline inclusions to escape and recombine with luminescence centres (if the temperature of the heating process was sufficiently high).

On cooling the crystals are once more subjected to a natural radiation environment arising from trace amounts of the uranium, thorium and potassium radioactive series which are present in most clay materials. This radiation, which is essentially constant over archaeological times, causes the ionization and subsequent trapping of electrons as shown in Fig. 1.1.

The accumulation of trapped electrons is a dynamic process which will continue over archaeological time so that the thermoluminescence observed is a direct measure of the radiation dose absorbed by the

crystal since last heating if the isothermal decay of electrons has been negligible at the ambient temperature of the material. The thermal stability of the various peaks in the glow curve of quartz is discussed in Section 1.7.

Having measured the thermoluminescence from the quartz it is then possible to determine the radiation dose which gave rise to it (i.e. the Archaeological Dose) by comparing this natural TL with the TL produced by the addition of a well-calibrated laboratory source.

The Dose-Rate is determined by analysis of the clay material for its content of uranium, thorium and potassium (Chapter VI) and hence the thermoluminescence age may be calculated.

It is convenient to introduce here the unit of radiation absorbed dose, the RAD, which is equivalent to 100 ergs of energy absorbed per gram of material.

The thermoluminescence age equation can then be written

$$\text{TL Age (yr)} = \frac{\text{Archaeological Dose (rad)}}{\text{Dose - Rate (rad/yr)}} \quad (1.12)$$

1.7 Isothermal Stability of the Glow Curve Peaks of Quartz

Garlick and Gibson (1948) demonstrated that the initial rise of luminescence well before the emission peak follows the same simple relation for both first and second order kinetics

$$I(T) = C \exp (-E/kT) \quad (1.13)$$

where C is a constant equal to $n_0 s$ for first order and $(n_0^2/N)s$ for second order.

Thus a plot of $\ln I$ vs $1/T$ should yield a value of $(-E/k)$ and hence E. Fleming (1969) carried out this "initial rise" experiment

for Norwegian α -quartz and obtained the values for E given in Table 1.1 for the three major peaks in the glow curve. The three peaks are situated at 110°C , 325°C and 375°C when the heating rate, β , is 20°Cs^{-1} . With these values and assuming first order kinetics, s may be calculated from equation (1.6) and hence the mean lifetime τ from equation (1.3). The values of s and of τ for different ambient temperatures (20°C , 25°C and 30°C) using Fleming's values for E are given in Table I.1.

It would appear from this Table that only the peak at 375°C is useful for archaeological dating purposes but this in fact is not the case. The application of the 110°C (at 20°Cs^{-1}) peak for dating is described in Chapter X while Wintle (1975) has shown that the initial rise method leads to an erroneous value of E for the 325°C peak.

She applied three different methods of trap depth determination to the 325°C peak in the glow curve of quartz and came up with the following results:

- | | |
|--------------------------------------|--------------------------------|
| (a) isothermal decay method | $E = 1.7 \pm 0.1 \text{ eV}$ |
| (b) variation of heating rate method | $E = 1.69 \pm 0.02 \text{ eV}$ |
| (c) initial rise method | $E = 1.05 \pm 0.03 \text{ eV}$ |

The difference between the first two values and the third one is thought to be due to thermal quenching, that is the decrease of luminescence efficiency with increasing temperature. This decrease in efficiency is caused by a rapid increase in the probability of non-radiative recombinations as the lattice becomes hotter and phonon activity increases. Methods (a) and (b) are unaffected by this but method (c) leads to a false result for E .

Using the value of 1.69 eV for E the following values of τ may be calculated for the 325°C peak in quartz:

TABLE 1.1

TRAPPING PARAMETERS BASED ON FIRST ORDER KINETICS

<u>T*(with $\beta=20^\circ\text{Cs}^{-1}$)</u>	<u>E(eV)</u>	<u>s(sec⁻¹)</u>	<u>20°C</u>	<u>τ (yr)</u>	
				<u>25°C</u>	<u>30°C</u>
110°C Peak	0.99	1.7×10^{13}	1.8 hr	55 min	29 min
325°C Peak	1.26	3.4×10^{10}	4×10^3	2×10^3	9×10^2
375°C Peak	1.66	7.5×10^{12}	1.5×10^8	5×10^7	2×10^7

$$\begin{aligned}
 \tau &= 2 \times 10^7 \text{ yr at } 20^\circ\text{C} \\
 &= 6 \times 10^6 \text{ yr at } 25^\circ\text{C} \\
 &= 2 \times 10^6 \text{ yr at } 30^\circ\text{C}
 \end{aligned}$$

It is evident, then, that this peak could also prove useful for archaeological dating although the added complication of changes in sensitivity (see next section) will limit this usefulness.

Before completing this section it is worth commenting on the appropriateness of using first order kinetics to describe the glow curve of quartz. Aitken and Fleming (1972) report that the 110°C peak exhibits almost pure first order kinetic behaviour whereas studies of the peak position movement with trap filling indicate that the 325°C and 375°C peaks obey first order kinetics for the most part but do exhibit some second order behaviour. They quote an example for the 375°C peak where filling of the electron traps from 5% to 100% moves the peak position 8°C lower. First order kinetics predicts no change (equation 1.6) whereas a second order peak should move some 50°C lower (equation 1.11).

Notwithstanding the contents of Section 1.5, it appears that first order kinetics is very nearly obeyed by the 325°C and 375°C quartz peaks and in any case if retrapping were present this would lead to a longer mean lifetime than that calculated in this Section.

1.8 Supralinearity and Sensitivity Changes in Quartz

(a) Low Doses

The growth of TL with increasing radiation dose is not a linear function over the whole range of the growth curve. For low dose levels (i.e. less than about 400 rads) the initial growth is faster than linear as illustrated in Fig. 1.4. This 'supralinearity' is exhibited by both

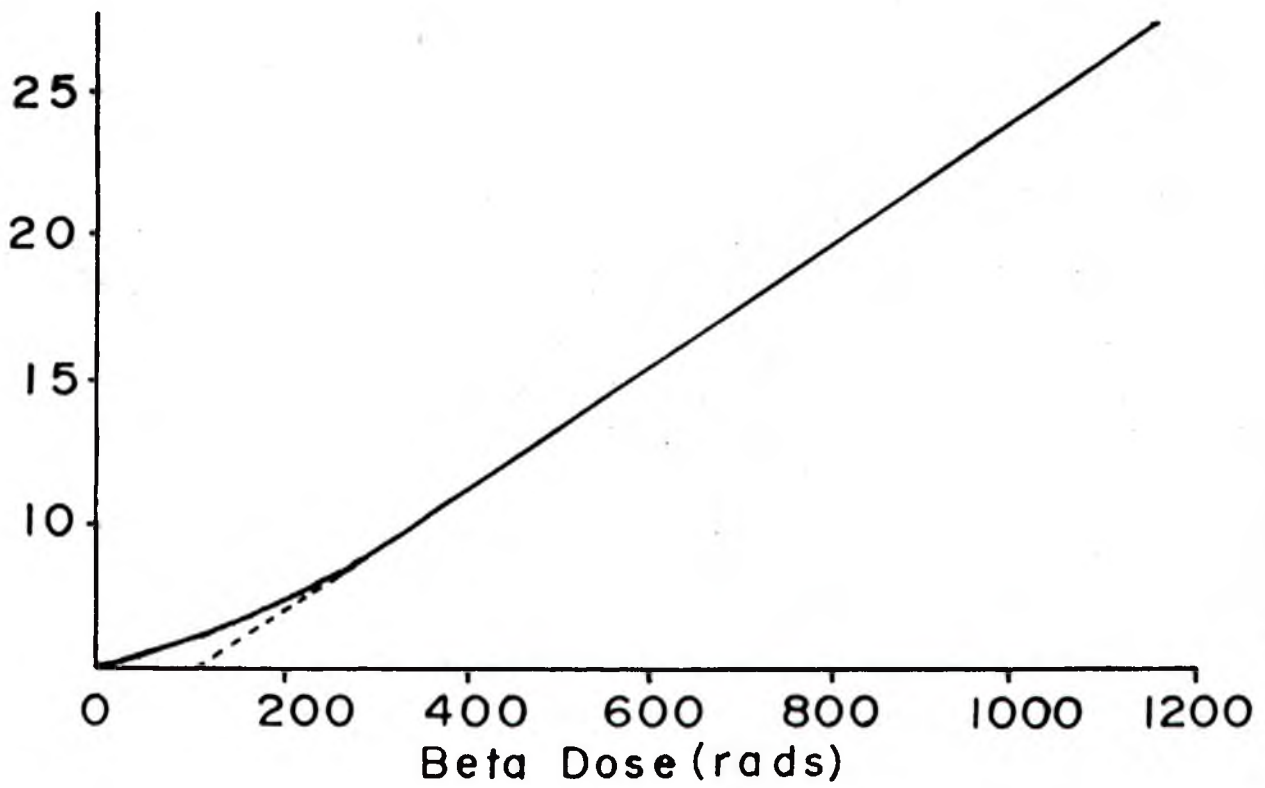


FIGURE 1.4: Low Dose Supralinearity of the TL Growth Curve of Quartz.

the 325°C and 375°C peaks (but not by the 110°C peak) and it is thought (Tite, 1966 and Fleming, 1969) to be due to competition during irradiation by a second set of trapping centres which do not give rise to TL. This second set of traps is assumed to have a higher capture cross section than the thermoluminescence traps, and to saturate much earlier leaving the form of the growth curve linear above 400 rads until the TL traps themselves begin to saturate. This occurs at a level which will vary from sample to sample but is of the order of several thousand rads.

The phenomenon of trap competition is not only thought responsible for the supralinearity effect just described but can also give rise to TL sensitivity changes. During geological times the quartz inclusions in the clay material would have received sufficient radiation doseage to saturate both competing trapping levels. Subsequently when the material was heated by ancient man, the degree to which the respective traps were emptied will depend on the firing temperature.

Heating to approximately 500°C will empty the TL traps responsible for the 325°C and 375°C peaks and Fleming (1969) has shown that this is also sufficient to empty the competing trapping levels for the 375°C peak but not for the 325°C peak. Hence the degree of supralinearity for the 375°C region may be assessed by artificially inducing a second glow-curve after the first natural glow-curve has been drained to 500°C . An example of this is shown in Fig. 1.5.

For the 325°C peak, however, this does not work because the 500°C heat treatment is not sufficient to empty the competing trapping sites and hence a second growth curve will have an increased sensitivity and a decreased supralinearity factor due to the lack of competing traps. This is illustrated in Fig. 1.6.

In order to assess a valid supralinearity correction from a second glow curve, it is necessary to restrict the analysis to the 375°C region.

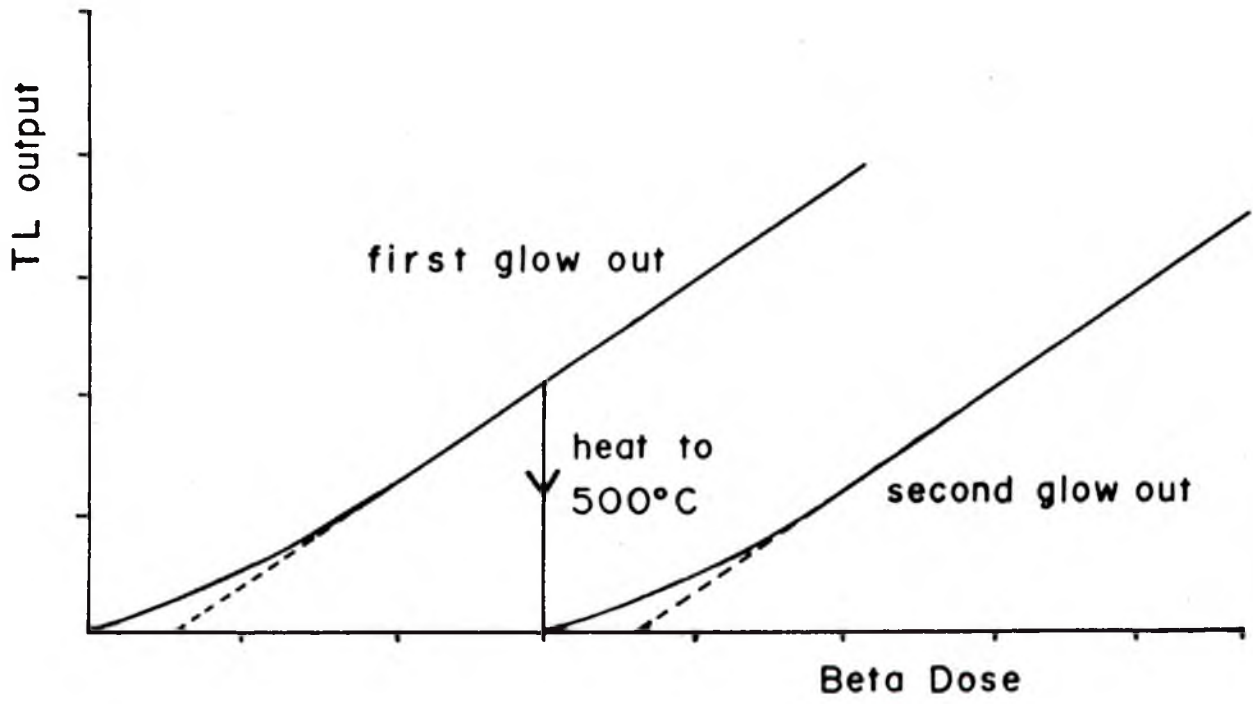


FIGURE 1.5: Second Glow-Out Growth Curve Parallel to the First giving the Same Supralinearity Correction.

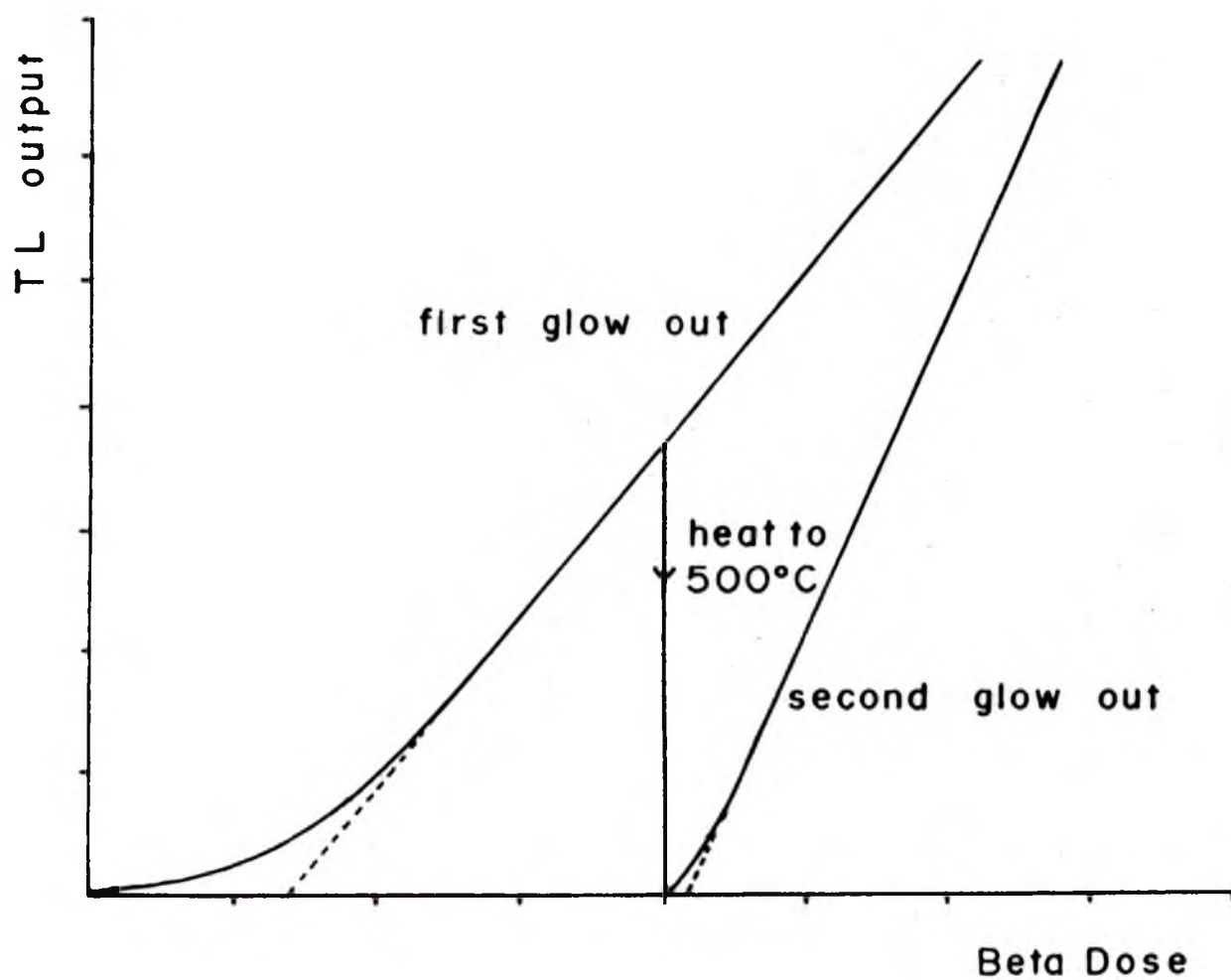


FIGURE 1.6: Second Glow-Out Growth Curve not Parallel to the First giving a Different Supralinearity Correction.

The TL sensitivity and the supralinearity of each of the two peaks depends on the relative concentrations of thermoluminescence traps and the non-TL competing traps. It is to be expected that this will vary from sample to sample and that in certain cases, the lower, 325°C , peak will be dominant giving a certain degree of overlap with the higher, 375°C , peak.

(b) High Doses

At the other end of the growth curve, the high dose region, non-linearity again sets in. This occurs when the TL traps begin to saturate. The curve does not level off completely but increases in a non-linear fashion (Fig. 1.7) above the saturation level. This continued increase is due to radiation damage within the crystal structure creating defects which can form additional thermoluminescence trapping sites.

Fleming (1969) has shown that the radiation-induced defects become considerably mobile and diffuse through the crystal lattice to form thermoluminescence sites only when they are in a charged state (i.e. have trapped electrons) and are subjected to heat treatment. Neither the electron excitation nor the intervention of heat alone can cause this site creation. The actual temperature dependence of the site formation is rather complex but it appears that at least 300°C is necessary to 'activate' the process. A sensitivity enhancement of $\times 340$ was measured for a pre-dose of 1.2 Megarads and the increase in sensitivity for lower pre-dose levels is shown in Fig. 1.8.

1.9 'Additive' Procedure for Determining Archaeological Dose

To avoid any possible error due to sensitivity changes after obtaining the first glow curve by heating to 500°C (whether it be due to overlap of the lower 325°C peak, to any pre-dose effect or any other

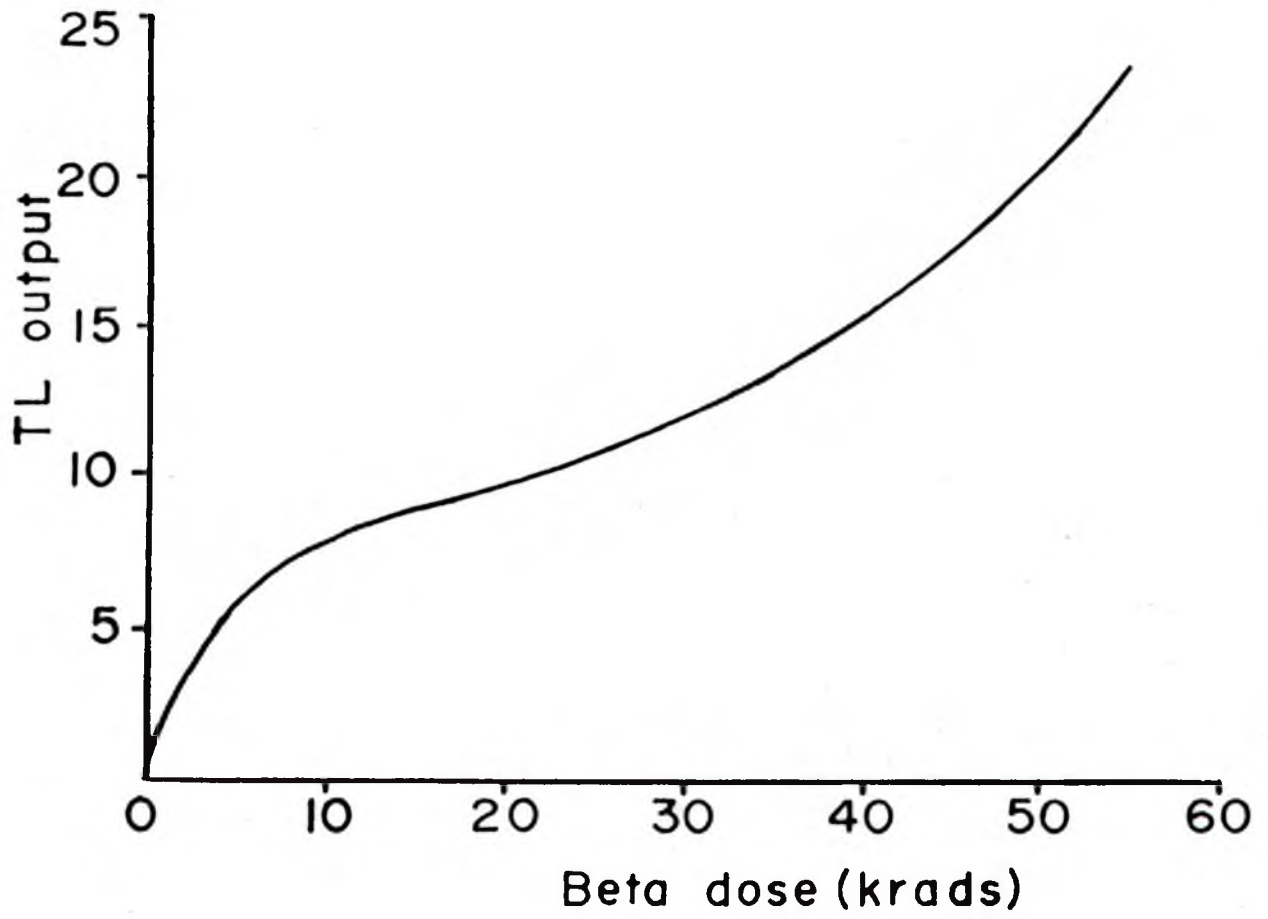


FIGURE 1.7: High Dose Saturation of the TL Growth Curve of Quartz.

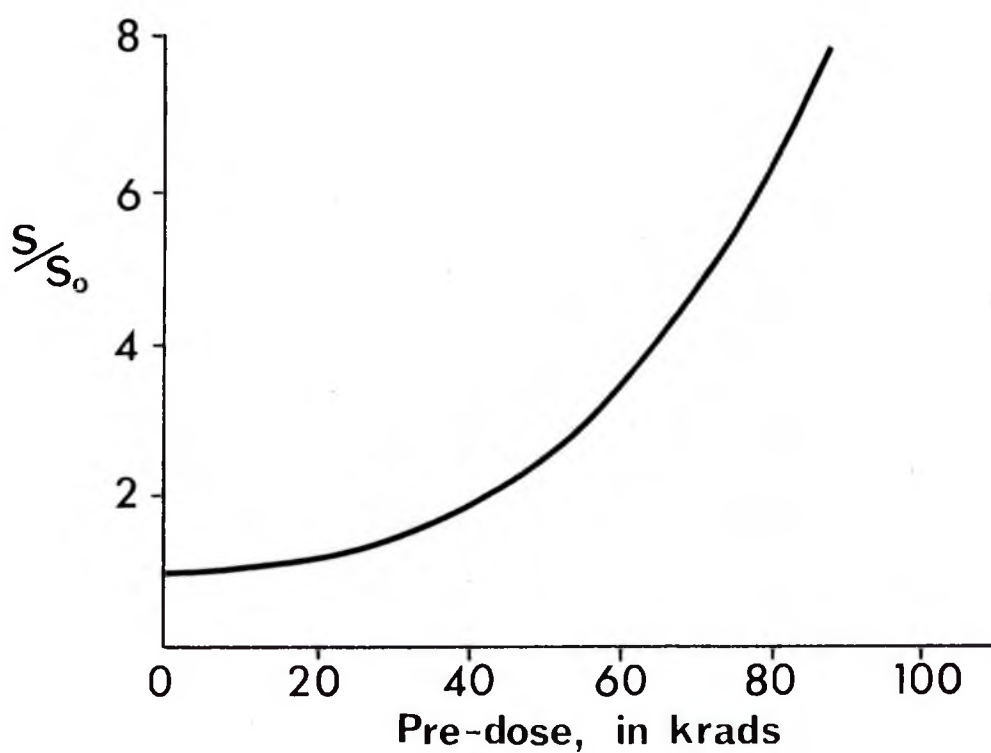


FIGURE 1.8: Pre-dose Sensitivity Enhancement of Quartz.

S_0 is the TL sensitivity measured for zero pre-dose and S is the sensitivity for the given pre-dose.

unknown phenomena), the 'additive procedure' illustrated in Fig. 1.9 is adopted. The natural archaeologically accrued TL is measured (N) from a known fraction of the sample. A second identical fraction is given an artificial laboratory beta dose (β_1) and the TL from this natural plus beta dose is measured ($N + \beta_1$). This procedure may be extended for several different beta doses (β_2, β_3, \dots) and is repeated for many different identical fractions at each dose level. A straight line through all of these points intersects the x-axis to give the equivalent dose (ED) which, however, still neglects the supralinearity of the initial response.

The supralinearity correction (I in Fig. 1.9) is determined by replotting the growth curve after drainage of the natural TL from each of the identical portions of sample. If no sensitivity changes have occurred and there is no overlap from the lower temperature peak then the slope of the second line, curve (b) in Fig. 1.9, should be the same as that of the first, curve (a) (Fleming, 1970).

The supralinearity correction, I , is added to the equivalent dose, ED, to give the total archaeological dose to be used in equation (1.12).

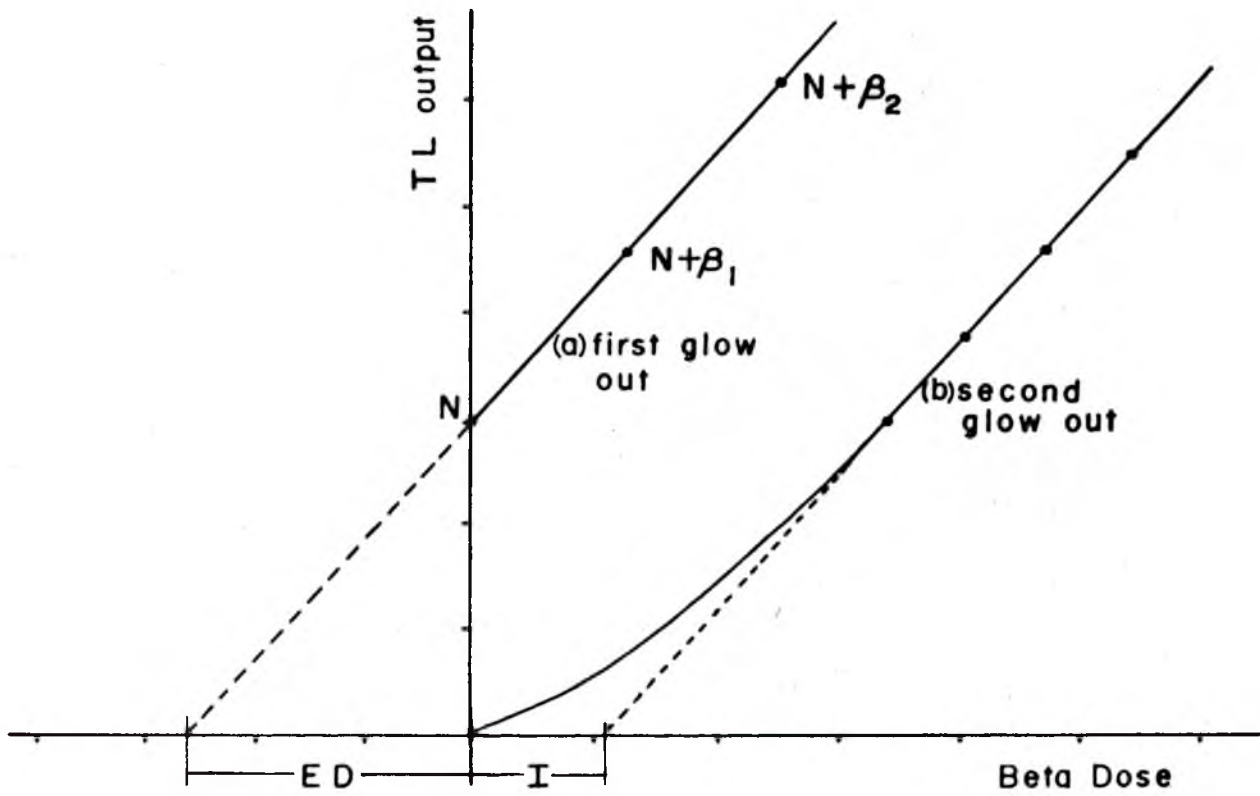


FIGURE 1.9: The 'Additive Procedure' for Determining the Equivalent Dose, ED , and the Supralinearity Correction, I .

CHAPTER II

TL EQUIPMENT - SETTING UP AND CALIBRATION

2.1 Introduction

The main criterion to be satisfied in the design of a thermoluminescence measuring system is that of detecting the very low light levels (typically 10^5 photons/s/sr) produced by the sample while at the same time minimising the effects of black-body thermal radiation (incandescence) and spurious, non-radiation induced thermoluminescence.

The system employed throughout these present studies is essentially the same as that described by Aitken and Fleming (1972) the main features of which are shown in Figure 2.1 and are described in Section 2.2.

2.2 Equipment

A highly sensitive photomultiplier (EMI 9635 QB) which has a spectral response biased towards the blue is selected. The spectral response of this tube is shown in Figure 2.2 and can be seen to fall off rapidly for wavelengths above $0.5 \mu\text{m}$. To further discriminate against black-body radiation a system of optical filters is introduced which consists of a blue-violet transmitting filter (Corning 7-59) combined with an infra-red rejecting filter (Chance Pilkington HA3).

Spurious or non-radiation induced thermoluminescence as a phenomenon is not well understood but it has been established (Aitken et al., 1968) that if the sample is heated in an atmosphere of dry, oxygen-free argon (or nitrogen) then the spurious TL is reduced by several orders of magnitude. Fleming (1969) has shown that the spurious TL lies more towards the red end of the spectrum than does the radiation-induced TL

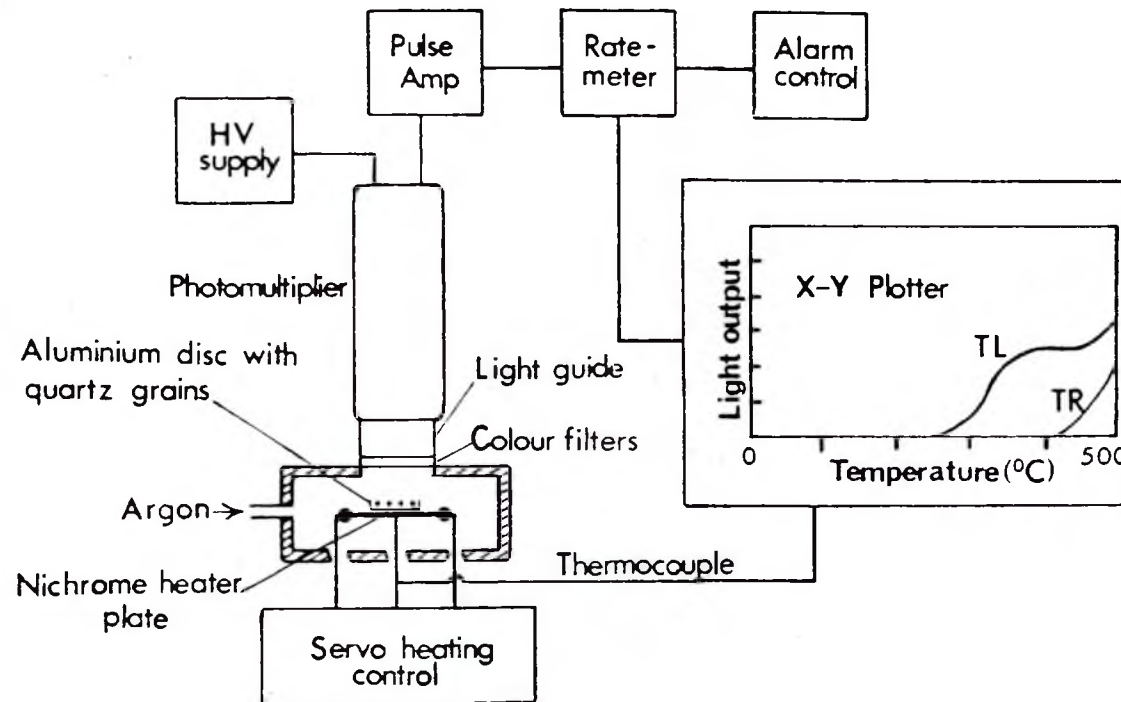


FIGURE 2.1: Diagrammatic Representation of the Thermoluminescence Dating Apparatus.

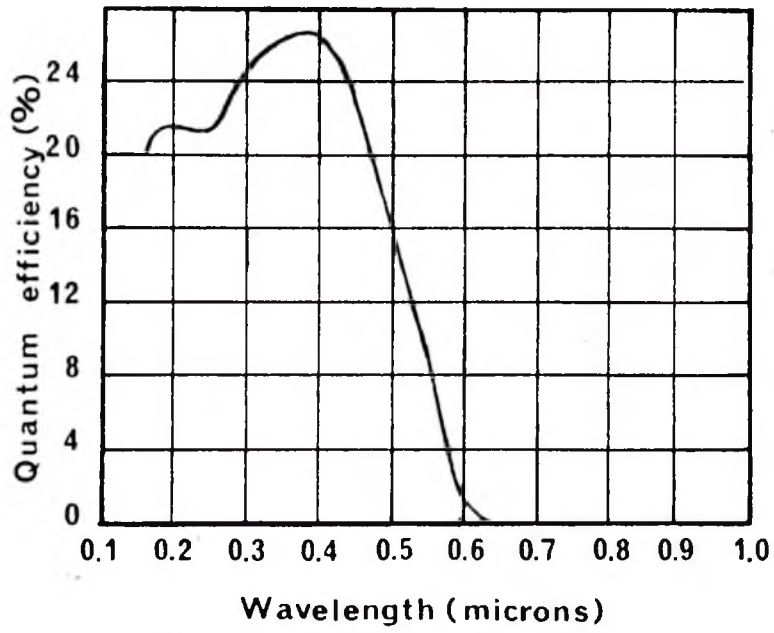


FIGURE 2.2: Spectral Response of the EMI 9635-QB Photomultiplier.

so that the filter system already described also provides useful discrimination against the former.

The sample itself rests on a two inch wide, water cooled nichrome heating strip. The heating rate is servo-controlled to be constant and reproducible to within $\pm 1\%$. The nichrome strip is shielded by a copper plate (mounted on insulating pyrophyllite strips) with a central hole below which the sample is positioned. A thermocouple is attached to the heating strip and the output from this drives both the servo-control mechanism and the X-axis of the chart recorder (Yokogawa Type 3077).

The photomultiplier, housing, filters, heating oven and servo-control mechanism were all supplied by Littlemore Scientific Engineering Co., Oxford.

The output from the anode of the photomultiplier is fed to a pulse amplifier (Ortec Model 113 pre-amp and Model 485 main amp) then through a pulse-height discriminator (Ortec Model 406) to a ratemeter (Ortec Model 441) which converts the pulsed signal to a form suitable for driving the Y-axis of the chart recorder. This 'photon-ratemeter' system has been shown by Aitken et al. (1968) to be superior to the 'dc' mode of operation but it does suffer the disadvantage of pulse pile-up at the amplifier and ratemeter when high pulse rates are encountered. An alarm control (Ortec Model 461) monitors the output and gives an audible and visual alarm when pile-up occurs. This problem is discussed more fully in Section 2.4. The high voltage is supplied to the photomultiplier by an Ortec Model 456 H.V. Supply. The above units are pictured in Figure 2.3.

2.3 Setting-Up of the Photon Detector

The EMI 9635 QB photomultiplier supplied with the apparatus has a recommended voltage of 1220 V for an overall sensitivity of 2000 A/lm and a dark current of 3 nA. With the high voltage set at this figure, the

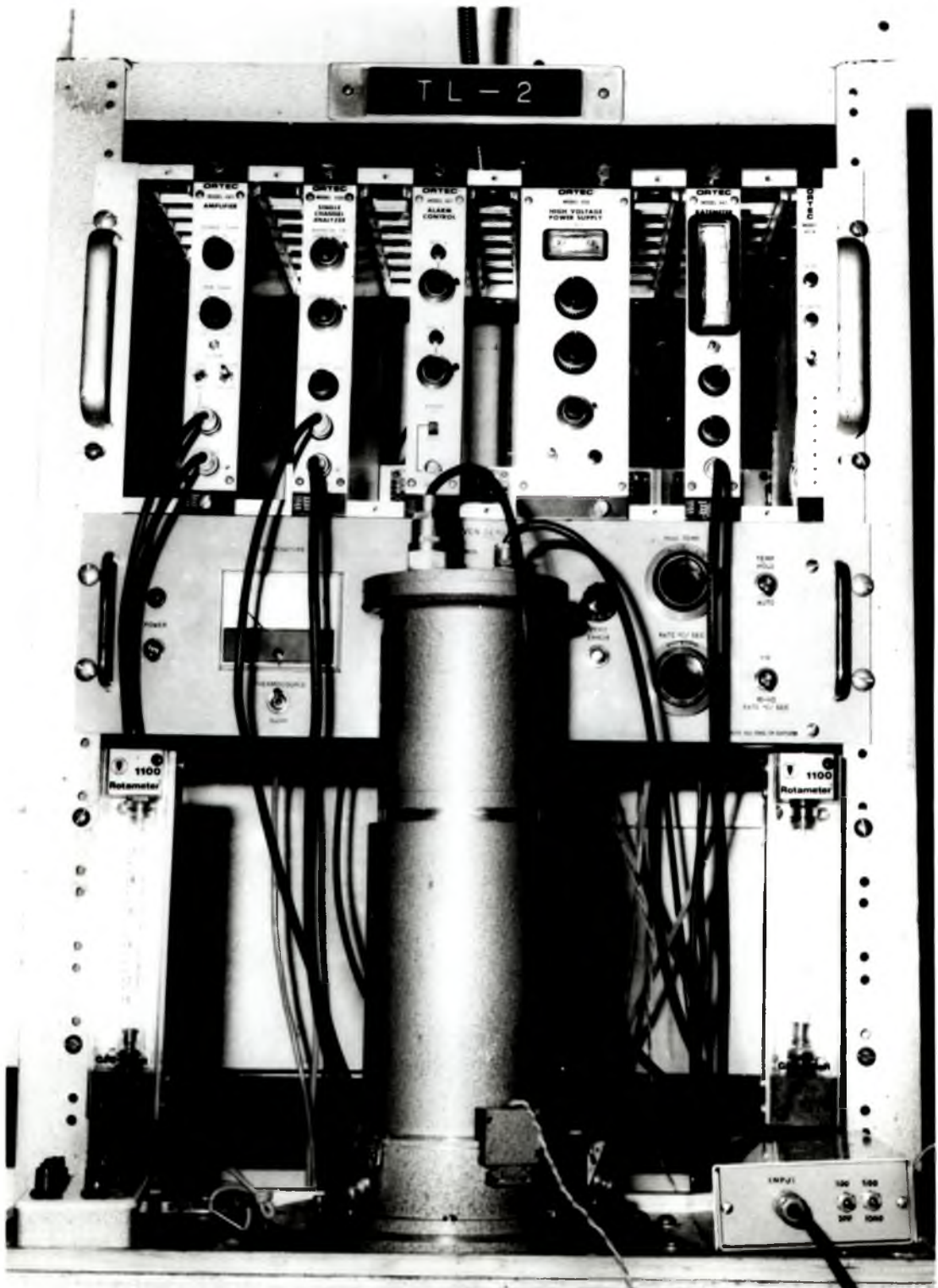


FIGURE 2.3: The Thermoluminescence Dating Apparatus.

gain of the amplifier was adjusted to prevent saturation on large pulse heights.

The discriminator lower level was then determined by placing the photomultiplier on the "Beta-light" source (a tritium encapsulated phosphor) supplied with the equipment the output from which can be assumed to be reasonably constant over the period of the experiment. The threshold was varied from 1.0 Volt downwards noting the output from the ratemeter at each setting and the resulting graph (Fig. 2.4a) was extrapolated backwards to zero threshold. The optimum working threshold for a good signal to noise ratio should be at a value which gives 85% of the output extrapolated back to zero. The value for the present system was found to be 0.3 Volts. The photomultiplier was then placed on the oven with only the black-body shield on the heating strip. The black-body output was measured at 450°C for the various threshold settings from 1.0 Volts downwards and the ratio of black-body to "Beta-light" output was plotted against threshold (Fig. 2.4b). This ratio is seen to increase rapidly below 0.1 Volts so that the threshold of 0.3 Volts provides an optimum working condition. The ratemeter range is adjusted to suit the brightness of the sample and the time constant is normally set at 0.05 sec.

2.4 Pulse Pile-Up and Non-linearity

The main advantages of using the photon-ratemeter system are that firstly it provides better discrimination against photomultiplier noise and secondly it is much less sensitive to changes in photomultiplier voltage and amplifier gain. A serious disadvantage, however, is that it lacks dynamic range with pile-up of pulses occurring at both the amplifier and ratemeter whenever high pulse rates are encountered. This pile-up, and the resultant non-linearity of response, might be

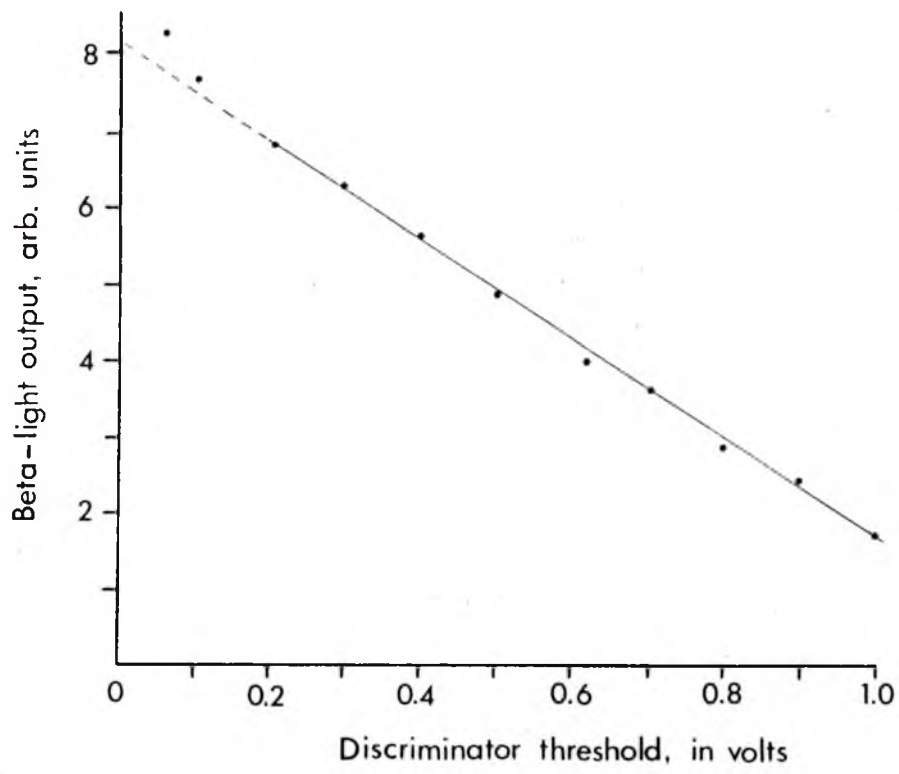


FIGURE 2.4a: "Beta-light" Output from the Ratemeter
versus Discriminator Threshold.

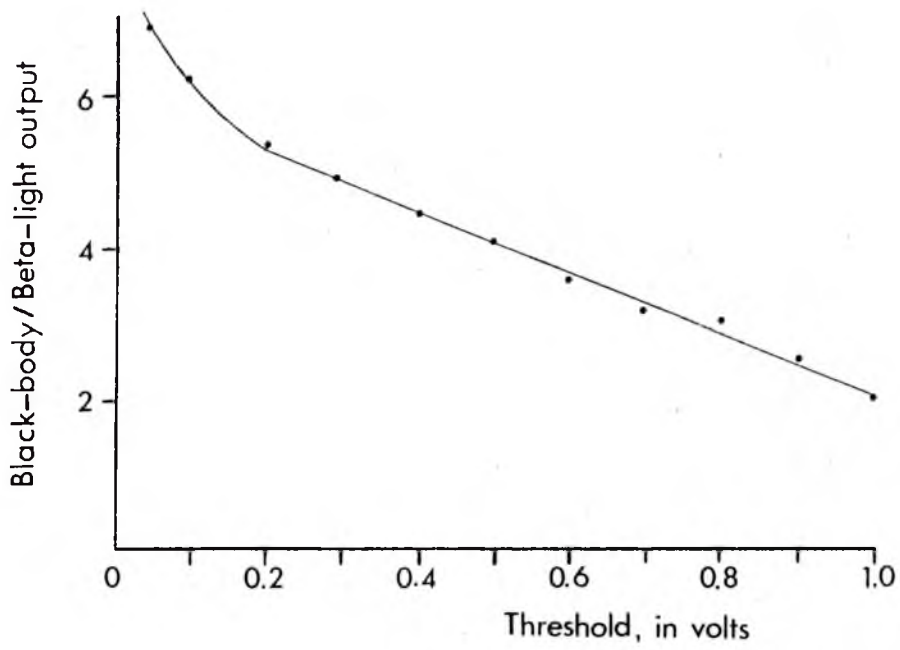


FIGURE 2.4b: Ratio of Black-body to "Beta-light" Output versus Threshold.

slightly improved by faster electronics but the ultimate limit will be the ability of the system to distinguish between overlapping pulses.

To overcome this problem studies were carried out of the non-linearity and efforts made to confine the signals to a linear region. The photomultiplier was placed on the "Beta-light" source with neutral density filters of different transmission factors (Balzers filters, No. 1 to No. 12) interposed between the two in turn. The output for a given filter is plotted against the transmission factor and the resultant curve (Fig. 2.5) is seen to become non-linear when the count-rate is approximately 30 K cps.

The count-rate is kept below this figure for very bright samples by attaching a thin aluminium plate with a small central hole over the aperture in the photomultiplier housing thus decreasing the effective size of the photocathode and hence the count-rate. An alarm control which gives an audible buzz and a visual red light monitors the output of the ratemeter and activates when the count-rate is equal or greater than 30 K cps.

The pile-up experiment described above was repeated several times throughout the course of the present studies and it was found that the initial slope of the curve in Figure 2.5 decreased slightly with time (probably due to ageing of the photomultiplier) but that the pulse-rate at which pile-up started to occur was consistently 30 K cps.

2.5 Alpha-Counting Equipment

The dose-rate from the uranium and thorium series may be assessed by measurement of the alpha activity of the sample by conventional counting methods (Turner et al., 1958). The conversion from actual alpha activity to dose-rate is described fully in Chapter VI.

To measure the activity of a sample the apparatus illustrated in

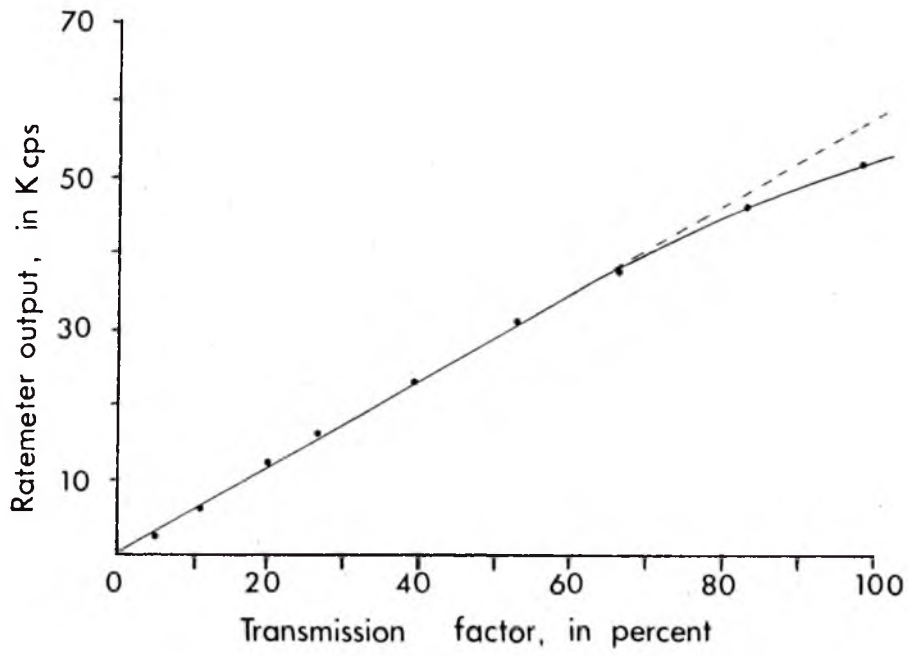


FIGURE 2.5: Non-linearity of the Response of the TL Apparatus at High Photon Count-Rates.

Figure 2.6 and diagrammatically in Figure 2.7 is used. The complete alpha counting set-up was supplied by Littlemore Scientific Engineering Co., Oxford and the calibration of the system is described in Appendix B.

The sample is gently crushed in a mortar and pestle and approximately 2 gm are placed in contact with the ZnS scintillation screen. This screen is constructed by attaching sellotape to the base of an aluminium ring and then sprinkling the ZnS powder over the sellotape. The ring is placed in the perspex holder and the sample poured into it to be in contact with the scintillating powder. The lid is then screwed onto the perspex holder and the assembly is mounted into the photomultiplier housing of the alpha-counting equipment. The component parts of the sample holder are pictured in Figure 2.8.

The alpha particles from the sample strike the screen and cause scintillations which are picked up by the photomultiplier and passed through a pulse amp and discriminator to a counter and printer. The printer prints-out the number of counts accumulated in a set interval (usually set to 25 min i.e. 1.5 ksec) as well as the total number of counts for the sample.

If N is the number of α -particles emitted per unit volume of active material per unit time then the number dN_o which are emitted in a small volume of area dA and height dh is

$$dN_o = N \cdot dA \cdot dh \quad (2.1)$$

Consider Figure 2.9, then the fraction of those emitted which pass through the circular cross section AB is

$$dN_o = \frac{N}{2} \left(1 - \frac{h}{R}\right) \cdot dA \cdot dh \quad (2.2)$$

Figure 2.6 and diagrammatically in Figure 2.7 is used. The complete alpha counting set-up was supplied by Littlemore Scientific Engineering Co., Oxford and the calibration of the system is described in Appendix B.

The sample is gently crushed in a mortar and pestle and approximately 2 gm are placed in contact with the ZnS scintillation screen. This screen is constructed by attaching sellotape to the base of an aluminium ring and then sprinkling the ZnS powder over the sellotape. The ring is placed in the perspex holder and the sample poured into it to be in contact with the scintillating powder. The lid is then screwed onto the perspex holder and the assembly is mounted into the photomultiplier housing of the alpha-counting equipment. The component parts of the sample holder are pictured in Figure 2.8.

The alpha particles from the sample strike the screen and cause scintillations which are picked up by the photomultiplier and passed through a pulse amp and discriminator to a counter and printer. The printer prints-out the number of counts accumulated in a set interval (usually set to 25 min i.e. 1.5 ksec) as well as the total number of counts for the sample.

If N is the number of α -particles emitted per unit volume of active material per unit time then the number dN_o which are emitted in a small volume of area dA and height dh is

$$dN_o = N \cdot dA \cdot dh \quad (2.1)$$

Consider Figure 2.9, then the fraction of those emitted which pass through the circular cross section AB is

$$dN_o = \frac{N}{2} \left(1 - \frac{h}{R}\right) \cdot dA \cdot dh \quad (2.2)$$

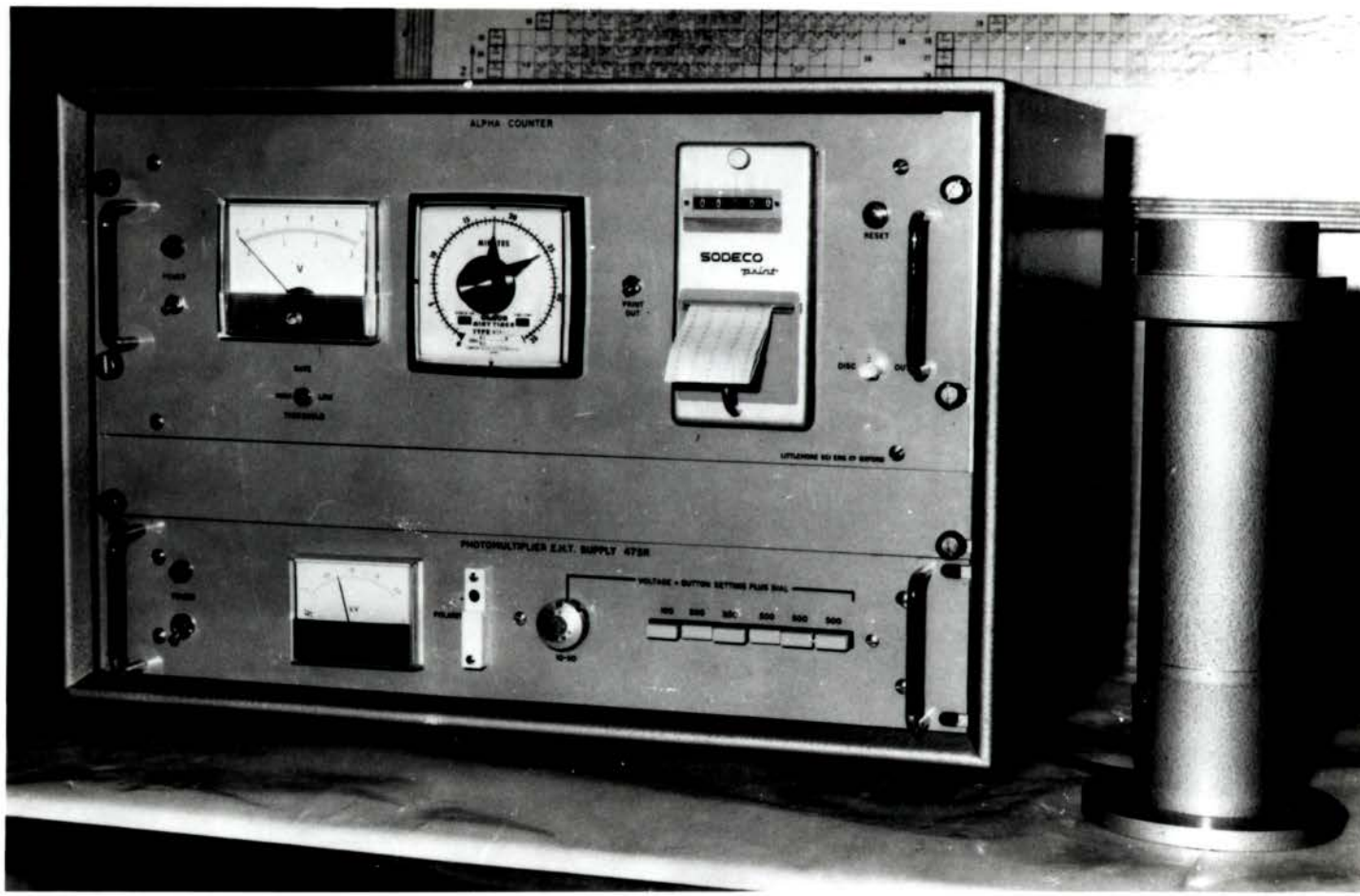


FIGURE 2.6: The Alpha-Counting Apparatus.

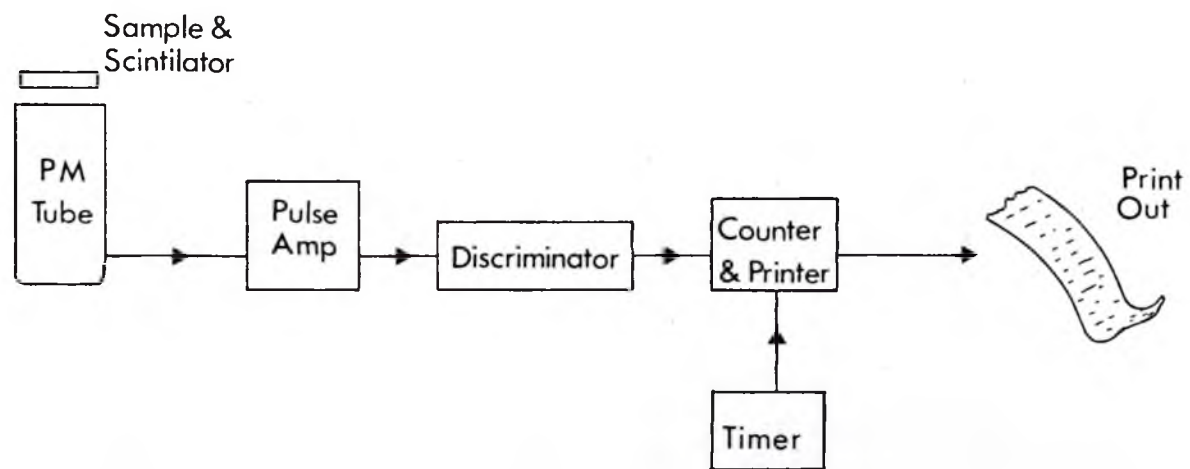


FIGURE 2.7: Diagrammatic Representation of the Alpha-Counting Apparatus.

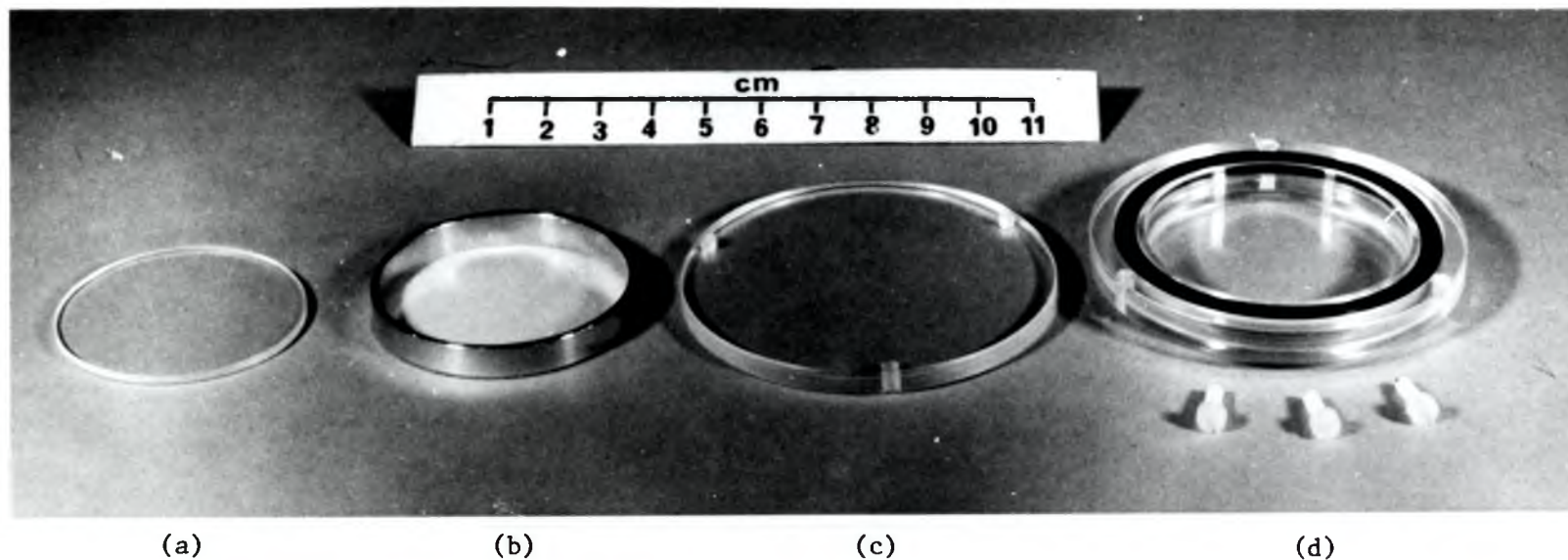


FIGURE 2.8: The Component Parts of the Alpha-Counter Sample Holder.

- (a) perspex spacer, (b) aluminium ring with ZnS scintillating screen,
(c) perspex lid, and (d) perspex body of sample holder and screws.

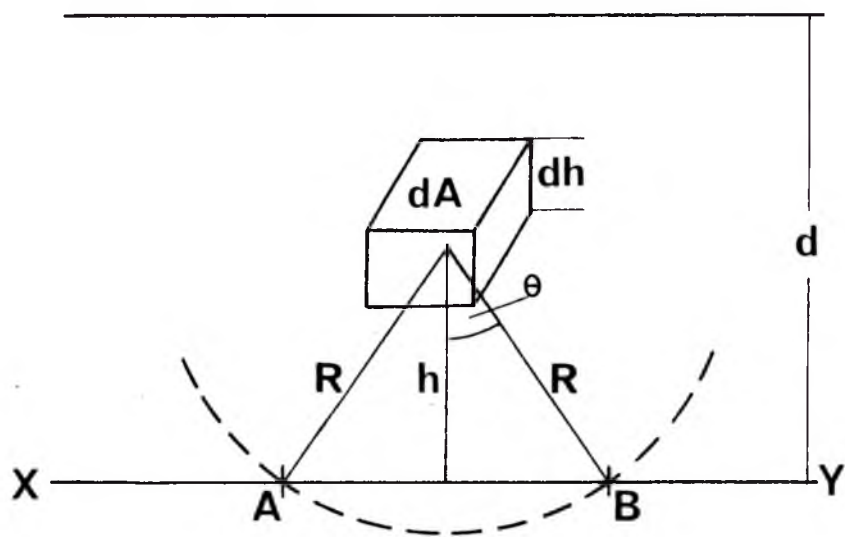


FIGURE 2.9: Geometry used for Alpha-Counting Activity Calculations.

where R is the range of an α -particle in the active medium, h is the height of the elemental volume $d\Lambda \cdot dh$ above AB and d is the thickness of the sample.

The total number of α -particles emerging per unit area of the sample per unit time, N_A , is then

$$\begin{aligned} N_A &= \frac{N}{2} \int_{h=0}^{h=d} (1 - h/R) \cdot dh \\ &= \frac{Nd}{2} (1 - d/2R) \end{aligned} \quad (2.3)$$

The range of α -particles in most clay materials is of the order of 20 to 30 microns whereas the thickness of the sample is likely to be of the order of a few millimetres at least. Hence it is possible to replace the upper limit of the integral in equation (2.3) by $h=R$, therefore

$$\begin{aligned} N_A &= \frac{N}{2} \int_{h=0}^{h=R} (1 - h/R) \cdot dh \\ &= \frac{NR}{4} \end{aligned} \quad (2.4)$$

If S , the activity, is the number of α -particles emitted per unit mass per unit time then S equals N/ρ where ρ is the density of the active material, thus

$$S = \frac{4N_A}{R \rho} \quad (2.5)$$

N_A is the number of α -particles emerging per unit area per unit time, so assuming they all give rise to a scintillation event, then if

C_{α} is the number of alpha-counts measured per unit time over an area A ,
 S may be written:

$$S = \frac{4 \cdot C_{\alpha}}{R \rho \Lambda} \quad (2.6)$$

The area A is calculated from the internal diameter of the aluminium ring which is 42 mm. Equation (2.6) will be used in Chapter VI for calculating dose-rates based on alpha activity.

CHAPTER III - ALPHA PARTICLE DOSIMETRY

3.1 The Attenuation of Radiation Through Interactions with Matter

The radiation emitted during the nuclear disintegration processes of the uranium, thorium and potassium series is of two basic forms - (i) charged particles and (ii) electromagnetic radiation. The latter form is dealt with in Chapter V whereas the former must be further divided into heavy charged particles (and more specifically alpha particles) which are covered in this Chapter and light charged particles (electrons and positrons) covered in the next.

The interaction of charged particles with matter is mainly via collision processes which in their course bring about a diminution in energy and a deflection of the particles' motion. These collisions can be either elastic or inelastic and can take place with either atomic electrons or nuclei. In the energy range considered here and for the charged particles of interest the preponderant mode of energy loss is by inelastic collisions with atomic electrons of the absorber material. The electrons are thereby raised to higher energy levels in the atom and may, as happens in the majority of cases, have sufficient energy transferred to them to cause them to be ejected from the atom altogether.

Thus the principal mode of energy loss of charged particles is ionization of atomic electrons, the very process which was described in Chapter I (Fig. 1.1) as giving rise to the thermoluminescence effect. This Chapter deals with the efficiency of alpha particles at producing TL and the attenuation of the alpha dose as the particle passes through a quartz grain.

3.2 Inefficiency of Alpha Particles to Induce Thermoluminescence

Woodley and Johnson (1965) first noted the relative inefficiency of heavy charged particles compared to electrons to induce thermoluminescence. Zimmerman (1972) made a study of the relative thermoluminescence response to alpha and beta radiation of six phosphors (including quartz) and obtained good agreement between experimental results and predicted alpha efficiencies based on an 'energy density' model.

This model may be understood by treating the alpha particle as a source of very localised ionization along its track. Thermoluminescent traps within the volume of this track experience an extremely high energy density which is sufficient to saturate them, while beyond that region the energy density is zero and the traps remain empty. Hence the difference in TL response between alpha and beta radiation is due to the difference in spatial energy distribution, this being localised along the track for alphas and uniform throughout the sample volume for betas.

As an example, a 3.7 MeV alpha particle may be considered as producing a cylindrical ionization track through a phosphor grain. The radius of this track will be approximately 2×10^{-6} cm and the energy density within the track about 10^8 ergs/gm (10^6 rads). If the phosphor is saturated for this dose of beta radiation, then the ineffective dose from the alpha particle is dissipated thermally to the crystal lattice and thus an alpha efficiency factor, k , may be defined as the ratio of the TL produced per unit energy by alpha radiation to the TL per unit energy for beta radiation, i.e.

$$k = \frac{(\text{TL/rad})_{\text{alpha}}}{(\text{TL/rad})_{\text{beta}}} \quad (3.1)$$

k-values are always < 1 and typical values for the 375°C peak of quartz are about 0.1 (Zimmerman, 1972).

3.3 The Attenuation and Range of Alpha Particles

The collision with and consequent ionization of the atomic electrons of the stopping material by the incident alpha particles is fundamentally a quantum-mechanical problem. The result of this treatment, incorporating relativistic considerations and other corrections, leads to the well-known Bethe equation for the Stopping Power of an absorber which reads (Bichsel, 1968)

$$-\frac{dE}{dx} = \frac{4\pi z^2 e^4 N Z}{m_e v^2} \left[\ln(2m_e v^2/I) - \ln(1 - \beta^2) - \beta^2 - \Sigma(C_i/Z) \right] \quad (3.2)$$

where z is the atomic number and v the velocity of the incident particle;

e is the electron's charge;

m_e is the mass of an electron;

N is the number of atoms per unit volume and

Z is their atomic number;

I is the mean excitation potential of the medium and

$\beta = v/c$ (c the velocity of light).

The term $\Sigma(C_i/Z)$ is a correction for the non-participation of bound electrons in the slowing-down process and is especially important for low velocity particles i.e. when v is comparable to the velocity of an electron in orbit.

The Range of an alpha particle may be defined as the path length of the particle to a point where all of its kinetic energy has been lost. This distance may be theoretically estimated by the integration

$$R = \int_{E_0}^0 (dE/dx)^{-1} dE \quad (3.3)$$

where E_0 is the initial particle energy.

Here (dE/dx) is the mean energy loss per unit path length. Since the alpha particle is brought to rest by a large number of statistically distributed collisions, each of finite energy transfer, the actual ranges of individual particles straggle around the mean value and are slightly different from a discrete slowing down range (although only by about 1% or less). The mean range defined by equation (3.3) is known as the continuous-slowing-down-approximation (csda) range and in practice all range-energy relations in this work will implicitly refer to a csda range unless stated otherwise.

Comprehensive tabulations for the Stopping Powers and Ranges of heavy charged particles are given by Barkas and Berger (1964) and the application of these to different materials is described by Bichsel (1968).

3.4 Absorbed Dose from Alpha Particles

Spiers (1953) first studied the problem of energy deposition in one medium due to particles generated in another. Kononenko (1957) studied the absorbed dose in tissue cavities due to alpha-particle emitters in surrounding bone. Both workers made the assumption that the linear energy transfer (LET), that is the energy deposited at any point along the track of a single charged particle, is independent of the particle energy. Charlton and Cormack (1962) derived expressions for the absorbed dose in tissue cavities in bone taking account of the dependence of LET on alpha energy and Howarth (1965) developed methods for calculating these expressions and gave tabulated values.

The results of Charlton and Cormack's work may be expressed by a simple relation

$$D_{\alpha}(x) = \frac{n_o E_o}{m S} \cdot G_{\alpha}(x/R_o) \quad (3.4)$$

Where $D_{\alpha}(x)$ is the absorbed dose at a point distant x from the interface between the emitting and the absorbing media; n_o is the number of alphas, of initial energy E_o and range R_o in the absorber, emitted per unit mass of the emitter and $\frac{S}{m}$ is the ratio of the mass stopping powers derived from Equation (3.2) by dividing by the density, ρ (i.e. $\frac{1}{\rho} \cdot \frac{dE}{dx}$). $G_{\alpha}(x/R_o)$ is a geometrical function which depends on the shape of the interface and on the range-energy relationship for alphas.

For alpha particles of energy between 1 and 10 MeV, the range-energy relation may be expressed as

$$R = AE^m \quad (3.5)$$

where R is the range of an alpha particle as its energy drops from E to zero, and A and m are empirical constants.

Using equation (3.5) Howarth (1965) developed the forms of $G_{\alpha}(x/R_o)$ for

(i) a plane interface

$$G_{\alpha} \rightarrow P_{\alpha}(x/R_o) = \frac{1}{2} \int_0^{\arccos(x/R_o)} (1 - x/R_o \cos\phi)^{1/m} \sin\phi d\phi \quad (3.6)$$

(ii) a spherical interface

$$G_{\alpha} \rightarrow S_{\alpha}(x/R_o, D/R_o) = \frac{1}{2} \int_0^{\phi_{\max}} (1 - a/R_o)^{1/m} \sin\phi d\phi \quad (3.7)$$

and (iii) a cylindrical interface

$$G_{\alpha} \rightarrow C_{\alpha}(x/R_o, D/R_o) = \frac{1}{\pi} \int_0^{\phi_{\max}} \int_0^{\arccos(a/R_o)} \cos\theta (1 - a/R_o \cos\theta)^{1/m} d\theta d\phi \quad (3.8)$$

where D is the diameter of the spherical interface,

$$(D/2)^2 = (D/2 - x)^2 + a^2 + 2a(D/2 - x)\cos\phi \quad (3.9)$$

and

$$\cos\phi_{\max} = \frac{(D/2R_o)^2 - 1 - (D/2R_o - x/R_o)^2}{2(D/2R_o - x/R_o)} \quad (3.10)$$

for $(D - x) \geq R_o$

$$\phi_{\max} = \pi \quad \text{for } (D - x) \leq R_o \quad (3.11)$$

There are few accurate data concerning the range-energy relationships of alpha particles but Charlton and Cormack (1962) estimated the variation of LET with energy based on data, derived from proton ranges in water (Whaling, 1958). By fitting a curve to the data points they came up with an empirical relationship

$$\frac{dE}{dR} = \frac{2.16 \times 10^2}{E^{0.5}} \text{ keV}/\mu\text{m} \quad (3.12)$$

and hence a value of m in equation (3.5) of 1.5 i.e.

$$R = AE^{1.5} \quad (3.13)$$

Fleming (1969) performed a similar curve fitting procedure to Whaling's data for protons in neon ($Z = 10$, which is nearer the effective Z value of quartz than is water) giving

$$\frac{dE}{dR} = \frac{2.332 \times 10^2}{E^{0.45}} \text{ keV}/\mu\text{m} \quad (3.14)$$

which implies $m = 1.45$, in good agreement with the above results.

Howarth (1965) has used the value of $m = 1.5$ in his tabulations of $G_\alpha(x/R_0)$ and so this figure will be assumed in further discussions of alpha particle ranges in quartz.

3.5 Effective Alpha Dose to Quartz Inclusions

Fleming (1970) has shown that the major fraction of the radioactivity is concentrated in the clay matrix and the quartz inclusions are relatively radioactivity-free and, in addition, the quartz grains may be treated as spherical in shape even though many are visibly rhombohedroid. Hence the calculations of Howarth (1965) may be used to estimate the alpha dose absorbed by the quartz inclusions.

To apply equation (3.7) it is necessary to know the values for D , the particle diameter, and R_0 the range of an alpha particle in quartz. In Part II we shall see that a grain size fraction of between 90 and 120 μm is used for dating work which gives an average diameter of $D = 105 \mu\text{m}$. To calculate R_0 from the tables of Barkas and Berger (1964), values for the average energy of the alpha particles, the mean ionization energy I of quartz and Z/A for quartz ($Z = \text{atomic number}$;

A = atomic weight) are required.

From Chapter VI the average alpha energy of the uranium series is $\overline{E_\alpha} = 5.36$ MeV and for the thorium series $\overline{E_\alpha} = 5.99$ MeV.

For I of quartz, use must be made of Bragg's Law (NBS, 1961) which gives a value averaged over each of the constituents, i.e.

$$Z/A = \sum_i u_i (Z_i/A_i) \quad (3.15)$$

and

$$\ln I = (Z/A)^{-1} \sum_i u_i (Z_i/A_i) \ln I_i \quad (3.16)$$

where u_i is the fraction by weight of the i th element in the compound.

Using values of I_i for Si of 170 eV and for O_2 of 100 eV, as recommended by Bichsel (1968), gives the following for quartz,

$$Z/A = 0.49925 \quad \text{and} \quad I = 128.1 \text{ eV} \quad (3.17)$$

The ranges obtained for the two series are then

$$\text{Uranium, } \overline{E_\alpha} = 5.36 \text{ MeV} \quad R_O = 21.7 \text{ } \mu\text{m} \quad (3.18)$$

$$\text{Thorium, } \overline{E_\alpha} = 5.99 \text{ MeV} \quad R_O = 25.6 \text{ } \mu\text{m} \quad (3.19)$$

The variation of $S_\alpha (x/R_O, D/R_O)$ can now be interpolated from Howarth's (1965) data and this is illustrated in Figure 3.1 for each of the two series with a scale given for the penetration depth x .

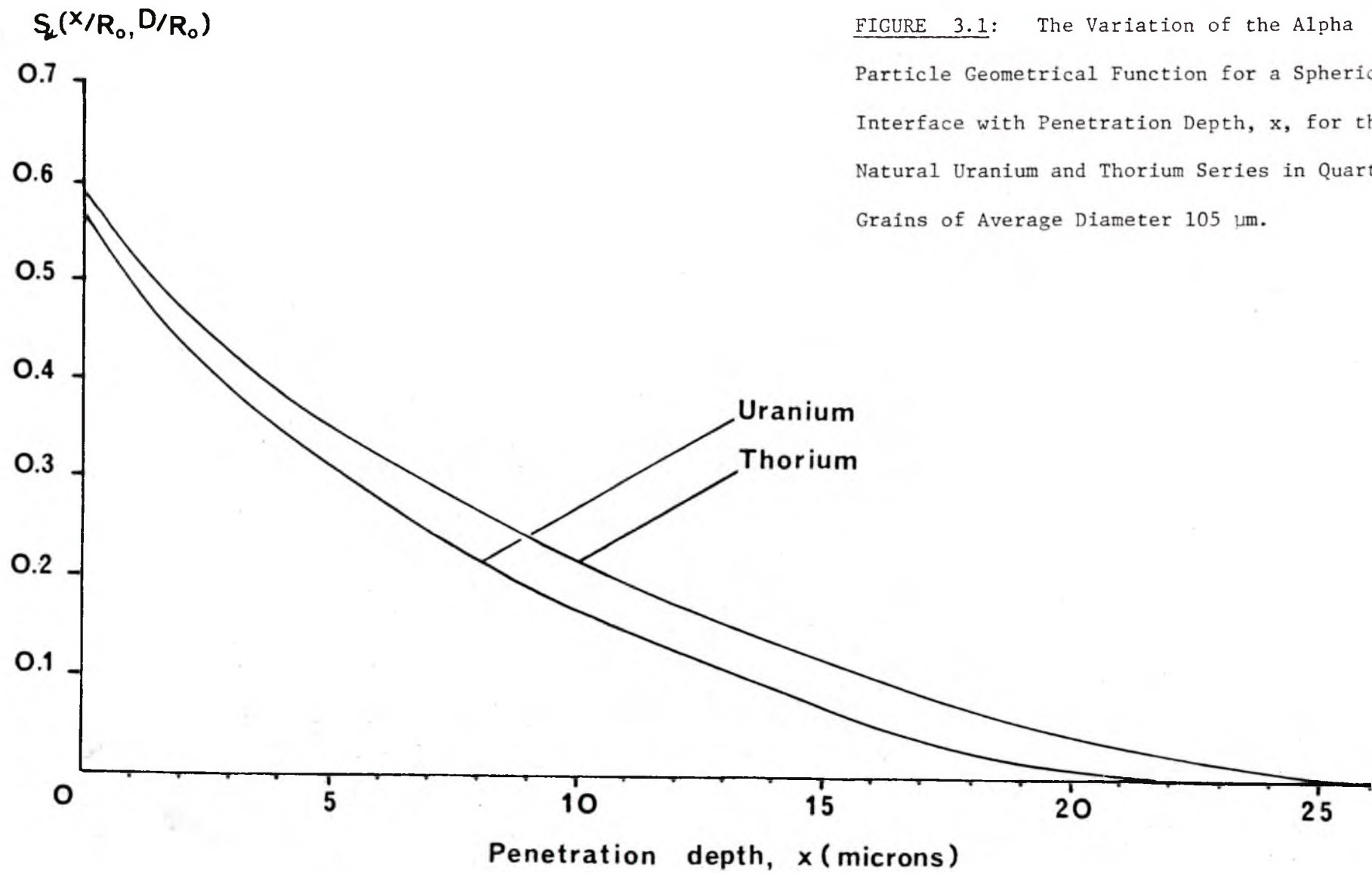


FIGURE 3.1: The Variation of the Alpha Particle Geometrical Function for a Spherical Interface with Penetration Depth, x , for the Natural Uranium and Thorium Series in Quartz Grains of Average Diameter $105 \mu\text{m}$.

Substituting $S_{\alpha}(x/R_o, D/R_o)$ in equation (3.4) gives $D_{\alpha}(x)$, the absorbed dose at a point x in a spherical grain, as

$$D_{\alpha}(x) = \frac{n_o E_o}{m S} \cdot S_{\alpha}(x/R_o, D/R_o) \quad (3.20)$$

To calculate the mean absorbed dose in a grain, $\overline{D_{\alpha}(\text{Abs})}$, $D_{\alpha}(x)$ must be integrated over the volume of interest in the grain, i.e.

$$\overline{D_{\alpha}(\text{Abs})} = \frac{n_o E_o}{m S} \cdot \frac{\int_{D/2-R_o}^{D/2} S_{\alpha}(x/R_o, D/R_o) r^2 \sin\theta dr d\theta d\phi}{\int_{D/2-R_o}^{D/2} r^2 \sin\theta dr d\theta d\phi} \quad (3.21)$$

$$= \frac{n_o E_o}{m S} \cdot \frac{\int_0^1 S_{\alpha}(u) \cdot (D/2R_o - u)^2 du}{\int_0^1 (D/2R_o - u)^2 du} \quad (3.22)$$

using $r = D/2 - x$ and substituting the variable $u = x/R_o$.

The integration in the numerator of equation (3.22) is evaluated for each of the uranium and thorium series by use of a simple Fortran computer programme based on Simpson's Rule for integration. The remainder of equation (3.22) may be evaluated analytically with the results for

Uranium:

$$\overline{D_{\alpha}(\text{Abs})}_U = 0.232 \times \frac{n_o E_o}{m S} \quad (3.23)$$

and Thorium:

$$\overline{D_{\alpha}(\text{Abs})}_{Th} = 0.251 \times \frac{n_o E_o}{m S} \quad (3.24)$$

3.6 The Reduction of the Effective Alpha Dose by Etching in Hydrofluoric Acid

In anticipation of the practical work to be described in Part II it is convenient to consider here some of the effects of the removal of part of the outer layers of the quartz grains by etching in hydrofluoric acid (HF). The full effects of this acid treatment are described in detail in Chapter VII but it is convenient to evaluate now the reduction in the effective alpha dose due to the removal of the outer grain boundaries.

For the sake of simplicity at this stage, spherical grain shape will be assumed throughout implying that the etching takes place at an even rate over the entire grain surface.

Equation (3.22) may be rewritten as

$$\overline{D_{\alpha}(\text{Abs})} = \frac{n_o E_o}{S_m} \cdot \overline{S_{\alpha}(\text{Abs})} \quad (3.25)$$

where $\overline{S_{\alpha}(\text{Abs})}$ is the mean shape factor for the whole grain and is defined by equation (3.22). If the outer regions of the grain are removed then the mean absorbed dose in the remainder of the grain, $\overline{D_{\alpha}(\text{Abs})}^*$, will be less than $\overline{D_{\alpha}(\text{Abs})}$ and the mean shape factor for the remaining alpha dose, $\overline{S_{\alpha}(\text{Abs})}^*$, may be defined by

$$\overline{D_{\alpha}(\text{Abs})}^* = \frac{n_o E_o}{S_m} \cdot \overline{S_{\alpha}(\text{Abs})}^* \quad (3.26)$$

To evaluate $\overline{S_{\alpha}(\text{Abs})}^*$, the limits of the integration must be defined. For the whole grain these limits were from $(D/2 - R_o)$ to $D/2$ but now the outer layer of thickness d has been removed (see Fig. 3.2) and hence the limits for the remainder of the grain are from $(D/2 - R_o)$ to $(D/2 - d)$.

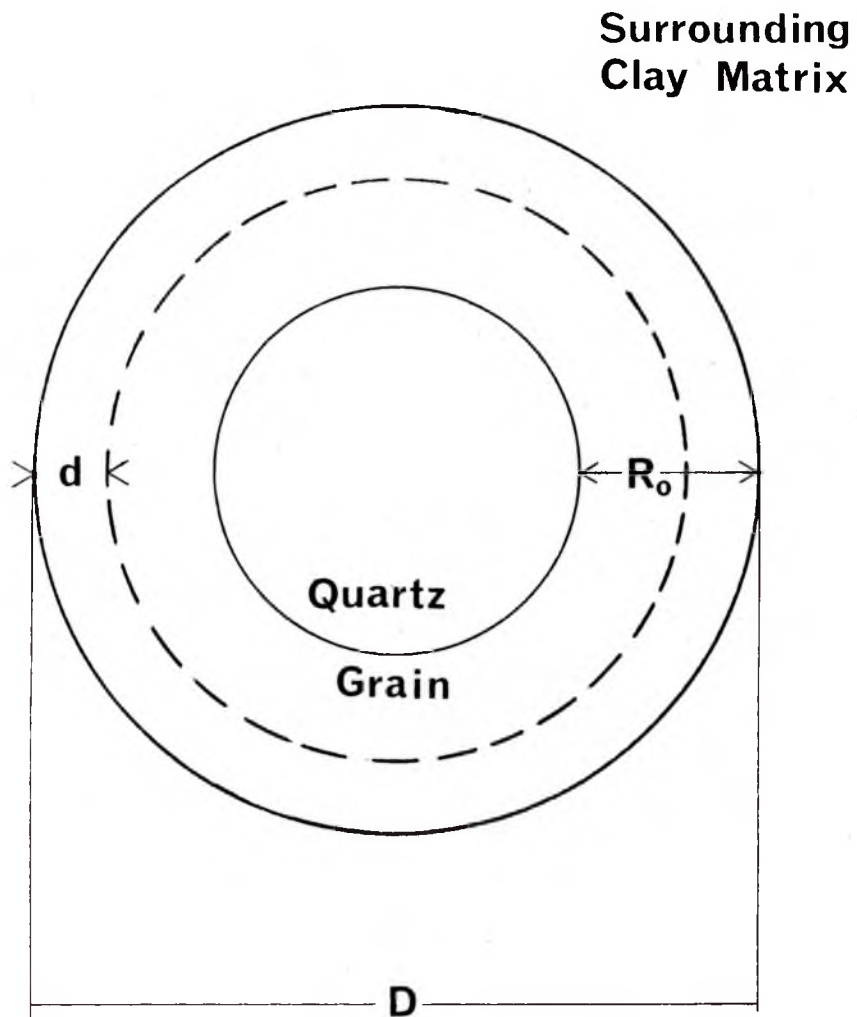


FIGURE 3.2: Geometry of a Quartz Grain with Thickness d removed by Etching in Hydrofluoric Acid.

Using the same substitutions as in equation (3.22) the mean absorbed dose in a grain which has had a layer of thickness d removed may then be written

$$\overline{D}_{\alpha}(\text{Abs})^* = \frac{n_o E_o}{S_m} \cdot \frac{\int_{d/R_o}^1 S_{\alpha}(u) \cdot (D/2R_o - u)^2 du}{\int_{d/R_o}^1 (D/2R_o - u)^2 du} \quad (3.27)$$

This integration is carried out as before for different values of d and the results are shown in Figure 3.3. Here the mean absorbed dose after etching is normalised to the mean dose before etching. The results of Fleming (1969, 1970) are also shown in Figure 3.3 and the difference is seen to be quite significant.

Assuming that the k -value does not vary with depth in the grain, then Figure 3.3 may be interpreted as the reduction in the thermoluminescence induced by alpha radiation as a function of the etching depth. These results will be used extensively in Part II when account is taken of this residual alpha-induced TL left after etching the quartz grain in HF.

3.7 Summary and Discussion of Results

In this Chapter it has been shown that alpha particles are only about one tenth as efficient as beta particles at inducing TL because of the very localised ionization density along the tracks.

In addition, alpha particles arising from nuclear disintegrations in the clay matrix surrounding the quartz grains will penetrate on average a distance of $21.7\mu\text{m}$ for the uranium series and $25.6\mu\text{m}$ for the thorium series.

On the basis of spherical geometry, shape factors have been

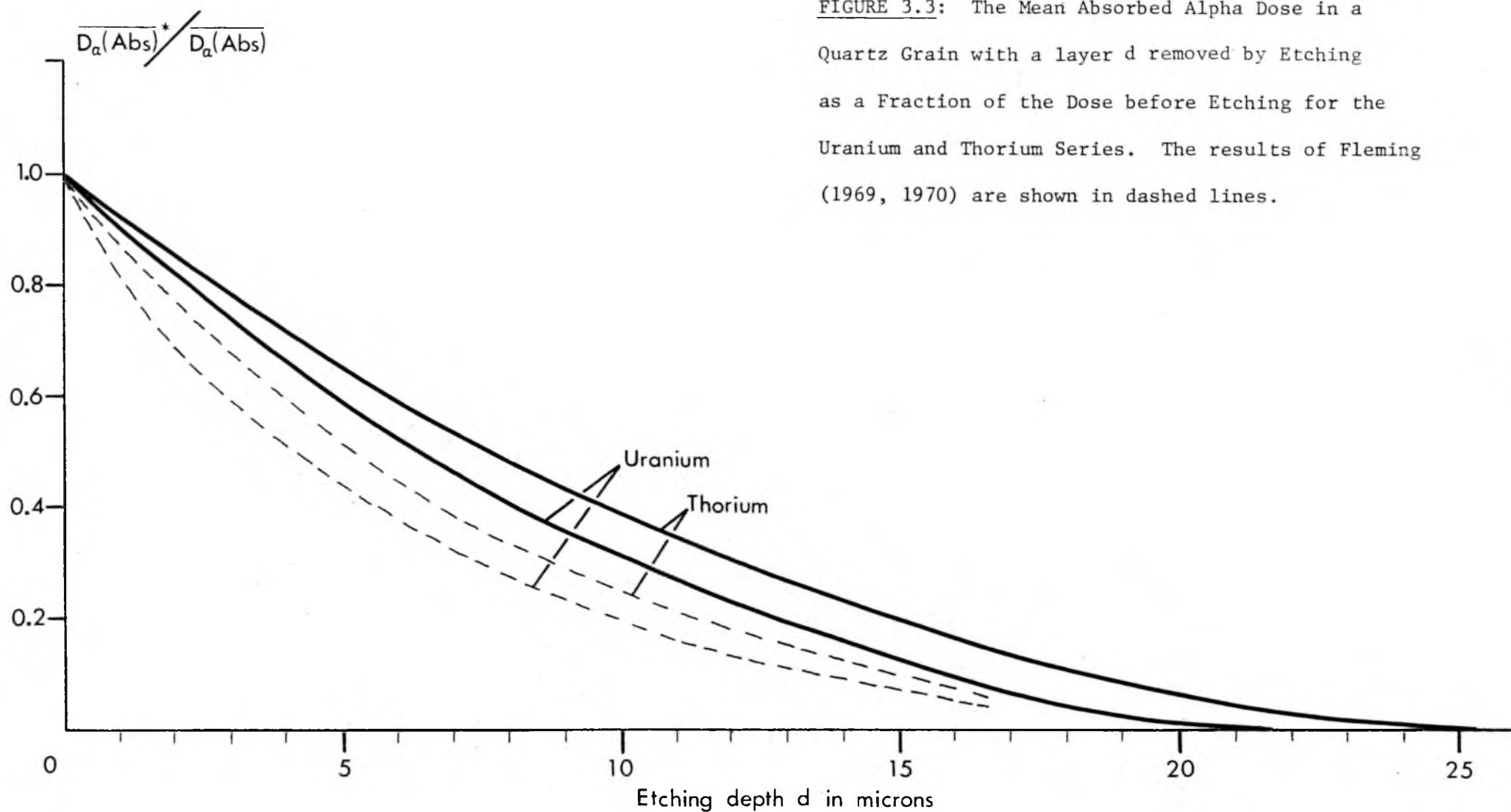


FIGURE 3.3: The Mean Absorbed Alpha Dose in a Quartz Grain with a layer d removed by Etching as a Fraction of the Dose before Etching for the Uranium and Thorium Series. The results of Fleming (1969, 1970) are shown in dashed lines.

deduced which indicate (Figure 3.1) that within a few microns of the grain's surface the absorbed dose has dropped to a fraction of the dose for zero grain size, $D_o (= n_o E_o / m S)$. It is worthwhile noting that even the surface dose of a $105\mu\text{m}$ grain is less than 60% of the zero grain size dose. By averaging over the whole of a $105\mu\text{m}$ grain it was found that the mean absorbed dose for the uranium series is 23.2% and for the thorium series 25.1% of D_o . Fleming (1970) quotes 21% and 25% for the uranium and thorium series respectively.

As an example of the consequences of this alpha dose dilution, consider a clay sample with 12ppm thorium and 3ppm uranium. The total alpha contribution from these typical levels of radioactivity is 1720 mrad/yr and the contribution from betas and gammas together only 174 mrad/yr (these figures are taken from Chapter VI). Thus the alpha radiation accounts for over 90% of the ionizing energy released by the decay of the two series.

If, however, account is taken of the dose dilution due to shape factors and assuming a k-value of 0.1, the alpha dose which effectively gives rise to thermoluminescence is reduced to only 41 mrad/yr or 19% of the total dose. (This is of course neglecting any beta or gamma dose attenuation due to grain size as described in the succeeding Chapters).

So, although over 90% of the ionizing energy released by nuclear disintegrations within the clay matrix is carried by alpha particles, only about 2% of this energy ever gives rise to thermoluminescence and this alpha-induced TL is concentrated in the outermost layers of quartz grains in the 90-120 μm size range.

The removal of these outer layers by etching in HF will serve to further reduce the alpha dosage as illustrated in Figure 3.3. The alpha dose from the uranium series is reduced by half on removal of $6.5\mu\text{m}$ of the grain and the dose from the thorium series is halved on removal of $8.0\mu\text{m}$.

These figures are significantly different from the values of $4.2\mu\text{m}$ and $5.4\mu\text{m}$ quoted by Fleming (1970) and as illustrated in Figure 3.3. The reason for the difference is thought to be mainly because Fleming (1969) evaluated his dose reduction curves for calcium fluoride and then assumed that to a "first order approximation" the curves would be the same for quartz. As can be seen in Figure 3.3, the curves are of the same order of magnitude. However, in the work of Chapter VII when an accurate assessment of the residual alpha dose is called for, the more rigorous treatment presented here is the more appropriate one to use.

The aforementioned attenuation factors all add up to give a residual alpha dose which is very much less than the dose from beta and gamma radiation. The quantification of the exact dosage requires information concerning the etching process (Chapter VII), but for grains in the size range $90\text{--}120\mu\text{m}$, it is always likely to be less than 19% of the total dose.

We have of course neglected to include possible variations in the mass stopping power ratio, S_m , in the above calculations. A Fortran computer programme was written which compared the mass stopping power of quartz to that of most of the samples investigated in Part II. The ratio was less than 1% different from unity in all cases and hence has been neglected in the alpha dose attenuation calculations.

CHAPTER IV - BETA PARTICLE DOSIMETRY

4.1 Introduction

The energy dissipation of beta particles passing through matter is a more complex problem than it is for alpha particles. This is because in an encounter with an atomic electron, a beta particle (an electron itself) can lose as much as half of its kinetic energy (compared to a fraction $\sim m_e/M$ for heavy charged particles) which results in a large amount of energy straggling about the mean csda path-length, r_0 , defined by

$$r_0 = \int_{E_0}^0 (dE/dr)^{-1} dE \quad (4.1)$$

In order that geometrical, or influence, functions can be evaluated for different interfaces, the csda range r_0 must be related to the actual straight-line range R because of the "drunken man's path" of the electrons as they traverse an absorber (see Fig. 4.1).

In addition, the variation of LET with energy must be taken into account although, as for alphas, this can be on an empirical basis only. The attempts of various authors to solve these problems are outlined below.

4.2 Various Methods for Absorbed Dose Calculations

Probably the first to approach the problem of the energy dissipation of electrons in an absorber was Spiers (1949) who was particularly concerned with the effect of the energy absorbed by tissue lying near or within bone. He assumed that the straight-line range, R , was 0.7 times the csda range r_0 , an assumption based on the experimental data of

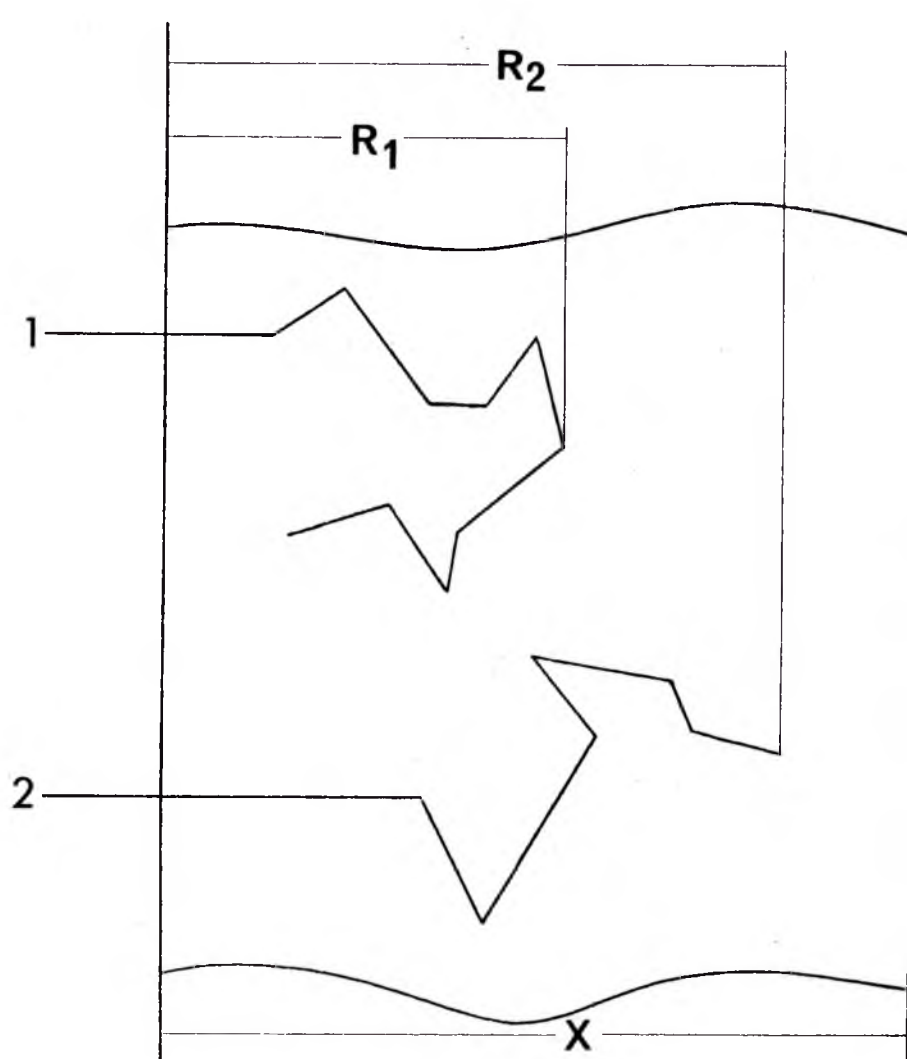


FIGURE 4.1: The "Drunken Man's Path" of an Electron in an Absorber of Thickness X . The two path-lengths are equal although the straight-line ranges, R_1 and R_2 , are not.

Williams (1930), and that the LET was independent of the electron energy.

Charlton and Cormack (1962a) modified Spiers' theory by taking account of the variation of LET with energy, i.e.

$$R = AE^m \quad (4.2)$$

{cf equation (3.5)}

but retained the assumption that $R = 0.7 r_0$. Howarth (1965a) developed this theory and produced tabulated results for $m = 1.75$.

Charlton and Cormack (1967) then varied the single-range assumption by incorporating a distribution of electron ranges from $R = 0.5 r_0$ to $R = 0.9 r_0$ but retaining $m = 1.75$. This and the other models mentioned so far are summarised in Table 4.1.

All of these models, however, take no account of the initial electron energy or of the medium in which the energy is being dissipated. Spencer (1959) calculated the average energy dissipated near point isotropic sources of monoenergetic electrons by a moments method of solution of the electron transport equation. He presented numerical values of a "de-dimensionalised energy dissipation distribution" $J(x)$ evaluated for electrons of various initial energies and travelling in various media (x is the distance from the source of electrons divided by r_0).

The results of Spencer are shown in Figure 4.2 for different media compared to the results of the previous models. It can be seen that the medium has an effect on the energy dissipation and that only the $M(1.75)$ model gives reasonable agreement, at least for carbon. Figure 4.3 illustrates the variation of energy dissipation with different initial electron energies and it is obvious that the dissipation is not very sensitive to changes in the initial energy.

Spencer's treatment has been extensively tested by Cross (1967, 1968) who has shown that over a wide range of spectral shapes there is excellent agreement between theory and experiment for distances from the source

TABLE 4.1

Various Models Used To Evaluate Influence Functions For Electrons

Author	Range	LET Value	Notation *
Spiers (1949)	$R = 0.7r_o$	$m = 1.00$	$R(1.00)$
Charlton and Cormack (1962a)/ Howarth (1965a)	$R = 0.7r_o$	$m = 1.75$	$R(1.75)$
Charlton and Cormack (1967)	$0.5r_o \leq R \leq 0.9r_o$	$m = 1.75$	$M(1.75)$

* The first letter refers to the choice of straight-line range.

i.e. R - straight range equal to $0.7r_o$; M - multiple ranges.

The number in brackets refers to the value of m.

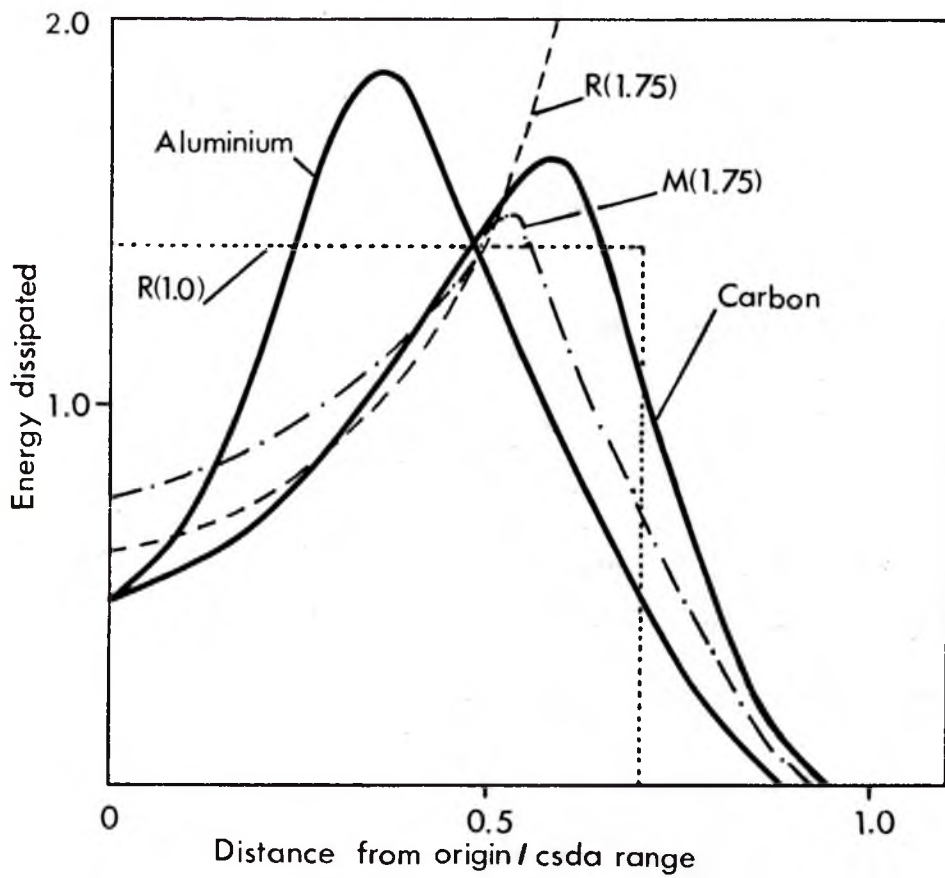


FIGURE 4.2: The Results of Spencer for the Energy Dissipation of Electrons in Aluminium and Carbon compared to the Predictions of the R(1.0), R(1.75) and M(1.75) Models.

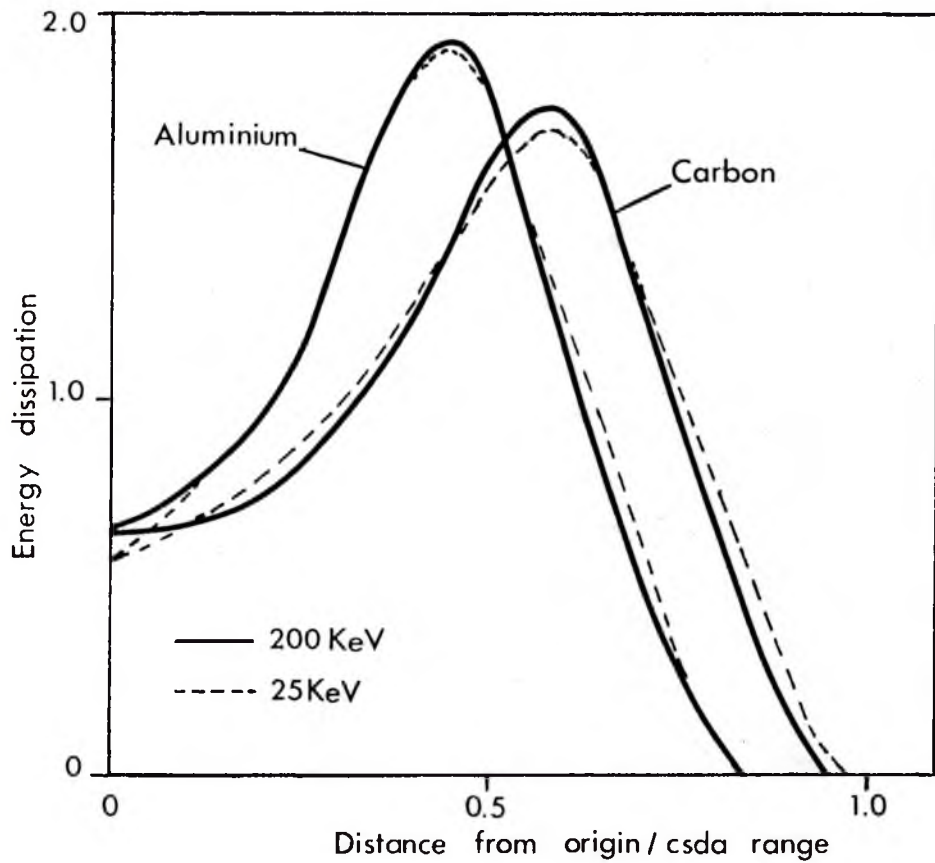


FIGURE 4.3: Spencer's Results for the Energy Dissipation of Electrons of Different Initial Energies in Carbon and Aluminium.

within which 95% of the energy is deposited.

Charlton (1970) has incorporated Spencer's theory into the convenient formalism introduced by Charlton and Cormack (1962a) in their treatment of the interface problem. His results for a spherical interface are presented in Section 4.3 and then extended to the case of quartz inclusions in Section 4.4 in order to evaluate the beta dose attenuation factors for the natural radioactive series.

4.3 The Attenuation of the Beta Dose in Spherical Geometry

Spencer's (1959) distribution function $J(x)$ is such that

$$J(x) \cdot (dE/dr)_{E_0} = I(r) \quad (4.3)$$

where $(dE/dr)_{E_0}$ is the stopping power of electrons of initial energy E_0 , and $I(r) \cdot dr$ is the average energy per electron dissipated in a spherical shell of radius r and thickness dr around the point source. Since $I(r)$ is normalised to one electron it can be used as an effective stopping power within the straight-path approximation i.e.

$$I(r) = (dE/dr)_r \quad (4.4)$$

The use of this analysis makes the variation of electron stopping power with energy over the entire track considerably more realistic in that it is dependent both on the initial energy and on the medium, factors which are not taken into account by the models described in Table 4.1.

Consider an infinite medium containing a uniform distribution of point sources of number density n_0 isotropically emitting electrons of energy E_0 . The energy dissipated per unit volume at some point P

in the medium is given by

$$D_o = \int_0^{2\pi} \int_0^{\pi} \int_0^{r_o} \frac{n_o r^2 \sin\theta}{4\pi r^2} \cdot (dE/dr)_p \cdot dr d\theta d\phi \quad (4.5)$$

From equation (4.4)

$$D_o = \frac{n_o}{2} \int_0^{\pi} \int_0^{r_o} \sin\theta \cdot I(r) \cdot dr d\theta \quad (4.6)$$

$$= \frac{n_o}{2} \int_0^{\pi} \int_0^{r_o} \sin\theta \cdot J(x) \cdot (dE/dr)_{E_o} \cdot dr d\theta \quad (4.7)$$

using equation (4.3) where $x = r/r_o$.

Hence

$$D_o = \frac{n_o E_o}{2} \cdot \int_0^{\pi} \sin\theta \int_0^1 J(x) \cdot (dE/dr)_{E_o} \cdot \frac{r_o}{E_o} \cdot dx d\theta \quad (4.8)$$

$$= n_o E_o \quad \text{since by definition,}$$

$$(dE/dr)_{E_o} \cdot \frac{r_o}{E_o} \cdot \int_0^1 J(x) dx = 1.0 \quad (4.9)$$

For a spherical interface between an active medium and a non-active sphere, the dose absorbed at a point P within the sphere, distance z from the interface is given by

$$D_{\beta}(z) = \frac{n_o E_o}{m} \cdot S_{\beta}(z/r_o, D/r_o) \quad (4.10)$$

where n_o is the number of electrons of initial energy E_o and range r_o

originating per unit mass of the active medium; S_m is the ratio of the mass stopping powers of the surrounding medium and the sphere; D is the diameter of the sphere and $S_\beta(z/r_o, D/r_o)$ is given by (Charlton, 1970),

$$S_\beta(z/r_o, D/r_o) = 1 - \frac{1}{2} \left(\frac{dE}{dr} \right)_{E_o} \cdot \frac{r_o}{E_o} \left[\int_0^{\theta_{\max}} \sin\theta \left\{ \int_0^1 J(x) dx \right\} d\theta + \int_{\theta_{\max}}^{\pi} \sin\theta \left\{ \int_0^{r_{\max}/r_o} J(x) dx \right\} d\theta \right] \quad (4.11)$$

where θ_{\max} and r_{\max} are defined in Figure 4.4.

Charlton has evaluated $S_\beta(z/r_o, D/r_o)$ numerically using the tables of Spencer for $J(x)$ and values of $(dE/dr)_{E_o}$ and r_o taken from Berger and Seltzer (1964), normalising $J(x)$ through equation (4.9) for any variations in the data used by Spencer. The results for various media are shown in Figure 4.5 for the centre of a sphere and are compared to the only other complete evaluation, that of Howarth (1965a). Howarth's $R(1.75)$ model assumes a straight-line range equal to $0.7r_o$ and hence the influence function drops to zero for $D/r_o = 1.4$.

The influence functions for a sphere are almost independent of the initial electron energy, varying by 5% at most over the energy range 0.025 to 1 MeV. Charlton (1970), therefore, gives tables of values of $S_\beta(z/r_o, D/r_o)$ for different media evaluated at 1 MeV. These can then be assumed independent of energy.

To evaluate $S_\beta(z/r_o, D/r_o)$ for quartz, interpolation between Charlton's values for carbon and aluminium has been carried out according to Spencer's (1959) recommendations i.e. interpolating the function

$$\{1/A \ln J(x) + x/(1 - x)\}$$

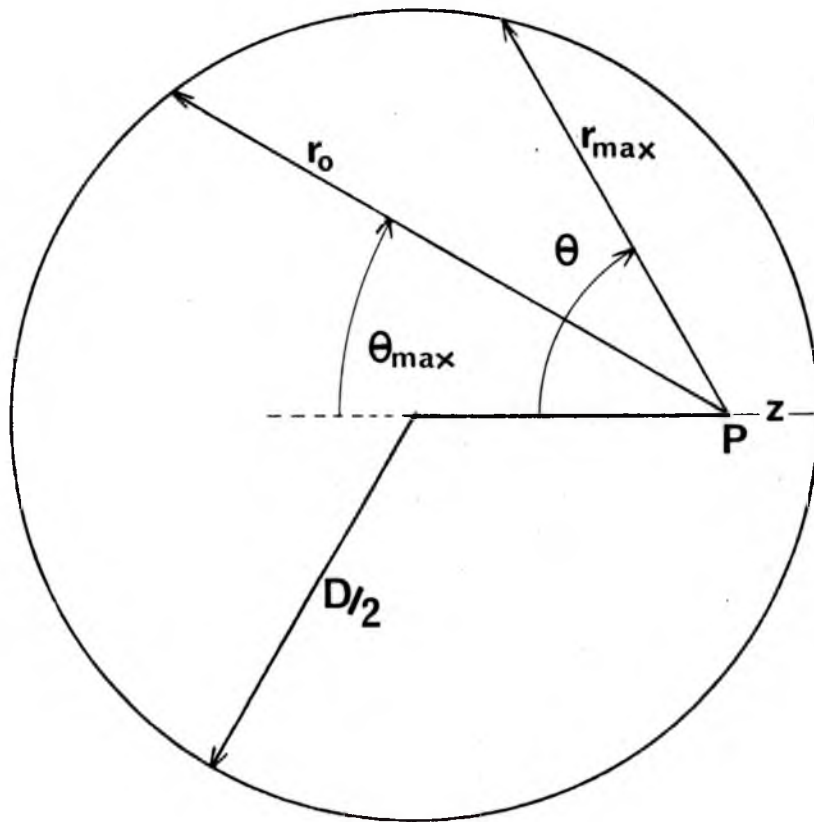


FIGURE 4.4: Geometry used in the Calculation of the Beta Dose Attenuation in Spherical Geometry.

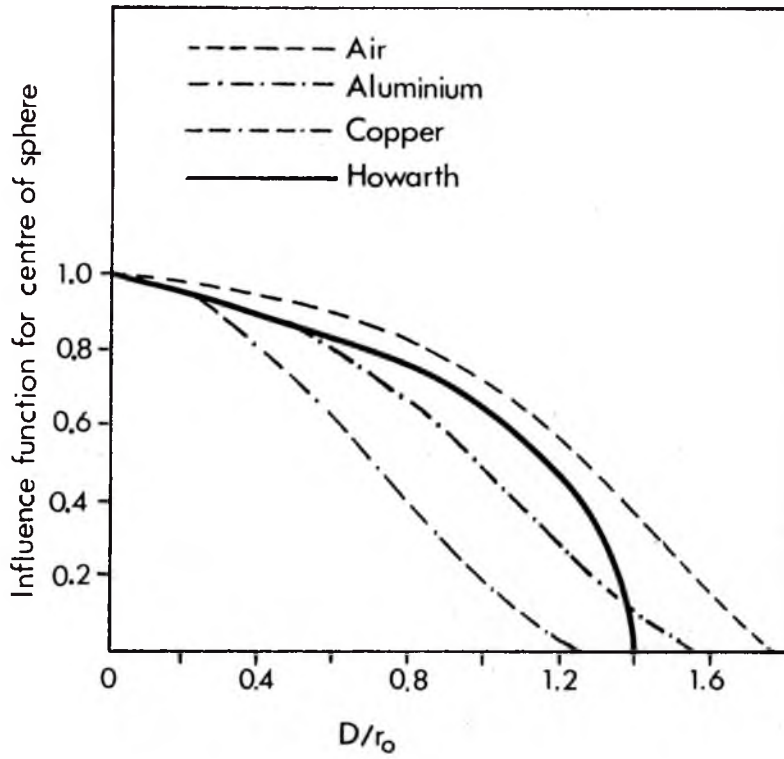


FIGURE 4.5: Beta Particle Influence Functions for the Centre of a Sphere for Different Media compared to the Results of Howarth.

rather than $J(x)$ itself, where A is a constant given by Spencer. The results are shown in Table 4.2.

4.4 The Attenuation of the Beta Dose in Quartz Inclusions for the Natural Radioactive Series

The added complication of the spectral distribution of energies for natural radioactive series makes the exact evaluation of beta dose attenuation an exceedingly complex problem. This is because when a nucleus decays through beta emission it also ejects a neutrino (a non-ionizing particle) with the transition energy being shared between the two. In a large number of transitions the energy released is divided up in a statistical manner such that both the beta particles and the neutrinos have energy distributions extending from zero to the maximum value. The maximum values and the average beta energies for each transition in each of the natural radioactive series are given in Chapter VI.

A complete evaluation of the beta attenuation should, therefore, include an integration over the whole energy spectrum for each transition of the series. Even if this were possible it would be an extremely lengthy procedure, but the lack of full information on the beta decay characterisation of many of the contributing radioisotopes makes this kind of analysis unfeasible.

It is fortunate, then, that the influence functions are not very sensitive to changes in the initial electron energy, and as a result, the average beta energy in each transition is used to calculate these functions in order to evaluate the beta attenuation in quartz inclusions. To confirm the validity of this approach, however, integrations over the complete energy spectra of a high energy (1.0 MeV) and a low energy (0.1 MeV) transition have been carried out in Appendix D. The influence functions

TABLE 4.2

Influence Functions for a Spherical Interface

QUARTZ

D/r_o	$\frac{z}{(D/2)}$										
	0.0	0.1	0.2	0.3	0.4	0.5	0.6	0.7	0.8	0.9	1.0
0.0	1.000	1.000	1.000	1.000	1.000	1.000	1.000	1.000	1.000	1.000	1.000
0.2	0.957	0.944	0.937	0.931	0.927	0.923	0.921	0.919	0.917	0.916	0.916
0.4	0.903	0.878	0.862	0.847	0.839	0.832	0.829	0.825	0.822	0.820	0.820
0.6	0.834	0.794	0.770	0.752	0.738	0.726	0.717	0.710	0.706	0.703	0.702
0.8	0.762	0.703	0.666	0.639	0.615	0.596	0.582	0.572	0.564	0.559	0.558
1.0	0.710	0.629	0.574	0.529	0.491	0.459	0.433	0.413	0.399	0.390	0.388
1.2	0.675	0.574	0.503	0.442	0.385	0.340	0.298	0.262	0.234	0.217	0.212
1.4	0.650	0.531	0.446	0.373	0.307	0.247	0.193	0.147	0.108	0.082	0.073
1.6	0.631	0.496	0.399	0.316	0.241	0.195	0.118	0.071	0.037	0.016	0.008
1.8	0.617	0.466	0.358	0.267	0.187	0.120	0.066	0.028	0.007	0.001	-
2.0	0.605	0.439	0.322	0.224	0.142	0.078	0.032	0.008	0.002	-	-

thus obtained are compared to those for the average beta energies of the transitions and the agreement is found to be excellent.

For each transition an average csda range, r_o , is calculated according to equation (4.1) with E_o taken as the average beta energy. A Fortran computer programme has been written which calculates the stopping powers of quartz and then integrates from E_o to 0 to evaluate r_o . The programme is based on the equations given by Berger and Seltzer (1964). The results for each radioactive beta emitting element in each series are shown in Table 4.3.

Knowing r_o and hence D/r_o , since $D = 105\mu\text{m}$, the values of the influence function can be evaluated for different values of z/r_o and then integrated over the volume of interest, i.e. the spherical quartz inclusion. The mean absorbed dose, $\overline{D}_\beta(\text{Abs})$, is given for each beta emitter by,

$$\overline{D}_\beta(\text{Abs}) = \frac{n_o E_o}{m S} \cdot \frac{\int_0^{D/2} S_\beta(z/r_o, D/R_o) \cdot r^2 dr}{\int_0^{D/2} r^2 dr} \quad (4.12)$$

$$= \frac{n_o E_o}{m S} \cdot \overline{S}_\beta(\text{Abs}) \quad (4.13)$$

By suitable substitution of variables equation (4.12) may be evaluated for each beta emitter with the following results for $\overline{S}_\beta(\text{Abs})$;

Uranium Series:

Th-234	$\overline{S}_\beta(\text{Abs})$	=	0.1946
Pa-234(0.13%)		=	0.8437
Pa-234m		=	0.9789
Pb-214		=	0.8590
Bi-214		=	0.9704
Pb-210		=	0.1549
Bi-210		=	0.9423

TABLE 4.3

Average Range of Beta Particles in Quartz

Element	E_0 (MeV)	r_0 (μm)
<u>Uranium Series:</u>		
Th-234	0.0456	17.3
Pa-234 (0.13%)	0.2308	2.60×10^2
Pa-234m	0.8372	1.56×10^3
Pb-214	0.2195	2.41×10^2
Bi-214	0.6413	1.12×10^3
Pb-210	0.0062	0.763
Bi-210	0.3945	5.76×10^2
<u>Thorium Series:</u>		
Ra-228	0.0141	2.26
Ac-228	0.3929	5.73×10^2
Pb-212	0.1067	75.1
Bi-212 (64.07%)	0.7649	1.40×10^3
Tl-208 (35.93%)	0.5719	9.62×10^2
<u>Potassium - 40:</u>		
K-40	0.583	9.85×10^2

Thorium Series:

Ra-228	$\overline{S}_{\beta}(\text{Abs})$	=	0.1567
Ac-228		=	0.9579
Pb-212		=	0.4267
Bi-212(64.07%)		=	0.9762
Tl-208(35.93%)		=	0.9654
Potassium-40	$\overline{S}_{\beta}(\text{Abs})$	=	0.9661

The mean dose attenuation factors for the whole of each series, $\overline{S}_{\beta}(\text{Abs})_{\text{U,Th}}$, can then be evaluated according to

$$\overline{S}_{\beta}(\text{Abs})_{\text{U,Th}} = \frac{\sum_i E_o^{(i)} \cdot \overline{S}_{\beta}(\text{Abs})_{\text{U,Th}}^{(i)}}{\sum_i E_o^{(i)}} \quad (4.14)$$

where the summation over i refers to each beta emitter in the series.

The mean absorbed doses for each series, $\overline{D}_{\beta}(\text{Abs})_{\text{U,Th}}$, are calculated to be for uranium,

$$\overline{D}_{\beta}(\text{Abs})_{\text{U}} = 0.938 \times \frac{n_o E_o}{S_m} \quad (4.15)$$

and for thorium,

$$\overline{D}_{\beta}(\text{Abs})_{\text{Th}} = 0.910 \times \frac{n_o E_o}{S_m} \quad (4.16)$$

Also for potassium,

$$\overline{D}_{\beta}(\text{Abs})_{\text{K}} = 0.966 \times \frac{n_o E_o}{S_m} \quad (4.17)$$

Internal conversion (IC) electrons are also emitted during radioactive decay as an alternative to gamma ray emission as discussed in Chapter VI. Once ejected from the parent atom, these IC electrons are in every way identical to beta particles. It is appropriate, therefore, to investigate here the attenuation of these electrons in passing through 105 μm diameter quartz grains.

The calculation is exactly the same as that worked through for the beta particles. Using equation (4.12) and the IC electron energies from Chapter VI, the mean dose, $\overline{D}_{\beta}(\text{Abs})_{\text{IC}}$, can be evaluated for each of the two

series, i.e.

$$\overline{D_{\beta}(\text{Abs})}_{U,IC} = 0.350 \times \frac{n_o E_o}{S_m} \quad (4.18)$$

and

$$\overline{D_{\beta}(\text{Abs})}_{Th,IC} = 0.400 \times \frac{n_o E_o}{S_m} \quad (4.19)$$

These values can now be included in equation (4.14) together with the values for the beta particles alone which were presented earlier in this Section. The total mean absorbed doses from each of the two series for the betas and IC electrons together, $\overline{D_{\beta}(\text{Abs})}_{U,Th}$, are thus found to be,

$$\overline{D_{\beta}(\text{Abs})}_U = 0.899 \times \frac{n_o E_o}{S_m} \quad (4.20)$$

and

$$\overline{D_{\beta}(\text{Abs})}_{Th} = 0.845 \times \frac{n_o E_o}{S_m} \quad (4.21)$$

4.5 The Effect of Hydrofluoric Acid Etching on the Beta Dose

Attenuation

The removal of the outer grain boundaries by etching in hydrofluoric acid (HF) has already been shown to drastically reduce the alpha dosage to quartz inclusions in the size range 90 to 120 μm (Section 3.6, Chapter III). We shall now consider the effects of this etching on the beta dose.

The geometry is the same as that depicted in Figure 3.2 and the mean influence function for the remainder of a grain after the outer thickness d has been removed is

$$\overline{S_{\beta}(\text{Abs})}^* = \frac{\int_0^{D/2-d} S_{\beta}(z/r_o, D/r_o) \cdot r^2 \cdot dr}{\int_0^{D/2-d} r^2 \cdot dr} \quad (4.22)$$

The mean absorbed dose in the quartz grains after etching is then

$$\overline{D_{\beta}(\text{Abs})}^* = \frac{n_o E_o}{S_m} \times \overline{S_{\beta}(\text{Abs})}^* \quad (4.23)$$

Equation (4.22) has been evaluated as before and the results are shown in Figures 4.6a,b and c for each beta emitter in the three series and for the IC electron component of the uranium and thorium series. The absorbed dose after etching is normalised to the value before etching in each of these Figures.

4.6 Summary and Discussion of Results

In this Chapter the attempts of various authors to solve the problem of the energy dissipation of beta particles passing through matter have been outlined. The more realistic approach of Charlton (1970) based on the work of Spencer (1959) has been described more fully and then applied to the case of a spherical quartz inclusion embedded in a radioactive matrix.

This treatment results in influence functions which predict that the beta dose to quartz grains of average diameter 105 μm is 93.8% of the zero grain size dose, D_0 , for the uranium series, 91.0% for the thorium series and 96.6% for potassium-40. When the attenuation of the IC electron component is included in the beta dose, it is reduced to 89.9% of D_0 for the uranium series and 84.5% for the thorium series.

For the typical clay sample considered in the last Chapter (Section 3.7) with 12ppm thorium and 3ppm uranium and in addition 1% K_2O , the zero grain size dose $D_0 = 146.4 \text{ mrad/yr}$. Accounting for the dose dilution predicted by the influence functions, as described by equations (4.17), (4.20) and (4.21), the beta dose which can effectively give rise to thermoluminescence is reduced to 134.2 mrad/yr or 91.7% of D_0 . This may be compared to the figure of 94% quoted by Aitken and Fleming (1972) which was based, however, on the R(1.75) model of Howarth (1965a) and which also did not take account of the IC electron component.

The results of etching the quartz grains in HF have been investigated and it was shown that only relatively minor dose dilution results from this treatment, compared to the more drastic effects on the alpha dose as

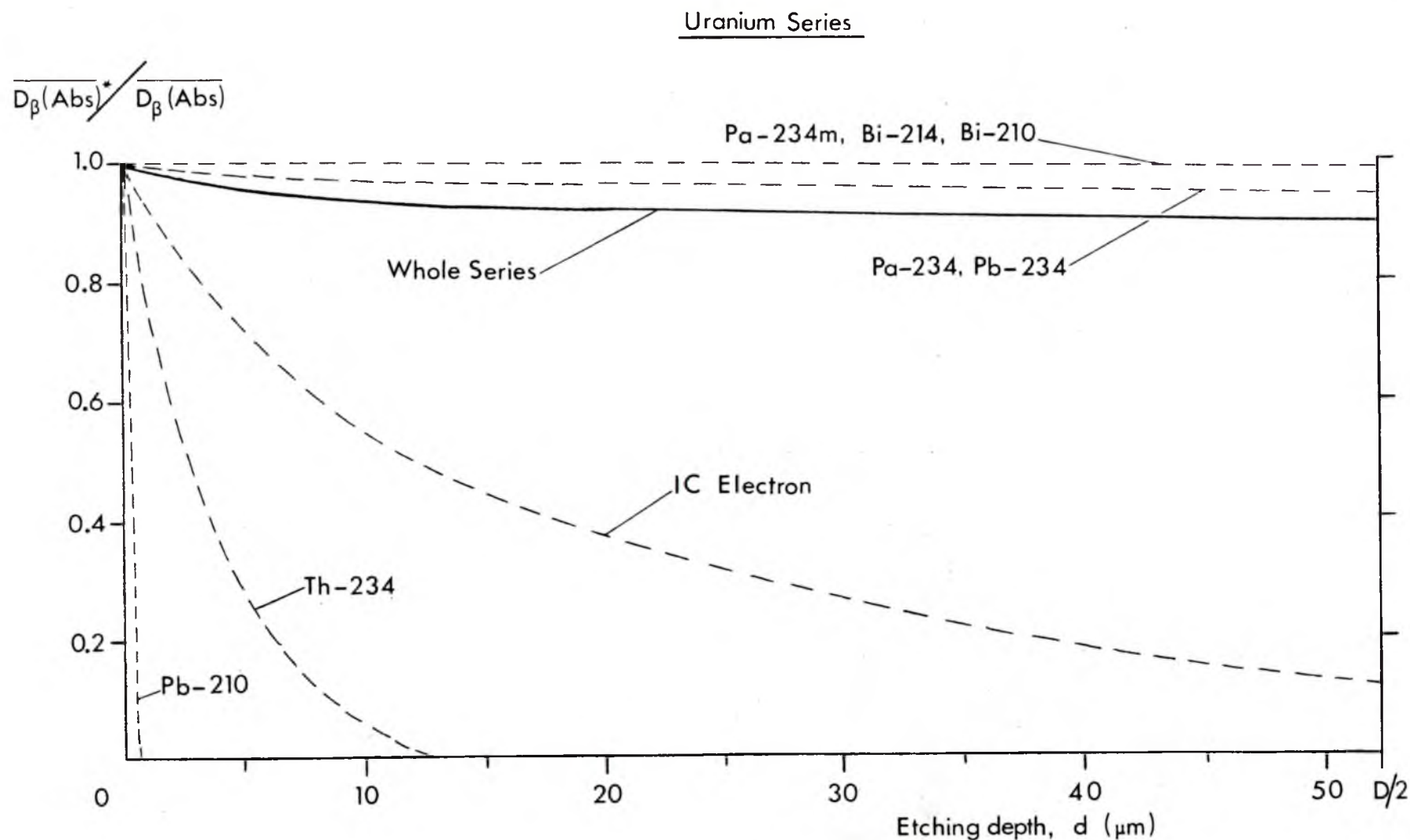


FIGURE 4.6a: Mean Absorbed Beta Dose in a Quartz Grain with a Layer d removed by Etching as a Fraction of the Dose before Etching for the Uranium Series.

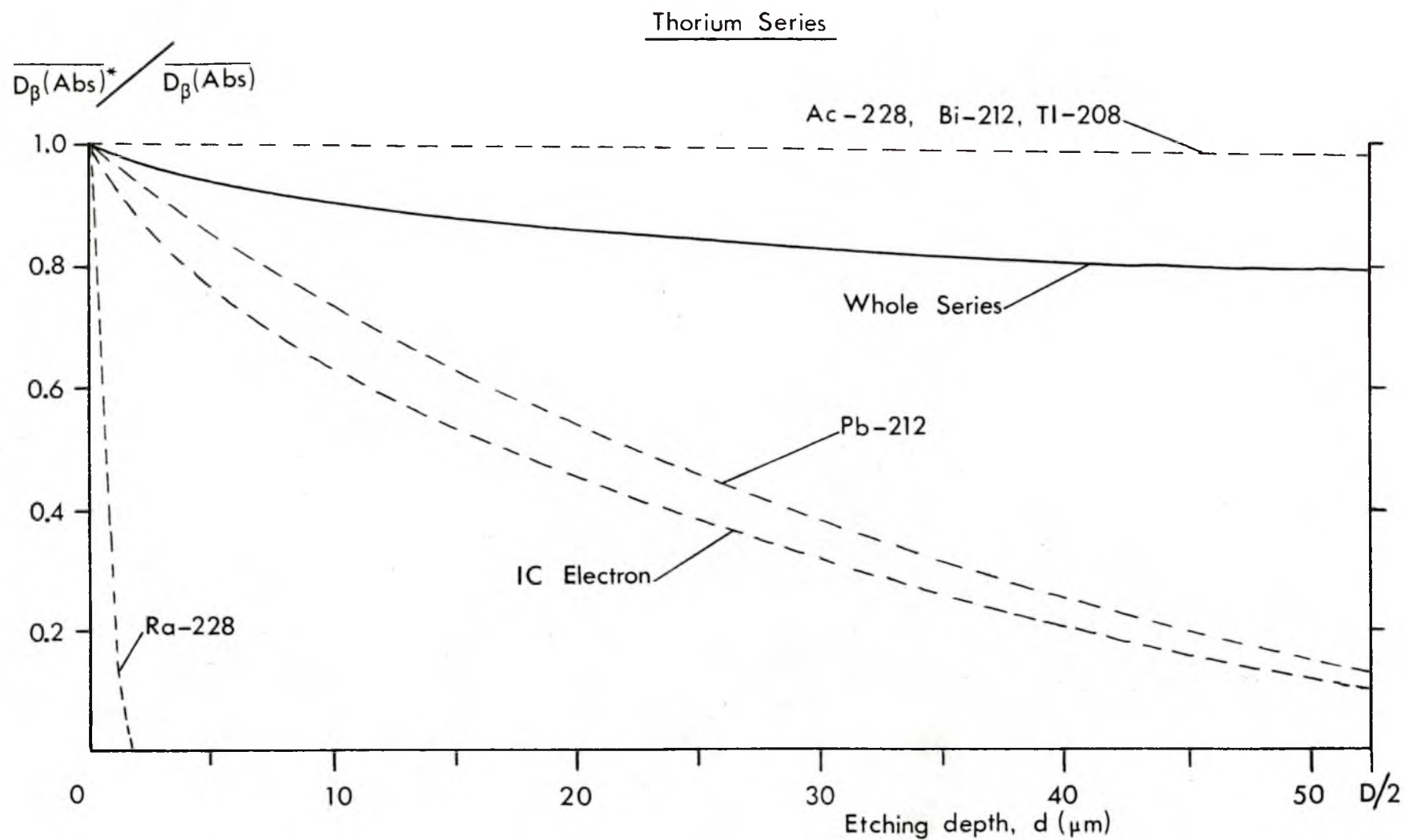


FIGURE 4.6b: Mean Absorbed Beta Dose in a Quartz Grain with a Layer d removed by Etching as a Fraction of the Dose before Etching for the Thorium Series.

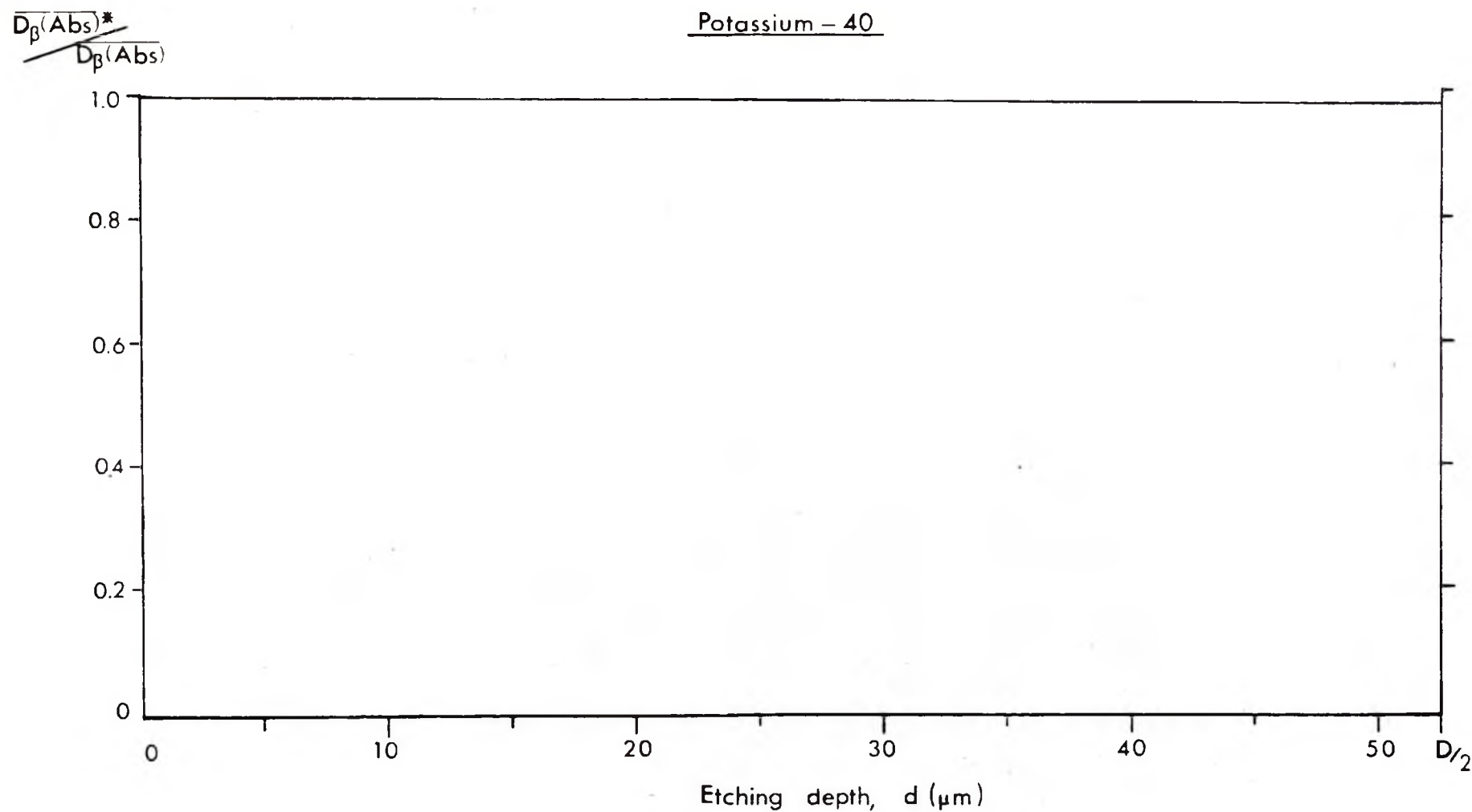


FIGURE 4.6c: Mean Absorbed Beta Dose in a Quartz Grain with a Layer d removed by Etching as a Fraction of the Dose before Etching for Potassium-40.

described in the last Chapter. A quartz grain which has had the outer 8 μm removed would have the total beta dose from the thorium series reduced by a factor of 0.93 and from the uranium series by a factor of 0.95. Since the potassium-40 beta dose suffers negligible attenuation at this etching depth, the overall dose from the typical clay sample described above is reduced by a factor of 0.97. The figure quoted by Aitken and Fleming (1972) for an etching depth of 8 μm is 0.95. The difference may be accounted for in the lack of the R(1.75) model to take account of the medium and the initial electron energy and also because these authors did not include the IC electron contribution in the beta dose.

As in the last Chapter the variations of S_m have been neglected. The computer programme used in Section 3.7 was modified to calculate the stopping power ratio of beta particles in the samples of interest here. As before the ratio was less than 1% different from unity and can thus be neglected.

CHAPTER V

GAMMA RAY DOSIMETRY

5.1 The Passage of Ionizing Radiation Through Matter

A qualitative difference exists between the passage of charged particles through matter and that of electromagnetic radiation such as gamma rays and X-rays. The difference is that the attenuation of gamma radiation as it passes through an absorber is evinced by an intensity diminution and not as an energy change as the particles slow down. Photons, the particles of which gamma radiation consists, have zero rest mass and they all travel at the velocity of light in the medium of interest.

As a beam of photons passes through matter, the interaction is characterised by the fact that each photon must be removed from the beam individually in a single event. If the intensity, or number of photons per cm^2 per sec., of the incident beam is I then the number removed per cm^2 per sec., ΔI , is proportional to I and to the distance traversed, Δx i.e.

$$\Delta I = -\mu I \Delta x \quad (5.1)$$

where μ is the constant of proportionality called the linear attenuation coefficient.

Integrating equation (5.1) gives

$$I = I_0 \exp(-\mu x) \quad (5.2)$$

where I_0 is the intensity of $x = 0$.

This exponential intensity diminution is brought about by the primary interactions of the gamma rays with matter which usually involve the production of energetic secondary electrons. It is the interactions of these secondary electrons which account predominantly for the ionization of the absorber atoms.

For example, a 1 MeV gamma ray travelling in quartz will produce, on average, a secondary electron of energy 440 KeV. This electron can then go on to ionize over 10,000 atoms before being brought to rest. The single primary ionizing event is therefore, negligible when compared to this large number of secondary ionizations.

In the energy range and for the materials of interest to be considered here, the primary interaction of the photons with absorber atoms is via three quite separate and distinctive processes.

(a) The Photoelectric Effect.

A photon gives up all of its energy to a bound electron (usually from the K or L shell) which is then ejected from the atom with a kinetic energy equal to the incident photon energy minus the binding energy of the electron in the atom. This effect is particularly important at low photon energies, i.e. less than 100 KeV, and for high Z absorbers. That part of the linear attenuation coefficient, μ , which is due to photoelectric interactions is characterised by the photoelectric absorption coefficient τ .

(b) The Compton Effect.

A photon is scattered, or deflected, from its original

direction by a collision with an atomic electron which results in a Compton scattered photon and a Compton recoil electron. If the energy of the incident photon is $h\nu_0$ and of the scattered photon $h\nu'$ then the recoil electron energy, T , is given by,

$$T = h\nu_0 - h\nu' \quad (5.3)$$

Compton scattering is important for photon energies around 1 MeV and for low and medium Z absorbers. The Compton contribution to the linear attenuation coefficient is characterised by the Compton collision coefficient, σ .

(c) Pair Production.

A photon travelling in the field of a nucleus, and to some degree the field of an electron, can be completely annihilated giving rise to an electron-positron pair i.e. $\gamma \rightarrow e^- + e^+$. A minimum incident photon energy of 1.02 MeV is required for pair production in the field of a nucleus, and a minimum of 2.04 MeV in the field of an atomic electron.

Pair production predominates at high energies and for large Z absorbers. The contribution to the linear attenuation coefficient is characterised by the pair production coefficient, κ .

The effects outlined above are described in much greater detail by Evans (1958, 1968) and Davisson (1968) as well as several other authors, and this present work can only hope to supplement this knowledge. The relative importance of the three types of interaction is shown in Figure 5.1 which is taken from Evans (1968).

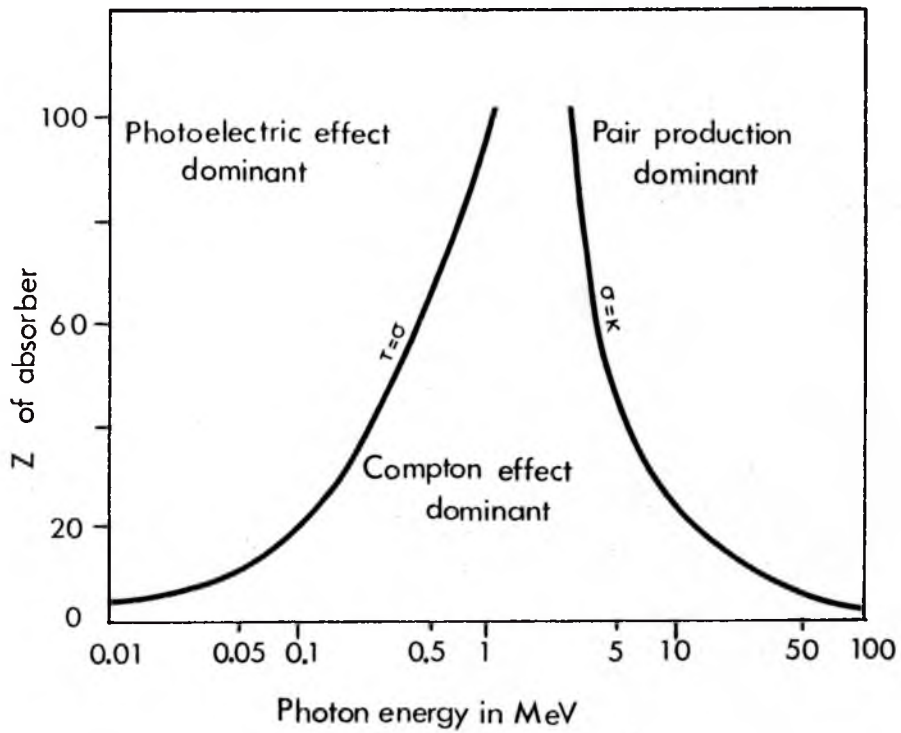


FIGURE 5.1: Relative Importance of the Three Types of Gamma-Ray Interactions.

5.2 Attenuation, Scattering and Absorption of Gamma Radiation

The attenuation of a beam of photons as described by equation (5.2) involves the deflection of photons from the beam with the imparting of energy to secondary electrons. In photoelectric and pair production events all of the photon energy is absorbed whereas in Compton collision events only part of the incident photon energy is imparted to a recoil electron with the balance merely being deflected and remaining with the scattered photon.

The linear attenuation coefficient can then be formed from a superposition of the three main effects (a), (b) and (c) i.e.

$$\mu = \tau + \sigma + \kappa \quad (5.4)$$

which can also be regarded as a superposition of energy absorption and energy scattering i.e.

$$\mu = \mu_s + \mu_a \quad (5.5)$$

where μ_s is the linear scattering coefficient and μ_a the linear absorption coefficient.

Since only the Compton process involves scattering, it is useful to divide σ into a scattering component, σ_s , and an absorption component, σ_a , and hence

$$\mu_s = \sigma_s \quad (5.6)$$

$$\text{and } \mu_a = \tau + \sigma_a + \kappa \quad (5.7)$$

It is convenient to introduce here the concept of a mass attenuation coefficient, μ/ρ , which is the linear coefficient divided by the density, ρ , of the absorber. In a similar fashion each of the other coefficients may be expressed as a mass-energy coefficient, hence

$$\frac{\mu}{\rho} = \frac{\mu_s}{\rho} + \frac{\mu_a}{\rho} = \frac{\tau}{\rho} + \frac{\sigma_a}{\rho} + \frac{\sigma_s}{\rho} + \frac{\kappa}{\rho} \quad (5.8)$$

When the problem of energy absorption is being considered, it is usually necessary to evaluate the absorption within a volume of interest. Energy can escape from this volume by means of scattered photons, annihilation radiation, bremsstrahlung and fluorescence radiation (see Evans, 1968, or Davisson, 1968, for full details of these phenomena). To allow for this escape of energy different mass-energy absorption coefficients have been defined, i.e.

$$\frac{\mu_a}{\rho} \quad - \quad \text{allows escape of Compton scattered photons only.}$$

$$\frac{\mu_{en}}{\rho} \quad - \quad \text{allows escape of Compton scattered, fluorescence, annihilation and bremsstrahlung photons.}$$

$$\frac{\mu_K}{\rho} \quad - \quad \text{allows escape of all of the above except bremsstrahlung photons.}$$

In general, the mass-energy absorption coefficient μ_a/ρ will be used in this thesis except where otherwise stated.

As a reference source for the work of later sections, the variation of certain of the mass-energy coefficients of quartz with energy have been calculated from the data of Hubbell (1969) and are presented in

graphic form in Figure 5.2.

5.3 Gamma-Ray Buildup Factors

In a volume distribution of γ -ray emitters not only the primary beam of photons gives rise to secondary electrons but the scattered photons will also go on to give rise to the ionization of atomic electrons until they either escape from the volume of interest or are completely absorbed as in a photoelectric event.

The primary photon absorption is easily calculable from the exponential attenuation, but the contribution from the scattered photons is a far more difficult problem. The energy buildup due to the scattered radiation is described by a so-called energy-absorption buildup factor, B_{en} , defined by,

$$B_{en} = \frac{\text{total absorbed dose-rate}}{\text{absorbed dose-rate due to primary photons}} \quad (5.9)$$

Evans (1968) has put forward an expression for B_{en} as,

$$B_{en}(\mu r) = 1 + a(\mu r)^k \quad (5.10)$$

where μr is the distance, r , from the source measured in mean free paths (the mean free path is equal to $1/\mu$ and is the average distance travelled by a photon before an interaction occurs) and k is a constant which depends on the photon energy and Z of the absorber. Also a is given by

$$a = \frac{1}{\Gamma(k+1)} \cdot \frac{\sigma_s}{\mu a} \quad (5.11)$$

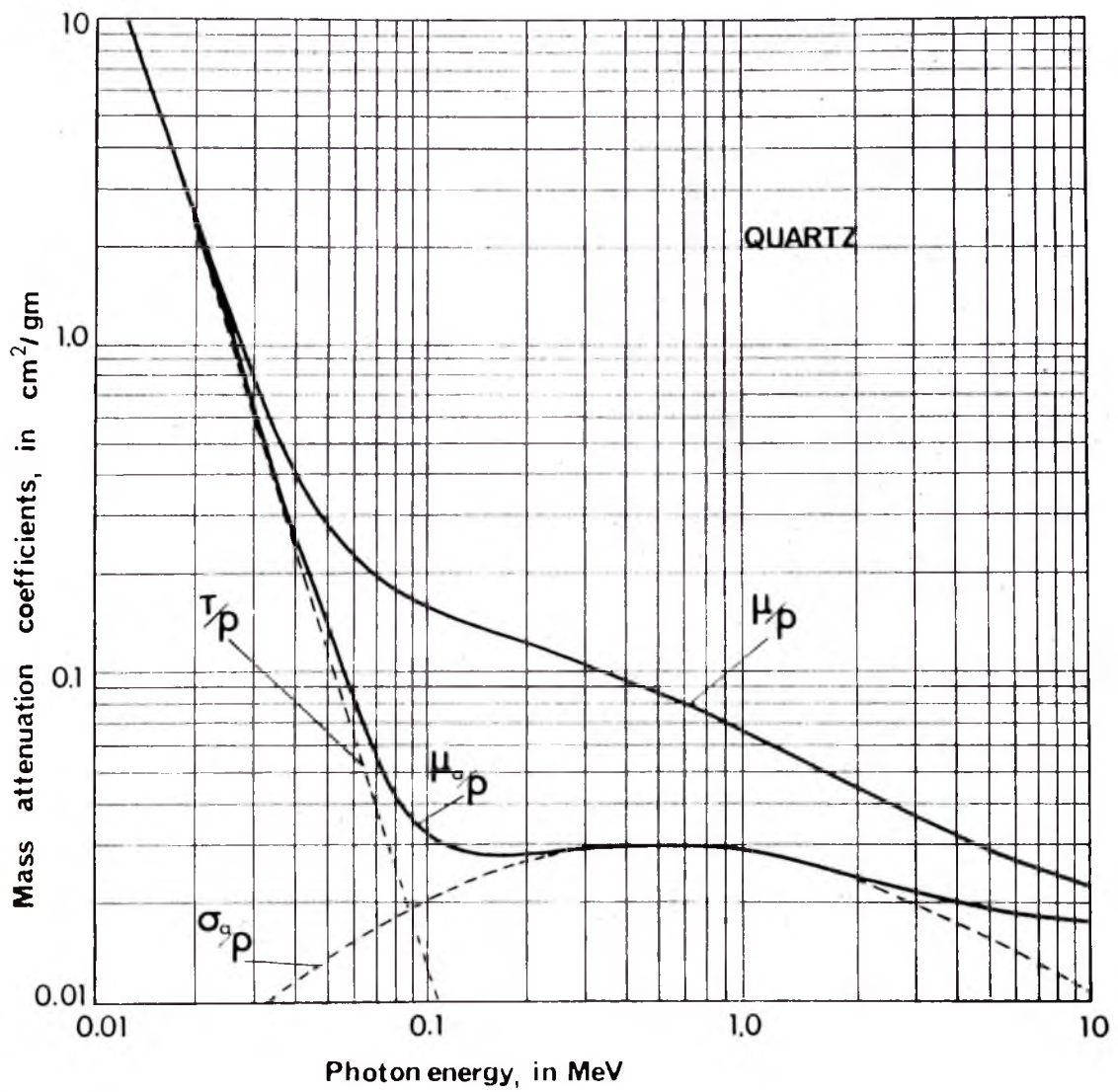


FIGURE 5.2: Mass Attenuation Coefficients of Quartz.

where $\Gamma(k + 1)$ is the gamma function of $k + 1$ and σ_s and μ_a are each evaluated for the primary photon radiation.

An oversimplified but useful approximation in the region of 1 MeV photons and for low Z absorbers is to take k as unity (Evans, 1955) i.e.

$$B_{en}(\mu r) \approx 1 + \frac{\sigma_s}{\mu_a} \cdot (\mu r) \quad (5.12)$$

Fleming (1969) used this to show that over 90% of the γ dose to a small volume in the centre of a radioactive clay medium derives from a sphere surrounding the volume with a radius of approximately 30 cm.

A more exact solution has been obtained by Berger (1968) who applied the moments method of Fano et al. (1959) to obtain values for the buildup factors for water. These results are expressed as a function of the mean free path (μr) and hence can be evaluated as a distance in materials of not-too-different atomic composition.

The absorbed dose at a point, P, distance r from the origin due to primary radiation alone is given by

$$D_{prim}(r) = n_o E_o \mu_a \exp(-\mu r) \quad (5.13)$$

where n_o is the number of gamma rays of energy E_o emitted per unit volume of the medium and μ_a and μ are the linear absorption and attenuation coefficients respectively.

The total absorbed dose due to primary and secondary radiation is, therefore, given by

$$D_{tot}(r) = n_o E_o \mu_a \cdot \exp(-\mu r) \cdot B_{en}(\mu r) \quad (5.14)$$

If we consider P now to be at the centre of a sphere of radius, R, then the absorbed dose at P due to the surrounding medium is given by

$$\begin{aligned}
 D_{\text{tot}}(P) &= n_o E_o \mu_a \cdot \int_0^{2\pi} \int_0^{\pi} \sin\theta d\theta \int_0^R \frac{\exp(-\mu r) \cdot B_{\text{en}}(\mu r) \cdot r^2 dr}{4\pi r^2} \\
 &= n_o E_o \cdot \frac{\mu_a}{\mu} \int_0^R \exp(-\mu r) \cdot B_{\text{en}}(\mu r) \cdot d(\mu r) \quad (5.15)
 \end{aligned}$$

Equation (5.15) can be integrated numerically as before for different values of R. This has been done for the thorium and uranium series and potassium-40 using Berger's values for $B_{\text{en}}(\mu r)$ and the value of R_{90} , the radius of a sphere the centre of which receives 90% of the dose to an infinite medium, has been calculated for a clay medium having a similar composition to quartz and a density of $\rho = 2.3\text{g/cm}^3$. The results are,

Thorium series,	$R_{90} = 30 \text{ cm}$
Uranium series,	$R_{90} = 29 \text{ cm}$
Potassium-40,	$R_{90} = 29 \text{ cm}$

These results are in good agreement with those of Fleming (1969) mentioned earlier in this Section.

5.4 Buildup Factors for an Overlying Layer

In anticipation of the practical work to be described in Chapter VII, the case of the energy absorbed from gamma-rays emitted in an overlying layer will be considered here. In Chapter VII this will be applied to the practical situation of a fireplace which has been covered by a

sedimentary layer of the same radioactivity to a height X cm, but above this is an overlying layer which has a 50% greater radioactivity content. It is necessary, therefore, to evaluate the absorbed dose at a distance X cm below an infinite plane interface.

The dose at a point P, distance X cm below the overlying layer, due to primary radiation only is

$$D_{\text{prim}}(P) = n_o E_o \mu_a \int_0^{2\pi} d\phi \int_0^{\pi/2} \sin\theta d\theta \int_X^{\infty} \frac{\exp(-\mu r) r^2 dr}{4\pi r^2} \quad (5.16)$$

$$= \frac{n_o E_o}{2} \cdot \frac{\mu_a}{\mu} \cdot \exp(-\mu X) \quad (5.17)$$

Hence the total dose due to primary plus secondary gamma-rays is

$$D_{\text{tot}}(P) = \frac{n_o E_o}{2} \cdot \frac{\mu_a}{\mu} \cdot \exp(-\mu X) \cdot B_{\text{en}}(\mu X) \quad (5.18)$$

The values of $B_{\text{en}}(\mu X)$ have been calculated from the data of Berger (1968) for different values of X and different photon energies assuming the density of the clay to be 2.28 gm/cm^3 (the average value as measured for the samples investigated in Chapter VII) and a similar atomic composition to quartz. The variation of $B_{\text{en}}(\mu X)$ with X for different energies is shown in Figure 5.3. In the range of $B_{\text{en}}(\mu X)$ used here, Berger (1968) estimates the accuracy to be between 2 and 3%.

Hence the dose for each energy shown in Figure 5.3 may be evaluated from equation (5.18). To find the dose for each of the natural series it would be necessary to average over each gamma energy in each series, but as there are several hundred such gamma-rays, the following procedure was adopted. A certain number of gamma-ray energy ranges were chosen and the contribution from gamma-rays falling within each range was

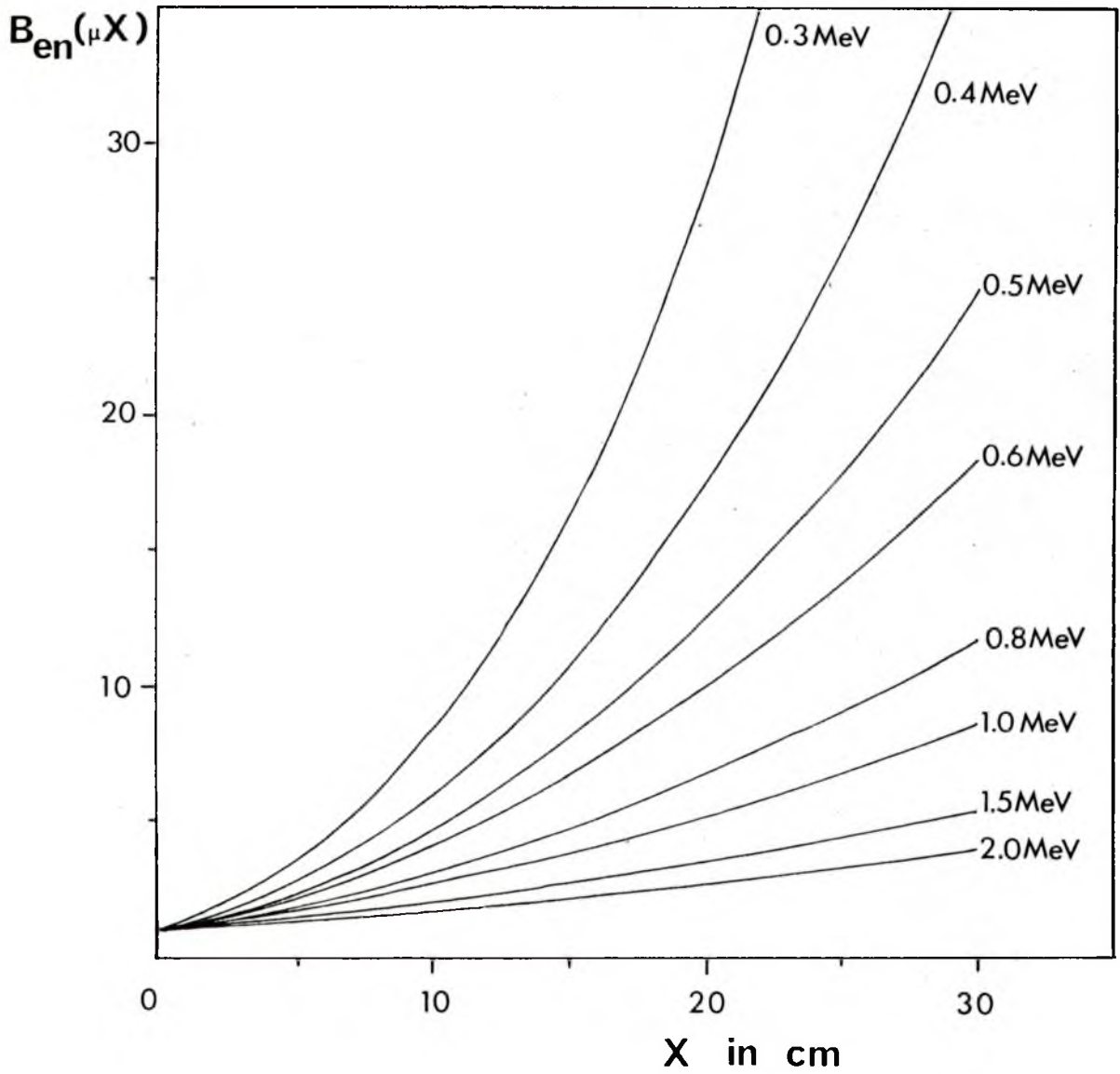


FIGURE 5.3: The Variation of $B_{en}(\mu X)$ with X for Different Photon Energies.

calculated as a percentage of the total contribution. The data on the gamma energies was taken from Chapter VI and the results are shown in Table 5.1.

The dose at a distance X cm below the overlying layer can then be evaluated by averaging over each energy range accounting for the percentage contribution of that range to the total dose. The results of this procedure are shown in Figure 5.4.

5.6 The Energy-Size Dependence of the TL Response

It has been shown in this Chapter that the principle mode of ionization, and hence the production of TL, is via the secondary electrons created by the initial photon collisions. When considering the problem of quartz inclusions embedded in a radioactive clay matrix it is useful to investigate the dependence of the TL response on photon energy and on particle size.

That the TL response should be dependent on photon energy can best be understood in terms of the photoelectric effect. At photon energies above 0.6 MeV, the Compton effect predominates and this effect is almost independent of the medium. Below 0.6 MeV, however, the photoelectric effect starts to become important. This effect is very dependent on the atomic number of the medium (approximately, τ is proportional to Z^4) so that the higher the Z value of the medium, the greater is the absorbed dose from a beam of photons at these low energies.

The particle size dependence follows directly from this if we consider a very small particle ($\sim 1 \mu\text{m}$) at very low energies ($\sim 10 \text{ KeV}$). The photoelectrons produced have very short ranges so that they can not escape from the grain nor can photoelectrons produced in the surrounding medium penetrate very far into it. As the photon energy increases, the energy of the photoelectrons and their range increases. In consequence

TABLE 5.1

Contribution to Total Dose from Gamma-rays
Within Certain Energy Ranges

<u>Energy Range (MeV)</u>		<u>Contribution to Total Dose (°/o)</u>
Thorium:		
\leq	0.3	5.695
	0.4	2.289
	0.5	0.907
	0.6	9.368
	0.8	4.408
	1.0	26.304
	1.5	2.524
	2.0	7.583
=	2.6147	40.754
Uranium:		
\leq	0.1	1.491
	0.15	0.035
	0.2	0.327
	0.3	4.599
	0.4	6.658
	0.5	0.610
	0.8	18.279
	1.0	3.242
	1.5	23.271
	2.0	27.464
	3.0	13.684
Potassium-40:		
=	1.4608	100.0

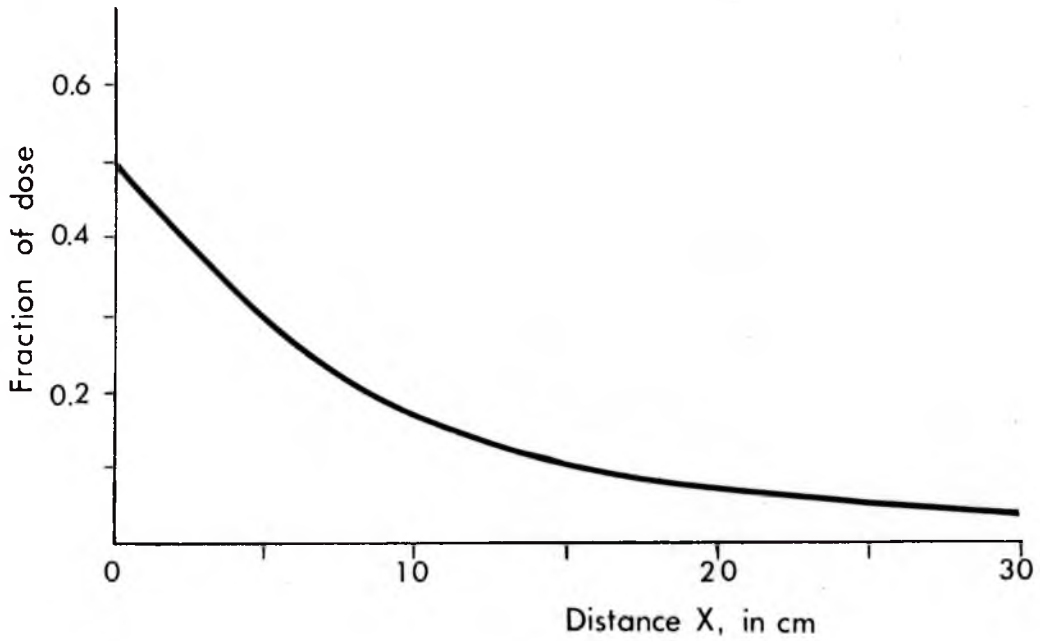


FIGURE 5.4: Fraction of the Gamma Dose experienced at a Point Distant X from an Infinite Plane Interface (i.e. an overlying layer). Note that the dose at $X = 0$ is only 0.5 times the dose that would be experienced if the interface were not present.

they can escape from a considerable depth in the grain and also the photoelectrons from the surroundings penetrate far into the grain. If the effective atomic number of the surrounding medium is greater than that of the grain then the electron energy entering the grain will be greater than the electron energy escaping from it and hence the TL response will increase. The converse is also true in that if the effective atomic number of the surrounding medium is less than that of the grain then the TL response will decrease. This effect is most marked at between 0.03 and 0.10 MeV.

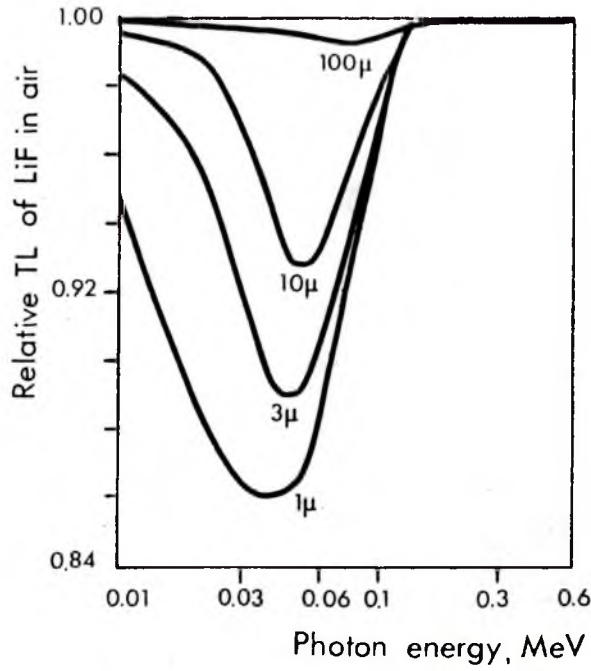
As the photon energy increases further the photoelectric effect declines in importance and the Compton effect begins to predominate. At about 0.2 MeV the Compton electrons have approximately the same energy as 0.01 MeV photoelectrons so the situation is similar to that described at 0.01 MeV. At still higher photon energies, all the electrons are Compton electrons with considerable ranges and since the mass energy absorption coefficient, μ_a/ρ , is almost independent of atomic number, the response is nearly independent of grain size.

This energy-size dependence of the TL response was first considered by Chan and Burlin (1970) who calculated the response of four thermoluminescent materials when irradiated in air and in teflon. Figure 5.5 shows their results for lithium fluoride. These effects are taken into account in Appendix C when lithium fluoride is used to calibrate the beta source against a calibrated cobalt-60 source.

It is useful to consider the possible implication of these effects for quartz grains embedded in a radioactive matrix and this is discussed in the following section.

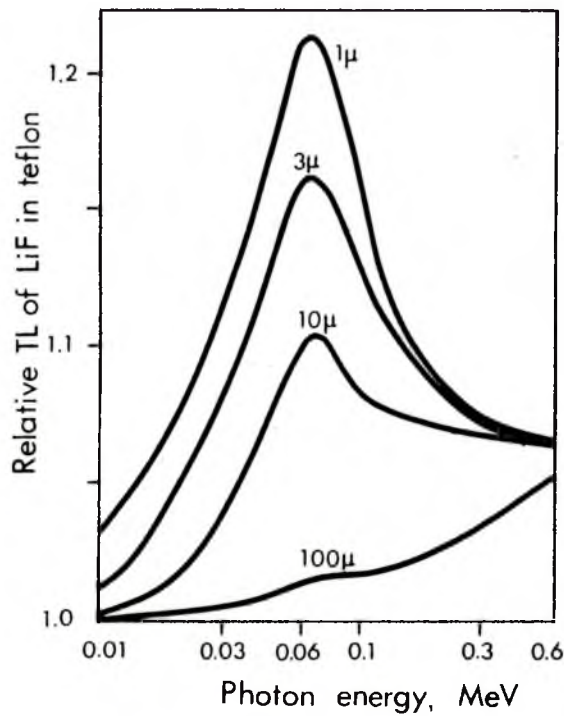
5.7 The Low Energy Photon Response of Quartz Grains in a Clay Matrix

The work of Chan and Burlin (1970) was based on a general theory of



(a)

(The relative TL is taken as the TL response of the grain sizes shown as a fraction of the response of a very large grain.)



(b)

FIGURE 5.5: The Energy-Size Dependence of the TL Response of LiF irradiated in (a) Air and (b) Teflon.

cavity ionization as proposed by Burlin (1966) for monoenergetic photons. The situation for the natural radioactive series is far from this simple however, with many γ -rays of different energies being emitted and each of these being scattered through many different energies until finally absorbed in a photoelectric event.

To assess accurately the low energy photon response of quartz grains some method of determining the photon spectrum is necessary. One such possible method is to make use of a computer technique known as the 'Monte Carlo' method. This technique traces the paths of individual gamma-rays through an absorber generating random numbers at various stages (hence the name) in order to characterise the type of interaction and the energy imparted to secondary electrons. Thousands of these gamma-ray case histories are summed in order to assess the average gamma interactions. Full details of such a method are given by Ellett et al. (1968) who used it to calculate absorbed doses in bounded tissue media.

At present computer programmes are being developed by the writer based on this technique to evaluate the photon spectrum from the uranium, thorium and potassium-40 γ -rays. No solutions are as yet available but it is hoped that the programmes will soon be complete and results will be forthcoming.

A qualitative picture can, however, be gained for the samples investigated in Chapters VII and IX by means of an elemental analysis of the clay of each sample. Just such an analysis has been carried out by dispersive X-ray fluorescence with the results shown in Table 5.2.

It may be seen from Table 5.2 that each of the samples has a very high quartz (SiO_2) content. The only elements of significantly higher atomic number which are present to any extent are the small amounts of calcium and iron but these may be balanced against the large amount of oxygen and the smaller percentage of carbon present both of which have a lower atomic number than quartz ($Z = 10.8$). Thus the atomic number of

TABLE 5.2

The Results of the X-ray Fluorescence Analysis for the Lake Mungo (F5 to F9)
and the Lake Jindabyne (JH2 and JH1) Fireplaces

	F5	F6	F7	F8	F9	JH2	JH1
SiO ₂	86.77	80.76	86.84	76.30	69.34	68.33	71.49
TiO ₂	0.330	0.355	0.355	0.350	0.355	0.440	0.515
Al ₂ O ₃	5.355	4.595	4.115	5.505	6.425	14.42	13.34
Fe ₂ O ₃	2.060	1.735	1.540	2.105	2.445	4.670	4.960
MnO	0.030	0.010	0.010	0.020	0.015	0.090	0.060
MgO	0.405	1.020	0.700	1.000	1.635	1.335	1.370
CaO	0.405	4.885	2.215	5.580	8.360	2.300	1.275
K ₂ O	0.885	0.725	0.665	0.825	0.985	2.650	2.965
P ₂ O ₅	0.040	0.040	0.025	0.040	0.070	0.055	0.110
S	0.005	0.010	0.010	0.010	0.015	0.000	0.005
CO ₂	0.318	3.834	1.738	4.379	6.561	1.805	1.001
H ₂ O	3.162	3.586	2.982	4.571	5.450	5.075	2.889
TOTAL	99.865	101.56	101.19	100.68	101.61	101.17	99.975

the surrounding matrix will be very similar to that of the quartz grains and the absorbed dose from gamma rays will be uniform throughout the sample (except of course in the presence of an interface as discussed earlier in Section 5.4).

This will not be the case for quartz grains embedded in a matrix with a considerably lower (or higher) atomic number. If we consider as an example a clay matrix which has approximately a 25% lower atomic number i.e. $Z \approx 8$, then the ratio of the mass-energy absorption coefficients of the quartz and clay is found to be 1.80 below about 100 KeV. In addition, the mass stopping power ratio is 0.93 in this energy region. The theory of Chan and Burlin (1970) predicts that under these circumstances very small grains of the order of $1 \mu\text{m}$ will absorb 4% more than the dose absorbed by the clay at 50 KeV and over 38% more at 20 KeV. Grains of the order of $100 \mu\text{m}$ will absorb 77% more than the matrix dose at 50 KeV and 80% more at 20 KeV.

The need to evaluate the photon spectrum from the natural radioactive series is therefore apparent in order to assess what fraction of the total photon energy is imparted at energies below about 100 KeV. This is especially true for $100 \mu\text{m}$ grains embedded in media which have significantly different atomic numbers to that of quartz.

5.8 Summary and Discussion

In this Chapter the essential qualitative difference between the interactions of gamma radiation and charged particles with matter has been described. This difference is evinced as an exponential intensity diminution which makes the concepts of stopping power and range inapplicable to gamma rays.

The principle mode of ionization, and the consequent creation of TL,

is via secondary electrons produced by three main types of interaction - photoelectric, Compton scattering and pair production.

If the volume of interest is large enough, the Compton scattered photons can go on to produce secondary electrons and the idea of buildup factors has been introduced to describe the absorbed dose from scattered radiation. This idea has been applied to the practical situation of an overlying clay layer with a higher radioactive level than the underlying one.

The energy-size dependence of the thermoluminescence response has been described and has been shown to be dependent on the atomic number of the surrounding medium. The necessity to assess the photon spectrum is therefore apparent and a method for this calculation was presented, a method which is currently being developed by the writer.

As an example, Mejdahl (1970) investigated experimentally the low energy response of quartz and feldspar inclusions embedded in clay tablets. He found that the response of the inclusions had a maximum value of 3.5 at 40 KeV relative to the response at 1.25 MeV. Unfortunately the elemental composition of the clay was not given so that the relative absorbed dose in the matrix and the grains could not be calculated. Gustafson and Brar (1964) have presented a gamma-ray spectrum which cut off, however, at 100 KeV. Mejdahl (1970) extrapolated this curve to lower energies and evaluated that the total response of inclusions in the clay tablet exceeded the true response by 5.3%.

For the samples investigated in Chapters VII and IX, X-ray fluorescence analysis indicates that the atomic numbers of the clays are very similar to quartz and hence the absorbed dose in the quartz grains will not differ significantly from the absorbed dose in the matrix.

CHAPTER VIRADIATION DOSE-RATEFROM THE NATURALLY-OCCURRING RADIOACTIVE SERIES6.1 Introduction

The assessment of the radiation dose-rate for thermoluminescence dating requires a knowledge of two factors - (i) the concentrations of the radioactive elements present in the clay matrix and (ii) the decay characteristics of all the contributing radioisotopes and hence the energy released for a given concentration of each of the uranium, thorium and potassium series.

The first of these factors is determined in this present work by alpha-counting, as described earlier in Chapter II, for the uranium and thorium series while for potassium-40, which has a well established natural abundance of 0.0118% of the total potassium content, the level of potassium is determined by dispersive X-ray fluorescence analysis. This is usually expressed as a percentage K_2O (see Chapter V, Table 5.2). Aitken and Fleming (1972) have described how thermoluminescent phosphors may also be used to evaluate the dose from the uranium, thorium and potassium series and in addition how the potassium content may be determined by flame photometry.

The second factor, the energy released by the radioactive decay of the three series, is described in the next Section and in Section 6.3 conversion factors from alpha counts and from actual concentrations to dose-rates are evaluated.

6.2 Radiation Data

When a radioactive nucleus decays it can do so by the emission of either an alpha or a beta particle. The decay of the parent can be to the ground state of the daughter nucleus alone or it can also be to one or more excited states. When this latter phenomenon occurs, the excited state of the daughter can then decay to the ground state (or a lower excited state) by the emission of either a gamma ray or by the transference of energy to an orbital electron which is then ejected from the atom as an internal conversion (IC) electron or, more commonly, by a combination of both of these processes.

In the case of IC electrons the hole left in the inner shell is filled by an electron from an outer shell, which gives rise to the emission of X-rays and Auger electrons. Vacancies created by the filling of the initial vacancy will in turn give rise to further X-rays and Auger electrons. These processes are described in greater detail by Martin and Blichert-Toft (1970).

An extensive survey of the available literature on the decay schemes of the radioisotopes of interest has been carried out. Most of the available information has been gleaned from the data published in 'Nuclear Data Sheets', a publication of the Oak Ridge National Laboratory's Nuclear Data Project. Data which is as yet unpublished was obtained from the Nuclear Data Project as computer print-out from their 'Evaluated Nuclear Structure Data File'. Table 6.1 gives the reference source for all of the data used in the compilation of the decay characteristics of the uranium and thorium series. (Note: the uranium series comprises of not only the uranium-238 series but also the uranium-235 series at a natural abundance of 0.72%). Using the information taken from these sources, the radiation data for the thorium-232 series and the uranium-238 and

TABLE 6.1

Reference Sources for the Uranium and Thorium Series

A-Value	Nuclei	Reference ¹	Date ²
207	Tl	B5	1971
208	Tl	B5	1971
210	Po, Bi, Pb	B5	1971
211	Po, Bi, Pb	B5	1971
212	Po, Bi, Pb	B8	1972
214	Po, Bi, Pb	ENSDF	*
215	Po	ENSDF	*
216	Po	17	1976
218	Po	ENSDF	*
219	Rn	ENSDF	*
220	Rn	17	1976
222	Rn	ENSDF	*
223	Ra	ENSDF	*
224	Ra	17	1976
226	Ra	ENSDF	*
227	Th, Ac	ENSDF	*
228	Th, Ac, Ra	17	1976
230	Th	B4	1970
231	Pa, Th	B6	1971
232	Th	B4	1970
234	U, Pa, Pa(m), Th	B4	1970
235	U	B6	1971
238	U	B4	1970

1. Reference gives the Nuclear Data Sheet volume number. ENSDF implies that the information was obtained as computer print-out from the Evaluated Nuclear Structure Data File.
2. Date gives the year the compilation was published except * which refers to the ENSDF.

uranium-235 series was assessed as detailed below and is presented in Tables 6.2, 6.3 and 6.4.

The alpha particle energy is the most straightforward to evaluate and is simply the sum of the energy of each alpha particle released during a nuclear decay times the abundance of that particular particle. The recoil energy of the nucleus has been neglected because of its very localised dissipation.

The beta energy is rather more complex because of the spectral nature of the beta emission. As already discussed in Chapter IV, the transition energy is shared with a neutrino so that the beta particles have an energy distribution up to a maximum value. β_{\max} is the sum of the maximum energy times abundance for each beta transition in each nuclear decay. β_{av} is the sum of the average energy times abundance for each decay. In most cases the average beta energy is given in the reference sources, but for those in which it is not, the method of Murthy (1971) has been applied to determine it.

The references of Table 6.1 usually list only the transition intensity for the gamma energy i.e. the abundance of transitions occurring from one excited state to another or to the ground state. These transitions can cause the release of energy from the atom in the form of electromagnetic radiation (gamma and X-rays) or as charged particles (IC and Auger electrons). For those transitions where the proportion of IC electrons to gamma rays (the internal conversion coefficient) is not given the tabulations of Hager and Seltzer (1968) have been used. They presented tables of K-, L- and M- shell internal conversion coefficients for certain energies and a computer-programme based on spline interpolation for those energies not listed. This was used when necessary to determine the energy and abundance of the IC electrons and gamma rays in each transition. The contribution from the N-, O- and

TABLE 6.2

Radiation Data for the Thorium-232 Series

Radioisotope	Half-Life	α (MeV)	β_{\max} (MeV)	β_{av} (MeV)	γ (MeV)	IC (MeV)
Th-232	1.405×10^{10} y	4.006	-	-	0.0001	0.0106
Ra-228	5.75 y	-	0.0550	0.0141	-	0.0015
Ac-228	6.13 h	-	1.1707	0.3929	0.9544	0.05855
Th-228	1.9131 y	5.399	-	-	0.0019	0.0191
Ra-224	3.66 d	5.675	-	-	0.0095	0.0022
Rn-220	55.6 s	6.292	-	-	0.00055	-
Po-216	0.15 s	6.7786	-	-	-	-
Pb-212	10.64 h	-	0.3713	0.1067	0.1055	0.0652
Bi-212 \rightarrow Po-212	60.60 m	-	1.3360	0.4901	0.1013	0.0015
\rightarrow Tl-208		2.1799	-	-	0.0039	0.0074
Po-212 (64.07%)	0.30 μ s	5.6295	-	-	-	-
Tl-208 (35.93%)	3.07 m	-	0.5804	0.2055	1.2070	0.0098
Positions not shown in decay schemes					0.0021	0.0006
X-rays					0.1197	
Auger Electrons						0.0094
TOTAL		35.959	3.5134	1.2093	2.50595	0.18585

TABLE 6.3

Radiation Data for the Uranium-238 Series

Radioisotope	Half-Life	α (MeV)	β_{\max} (MeV)	β_{av} (MeV)	γ (MeV)	IC (MeV)
U-238	4.49×10^9 y	4.185	-	-	0.0111	-
Th-234	24.10 d	-	0.1625	0.0456	0.0149	0.0087
Pa-234m	1.17 m	-	2.2647	0.8372	0.0112	0.0036
Pa-234(0.13%)	6.70 h	-	0.0009	0.0003	0.0016	0.0009
U-234	2.48×10^5 y	4.759	-	-	0.0001	0.0101
Th-230	7.7×10^4 y	4.677	-	-	0.0004	0.0117
Ra-226	1.6×10^3 y	4.775	-	-	0.0090	0.0033
Rn-222	3.824 d	5.4892	-	-	0.0004	-
Po-218	3.05 m	6.0025	-	-	0.0001	-
Pb-214	26.8 m	-	0.7055	0.2195	0.2285	0.0692
Bi-214	19.9 m	-	1.7762	0.6413	1.5088	0.0118
Po-214	163.7 μ s	7.689	-	-	0.0001	-
Pb-210	21.3 y	-	0.0243	0.0062	0.0019	0.0253
Bi-210	5.012 d	-	1.1610	0.3945	-	-
Po-210	138.4 d	5.306	-	-	0.00001	-
X-rays					0.0332	
Auger Electrons						0.0089
TOTAL		42.8827	6.09525	2.1446	1.82131	0.1535

TABLE 6.4

Radiation Data for the Uranium-235 Series

Radioisotope	Half-Life	α (MeV)	β_{\max} (MeV)	β_{av} (MeV)	γ (MeV)	IC (MeV)
U-235	7.1×10^8 y	4.3897	-	-	0.1485	0.0131
Th-231	25.52 h	-	0.2193	0.0627	0.0151	0.0503
Pa-231	3.25×10^4 y	4.9225	-	-	0.0237	0.0888
Ac-227	21.77 y	0.0689	0.0398	0.0102	0.0099	-
Th-227	18.2 d	5.8379	-	-	0.0988	0.0002
Fr-223(1.4%)	22 m	-	0.0159	0.0040	0.0007	-
Ra-223	11.43 d	5.8224	-	-	0.0865	-
Rn-219	3.96 s	6.7590	-	-	0.0576	-
Po-215	1.78 ms	7.3864	-	-	0.0003	-
Pb-211	36.1 m	-	1.3234	0.4564	0.0764	0.0025
Bi-211	2.15 m	6.5680	0.0017	0.0004	0.0491	0.0071
Po-211(0.28%)	0.52 s	0.0209	-	-	0.00002	-
Tl-207	4.79 m	-	1.4340	0.5054	0.0024	-
TOTAL		41.7757	3.0341	1.0391	0.57402	0.1620

higher shells was taken from Dragoun et al. (1971).

γ is the sum of the energy times abundance for the gamma rays in each transition and IC is the sum for the internal conversion electrons.

The hole created in the inner shell by the ejection of the IC electron is filled by an electron from an outer shell with the emission of either an X-ray or of an Auger electron. The fluorescence yield, ω , for a particular atomic shell is defined as the probability that a vacancy in that shell will result in the emission of an X-ray. The probability of Auger electron emission is, obviously, $1 - \omega$. Values of ω are taken from Bambynek et al. (1972) and are used to calculate the sum of the energy times abundance for the X-rays and Auger electrons for each series.

The radiation data for potassium-40 was taken from Martin and Blichert-Toft (1970) except for the average energy of the beta transition. This transition has a rather complex 'third forbidden unique' spectrum and the average beta energy was taken to be 0.583 MeV (Martin, 1975) at an abundance of 89.3%. In the remaining 10.7% of cases, potassium-40 decays by electron capture then gamma ray emission with an energy of 1.4608 MeV.

6.3 Assessment of the Dose-Rate

The uranium and thorium series consist of a whole chain of radioactive nuclei constantly decaying to their daughters until a stable isotope is reached. If we assume that the radioactive descendants of the first member remain with the original material, then after sufficient time has elapsed all members of the series will be present together, nuclei of any particular member being formed by its parent while other nuclei of the same member decay to its daughter. The relative amounts of all the nuclides will be constant when the decay series reaches

radioactive equilibrium, each nuclide decaying at the same rate at which it is formed. Hence the activity of each member of the series is precisely the same as that of any other member, i.e.

$$\lambda_1 N_1 = \lambda_2 N_2 = \lambda_3 N_3 - - - - - \quad (6.1)$$

where $\lambda_{1,2,3}$ etc. are the decay constants and $N_{1,2,3}$ etc. are the number of each radioactive nuclide per gram of material.

A serious hindrance to the achievement of radioactive equilibrium for the natural series is the presence of the gaseous daughters radon (Rn-222), halfway through the uranium-238 series, and thoron (Rn-220), halfway through the thorium-232 series. These radioactive gases have halflives of 3.824 days and 55.6 secs respectively and Tanner (1964) has shown that in very dry soil the mean migration distance of radon is about 2 m and of thoron is about 2 cm. It is possible that under certain circumstances the escape of radon, at least, could seriously affect the dose-rate. Because of this the dose-rates given in Table 6.5, for a given concentration of the parent nuclide, are listed for no gas loss and for 100% gas loss. The drastic effects of any gas loss on the gamma dose of the uranium series is immediately obvious. This problem is taken into account in the calculation of the dose-rates in Part II of this work.

The dose-rates quoted in Table 6.5 for the beta dose include the contributions from beta particles (using β_{av}), internal conversion electrons and Auger electrons. The gamma dose contributions include both the gamma rays and the X-rays.

In Chapter II equation (2.6) was derived for the alpha activity, S , of a sample based on the number of alpha-counts measured per unit time, C_α , over an area A . This is

TABLE 6.5

Dose-Rate (mrad/yr) for 1 ppm by Weight of Parent

	α	β	γ
Thorium Series:			
no thoron loss	73.8	2.86	5.14
100% thoron loss	30.9	1.03	2.08
Uranium Series:			
no radon loss	278.3	14.62	11.48
100% radon loss	126.2	6.09	0.56
Natural Potassium:			
1% K_2O	-	68.2	20.5

$$S = 4. \frac{C_{\alpha}}{R\rho A} \quad (6.2)$$

where R is the average range of an alpha particle in the material of density ρ .

Using values of 6.94 mg/cm^2 for $R\rho$ of the thorium series and 5.84 mg/cm^2 for $R\rho$ of the uranium series and in addition using threshold fractions of 0.85 and 0.82 for the thorium and uranium series respectively (Aitken and Bowman, 1975), the dose-rates per alpha particle counted per cm^2 per ksec may be calculated and these are presented in Table 6.6 for a sample containing only the uranium series and for a sample containing only the thorium series.

In practice, the number of alpha-counts measured will originate from a combination of the uranium and thorium series and hence some measure of the ratio of the abundance of the parents is necessary. For the samples investigated in Part II this was carried out by trace element dispersive X-ray fluorescence analysis. Another method for providing an estimate of the uranium to thorium ratio is the 'pairs technique' described by Aitken and Fleming (1972) in which a coincidence circuit records the number of times an alpha-count is followed by a second count within 0.2 sec of the first. This effectively determines the activity of Po-216 and hence the thorium series.

6.4 Summary of Results

The results of an extensive literature search for the decay characteristics of each contributing radioisotope in each of the natural radioactive series was presented in this Chapter. These values were then used to calculate dose-rate conversion factors for a given concentration of each series and for a given alpha-count measurement.

The conversion factors for the alpha-counts require an estimate of the

TABLE 6.6

Dose-Rate (mrads/yr) per Alpha Particle
Counted per cm² per ksec

	α	β	γ
Uranium Series	2274	119.4	93.8
Thorium Series	2055	79.7	143.2

uranium to thorium ratio. As an example consider a sample which has the combined activity of the parents uranium-238 and uranium-235 equal to the activity of the parent thorium-232. This corresponds to 3.167 ppm of thorium for every 1 ppm uranium. Thus for a thick source of diameter 42 mm (see Chapter II, Section 2.5) the conversion factors from alpha-counts per ksec to mrad/yr are 157, 7.24 and 8.49 for alpha, beta and gamma doses respectively assuming no gas loss.

The dose-rates presented in this Chapter have been based on the implicit assumption that the energy released per gram of the sample is everywhere equal to the energy absorbed per gram. As has been described in Chapters III, IV and V this is not always the case for quartz inclusions embedded in a radioactive clay matrix. The modification factors developed in these Chapters must, therefore, be taken into account when evaluating the dose-rates for the practical work in Part II.

PART II

APPLICATION OF THERMOLUMINESCENCE DATING
TECHNIQUES TO THREE ARCHAEOLOGICAL SITES IN AUSTRALASIA

CHAPTER VIITHE DATING OF ANCIENT ABORIGINAL FIREPLACES FROM LAKE MUNGO7.1 Introduction

The fundamental principles of thermoluminescence dating have been set down in Part I and the remainder of this thesis is concerned with the application of these principles to the practical problem of dating archaeological samples.

This Chapter deals with ancient Aboriginal fireplaces from Lake Mungo in western New South Wales, a site which has proven to be of great archaeological significance. The thermoluminescence ages for these fireplaces turn out to be in excess of 30,000 years. These ages are compared to previous radiocarbon ages in the next Chapter and the agreement is found to be good, although a small systematic difference appears to exist which, if real, might be explained in terms of variations in the cosmic ray flux, caused possibly by changes in the Earth's geomagnetic field.

Chapter IX deals with the dating of more Aboriginal fireplaces this time from Lake Jindabyne which is situated about 150 km south of Canberra. These fireplaces are much younger, being less than 3,000 years old. Then in Chapter X the final archaeological application of the technique is described and it is the dating of cooking stones from the Kuk Tea Research Station in New Guinea. These sites are less than 300 years old which serves to demonstrate the large time span over which thermoluminescence dating may be applied.

7.2 Archaeological Background of the Lake Mungo Site

During the Quaternary period large areas of western New South Wales and northern Victoria were covered by hundreds of lakes both large and small. Nearly all are dry today but some may still be recognised by the long low dune that follows the eastern shoreline. These dunes, which were formed by the prevailing westerly winds, have the shape of a crescent moon and are called lunettes.

A group of these lakes, the Willandra Lakes located approximately 100 km north-east of the town of Mildura, forms the terminal system of the Willandra Creek, a distributary stream of the Lachlan River (see Figure 7.1). The Willandra Creek now carries water only during peak or flood discharges but during Pleistocene time it flowed more freely and was able to maintain the lake system full of water for long periods.

The lakes appear to have been a focal point for the tribes of ancient Aborigines passing through this area and many traces of early human occupation have been found along the shoreline of nearly all the major lakes. Some of the best exposures have occurred on the lunette along the eastern shore of Lake Mungo (Bowler *et al.*, 1970). This lunette, known as the 'Walls of China', has suffered massive erosion in recent times and this has uncovered the sites of many ancient fireplaces. Charcoal from these fireplaces has been dated by Barbetti and Polach (1973) using the radiocarbon method and the ages place the lakeside dwellers at Mungo in an era of Australian prehistory over 30,000 years ago.

To fully appreciate the archaeological significance of the Mungo finds, we must consider the as yet unsolved problem of how and when the ancestral Aboriginal migrants colonised the continent of Australia. If indeed they originated in Asia, then the duration of their occupation of Australia is very relevant to this question. The answer may lie partly in the

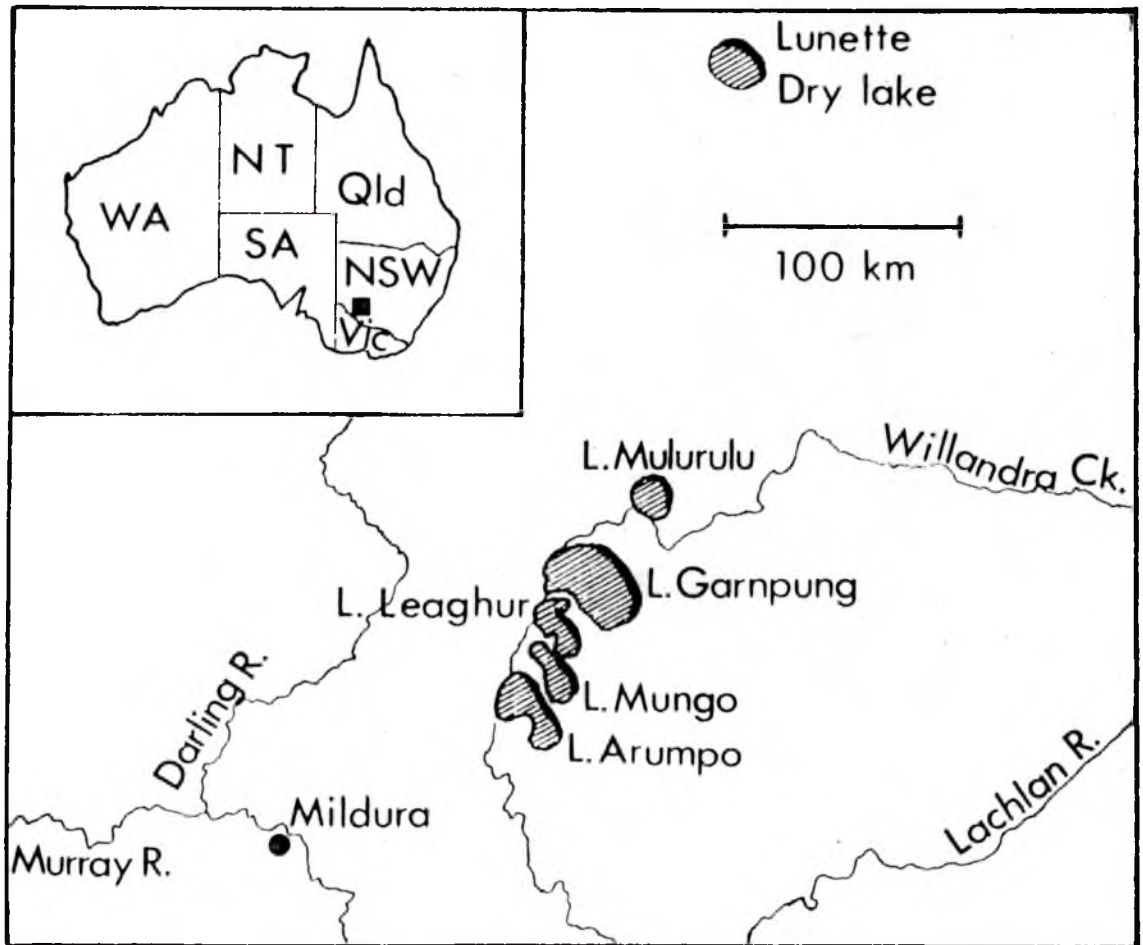


FIGURE 7.1: The Willandra Lakes System. The 'Walls of China' is the crescent-shaped lunette along the eastern shoreline of Lake Mungo. The inset shows the position of the region on the continent of Australia.

possibility that these Pleistocene explorers found a vastly different continent from that familiar to us today.

Firstly it was larger, since during the last ice age the sea-level dropped over 500 feet below its present level (this modern level was only attained between 6,000 and 3,600 years ago). As a result, Tasmania in the south and New Guinea in the north would both have been part of the continental mainland which was, in effect, much nearer Asia. Sea-levels rose and fell in cycles in accordance with fluctuations in the ice sheets and the last low stage appears to have been about 20,000 years ago, obviously too recent for consideration as a time for potential migration. The preceding lower ocean phase was earlier than 50,000 years ago and if human migration over narrower straits is postulated, then such an age must be considered as the minimal period of human occupancy (Mulvaney, 1975).

Secondly, with cooler temperatures and lower evaporation rates, Pleistocene regional conditions were more congenial. In the cool temperate and monsoonal belts the rain forests were less dense, so that travel across the continent would have been easy and relatively rapid. The exact routes followed by the ancient Pleistocene travellers still remain a mystery although it is very probable that many early coastal plain sites now lie deep below the Pacific Ocean.

Lake Mungo is one of the best studied early-man locations on lake-bordering lunettes but it should not be regarded as among the earliest. Northern sites must have been colonised en route, while the sophisticated exploitation of the natural resources around Mungo implies that the migrants were already well accustomed to Australian conditions. Similar settlement patterns appear to be emerging from at least two other sites, one at Keilor in Victoria and the other at Devil's Lair Cave in Western Australia, both of which are now giving ages of in excess of 30,000 years

based on the radiocarbon dating method.

Australian Prehistory is beginning to come of age and is starting to play an important role in the world-wide search for early man. The fireplaces at Mungo are a small but significant part of this search since they have important implications for the whole of south-east Asia if, as has already been stated, that region is assumed to be the migrational source for modern Australians. Because of the time necessary for migration across the Malayo-Indonesian area and across northern Australia*, the presence of a morphologically modern people in the Mungo area 30,000 years ago argues for the much earlier presence of similarly modern people on the south-east Asian mainland. This is supported by the morphology and probable age of the Niah skull found in Sarawak and dated to around 40,000 years (Brothwell, 1960). The Lake Mungo finds, therefore, suggest the presence of fully sapient populations in south-east Asia as early as, if not earlier than, their known presence elsewhere.

7.3 Aboriginal Fireplaces at Lake Mungo

The Mungo campsites are thought to have been utilised during the summer season with the groups dispersing over the drier plains in winter (Mulvaney, 1975). The presence of emu egg shells, however, suggests the probability of late winter-spring camps. The high protein diet of the Mungo people also comprised several marsupial and reptilian species hunted on the bushy plains in addition to the abundance of molluscs and fish in the four fathoms of freshwater in the lake.

According to Barbetti (1973) there were three types of ancient fireplaces found in the Willandra Lakes area. Ovens consisted of lumps of baked clay used as cooking stones arranged on top of a thin layer of ash

*see Appendix F for a simple model of this population expansion

and charcoal in a shallow depression. Hearths were small areas of blackened earth, without cooking stones, resulting from an open fire. The third type consisted of two mounds of baked clay with ash and charcoal underneath. The purpose of this third type of fireplace is not known (Barbetti, *op. cit.*).

Allen (1972) has reviewed the descriptions of the use of Aboriginal ovens as recorded by early European explorers and he cites Eyre (1845) on the use of an oven:

'The native oven is made by digging a circular hole in the ground, of a size corresponding to the quantity of food to be cooked. It is then lined with stones in the bottom (or clay balls where stones are unavailable), and a strong fire made over them so as to heat them thoroughly, and dry the hole. As soon as the stones are judged to be sufficiently hot, the fire is removed, and a few of the stones taken, and put inside the animal to be roasted if it be a large one. A few leaves or a handful of grass are then sprinkled over the stones in the bottom of the oven, on which the animal is deposited, generally whole, with hot stones laid on top of it. It is covered with grass, or leaves, and then thickly coated with earth, which effectually prevents the heat from escaping.'

One further challenging find for the archaeologist and anthropologist has been the discovery of fragments of four human cremations at Lake Mungo. The ceremony involved the smashing and re-burning of the bones and their interment in a round hole. Radiocarbon dating of the collagen fraction from one of the skeletal remains and also of charcoal from a hearth synchronous with the burial gives an age of $25,500 \pm 1000$ years BP (Bowler *et al.*, 1972) and hence it is possibly the earliest known human cremation ritual (Thorne, 1971). Also the recent discovery of an almost complete skeleton (Bowler and Thorne, 1976) further expands the morphological and cultural information available from the earliest known period of Man's occupation of the continent of Australia.

The sediment below the fires is believed to have been heated to a temperature in excess of 450°C (based on archaeomagnetic work carried out by Barbetti, 1976) which is sufficient to empty the traps of geologically-accrued TL. The testing of this assumption is described later. In addition, X-ray diffraction analysis indicated a high quartz content in the samples, later confirmed by X-ray fluorescence (see Chapter V, Table 5.2).

Preliminary work was carried out previously at this laboratory by Adams and Mortlock (1974) using the fine-grain technique of Zimmerman (1971). Initial studies by the writer showed that this particular technique is not applicable to these samples because of "anomalous" fading (Wintle, 1973), that is, the escape of electrons from traps without the intervention of heat. This phenomenon has been interpreted by Zimmerman (1977) as being due to phosphorescence which is almost temperature independent and which has emission spectra at different wave-lengths from that of the TL. The phosphorescence is qualitatively similar to the radiative recombination extensively studied in semiconductors. That "anomalous" fading had taken place in the Mungo samples was experimentally verified as follows:

Fine grain samples were heated to 500°C to empty the TL traps and were then given a known laboratory beta dose. Some samples were glowed out immediately while others were stored in darkness and glowed out progressively over a period of some three months. A 'monitor' sample of LiF was stored with the fine grain samples in order to correct for any drift in the apparatus over this time period.

The results obtained from this experiment were neither consistent nor reproducible. Values of between 10 and 30% fading were measured for nearly all the samples over this time indicating a serious danger in the application of the fine grain technique to these samples. "Anomalous"

fading manifests itself mostly among the clay minerals, and X-ray diffraction analysis indicates a fairly large percentage of calcite (of the order of 5%) together with much smaller amounts of illite and kaolinite present in these clays. The inclusion technique of Fleming (1970) utilises only quartz, which is not subject to this fading problem (see Chapter XI, however), and therefore this technique has been adopted throughout the present investigations.

TL work on baked ovenstones from Lake Mungo has recently been reported by Huxtable and Aitken (1977) who found that fine-grain samples were also subject to spurious thermoluminescence. They too adopted the inclusion technique. However, because of the small sample size of the ovenstones, the ages they report are subject to large standard errors. Nevertheless the mean ages are generally in good agreement with those presented in the following Sections, as will be discussed more fully in Chapter VIII.

7.5 Separation of Quartz Inclusions from the Clay Matrix

The first step in the preparation of samples for the quartz inclusion technique is to separate the grains of quartz from the surrounding matrix. All the stages of preparation right through to the final heat treatment itself were conducted under subdued red lighting. This is because ultra violet radiation can excite electrons from their traps in much the same way as heat and thus exposure to sunlight or artificial light with a high u.v. content will tend to 'bleach' the TL from the quartz.

Samples of the porous and friable Mungo sediment were supplied in blocks approximately 10 cm square and coated with polyurethane foam. These blocks had been prepared for archaeomagnetic research (Barbetti, 1973) and consequently many had 2.8 cm diameter cores cut from them for

this purpose. The location and coding of each sample block is given in Figure 7.2. Samples for TL dating were obtained by using a low speed drill to gently break loose material from different parts of each block, having first removed the outer couple of millimetres which had been exposed to sunlight. This material was then pooled together to form the clay samples from which the quartz could be extracted for each fireplace.

These clay samples were gently crushed in a mortar and pestle so as to break up any aggregates of smaller grains but not to fracture the larger ones and were then sieved to obtain the grain size fraction between 90 and 120 μm . This size fraction was passed through a Frantz magnetic separator which extracts the crystalline (non-magnetic) grains from the surrounding (magnetic) matrix. This device is shown in Figure 7.3 and consists of a chute divided into two channels down which the grains fall under the influence of a magnetic field at right angles to the direction of motion. The chute may be tilted side-ways so that grains deflected by the magnetic field (i.e. magnetic ones) must travel 'uphill' against gravity and thus by varying the angle of tilt and the magnetic field, the magnetic grains can be deflected into one channel of the chute and collected in one bucket while the non-magnetic grains pass unaffected down the second channel and are collected in a second bucket. No hard and fast rules can be applied to the setting of the angle or the magnetic field as each sample requires a slightly different treatment. On average, however, the angle of tilt was approximately 10° and the magnetic field (measured as a current through the coils) the equivalent of 2 amperes.

The crystalline fraction thus obtained was then washed in dilute hydrochloric acid (HCl) to clean the grains and dissolve most of the calcite present. The remaining grains will comprise quartz and a very small amount of feldspars. These grains were then etched in hydrofluoric acid (HF) at a temperature and concentration as described later. This not

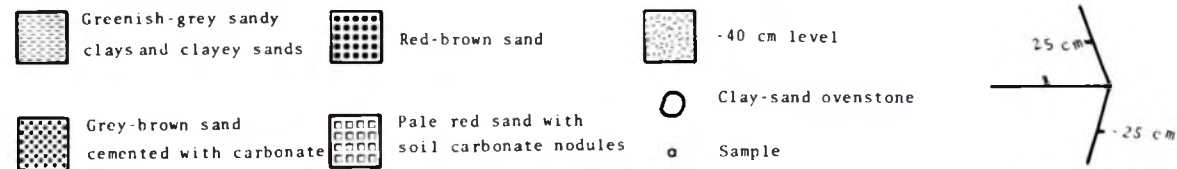
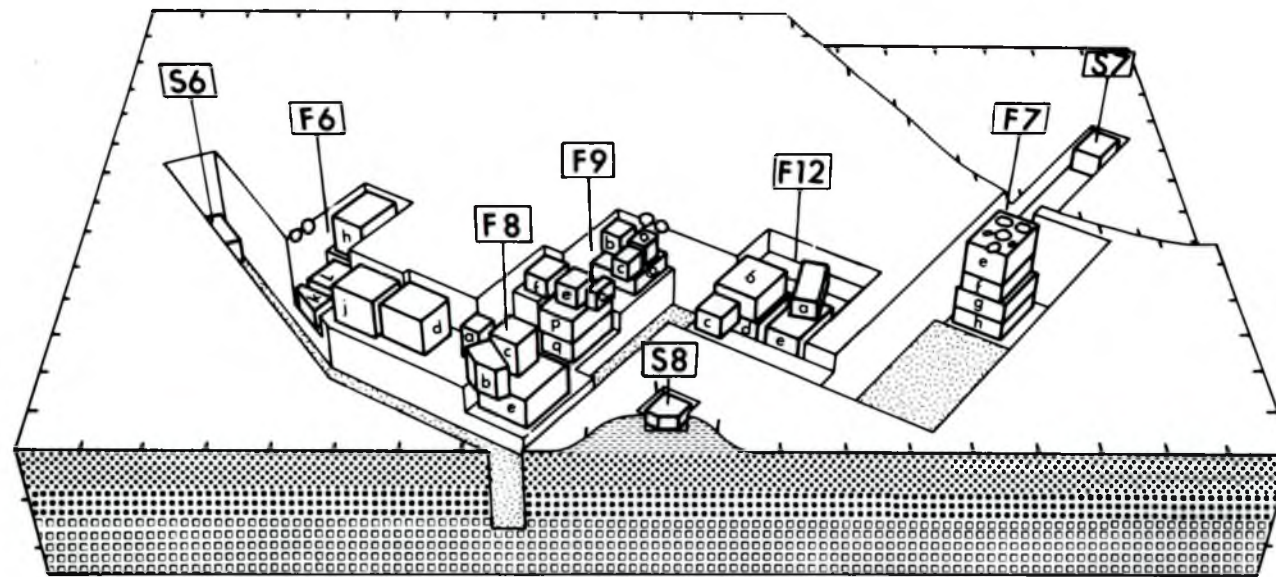


FIGURE 7.2: Sample Location relative to Overlying Zanci Layer (reproduced by kind permission of Dr. M. Barbetti).

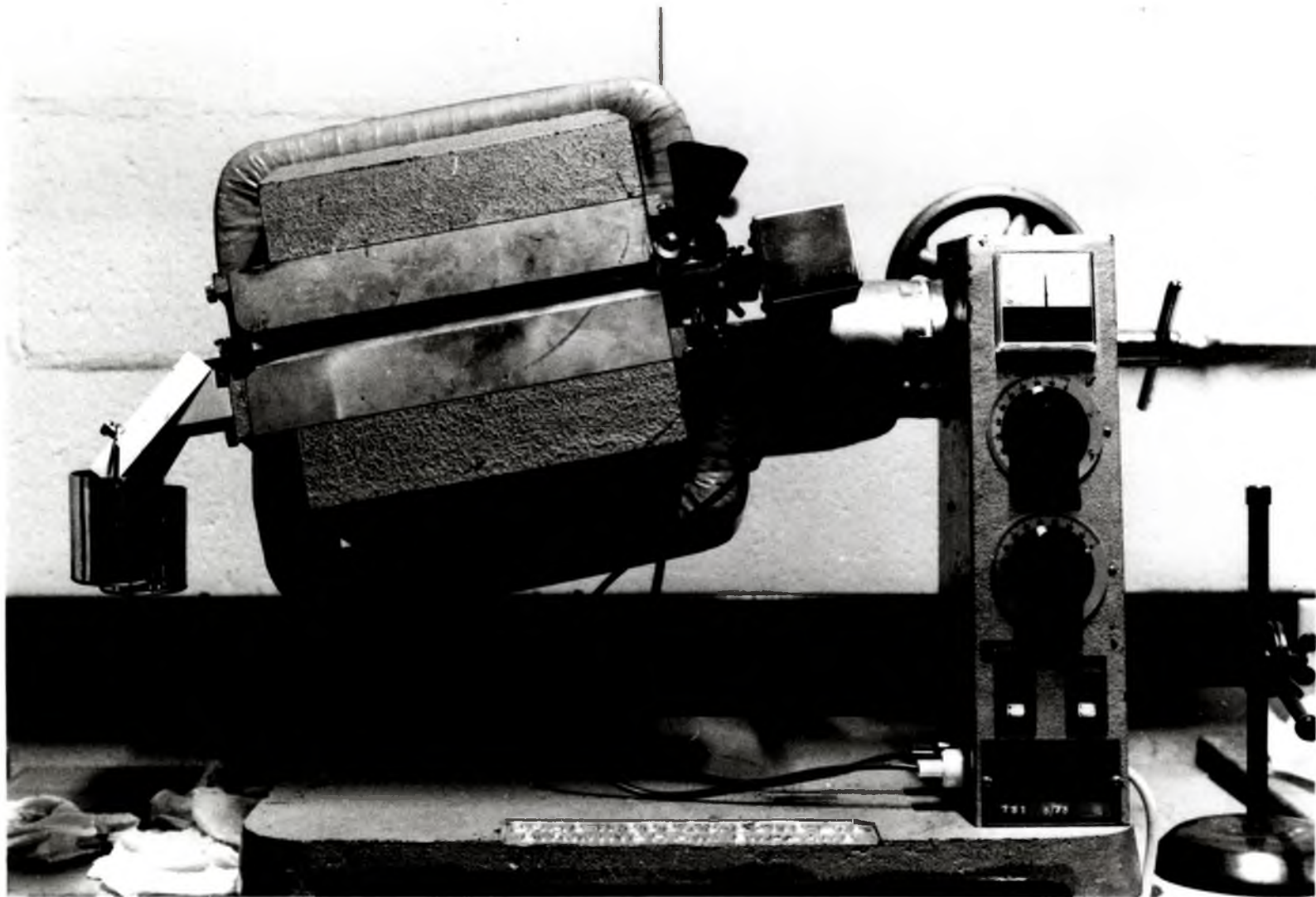


FIGURE 7.3: The Franz Magnetic Separator.

only dissolves almost all feldspars present but also eats away part of the surface of the quartz grains. This latter effect is described fully in the next Section but the result of the former was to produce samples which were almost 100% pure quartz. X-ray diffraction analysis indicated that this preparation produces samples in which no other mineral but quartz could be detected (see Figure 7.4).

7.6 The Effect of HF Etching on the Morphology of Quartz

Inclusions

In the "classical" quartz inclusion dating technique of Fleming (1970) it has been usual to assume that the HF acid treatment of the quartz inclusions removed a layer from the surface of the grains in a reasonably uniform fashion. This assumption implies the isotropic removal of the outer boundaries which contain not only diffused impurities and hence modified TL centres, but also the residual thermoluminescence induced by alpha radiation from the surrounding matrix. It is known, however, that quartz often etches very irregularly, with a much higher rate along dislocation lines in the crystal lattice structure (Lang and Miuscov, 1967) and so the validity of the assumption of isotropic etching has been tested by optical and scanning electron microscopy on etched and unetched quartz inclusions.

A sample of quartz grains, which had been separated as described in the last Section, was divided into four parts which were each subjected to different etching times in HF, these being no etch, 10 min, 40 min and 100 min acid treatment at room temperature. The grains were then viewed optically in a binocular microscope and also in a Cambridge Stereoscan scanning electron microscope (SEM).

Optically the unetched grains appeared fairly consistent in size with many grains appearing slightly coloured. About 75% of the grains

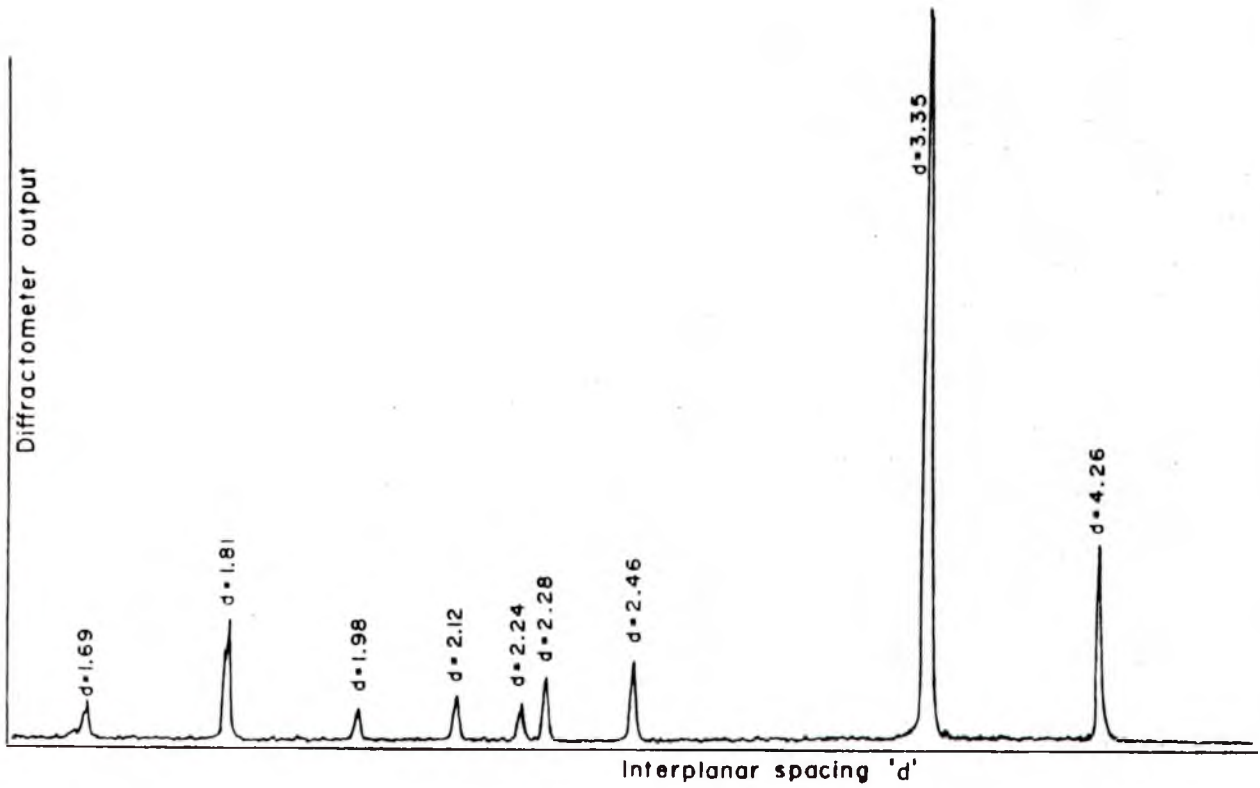


FIGURE 7.4: Typical X-ray Diffraction Pattern from a Prepared Sample of Quartz Grains from a Lake Mungo Fireplace. All the peaks shown correspond to quartz peaks with no other mineral detectable.

appeared "frosty" with the remainder describable as optically "shiny". After a 10 min etch the colouring on the grains had disappeared indicating a surface phenomenon, whilst the proportion of shiny grains appeared to increase. A photograph of a typical collection of these grains etched for 10 min is shown in Figure 7.5. For the 40 min and 100 min etched samples the proportion of shiny grains became greater, with over 60% falling into this category for the 100 min grains. In addition, for these longer etching times a greater variation in grain size became apparent.

A closer investigation of the grains was achieved with the SEM. Individual grains from each sample were sorted by hand (no efficient mass method of separation was devised) into either an optically frosty or shiny category and were examined and photographed in the SEM. Figure 7.6 shows typical frosty and shiny unetched grains and Figure 7.7 frosty and shiny grains from the 100 min etched fraction. The drastic effect on the 100 min frosty grain is immediately obvious, with deep etch pits gouged out of the body of the grain.

Figures 7.8a - d show aggregates of the grains after each of the four etching times. It is apparent that as the etching time increases, some grains are attacked more severely by the acid than others and become smaller in diameter by a factor or two or more. Also some grains lose a substantial part of their inner volume as etching tunnels are eaten right through the grains. Although all of the data presented here are from quartz from Mungo fireplaces, similar effects have been noted on quartz from ancient pot sherds from other areas such as Cyprus, Mexico, England and France (Bell and Zimmerman, 1978).

From the SEM photographs it appears that the etching rate can vary considerably between grains and also that the assumption of isotropic removal of material can be grossly incorrect especially for long etching times. Some grains will have a larger fraction of the residual alpha dose

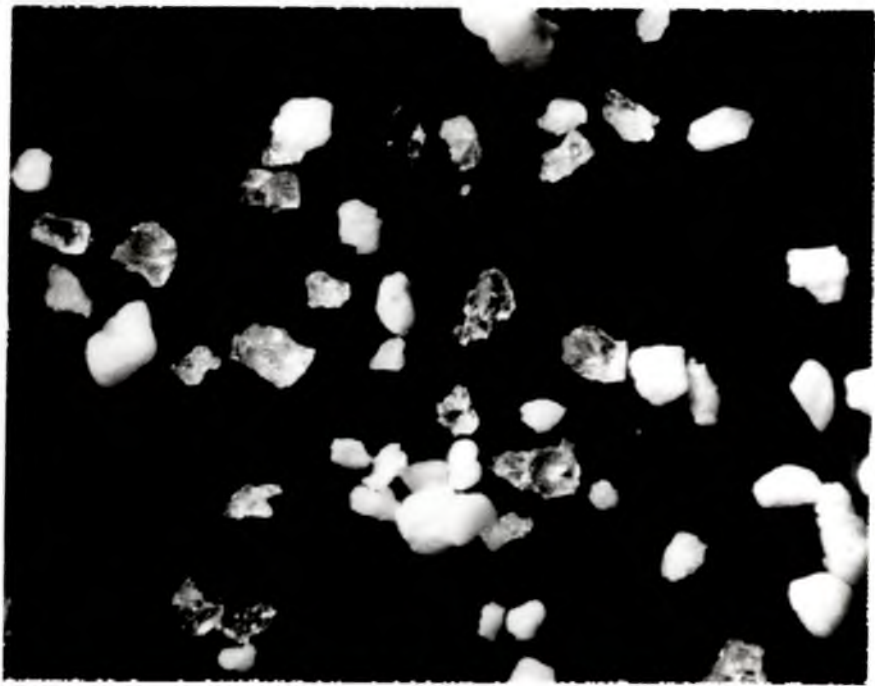
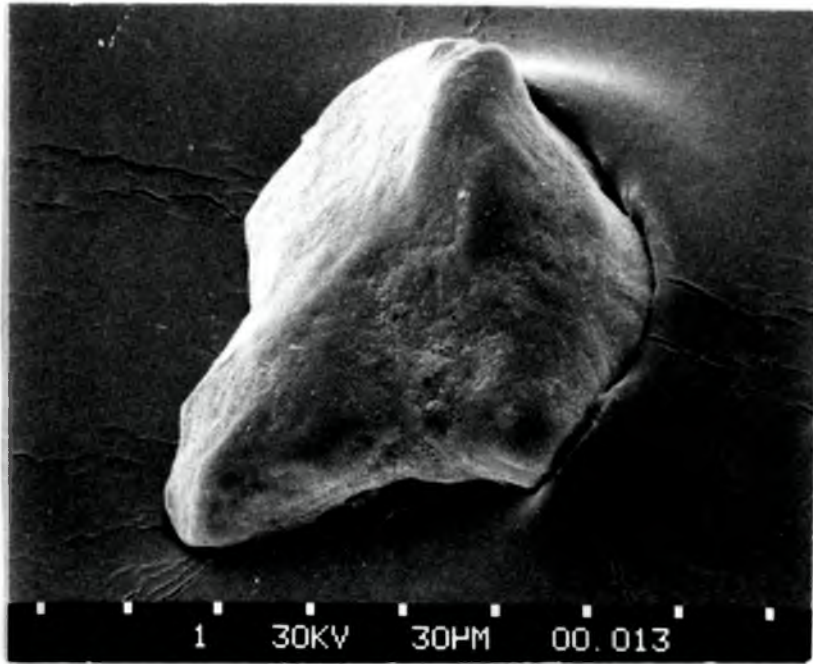
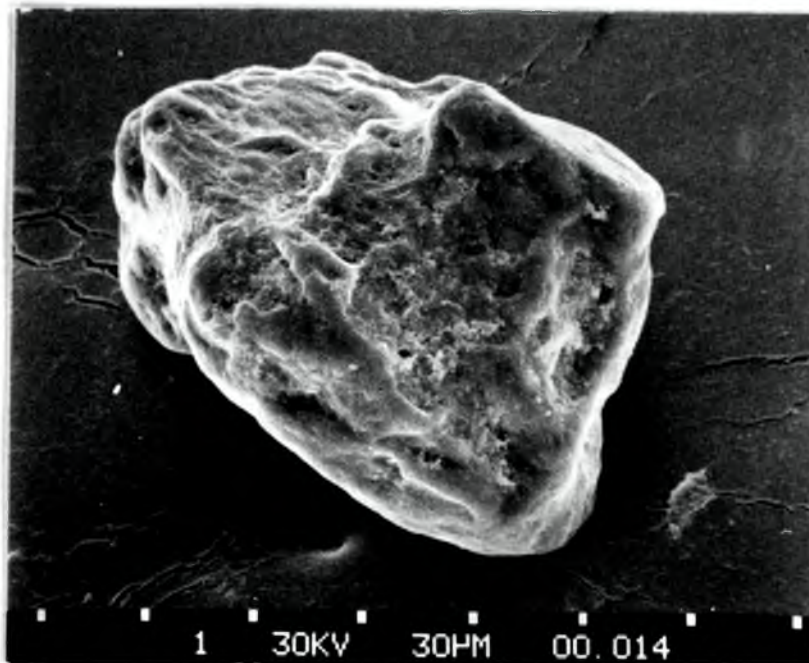


FIGURE 7.5: Optical Photograph of Quartz Grains Etched for
10 min in HF.

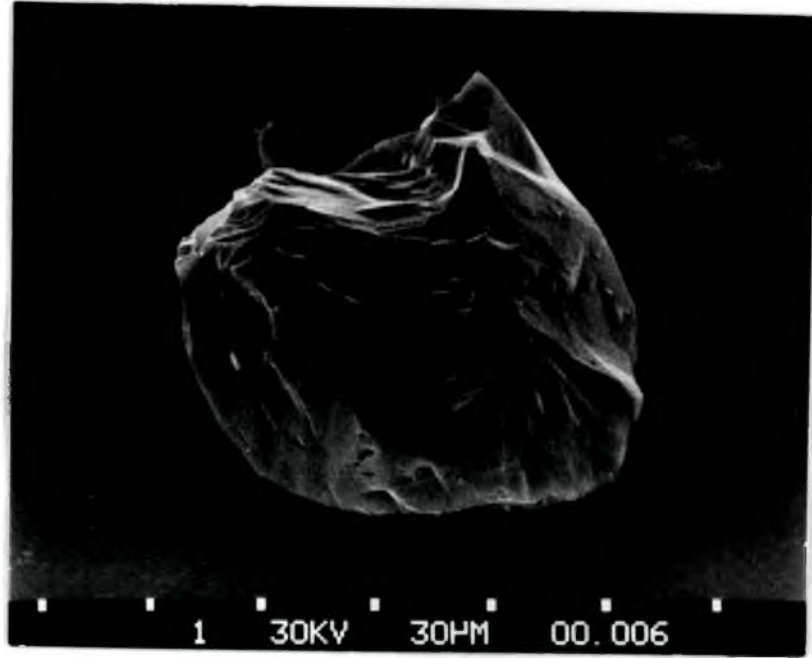


(a)

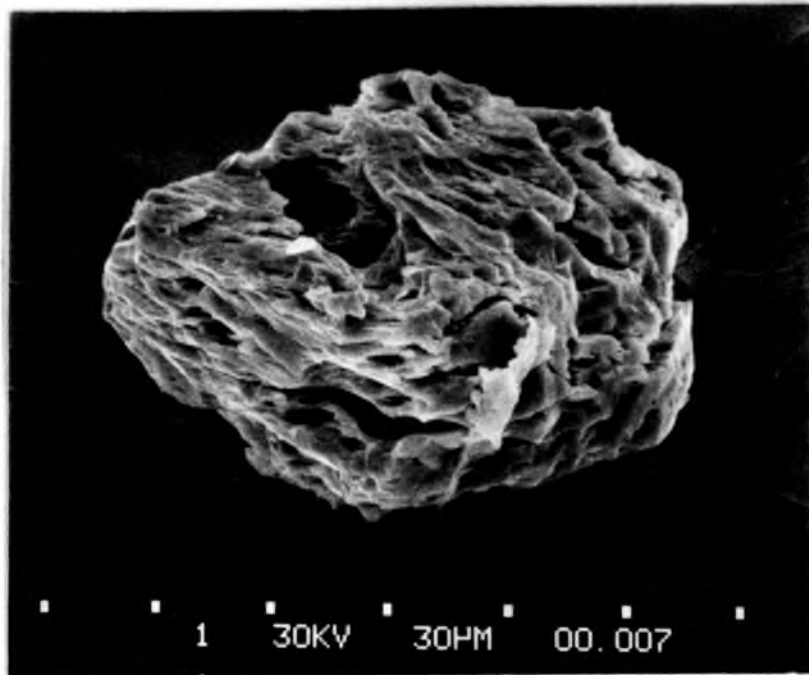


(b)

FIGURE 7.6: SEM Photographs of Individual Unetched Quartz Grains;
(a) shiny and (b) frosty.



(a)



(b)

FIGURE 7.7: SEM Photographs of Individual Quartz Grains Etched for 100 min in HF; (a) shiny and (b) frosty.

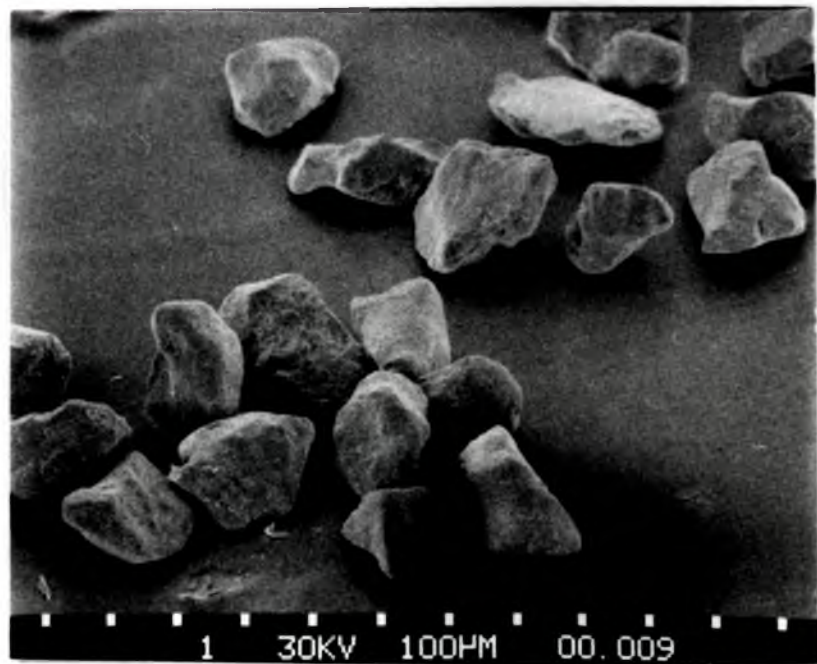
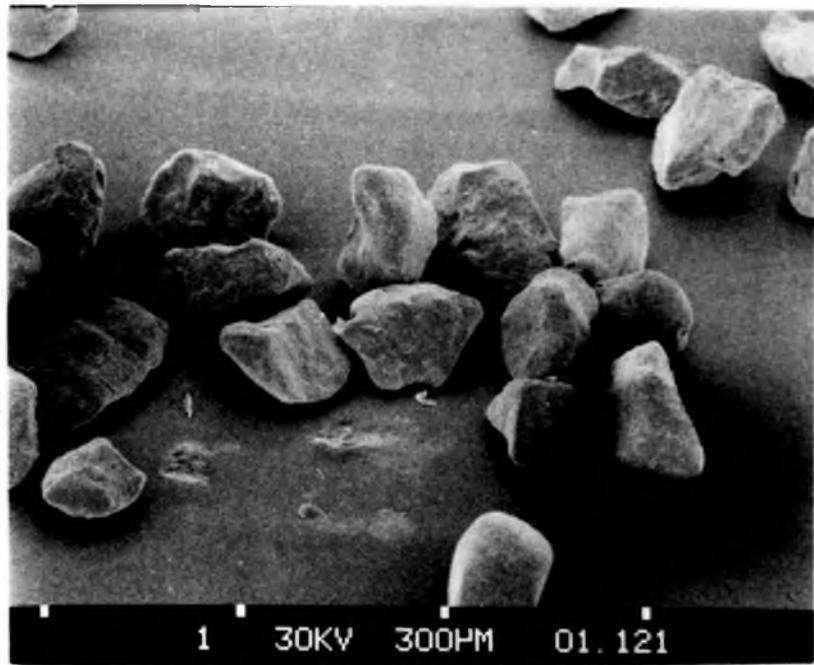


FIGURE 7.8a: SEM Photographs of Unetched Quartz Grains.

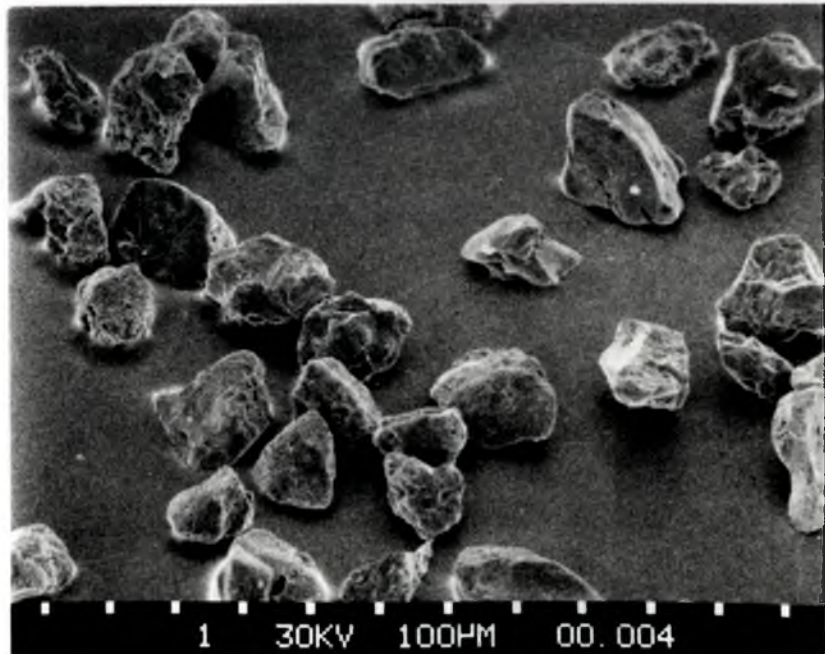
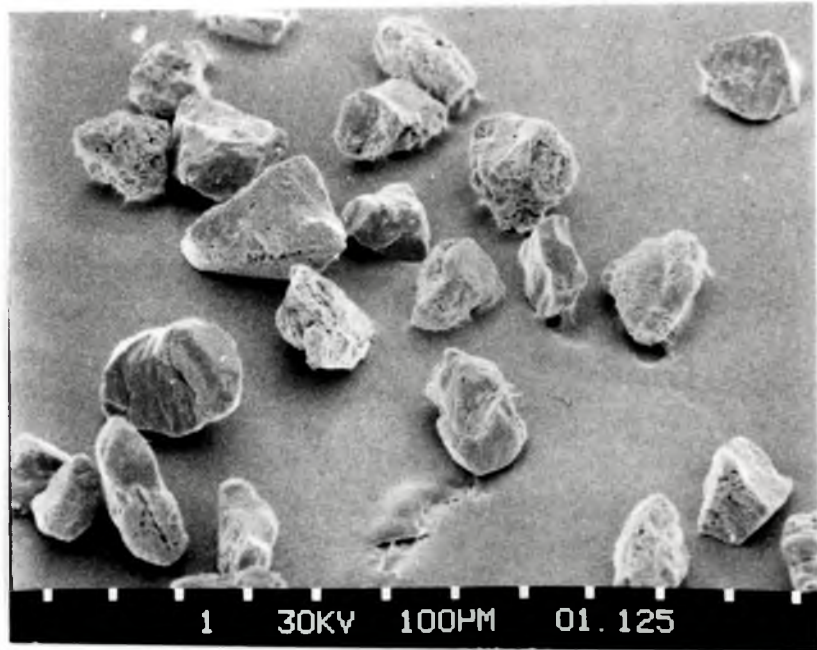


FIGURE 7.8b: SEM Photographs of Quartz Grains Etched for 10 min in HF.

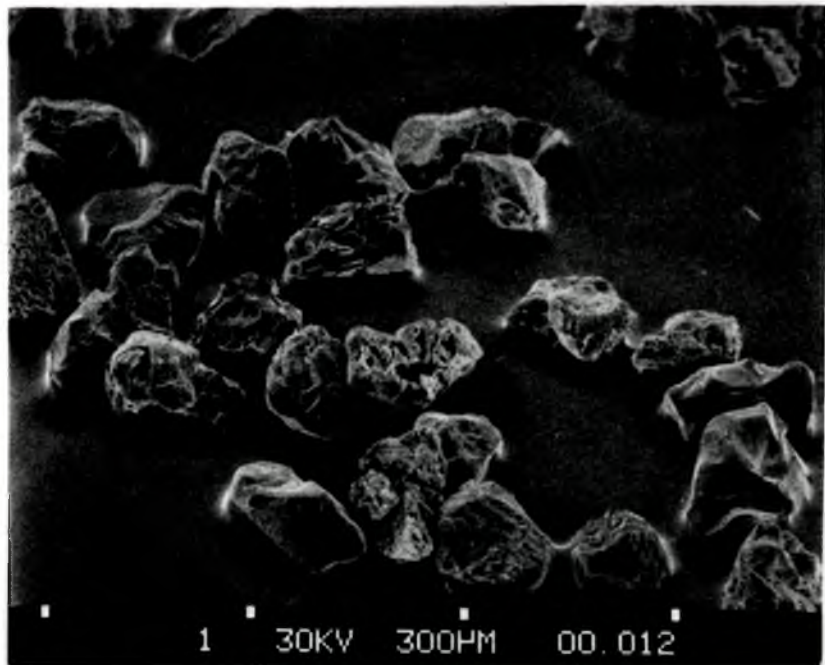
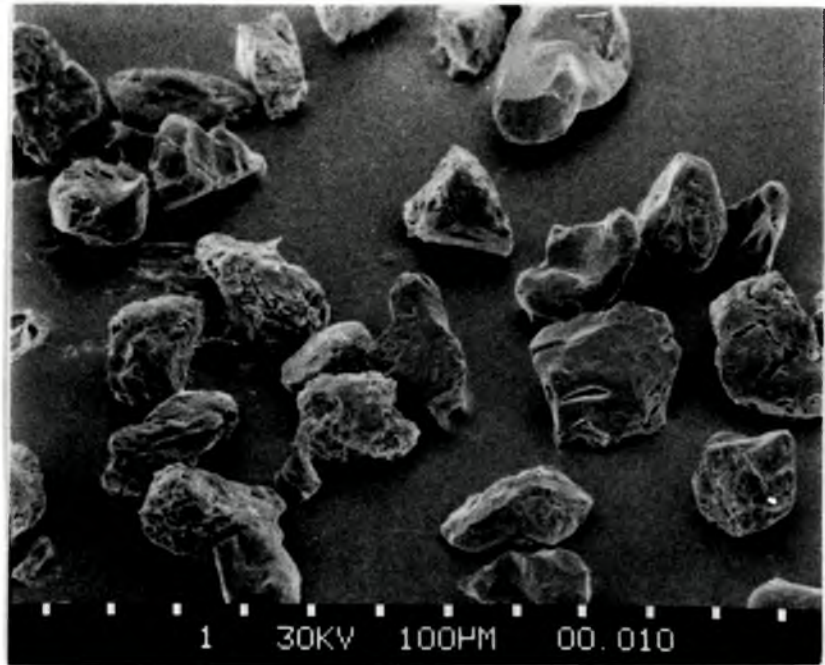


FIGURE 7.8c: SEM Photographs of Quartz Grains Etched for 40 min in HF.

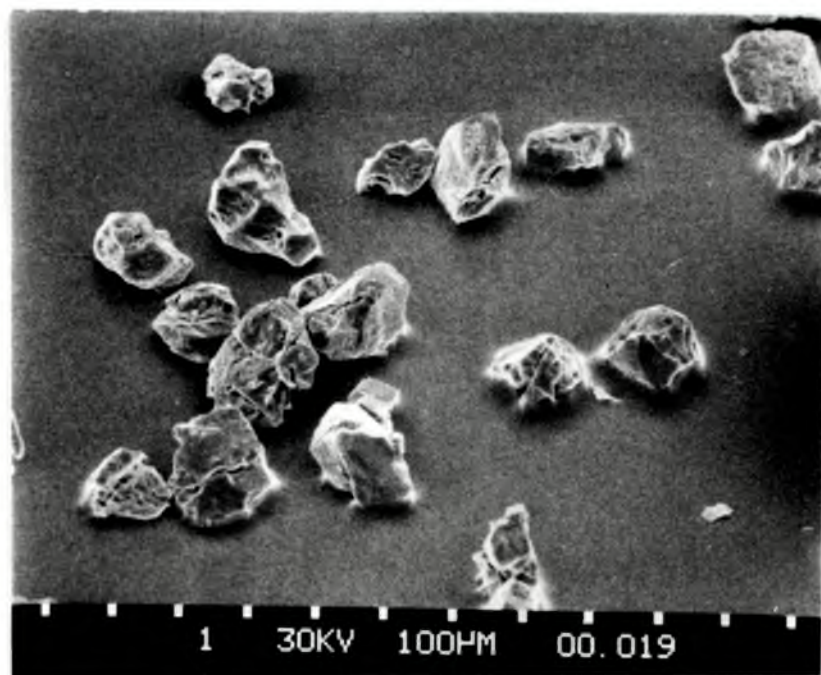
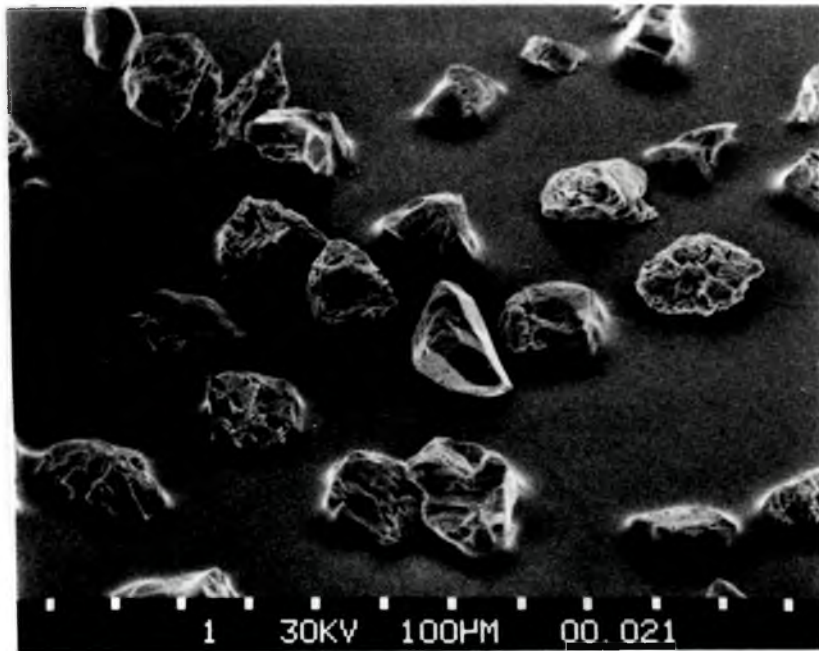


FIGURE 7.8d: SEM Photographs of Quartz Grains Etched for 100 min in HF.

removed than others. To confirm the variation in etching rates, weight loss experiments were performed on the frosty and shiny separates which had both been etched in HF as described above for 40 min. The weight of the frosty category was reduced by a factor of 0.50, corresponding to an isotropic etching depth of $\sim 10\mu\text{m}$. The shiny category was reduced in weight by a factor of 0.82, corresponding to an isotropic etching depth of $\sim 3\mu\text{m}$. The variation amongst individual grains will be even greater.

To ascertain whether this variable etching process is dependent on any visible internal differences in the grains, frosty and shiny grains were mounted and polished and then observed optically (Bell and Zimmerman, 1978). No internal differences were visible, in agreement with the observations of Lang and Miuscov (1967) that there was a direct correlation between HF acid etch tunnels and X-ray topographic images of dislocations in the crystal lattice structure.

For a sample matrix containing 12ppm thorium, 3ppm uranium and 1% K_2O and assuming a k-value of 0.1, the alpha contribution to the total effective dose is 14%. In the extreme, hypothetical case where all the material lost has occurred by complete dissolution of a small number of the grains with essentially no loss of material for the remainder, then the remaining sample would have no reduction of this alpha dose. In practice it is difficult to assess accurately the average reduction in the alpha dose because the variations in etching rate are so large. In certain cases it appears that the residual alpha contribution could be larger than 5% even after 40 min HF etching and hence would not be negligible contrary to the basic assumption of the quartz inclusion technique as proposed by Fleming (1970).

There are two obvious approaches for overcoming this problem but neither appears to offer a completely straightforward solution. The first would be to use an extremely long etching time in an attempt to

remove all of the alpha-dosed material. However, it is not clear how to be certain that the material remaining after such a long etch did not consist in part of the outer layers of some grains. Also there is the possibility that long etching times may have some influence on the TL output. This was tested by taking TL measurements on frosty and shiny separates after a 40 min etch. It was found that both fractions gave the same TL glow curve shape and sensitivity to within 10% reproducibility. The same glow curve shape was also observed for each of the different etching times indicating that the acid attack has negligible effect on the TL from the grains. In addition, the large reduction in sample size associated with long etching times would in some cases be quite untenable although this is not the case for the Mungo samples.

The second approach would be to etch for a minimum length of time, just sufficient to dissolve any feldspar grains present in the samples and to remove the discolouration from the surface of the quartz grains. The grains will then deviate as little as possible from the isotropic removal assumption and this would make the calculation of the alpha contribution for each sample easier. This method may still not be straightforward in all cases as the alpha efficiency can vary with depth in the outer grain layers due to the diffusion of impurities into these regions as reported by Fleming (1970). This second approach has, however, been adopted for the inclusion dating described in this thesis as the problems associated with its use appear to be much less difficult than those associated with the first method. The justification of the use of a minimum etching time is, therefore, given below.

For the Mungo samples the minimum etching time appears to be approximately 10 min in concentrated HF at room temperature. After this length of etching time the discolouration on the grain's surface has completely disappeared and X-ray diffraction analysis indicates that only quartz

grains remain present in the samples (see Figure 7.4). Weight loss experiments were carried out (i.e. the weight of quartz dissolved for a given etching time) and if we assume constant density and isotropic removal, the etching depth may then be calculated. For 10 min in HF as above, this etching depth is calculated to be 2.5 μm .

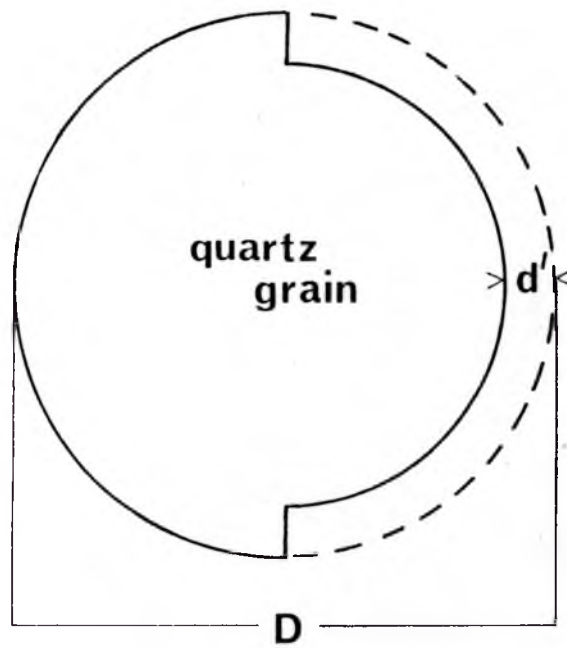
It is necessary to show that this isotropic etching depth (i.e. one based on weight loss experiments) may be used to assess accurately the alpha particle contribution when the actual etching process is a much more irregular process. To aid the calculations a non-isotropic case which has a high degree of symmetry is assumed and is shown in Figure 7.9a. This is a spherical grain of diameter D which has a layer d' removed from only half its surface. The normal isotropic removal case is shown in Figure 7.9b with a spherical grain of diameter D which has a uniform layer d removed from its surface. Obviously if we postulate that the weight removed from both grains is equal then $d' > d$. If $Y = d'/d$ then it can be shown by simple geometry that

$$Y = \frac{1}{d} \left\{ D/2 - \left[2(D/2 - d)^3 - (D/2)^3 \right]^{1/3} \right\} \quad (7.1)$$

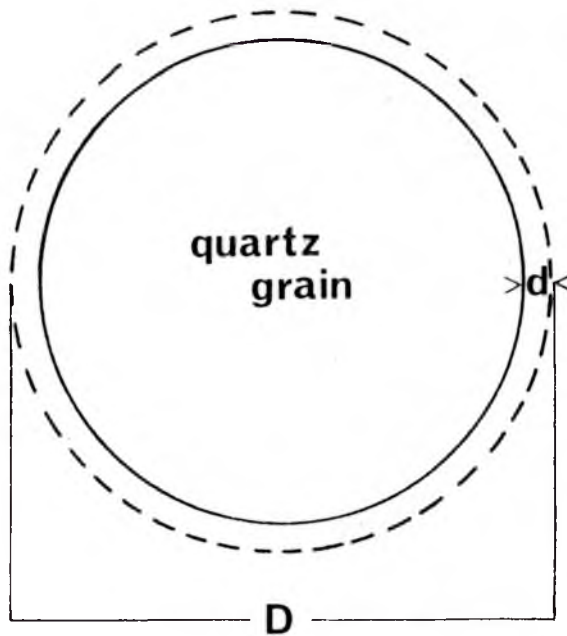
and values for Y may be calculated for $D=105 \mu\text{m}$ as given in Table 7.1.

The fraction of the alpha dose removed in a given layer may be taken from Chapter III and from the symmetry of Figure 7.9a it can be seen that the fraction of the dose removed by etching a complete layer d' is double that fraction removed by etching a layer d' over only half the grain's surface (as in Figure 7.9a). The fraction of the dose removed by etching an isotropic layer d , $\phi_\alpha(d)$, and the fraction removed by etching a non-isotropic layer d' over half the grain's surface, $\phi_\alpha(d')$, are compared in Table 7.2 for both the uranium and thorium series.

For values of d up to 5 μm the alpha dose removed from an isotropically etched grain is not significantly different from that removed from a



(a)



(b)

FIGURE 7.9: Isotropic and Non-isotropic Etching of Quartz Grains to give equal Weight Loss.

TABLE 7.1

Values of Y , the isotropic/non-isotropic
removal factor for a grain diameter D of $105\mu\text{m}$

<u>d (μm)</u>	<u>Y</u>
1.0	2.04
2.5	2.11
5.0	2.27
10	3.18
15	5.77
20	4.74

TABLE 7.2

Fraction of the alpha dose removed, in percent,
by etching isotropically and non-isotropically
(to give the same weight loss) for the uranium
and thorium series.

<u>d(μm)</u>	<u>Uranium</u>		<u>Thorium</u>	
	<u>Φ_α (d)</u>	<u>Φ_α (d')</u>	<u>Φ_α (d)</u>	<u>Φ_α (d')</u>
1.0	9.0%	9.0%	7.0%	7.3%
2.5	22.0	21.3	17.5	17.8
5.0	40.5	37.0	34.0	32.3
10.0	68.0	50.0	60.5	50.0
15.0	88.0	50.0	79.5	50.0
20.0	98.5	50.0	93.5	50.0

non-isotropically etched grain. Beyond $5\mu\text{m}$ the doses do become significantly different. At $2.5\mu\text{m}$, the isotropic etching depth used for the Mungo samples, the isotropic and non-isotropic doses are only 3.2% and 1.7% different for the uranium and thorium series respectively. This has been proven, of course, only for the particular case as depicted in Figure 7.9. Because of the approximately linear region in the initial stages of the alpha dose attenuation curve (see Figure 3.3), however, it is to be expected that for small etching depths even highly unsymmetrically etched grains will have an alpha dose attenuation similar to the isotropic case for equal weight loss. In addition, the restricted etching depth implies that the alpha dose removed will be small particularly when compared to the total dose (alpha plus beta plus gamma) and any errors in the estimation of the alpha dose removed will therefore also be small by comparison.

7.7 TL Response of the Outer Layers of the Quartz Grains

Fleming (1970) has shown that the diffusion of elemental impurities from the host clay matrix into the outer regions of the quartz grains during the firing process in antiquity can cause not only discolouration of the grains due to the formation of colour centres but also the creation of thermoluminescent centres in these outer layers. Etching for a limited time in HF to remove the discolouration will improve the transparency of the grains but it is necessary to determine whether it also removes the layers containing modified TL centres or, failing that, whether these layers significantly affect the overall TL from the grain.

To investigate this problem, the four samples of quartz grains which had received the different etching times (i.e. 0, 10, 40 and 100 min) were each crushed to fine grains and the 1 to $8\mu\text{m}$ size range was deposited on aluminium discs from a suspension in acetone as described by Zimmerman (1971). If the outer impurity diffused layers do significantly modify the

TL from the whole grain, then the alpha efficiency factors, k , will be quite different for these outer regions and the TL response to a given alpha dose for the four etched fractions should therefore be noticeably different.

To test this possibility, the crushed samples as prepared above were drained of any residual TL by heating to 500°C and then given a known alpha dose from a ^{242}Cm source (calibration details are given in Appendix A). The TL output from this is compared to the output for a known beta dose from a ^{90}Sr source (calibration details in Appendix C) for each of the etching times and the resultant alpha efficiency factors, k (as defined by equation 3.1), are given in Table 7.3.

As can be seen from Table 7.3 the k -values for each etching time are the same within experimental errors. The values for the no etch fraction are, perhaps, slightly higher on average but the difference is much less than the quoted errors. This implies that any modification of the TL from the outer layers due to impurity diffusion does not significantly affect the overall TL from the whole grain, particularly after a 10 min etch which removes a layer of approximately $2.5\mu\text{m}$ (based on isotropic weight loss).

To show this numerically, the volume fraction of a $105\mu\text{m}$ grain that is lost after 10 min etching is found to be about 14%. Considering the hypothetical case where the k -value of the outer $2.5\mu\text{m}$ was double the k -value of the inner grain volume, then the alpha induced TL from the crushed sample would be 14% higher than if the whole grain volume had the same k -value. If we assume that the limit to which we can experimentally differentiate the TL levels is 5%, then the maximum value the k -value for the outer $2.5\mu\text{m}$ can have is about one third higher than that of the rest of the grain volume. Now from the etching data of Chapter III, we have that approximately 18% of the alpha dose from the natural radioactive

TABLE 7.3

Alpha Efficiency Factors for the Different Etching Times

Fireplace	No Etch	10 min.	40 min.	100 min.
F6	0.065 ± 0.003	0.064 ± 0.003	0.065 ± 0.003	0.064 ± 0.003
F7	0.069 ± 0.004	0.067 ± 0.004	0.066 ± 0.004	0.064 ± 0.003
F8	0.063 ± 0.003	0.061 ± 0.003	0.062 ± 0.003	0.060 ± 0.003
F9	0.063 ± 0.003	0.060 ± 0.003	0.064 ± 0.003	0.061 ± 0.003
S7	0.067 ± 0.004	0.068 ± 0.004	0.066 ± 0.004	0.066 ± 0.004

series is contained in the outer $2.5\mu\text{m}$ and hence for a k-value one third higher in these regions, the overall natural TL from the alpha dose would be a maximum of 6% higher than for a grain with the same k-value over the whole volume. However, since the alpha dose is only about 10% of the total archaeological dose received by the samples, then the maximum error involved would be only 0.6%.

The same is true if the k-value was in fact double for the outer layers but the impurity diffusion had only taken place to a distance of $1\mu\text{m}$ from the grain's surface. Just over 5% of the grain's volume is contained in the outer $1\mu\text{m}$ and 7.5% of the alpha dose lies there also. Hence at a limit of 5% experimental differentiability, the k-value could be double. This gives a possible maximum error of 7.5% in the natural TL alpha dose, and hence a maximum error of 0.75% in the overall dose assessment.

Since no observable difference in the k-values could be detected, it is assumed that the situation for the Mungo quartz is either i) the k-value for the outer $2.5\mu\text{m}$ is very similar to that for the rest of the grain, or ii) the k-value is dissimilar for the outer layers but the diffusion front is much less than $2.5\mu\text{m}$, or, more probably iii) a combination of the above two cases has taken place. Hence, the k-value measured for the 10 min etch fraction, i.e. the fraction with an isotropic layer of $2.5\mu\text{m}$ removed, is the value used in the determination of the residual alpha dose for each fireplace.

7.8 Measurement of the Archaeological Dose

The 'additive' procedure as described in Chapter I was the method adopted for the measurement of the Archaeological Dose (AD) received by the Mungo samples. This method involves the application of artificial

laboratory beta doses in addition to the natural radiation dose the samples have received in order to suppress any possible errors due to sensitivity changes during the glowing out process. This has already been discussed in Section 1.8 particularly with regard to the measurement of the supralinearity correction, I.

The quartz grains, prepared as detailed in the previous Sections, were deposited on aluminium discs approximately 1 cm in diameter by means of the dispenser illustrated in Figure 7.10 which was designed and built specifically for this purpose. A hole in the rectangular block is filled with grains and then levelled with a straight edge. The grains are then dumped gently through the funnel onto the aluminium disc. The weights of over two hundred such dispensings were noted and it was found that just under 5 mg of the quartz grains were deposited with a standard deviation in the individual weights of less than 2%.

The disc with the quartz grains is then placed on the nichrome heating strip (Figure 7.11a) and the heat shield placed in position (Figure 7.11b) in order to measure the TL output. Beta irradiations are performed on the heating strip by placing a source holder in position (Figure 7.11c) to carry the ^{90}Sr source which was calibrated in this position (see Appendix C). Lead shields are placed around the apparatus when irradiations are taking place.

The heating rate used throughout these studies was 5°C per sec. This slower heating rate (compared to the more usual 20°C per sec) was used because of the problem of thermal lag between the grains and the aluminium discs. The results of the slower heating rate are: i) a decrease in the TL intensity as predicted by both equations (1.4) and (1.10) - this decrease is not a serious drawback here because of the extremely high light levels from the samples even at 5°C per sec; and ii)

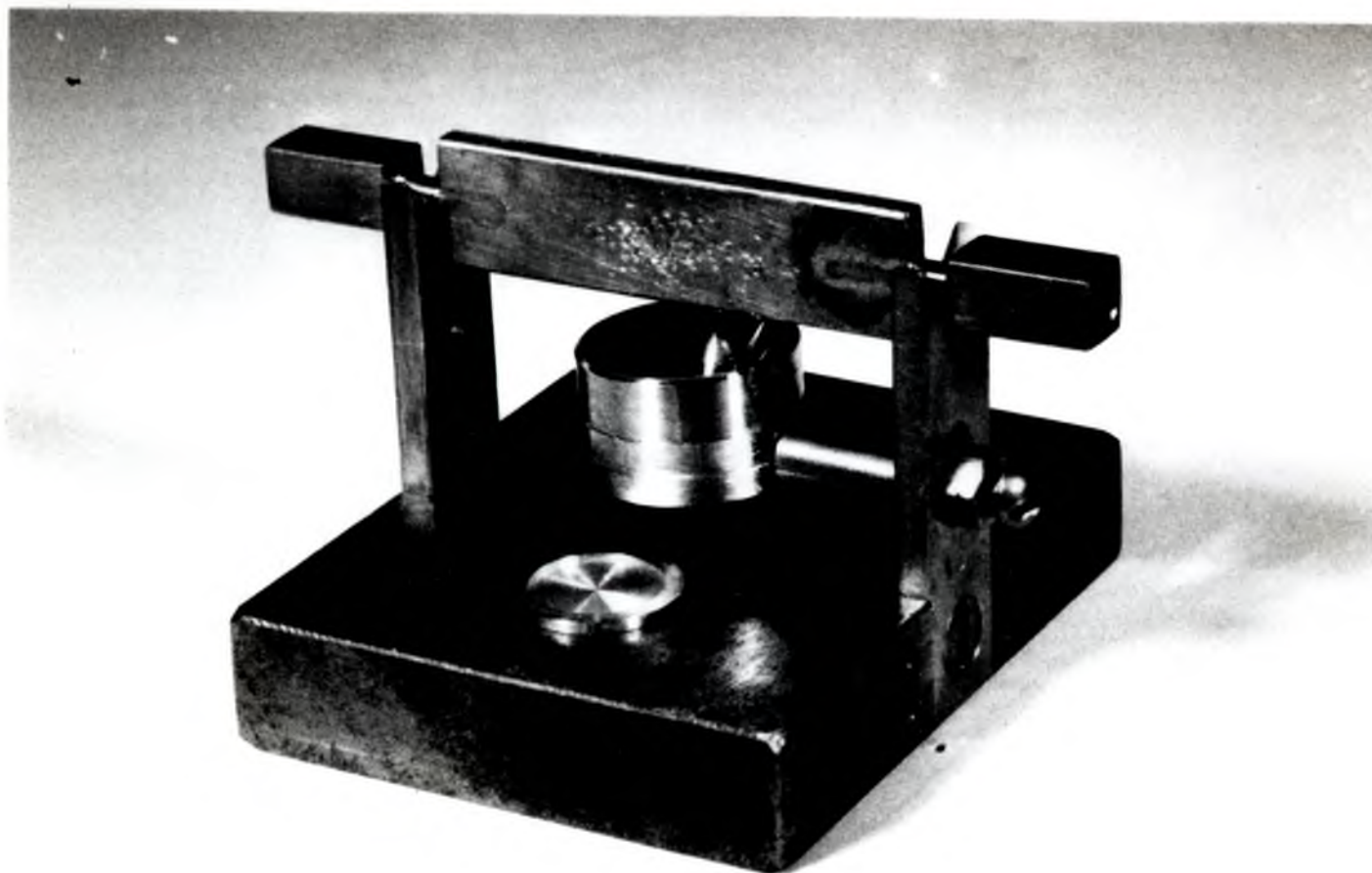


FIGURE 7.10: Dispenser for depositing Quartz Grains on Aluminium Discs.
Equal portions (approximately 5 mg) are dispensed onto each disc.

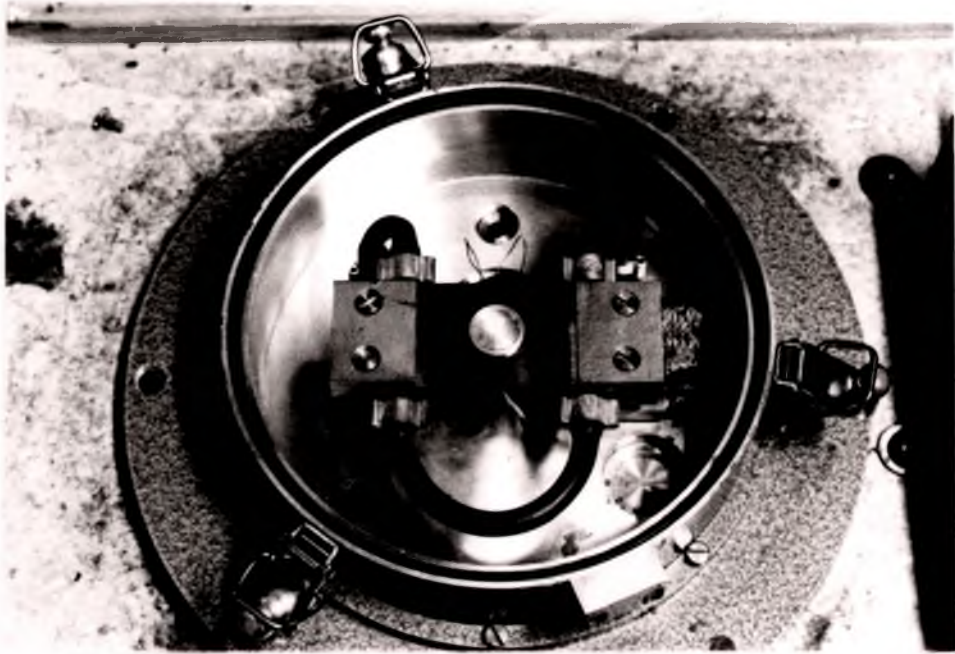


FIGURE 7.11a: Aluminium Disc with Quartz Grains Resting
on Nichrome Heating Strip.

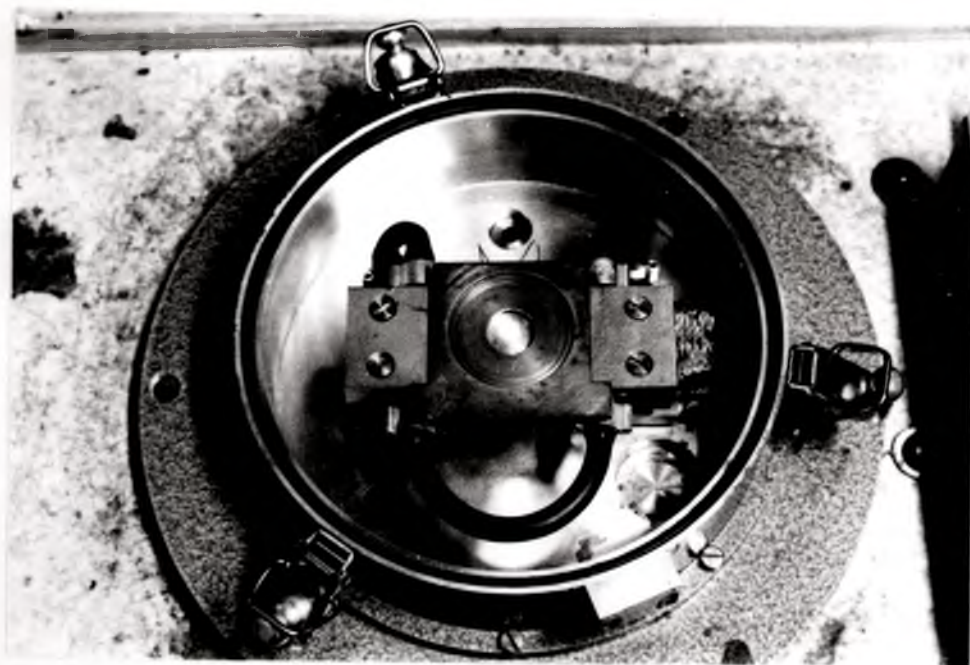


FIGURE 7.11b: Heat Shield in position on Nichrome Heating Strip.

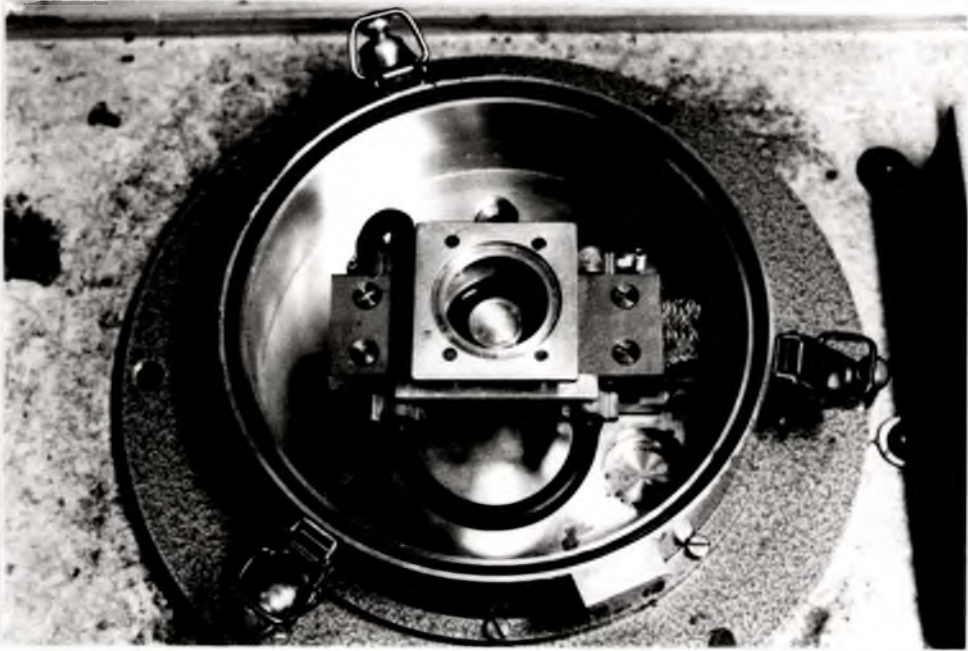


FIGURE 7.11c: Beta Source Holder in position on Heating Strip.

a shifting of the so-called '375°C' peak to a lower temperature as predicted by both equations (1.6) and (1.11). For the Mungo quartz the main peak was seen to occur at about 355°C (as depicted in Figures 7.13 - 7.17).

The intensity of the light output at any given temperature and heating rate is proportional to the absorbed radiation dose and therefore measurements of the peak heights are used in determining the AD. The height of the glow curve much below the peak will probably suffer interference from the malign lower temperature peak (see Chapter I, Section 1.8) whereas the height of the glow curve much above the peak will suffer interference from the thermal black-body radiation.

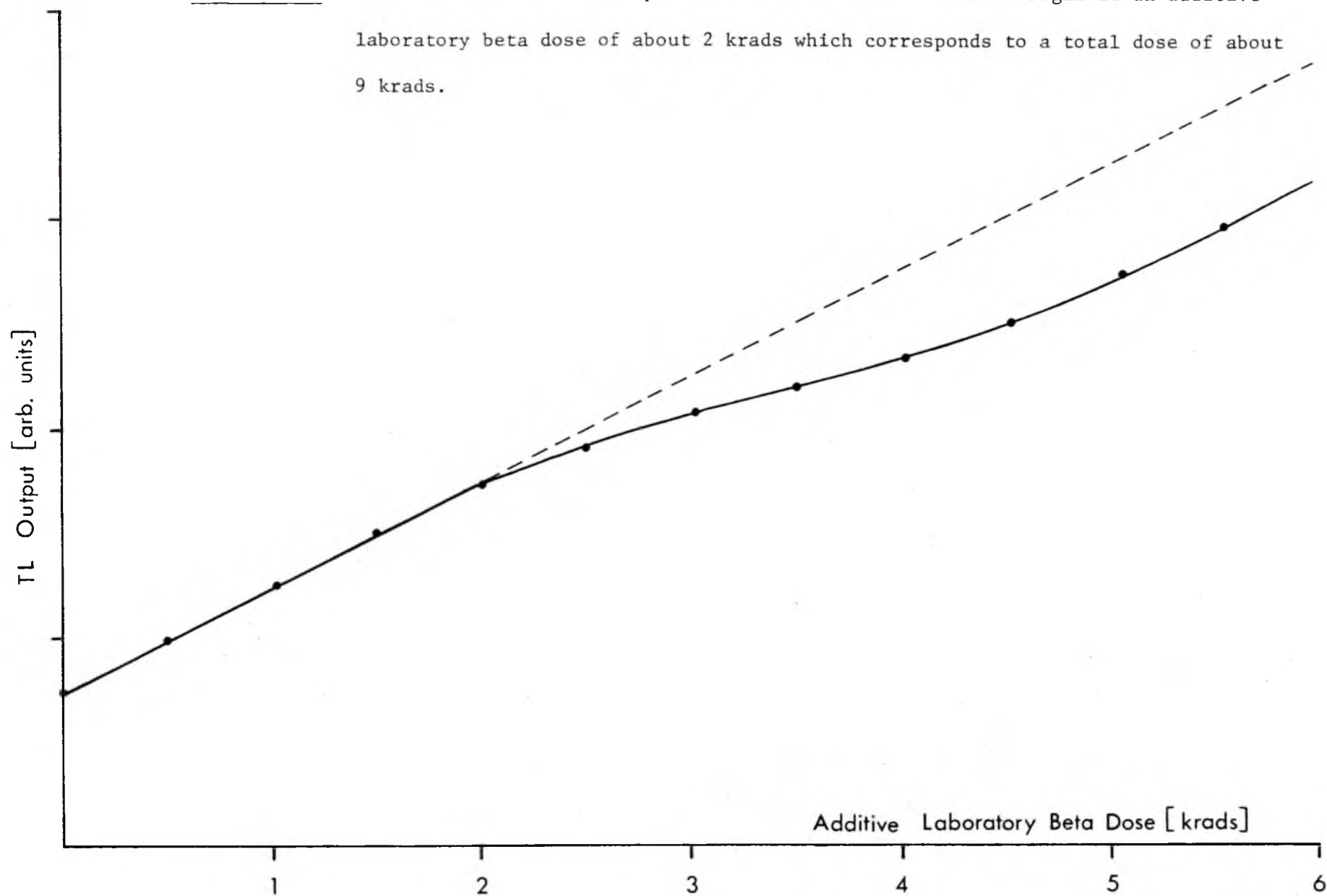
7.9 Saturation Tests on the Mungo Quartz

In Section 1.8(b) the saturation of the TL traps due to high radiation doses was discussed. In view of the high AD the Mungo quartz has received it was thought propitious to investigate what levels of additive laboratory beta doses could be applied to the samples before the non-linearity associated with the saturation effect set in.

Prepared samples from each of the fireplaces were given laboratory beta doses in addition to the natural archaeological dose they had already received. For each fireplace three discs were used for each dose level and the mean value taken. Additive laboratory beta doses up to a value of approximately 9 krads were administered to the samples in steps of approximately 500 rads (the word 'approximately' is used here because the actual doses were measured accurately by the time of irradiation, i.e. in seconds, and then converted to rads using the source calibration figure. The true value was 506 rads which corresponds to 210 secs, or 3½ min, of irradiation with the beta source).

The results of this experiment are shown in Figure 7.12 for fireplace F9, the fireplace which has received the highest AD as will be

FIGURE 7.12: Saturation Curve for Fireplace F9. Saturation is seen to begin at an additive laboratory beta dose of about 2 krad which corresponds to a total dose of about 9 krad.



shown in later Sections. It can be seen that the increase of TL with dose is linear up to a total (AD plus laboratory dose) of approximately 9 krad. Above this value the response becomes less than linear because of the onset of saturation of the TL traps. The curve does not completely level off but increases in a non-linear fashion due to radiation damage within the crystal lattice structure creating defects which can form additional TL trapping sites (Fleming, 1969). Figure 7.12 can be compared with Figure 1.7 in Chapter I which is the high dose saturation curve for Norwegian alpha quartz taken from Fleming (1969). The shapes of the two curves are seen to be quite similar.

Each of the other fireplaces gave almost exactly the same curve shapes and, within experimental errors, the same limit of linearity. That is to say, for each of the fireplaces tested in this present investigation, the non-linearity associated with the onset of TL trap saturation sets in when the quartz has received a total dose of about 9 krad. Thus only additive beta doses which give a total dose of less than 9 krad were used throughout the present experiments.

7.10 Results of the Archaeological Dose Measurements

In all, five fireplaces (F5, F6, F7, F8 and F9) and two samples from supposedly unbaked clay (S6 and S7 were tested). The unbaked samples were studied as a check that the geological TL was still present and that the TL from the fireplaces was not itself geological. S6 gave results which appeared to indicate saturation, i.e. a very high natural TL level and the increase in TL for additive laboratory doses small, predicting an age of several hundred thousand years. It was surmised, therefore, that this material had suffered no heat treatment, at least during archaeological times. S7, however, did give light levels and an archaeological dose consistent with those of the other fireplaces. Barbetti (1976) has measured

the thermoremanent archaeomagnetism (see next Chapter) of all of these samples and he too found that S7 appears to have been baked. Thus, although perhaps not a fireplace in the archaeological context, it is included here as such.

Fireplace F5 is not situated with the other fireplaces in the Walls of China but is located actually down on the lake bed. Since the lake dried up some 16,000 years ago, this fireplace must be younger than this. In fact it appears to be much younger, hence a different TL dating technique, that known as the 'Pre-dose technique' (Fleming, 1973) described in Chapter X, was used for this fireplace alone.

The peak heights of the glow curves were measured for the natural TL output and for the natural plus additive laboratory beta doses in steps of 500 rads to a maximum total dose of not more than 9 krad. Typical glow curves for the natural and natural plus beta dose are shown for each of the fireplaces in Figures 7.13 - 7.17. Very many discs were glow out at each level in order to overcome the statistical uncertainties of having the points on the TL growth line relatively close together. A minimum of 50 discs was used for each fireplace.

To avoid errors due to any pre-dose effect (see Figure 1.8), only those discs which had been used to measure the natural TL were given a laboratory beta dose and glow out a second time to measure the supra-linearity correction I. In this way all the discs which were glow out a second time had received the same pre-dose (i.e. the AD) and hence any sensitivity enhancement should be constant.

To test whether the trapping centres responsible for the peak in the TL glow curve are of sufficient depth to have lifetimes sufficiently long for dating purposes, the 'plateau test' (Aitken and Fleming, 1972) was carried out for each fireplace. This was done by comparing the glow curve shape of the natural TL with that of the natural plus laboratory beta dose.

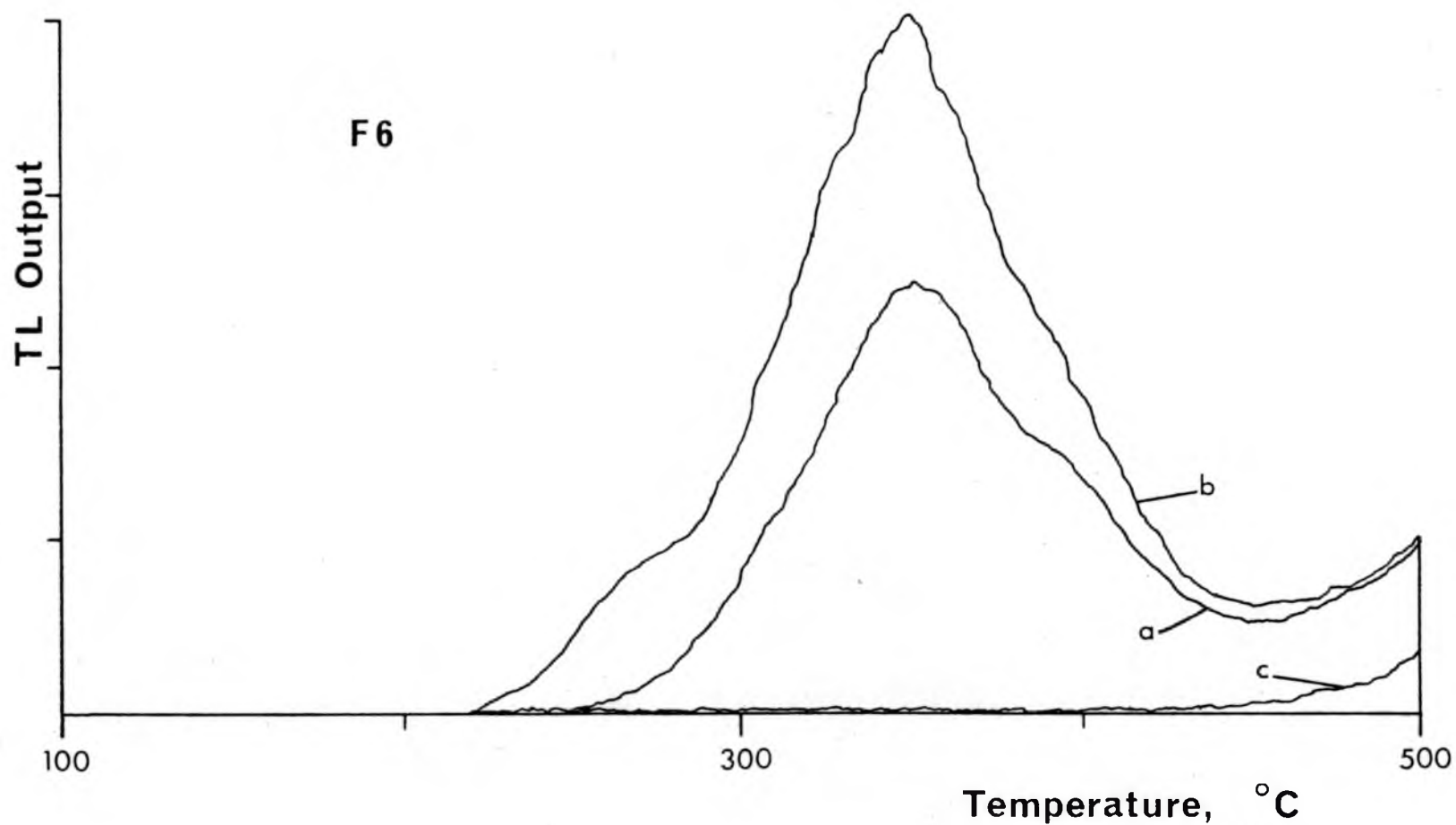


FIGURE 7.13: Actual TL Glow Curve for Fireplace F6. The heating rate was $5^{\circ}\text{C sec}^{-1}$ and the peak occurs at 355°C . Curve a is the natural TL; curve b is the natural plus additive laboratory radiation dose and curve c is the background black-body glow obtained by heating the sample a second time to 500°C after it has cooled. The true TL response is given by curve a or curve b minus curve c.

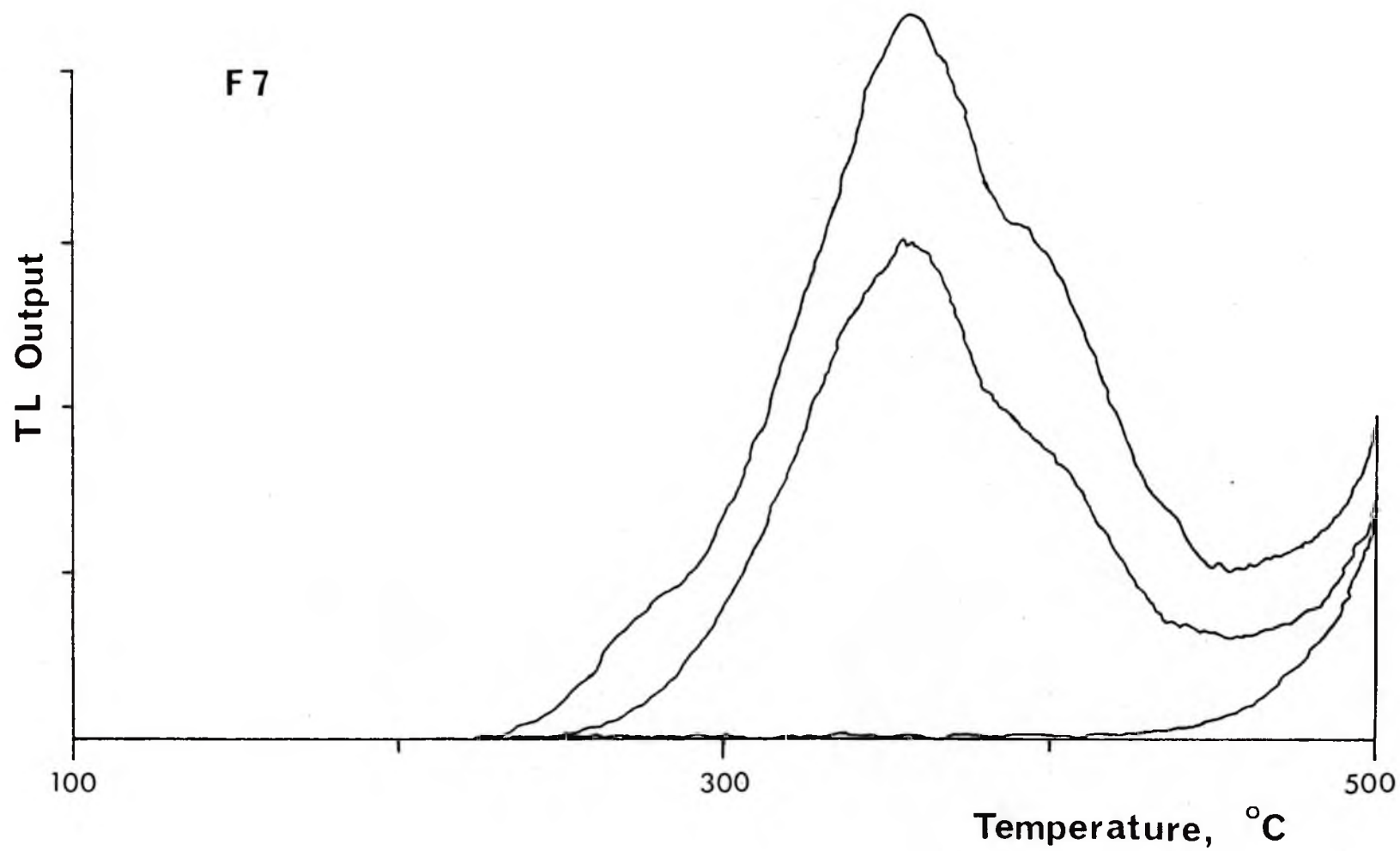


FIGURE 7.14: Actual TL Glow Curve for Fireplace F7.

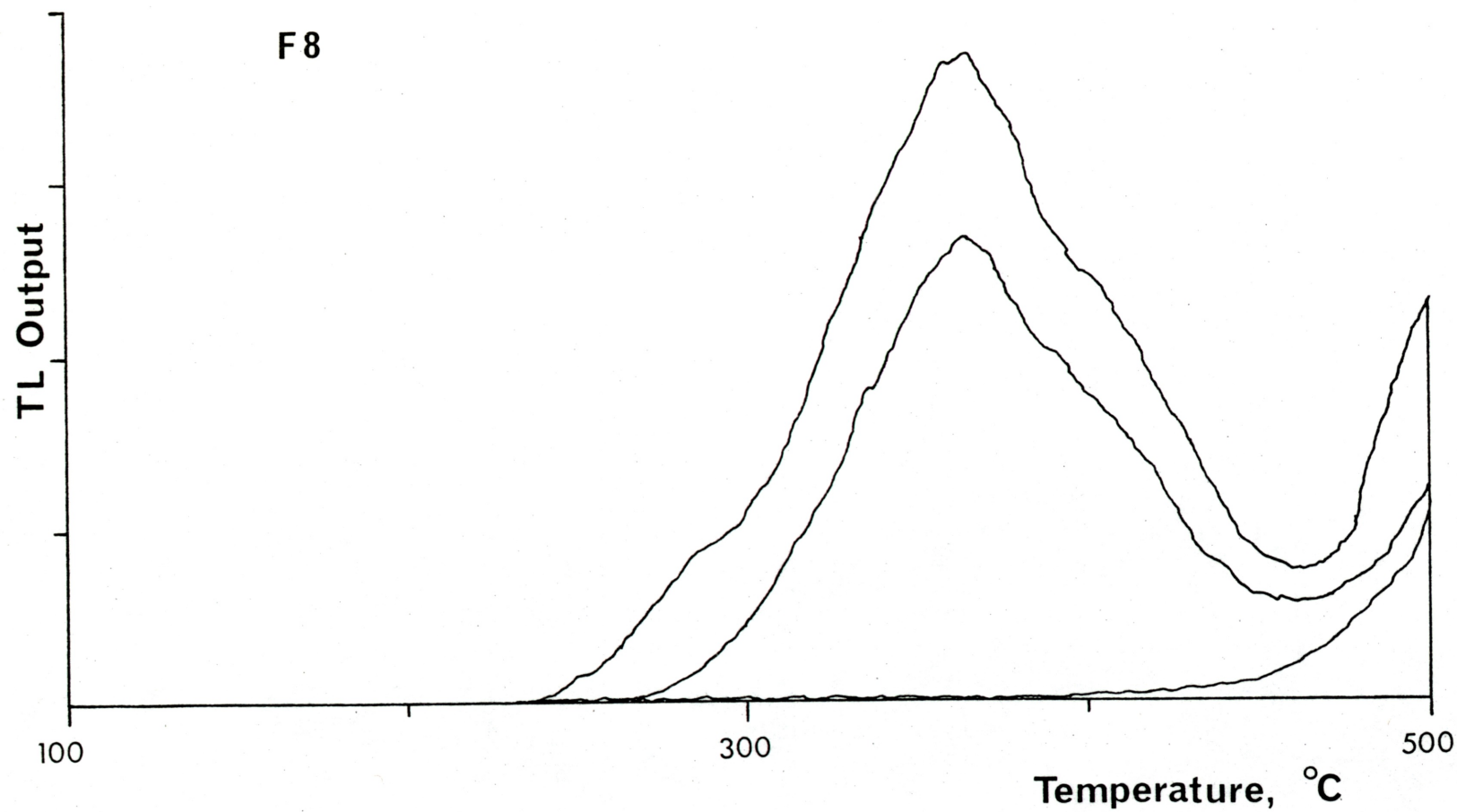


FIGURE 7.15: Actual TL Glow Curve for Fireplace F8.

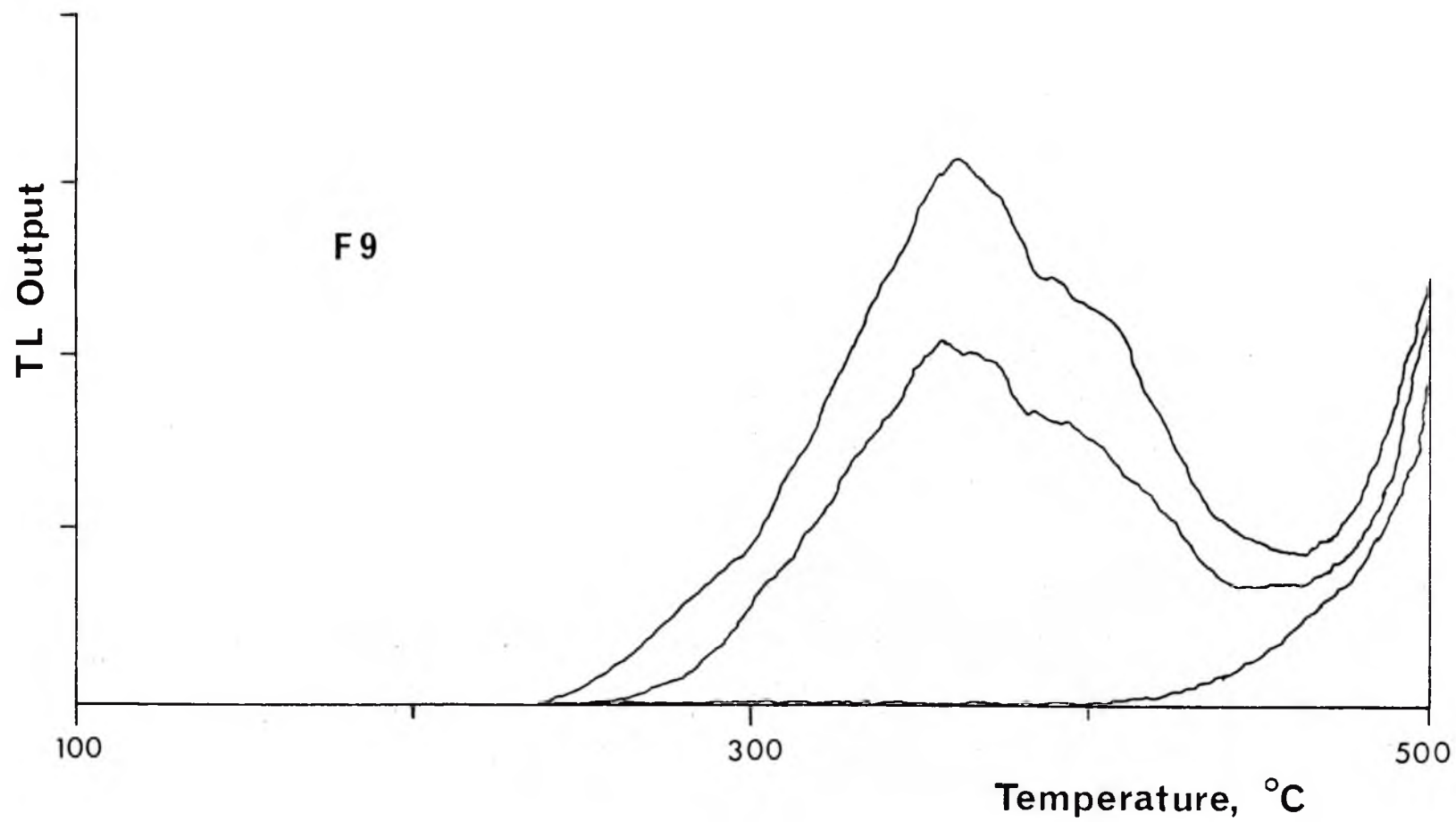


FIGURE 7.16: Actual TL Glow Curve for Fireplace F9.

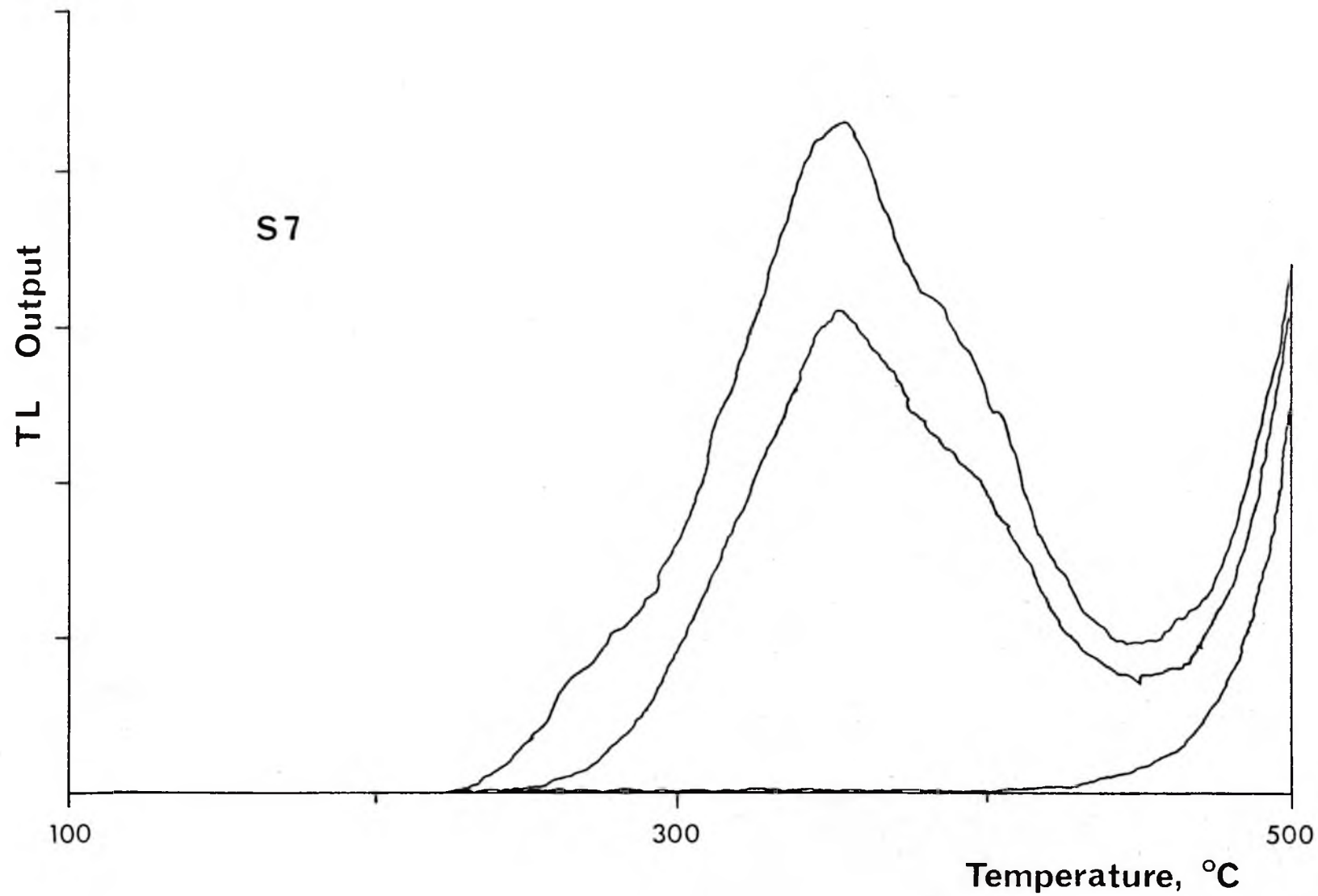


FIGURE 7.17: Actual TL Glow Curve for Fireplace S7.

If A is the natural TL output at any given temperature and B is the output for the natural plus beta dose at the same temperature, then the ratio $A/(B-A)$ may be calculated as a function of temperature in steps of 25°C . The plateaux for each of the fireplaces are shown in Figure 7.18 a-e. As can be seen, below about 225°C the ratio is effectively zero but it rises sharply to a constant level at about 325°C . This plateau is evidence that there is a temperature range over which there is no fading of the natural TL. For every fireplace it includes the range about 355°C , at which temperature the glow curve maximum is seen to occur. It should be noted that all of the discs for each fireplace were held at 150°C for 5 minutes before the actual glow out was made in order to ensure that the laboratory induced TL in the high temperature region of the glow curve was indeed associated with sufficiently deep traps (Aitken and Fleming, 1972).

To illustrate the variability of the experimental data and also to show how the data are used to evaluate the AD, an actual example is worked through below. The example chosen is fireplace F7 which turns out to be the oldest fireplace investigated here. A total of 63 discs were glow out for F7 and Table 7.4 shows the results of these tests. In this Table, N refers to the natural TL output and β refers to the output induced by a laboratory beta irradiation of $3\frac{1}{2}$ mins (i.e. 506 rads). Hence $N + \beta$ is the TL output of the natural plus beta dosed samples. The TL output figures quoted are in arbitrary light units measured at 355°C and are the mean values for the number of discs glow out at that level. S.D. is the standard deviation of the mean. The results are shown graphically in Figure 7.19 which may be compared with Figure 1.9.

The results for each of the discs are then fed into a computer programme which performs a linear 'least squares fit' to all of the data points and extrapolates the line to give the intercept on the dose axis for both ED and I. The programme then calculates the standard error in

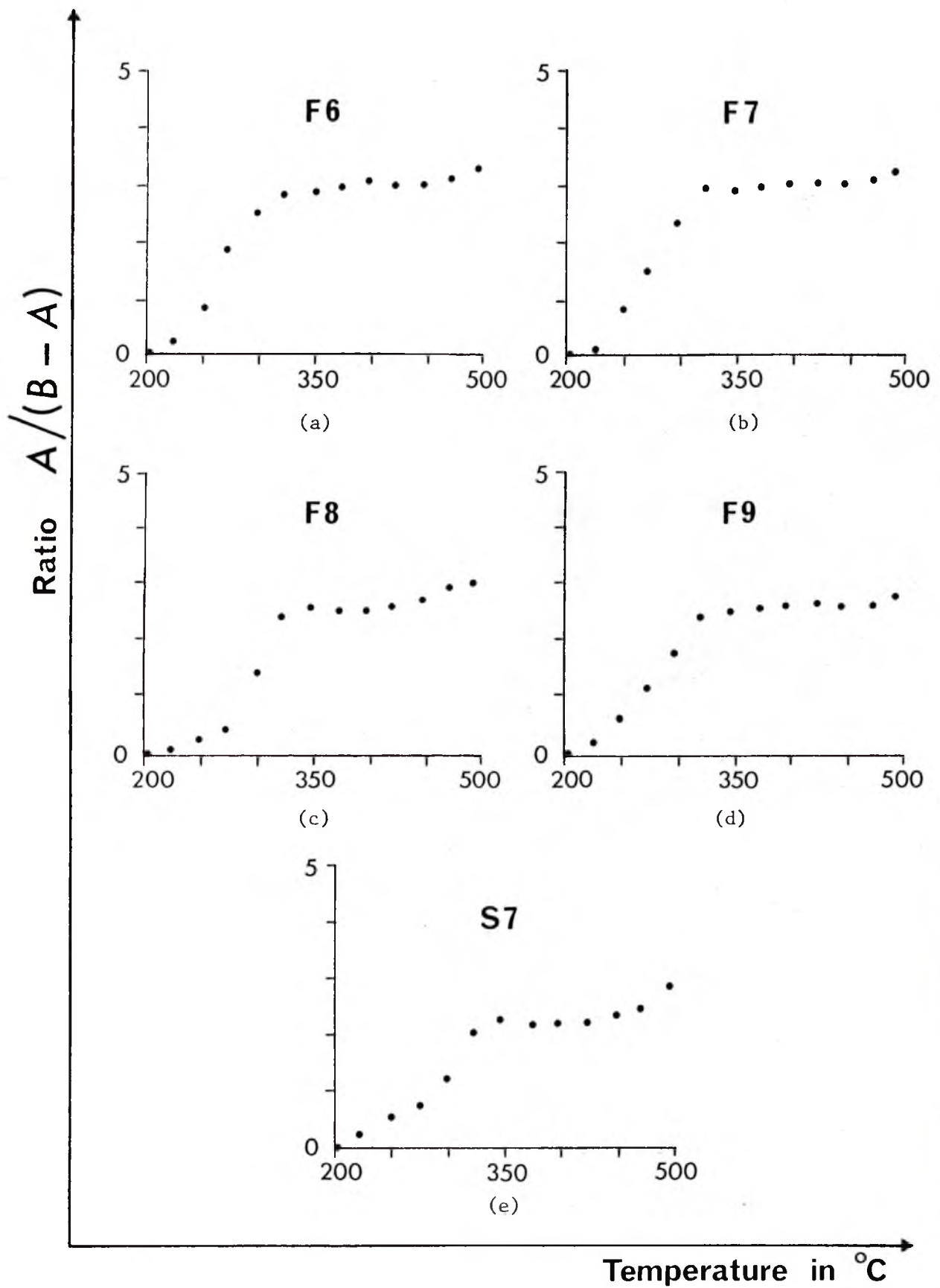


FIGURE 7.18: Plateau Test for each of the Lake Mungo Fireplaces.

TABLE 7.4

Experimental Data for Fireplace F7

<u>ED</u>			
<u>TL Level</u>	<u>No. of Discs</u>	<u>TL Output</u>	<u>S.D.</u>
N	20	63.9	2.3%
N + β	10	68.9	3.1%
N + 2 β	12	73.8	3.2%
N + 3 β	11	79.6	2.9%
N + 4 β	10	84.5	2.7%
 <u>I</u>			
β	4	1.3	5.4%
2 β	4	6.6	5.7%
3 β	4	11.6	6.5%
4 β	4	16.8	6.1%
5 β	4	21.8	6.3%

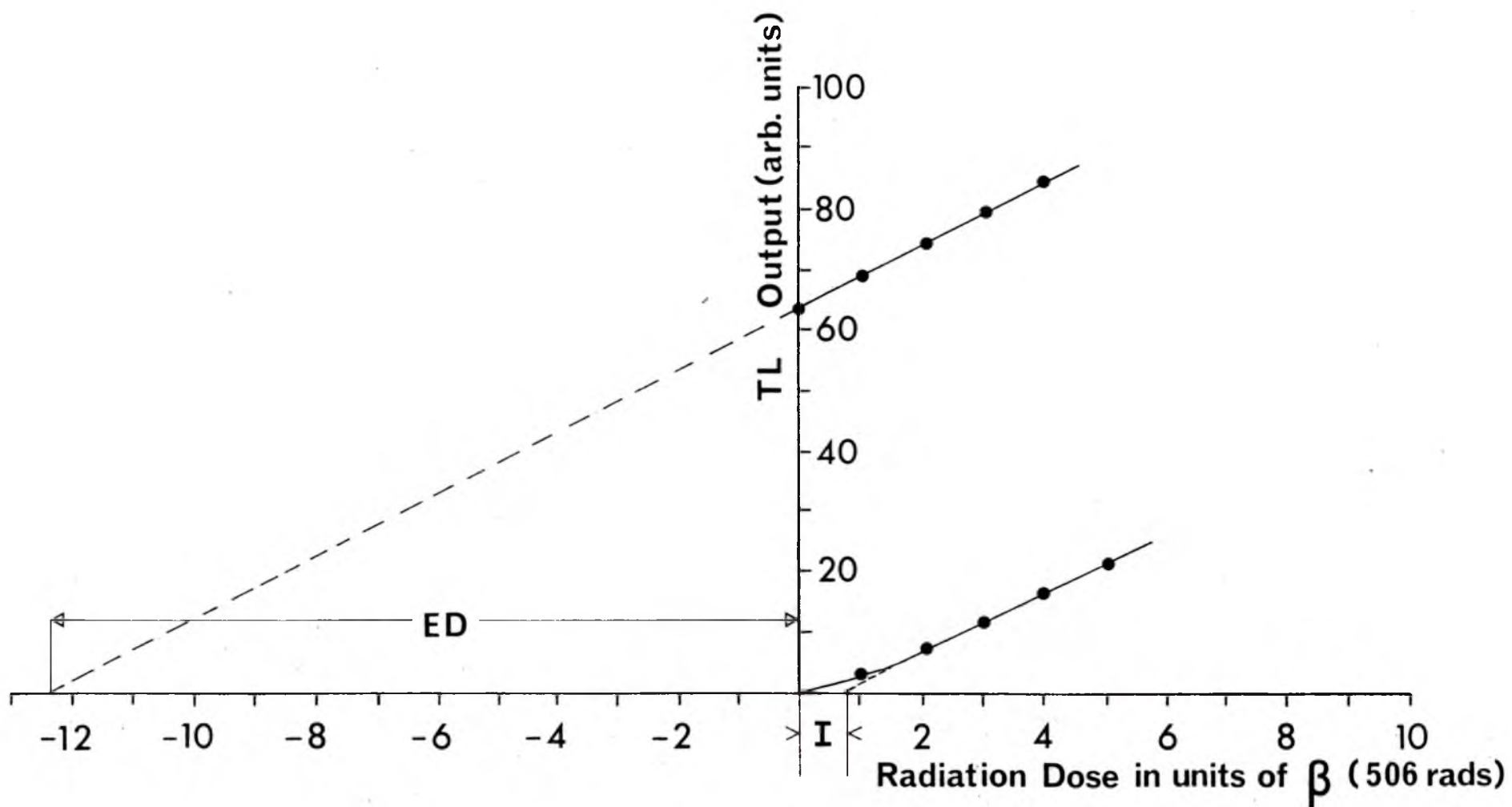


FIGURE 7.19: Additive Procedure for Fireplace F7. The archaeological dose is given by the equivalent dose ED, plus the supralinearity correction, I.

each of the intercepts (full details of the statistical formulae used in the programme are given in Appendix E). The results for F7 at 355°C are:

$$ED = 6220 \pm 250 \text{ rads}$$

$$I = 370 \pm 120 \text{ rads}$$

In addition, the ratio of the slopes of the first and second glow outs are calculated to check if sensitivity changes have occurred during the first glow out and/or if there is any interference from the lower temperature peak. If neither of these effects has taken place then the slope of the first glow out should be the same as that of the second and the supralinearity figure, I , calculated from the second glow out is a valid approximation of the first part of the original TL growth curve. If the ratio is not unity then the supralinearity correction will be different as has already been illustrated in Figures 1.5 and 1.6. Fleming (1970) introduced a 'parallel slopes' criterion which implied that the supralinearity correction was valid only if the slopes were parallel to within an accuracy of $\pm 5\%$. As can be seen in Table 7.5 some of the fireplaces do not quite satisfy this criterion. However, they all do satisfy a criterion of $\pm 10\%$ and since the supralinearity correction is in all cases less than 6% of the AD, this small change in sensitivity will not be significant. For F7 the ratio of first to second glow out slopes is 1.01 at 355°C and hence the AD is given by $ED + I$, which is equal to 6590 rads.

The results for each of the other fireplaces were evaluated in exactly the same way (with the exception of F5, as discussed earlier in this Section) and these data are presented in Table 7.5 for the 355°C peak in the glow curve of the Mungo quartz for each fireplace. In addition, measurements were made 25°C above the peak (i.e. at 380°C) and at 25°C below the peak (i.e. at 330°C) and these results are given in Table 7.6. The values of AD for each of the three temperatures are extremely close, indicating good uniformity over most of the plateau region. As stated

TABLE 7.5

Archaeological Dose Measurements for
the Lake Mungo Fireplaces

<u>Fireplace</u>	<u>Slope Ratio of first glow/second glow</u>	<u>ED (rad)</u>	<u>I (rad)</u>	<u>AD (rad)</u>
F6	1.04	5210 \pm 200	320 \pm 100	5530 \pm 225
F7	1.01	6220 \pm 250	370 \pm 120	6590 \pm 280
F8	1.10	6100 \pm 250	380 \pm 120	6480 \pm 280
F9	0.93	6670 \pm 270	400 \pm 130	7070 \pm 300
S7	1.09	6490 \pm 250	390 \pm 120	6880 \pm 280
F5	-	-	-	89 \pm 5

TABLE 7.6

Archaeological Dose Measurements at Three Different Temperatures

Fireplace	330°C			355°C			380°C		
	<u>ED</u>	<u>I</u>	<u>AD</u>	<u>ED</u>	<u>I</u>	<u>AD</u>	<u>ED</u>	<u>I</u>	<u>AD</u>
F6	5230	200	5430	5210	320	5530	5380	110	5490
F7	6080	280	6360	6220	370	6590	6290	310	6600
F8	6070	330	6400	6100	380	6480	6430	110	6540
F9	6640	340	6980	6670	400	7070	6880	260	7140
S7	6610	170	6780	6490	390	6880	6540	310	6850

earlier, the values of the AD at the peak temperature of 355°C are the figures used, together with the annual dose-rates calculated in the next Section, in evaluating the ages of the Mungo fireplaces.

7.11 Annual Dose-Rate Calculations

The archaeological dose is delivered to the quartz grains by trace amounts of the natural radioactive series of uranium and thorium and by potassium-40. The dose from the uranium and thorium series is assessed by measuring the alpha activity of the sample as described in Chapter II and then applying the conversion factors evaluated in Chapter VI. These conversion factors require some knowledge of the relative amounts of the uranium and thorium series present in the samples. This ratio was measured by trace element dispersive X-ray fluorescence and was found to be approximately six parts thorium for every one part uranium for all of the fireplaces. The levels of potassium-40 were assessed by measurement of the total potassium content (see Table 5.2) by dispersive X-ray fluorescence and using the natural abundance of 0.0118% for potassium-40. The dose is then evaluated using the conversion factors of Chapter VI.

The calibration of the alpha counting equipment is described in Appendix B while the X-ray fluorescence measurements were carried out in the Department of Geology at this University. These measurements, however, give only the zero grain size dose in an infinite homogeneous medium. To calculate the radiation dose actually absorbed by $105\mu\text{m}$ diameter quartz grains a number of correction factors must be applied to the three types of radiation emitted by the natural radioactive series. These factors are described in detail below.

Grain Size Attenuation Factors

Because of the finite size of the quartz grains, i.e. on average 105 μ m in diameter, the various types of radiation penetrating the grains will suffer some attenuation. In Chapter III and Chapter IV influence functions (or shape factors) were evaluated for the alpha and beta radiations of the natural series (gamma radiation effectively suffers no attenuation on passing through a quartz grain of the size considered here). Hence for the alpha particles, the mean absorbed dose for the uranium series is 23.2% and for the thorium series is 25.1% of the zero grain size dose. For the beta particles (including the IC electron component), the mean absorbed dose for the uranium and thorium series and potassium-40 were found to be 89.8%, 84.5% and 96.6% of the zero grain size dose respectively. These factors must be applied to the alpha and beta dose for each fireplace.

Alpha Efficiency Factors

The alpha efficiency factors, k , have already been discussed in this Chapter (Section 7.9) and their values, which range from 0.060 - 0.068, are given in Table 7.3. These factors were applied to the alpha dose for each fireplace.

HF Etching Factors

As stated earlier in this Chapter the quartz grains from the Mungo fireplaces were etched in HF acid for 10 min which, based on weight loss experiments, corresponds to the isotropic removal of a layer 2.5 μ m thick. In Chapter III and Chapter IV the effects of this acid etching on the absorbed radiation doses have been investigated. The alpha dose reduction factor for the removal of a 2.5 μ m layer is 78% of the unetched dose for the uranium series and 82% for the thorium series from Chapter III. For

the beta dose, the reduction factors are 98.0% and 97.5% of the unetched dose for the uranium and thorium series respectively from Chapter IV. The potassium-40 beta dose suffers negligible attenuation at this etching depth. These further reduction factors must, therefore, be applied to the alpha and beta doses of the Mungo fireplaces.

Ground Water

The presence of ground water in the samples has the effect of diluting the radiation dose delivered to the quartz grains. The attenuation may be calculated for each type of radiation from the equation given by Zimmerman (1971), namely

$$\frac{D(\text{dry})}{D(\text{wet})} = 1 + A \left[\frac{\text{sample weight, wet}}{\text{sample weight, dry}} - 1 \right] \quad (7.2)$$

where $D(\text{dry})$ and $D(\text{wet})$ are the dose-rates for the sample dry and wet respectively; A in the case of alphas and betas is the ratio of the mass stopping powers of water and sample, and for gammas it is the ratio of the mass absorption coefficients. The values of A given by Zimmerman (1971) are 1.50, 1.25 and 1.14 for alpha, beta and gamma radiation respectively. To evaluate equation (7.2) the fractional increase in weight of the Mungo clay when completely saturated was measured and found to be approximately 20%. Next the average fraction of the saturation level that the samples have experienced over the period under consideration must be assessed. The climate of this area has been very dry over the last 30,000 years or so and hence the major contribution to ground water would have been fairly small rainfall and, since the fireplaces are situated well above the water-table, this rain water would soon drain away (Bowler, 1976). The water content of the Mungo clay, therefore, is expected to have been about 10%, on average. Putting these values into equation (7.2)

gives reduction factors of 97.1%, 97.6% and 97.8% of the dose-rate of the sample dry for the alpha, beta and gamma doses respectively and again these values are to be applied to each fireplace.

Radon

The presence of the gaseous daughter radon (Rn-222) halfway through the uranium series has already been pointed out in Chapter VI. Radon emanation will not, however, be a problem for the material of the fireplaces themselves since any flow of gas outwards would be balanced by a flow inwards. This would not be the case near the surface in the stratigraphic clay layer overlying the Mungo fireplaces (see below), so the problem of radon escape was investigated. Following the method of Zimmerman (1971), all of the fireplaces and the material of the overlying clay layer were alpha-counted with the perspex sample holder (see Figure 2.8) unsealed and then measured again after the sample had been sealed for two weeks or more. For all the samples tested the alpha counts were identical within statistical variations indicating that radon escape does not constitute a problem.

Overlying Clay Layer

All of the fireplaces are located in the sedimentary layer known as the Mungo Unit (Barbetti and McElhinny, 1976) which extends almost 2 metres in depth. Above it is a layer of greenish-grey clay known as the Zanci Unit which originated on the lake bed but was swept rapidly over the lunette by the prevailing westerly winds when the lake last dried up, some 16,000 years ago. This clay contains many of the soluble uranium, thorium and potassium salts which were dissolved in the lake water and deposited when the lake dried up. Consequently the clay of the Zanci Unit has

a measured 50% higher alpha count and more than double the potassium level ($2.17\% \text{ K}_2\text{O}$) of the Mungo Unit below it and will contribute significantly to the gamma dose experienced by the fireplaces. Also the thorium/uranium ratio of the Zanci clay was measured by X-ray fluorescence and was found to be 8.5/1 indicative of the slightly higher solubility of thorium salts over uranium salts. The contribution to the gamma dose will depend on the depth of the fireplaces in the Mungo Unit i.e. the distance from the interface with the overlying layer. These distances are taken from Figure 7.2 knowing the sample code letters each of which are given in Table 7.7.

In Chapter V (Section 5.4) the fraction of the gamma dose experienced at a point below an infinite plane interface has been evaluated. The gamma dose fraction from the Zanci Unit reaching the fireplaces can thus be calculated and this is also given in Table 7.7. The Zanci Unit, however, was deposited rapidly between 17,000 and 15,000 years ago when the lake was drying up so that the gamma dose from the overlying layer would only have been experienced by the fireplaces for approximately half of their archaeological age. In addition, the gamma dose from the Mungo clay itself would be reduced by the same fraction as that of the gamma dose it receives from the Zanci Unit, but this would have taken place over virtually the whole of the archaeological age of the fireplaces. Hence for each fireplace the gamma dose from the overlying layer is calculated from the fractions given in Table 7.7 and then halved to account for the time the layer has been in position. The gamma dose from the Mungo clay itself is reduced by the same fraction and the Zanci contribution added to this to give the total gamma dose.

Internal Radioactivity of Quartz Grains

TABLE 7.7

Sample Location Relative to the Zanci Unit
and the Fraction of the Gamma Dose Experienced
by the Fireplaces.

<u>Fireplace</u>	<u>Code Letter</u>	<u>Distance from Zanci Unit (cm)</u>	<u>Fraction of Gamma Dose</u>
F6	k	25.0	0.055
F7	f	14.6	0.118
F8	d	16.7	0.103
F9	f	10.4	0.153
S7	-	9.95	0.165

It has generally been assumed that quartz grains are almost entirely free of internal self-radioactivity (Fleming, 1970). However, Sutton and Zimmerman (1977) have shown that alpha counts on certain quartz extracts indicate that in some samples the internal alpha dose may be significant. Zimmerman(1977a) has carried out tests on the Mungo fireplaces and he found that, on average, the internal radioactivity of the Mungo quartz was 1.3ppm thorium and 0.4ppm uranium. Using the dose-rate conversion factors from Chapter VI, the alpha efficiency factors from Table 7.3 and the alpha and beta dose grain-size absorption factors detailed above, a contribution to the dose-rate from internal self radioactivity of 9 mrad/yr alpha dose and 1 mrad/yr beta dose is calculated for each of the fireplaces. These values must be added to the overall radiation dose-rate together with a figure of 15 mrad/yr to account for the dose due to cosmic rays.

To illustrate how the many complicated correction factors detailed above are applied in calculating the annual dose-rates for the fireplaces an actual example is worked through below. The example chosen is again fireplace F7.

Example - Annual Dose-Rate for F7

From Appendix B, the calibration of the alpha counter, the conversion factors from alpha counts per kilosecond to mrad/yr are 170.5, 7.69 and 9.84 for the alpha, beta and gamma doses respectively, assuming a Th/U ratio of 6/1. If D_{α} is the alpha dose-rate in mrad/yr, D_{β} the beta dose and D_{γ} the gamma dose-rate then

$$D_{\alpha} = 170.5\alpha$$

$$D_{\beta} = 7.69\alpha + 68.2K$$

$$D_{\gamma} = 9.84\alpha + 20.5K$$

where α is the alpha count per ksec and K is the percentage K_2O . For F7,

$$\alpha = 5.473 \text{ cts/ksec}$$

$$\text{and } K = 0.665\% K_2O$$

hence

$$D_{\alpha} = 933$$

$$D_{\beta} = 42.09 + 45.35$$

$$D_{\gamma} = 53.86 + 13.63$$

Grain Size Attenuation Factors for the uranium and thorium alpha doses are 23.2% and 25.1% respectively. For a Th/U ratio of 6/1 the resultant overall factor is 24.8% and hence

$$D_{\alpha} = 933 \times 0.248 = 231.4$$

For the beta dose the factors are 89.8% and 84.5% for uranium and thorium series respectively or 85.3% accounting for the Th/U ratio. For potassium-40 the factor is 96.6%, hence

$$\begin{aligned} D_{\beta} &= 42.09 \times 0.853 + 45.35 \times 0.966 \\ &= 35.90 + 43.81 \end{aligned}$$

The Alpha Efficiency Factor for F7 is 0.067 and hence the alpha dose becomes

$$D_{\alpha} = 0.067 \times 231.4 = 15.5$$

The HF Etching Factors for the alpha doses of uranium and thorium are 78.0% and 82.0% respectively which results in an overall figure for the two series of 81.4%. Hence,

$$D_{\alpha} = 15.50 \times 0.814 = 12.6$$

For the beta doses the respective values are 98.0% and 97.5% giving a resultant 97.6%. Therefore, since potassium-40 is unaffected,

$$\begin{aligned} D_{\beta} &= 35.90 \times 0.976 + 43.81 \\ &= 35.04 + 43.81 \end{aligned}$$

Ground Water in the samples reduces the alpha, beta and gamma doses to 97.1%, 97.6% and 97.8% respectively of the dose-rates of the samples dry. Hence,

$$D_{\alpha} = 0.971 \times 12.6 = 12.3$$

$$\begin{aligned} D_{\beta} &= 0.976 (35.04 + 43.81) \\ &= 34.20 + 42.76 \end{aligned}$$

$$\begin{aligned} D_{\gamma} &= 0.978 (53.86 + 13.63) \\ &= 52.68 + 13.33 \end{aligned}$$

The Overlying Clay Layer has a total gamma dose of 145 mrad/yr. From Table 7.7 the fraction of this dose which reaches F7 is 0.118. The dose-rate from the Zanci Unit is therefore 17.1 mrad/yr. However, because the overlying layer has been in position for only half of the archaeological age of the sample, the effective dose-rate will be 8.6 mrad/yr. Also, D_{γ} for F7 will be reduced by the fraction 0.118 and hence

$$\begin{aligned} D_{\gamma} &= 0.882 (52.68 + 13.33) \\ &= 46.46 + 11.76 \end{aligned}$$

The Internal Radioactivity of the quartz grains gives rise to a further alpha dose of 9 mrad/yr and beta dose of 1 mrad/yr.

Cosmic Rays introduce a further 15 mrad/yr.

So for the alpha dose we have 12.3 mrad/yr from the clay plus 9 mrad/yr internal dose, totalling 21.3 mrad/yr. The beta dose is 77 mrad/yr plus 1 mrad/yr internal giving a total of 78 mrad/yr. The gamma dose is 58 mrad/yr plus 8.6 mrad/yr from the overlying Zanci Unit, which gives a total of 66.6 mrad/yr. Together with the 15 mrad/yr cosmic ray dose this gives a total annual dose-rate of 181 mrad/yr. These values together with those for each of the other fireplaces are given in Table 7.8. Before using these annual dose-rates together with the archaeological doses calculated in the last Section to determine the ages of the

TABLE 7.8

Component Parts of the Annual Dose-Rates
(mrad/yr) for the Lake Mungo Fireplaces.

Fireplace	Alpha	Beta(U & Th)	Beta(K)	Gamma(U & Th)	Gamma(K)	Gamma(Overlying)	Total*
F5	-	68	56	105	18	-	272
F6	11	31	46	45	14	4	176
F7	12	34	43	46	12	9	181
F8	12	36	53	50	15	7	198
F9	12	36	63	47	17	11	211
S7	13	36	52	49	13	12	200

* Total includes: 15 mrad/yr cosmic ray dose
9 mrad/yr internal alpha dose
1 mrad/yr internal beta dose

samples, some estimate of the errors involved in the final age determination is necessary and this is derived in the next Section.

7.12 Error Analysis and Age Determination

The error analysis to be described in this Section is based almost entirely on the work of Aitken and Alldred (1972) which was later revised by Aitken (1976).

It is convenient to define here the following symbols: as before D_α , D_β and D_γ are the dose-rates from alpha particles, beta particles and gamma rays respectively, and D is the total effective dose-rate. The component of D_β arising from the uranium and thorium series is $D_{\beta,U,Th}$ and from potassium-40 is $D_{\beta,K}$; likewise for D_γ . The fractional components of the dose-rate are defined as

$$f_\alpha = \frac{kD_\alpha}{D}, \quad f_\beta = \frac{D_\beta}{D}, \quad f_\gamma = \frac{D_\gamma}{D} \quad \text{etc.}$$

The error analysis can now be divided into i) random errors and ii) systematic errors.

Random Errors

Estimating the errors in the evaluation of ED , I and k to be δED , δI and δk respectively (at one standard deviation) then the corresponding percentage error in the age σ_1 is given by

$$\sigma_1^2 = \left[100(1-f_\alpha) \frac{\delta ED}{ED} \right]^2 + \left[\frac{100\delta I}{ED + I} \right]^2 + \left[100f_\alpha \frac{\delta k}{k} \right]^2 \quad (7.3)$$

As explained in Section 7.10, δED and δI are evaluated by the programme which performs the 'least squares fit' to the individual data points and they are given in Table 7.5 for each fireplace. The values of δk are based on the experimental determinations of the k -values and these are given in

Table 7.3 for the 10 min etch fraction.

The random error in the alpha-counting is taken to be 5% (Aitken, 1976) while the errors quoted for the dispersive X-ray fluorescence measurements of the potassium contents are said to be 3%. Hence the relevant random error for alpha-counting and potassium analysis σ_2 is given by

$$\sigma_2^2 = 25 \left\{ f_\alpha + f_{\beta, U, Th} + f_{\gamma, U, Th} \right\}^2 + 9 \left\{ f_{\beta, K} + f_{\gamma, K} \right\}^2 \quad (7.4)$$

Systematic Errors

Systematic errors arise from uncertainties in the calibration of the alpha and beta sources, the alpha-counter and the potassium analyser.

The alpha source has been calibrated indirectly by comparing the k-values of thermoluminescent phosphors supplied by the Research Laboratory for Archaeology, Oxford (see Appendix A). The calibration of the Oxford alpha source has an error of 5% (Aitken, 1976) and assuming an experimental inter-calibration error of 3% then the total error in the alpha source calibration is 6%.

The beta source has been calibrated directly as described in Appendix C and the error is thought to be 3%.

The calibration of the alpha-counter is described in Appendix B and a value of 5% is assumed for the error. The X-ray fluorescence analyser is quoted as being accurate to within $\pm 5\%$ at 95% confidence levels which implies a standard error of approximately 2.5%.

These lead to a systematic error in the age due to calibration errors given by

$$\sigma_3^2 = 36f_\alpha^2 + 9 \left\{ 1 - f_\alpha \right\}^2 + 25 \left\{ f_\alpha + f_{\beta, U, Th} + f_{\gamma, U, Th} \right\}^2 + 6 \left\{ f_{\beta, K} + f_{\gamma, K} \right\}^2 \quad (7.5)$$

As pointed out by Aitken (1976) it has been usual to include a systematic error term to allow for uncertainties in the uranium to thorium ratio mainly because of the large differences between the two series for both the beta doses and gamma doses. For the Mungo fireplaces, however, the beta dose and most of the gamma dose derive from the same material. From Table 6.6 it can be seen that although the individual contributions vary quite significantly between the two series, the totals of the beta plus gamma doses differ by less than 5%. Add to this the fact that an estimate of the ratio has been obtained by trace element X-ray fluorescence and it appears that negligible systematic error need be added for these samples.

A further systematic error term needs to be added to account for the possible effects of radon emanation and ground water. The former effect has been shown to have negligible effect whereas the latter depends on an accurate knowledge of past climatic conditions. This is not known so following Aitken and Alldred (1972) a value of 2% is allowed to cover radon and ground water effects. Hence the error in the age is given by

$$\sigma_4^2 = 4 \quad (7.6)$$

The final systematic error term that must be added is one to account for the possible errors in evaluating the internal alpha dose to the quartz grains. This alpha dose was evaluated using the average value for the radioactivity level within the grains since the experimental errors associated with the individual determinations were larger than the individual differences. The error in the average value is thought to be 10% at a 95% confidence limit, or 5% at one standard deviation. Allowing also an error of 5% to account for the possibility of the non-homogeneous distribution of alpha emitters within the quartz grains (Sutton and Zimmerman, 1977), the resulting error in the value of 9 mrad/yr used in

the dose-rate determinations is 7%. The error in the age is therefore

$$\sigma_5^2 = 49 f_{\alpha, I}^2 \quad (7.7)$$

where $f_{\alpha, I}$ is the fraction the internal alpha dose is of the total dose-rate.

The overall error σ is then

$$\sigma^2 = \sigma_r^2 + \sigma_s^2 \quad (7.8)$$

where σ_r and σ_s are the combined random and systematic errors respectively and are given by

$$\sigma_r^2 = \sigma_1^2 + \sigma_2^2 \quad (7.9)$$

$$\sigma_s^2 = \sigma_3^2 + \sigma_4^2 + \sigma_5^2 \quad (7.10)$$

To evaluate equations 7.3 - 7.10 the fractional components of the error terms for each fireplace must be determined. These figures are given in Table 7.9. Using these values the random and systematic errors have been calculated and are presented in Table 7.10.

The thermoluminescence age equation has already been given in Chapter I and is

$$\text{TL Age (yr)} = \frac{\text{Archaeological Dose (rad)}}{\text{Dose-Rate (rad/yr)}} \quad (7.11)$$

Combining the archaeological dose values from Table 7.5 with the dose-rates given in Table 7.8 allows the TL ages of the Mungo fireplaces to be calculated along with their associated errors. These ages are now presented in Table 7.11.

The ages of fireplaces F6, F7, F8 and F9 are of great archaeological significance even if only because they confirm the extreme antiquity of the sites as already proposed by Barbetti and Polach (1973) who carried out radiocarbon dating on charcoal from each fireplace. A direct comparison of the TL and radiocarbon ages is given in the next Chapter. As

TABLE 7.9

Fractional Error Components for the Mungo Fireplaces

Fireplace	f_{α}	$f_{\alpha,I}$	$f_{\beta,U,Th}$	$f_{\beta,K}$	$f_{\gamma,U,Th}$	$f_{\gamma,K}$	$\delta ED(rads)$	$\delta I (rads)$
F5	-	-	0.254	0.206	0.386	0.066	-	-
F6	0.114	0.051	0.182	0.261	0.272	0.086	200	100
F7	0.116	0.050	0.193	0.238	0.292	0.078	250	120
F8	0.106	0.045	0.187	0.268	0.277	0.086	250	120
F9	0.100	0.043	0.175	0.299	0.259	0.096	270	130
S7	0.110	0.045	0.185	0.260	0.287	0.084	250	120

TABLE 7.10

Error Terms for the Mungo Fireplaces

Fireplace	$\sigma_1(\%)$	$\sigma_2(\%)$	$\sigma_3(\%)$	$\sigma_4(\%)$	$\sigma_5(\%)$	$\sigma_r(\%)$	$\sigma_s(\%)$	$\sigma(\%)$
F5	5.62	3.45	4.55	2.00	0.23	5.92	4.97	8.26
F6	3.89	3.02	4.04	2.00	0.36	4.93	4.52	6.69
F7	4.03	3.15	4.14	2.00	0.35	5.12	4.61	6.89
F8	4.14	3.04	4.06	2.00	0.31	5.14	4.54	6.85
F9	4.11	2.92	3.96	2.00	0.30	5.04	4.45	6.73
S7	3.88	3.09	4.09	2.00	0.31	4.96	4.56	6.44

TABLE 7.11

TL Ages of the Lake Mungo Fireplaces

Fireplace	TL Age (yr)
F5	330 \pm 27
F6	31,400 \pm 2100
F7	36,400 \pm 2500
F8	32,700 \pm 2200
F9	33,500 \pm 2300
S7	34,400 \pm 2200

argued in the introductory Sections of this Chapter, the presence of a morphologically modern people in the Mungo area more than 30,000 years ago suggests the presence of similarly modern people on the south-east Asian mainland in much earlier times. This appears to have been established by the ages of the Mungo fireplaces.

From a scientific point of view, the successful extension of the thermoluminescence inclusion dating technique to the quartz from baked sediments below ancient fireplaces greater than 30,000 years old is extremely encouraging. Although the numerous and complicated correction factors called for in the age calculations preclude a routine application of such a dating programme, this work has demonstrated that this type of dating programme can be successful if and when research time and facilities are available.

7.13 CONCLUSION

In this Chapter the basic principles of thermoluminescence dating, which were developed in Chapter I, have been applied to the baked clay of Aboriginal fireplaces from Lake Mungo.

The archaeological context of the sites has been described and the discussion has examined the overall significance of the ages of the fireplaces to the prehistory of south-east Asia.

The preparation of the samples was described in detail with particular attention being paid to the etching of the quartz grains in hydrofluoric acid. It was seen that this etching takes place at an uneven rate over the surface of some grains and therefore the assumption that the outer, alpha-dosed layers are isotropically removed is not strictly valid. Hence an etching time was chosen to be just sufficient to remove any discolouration arising from the diffusion of impurities into the outer layers and

hence improve the transparency. An etching time of 10 min in concentrated HF at room temperature was used. Some of the residual alpha dose will remain in the grains, and thus the alpha efficiency factors for the Mungo quartz were investigated.

The archaeological dose was measured by the 'additive procedure' described in Chapter I with many discs (more than 50) being glowed out for each site. The extreme ages of the Mungo fireplaces are useful in that they provide a large TL signal but as a consequence care is required when administering additive laboratory beta doses lest the TL traps become saturated. Saturation tests were made and it was found that the TL traps just began to saturate when the total (natural plus laboratory) dose reached 9 krads. Thus the additive laboratory doses were designed to keep the total dose below 9 krads.

The dose-rates for each of the fireplaces were evaluated taking into account the many correction factors necessary for these sites. In addition to the grain size, k-value, HF etching and ground water attenuation factors, the presence of a more highly radioactive, overlying clay layer and the internal radioactivity of the quartz grains themselves have each been allowed for.

A complete error analysis of the random and systematic errors involved in the dating procedure was then presented (the possibility of other more subtle errors is discussed in Chapter XI). Following this the TL ages were evaluated for each fireplace and found to range from 31,400 - 36,400 years (apart from F5 which is 330 years), ages which are in reasonable agreement with previous radiocarbon ages for the same fireplaces. There is, however, a small systematic displacement between the TL and the radiocarbon ages for each fireplace and this is the subject of the next Chapter.

CHAPTER VIII

THE COMPARISON OF THERMOLUMINESCENCE

AGES WITH RADIOCARBON AGES FOR

THE MUNGO FIREPLACES

8.1 Comparison of TL and Radiocarbon Ages

As mentioned in the previous Chapter, the thermoluminescence ages of fireplaces F6, F7, F8 and F9 confirm the extreme antiquity of the sites as already proposed by Barbetti and Polach (1973) based on radiocarbon dates. These radiocarbon ages for each fireplace are given in Table 8.1 and it should be noted that they are calculated using the conventional 5568 year C-14 half-life. To find the age using the more appropriate 5730 year half-life it is necessary to increase the ages in Table 8.1 by 2.9%. A direct comparison of the TL and radiocarbon ages which have been corrected in this manner is presented in Table 8.2. Here the difference in the ages in years and the 'z' ratio are both given.

The 'z' ratio is directly analogous to the more familiar 't' ratio and it has been used previously to intercompare radiocarbon dates (Polach *et al.*, 1972). The equation for 'z' can be written (Mood and Graybill, 1963),

$$z = \frac{\bar{X}_1 - \bar{X}_2}{(\sigma_1^2 + \sigma_2^2)^{1/2}} \quad (8.1)$$

where \bar{X}_1 and \bar{X}_2 are the two mean values to be compared and σ_1 and σ_2 are their respective standard deviations. The z statistic is normally distributed with zero mean and unit variance.

The values of 'z' given in Table 8.2, therefore, indicate that the

TABLE 8.1

Radiocarbon Ages of Lake Mungo Fireplaces

<u>Fireplace</u>	<u>Radiocarbon Sample Number</u>	<u>Radiocarbon Age (yr BP)</u>
F6	ANU-667	26,270 \pm 470
F7	ANU-680	30,780 \pm 520
F8	ANU-681	28,310 \pm 410
F9	ANU-682	27,530 \pm 340

TABLE 8.2

Comparison of TL and Radiocarbon Ages

<u>Fireplace</u>	<u>TL Age ($\times 10^3$ yr)</u>	<u>Radiocarbon Age ($\times 10^3$ yr)</u>	<u>Difference ($\times 10^3$ yr)</u>	<u>'z' ratio</u>
F6	31.4	27.0	4.4	2.0
F7	36.4	31.7	4.7	2.0
F8	32.7	29.2	3.5	1.7
F9	33.5	28.4	5.1	2.2

probability of the two ages for each fireplace being merely part of the same distribution about some common mean value is less than 5% or 0.05. For two fireplaces this probability is 0.05×0.05 or 0.25%. The probability that the TL and radiocarbon ages for all four fireplaces are the same for each site is $6.25 \times 10^{-4}\%$, i.e. extremely small.

Thus it appears that the systematic difference between the TL and radiocarbon ages may be quite significant if we accept that the errors quoted for both dating methods are valid. Before putting forward possible explanations of this discrepancy, it is appropriate to present here a very brief explanation of the radiocarbon dating method.

8.2 The Radiocarbon Dating Method

Radiocarbon (C-14) is produced in the Earth's upper atmosphere (the stratosphere) through its constant bombardment by cosmic rays from outer space. The cosmic ray flux consists of charged particles, mainly protons and He, C, N and O nuclei, with energies distributed over a broad spectrum (Rossi, 1964, has indicated that a few cosmic ray particles may have energies above 10^{19} eV). The cosmic ray particles undergo a complex chain of nuclear reactions which can result in the production of thermal energy neutrons, as well as many other nuclear fragments. These secondary neutrons have a high capture cross section with the abundant atmospheric nitrogen nuclei to produce C-14 by the following (n,p) reaction:



C-14 is then oxidised to ${}^{14}\text{CO}_2$ in the stratosphere by a mechanism and at a rate that is not well known. As a gas, the ${}^{14}\text{CO}_2$ mixes within the atmosphere in the same manner as other gas molecules. Plants take up CO_2 from the atmosphere and animals generally consume organic material thereby absorbing carbon, a tiny fraction of which (*ca.* $1.2 \times 10^{-10}\%$) will

be in the form of C-14. At the sea surface the transfer or exchange of CO_2 is controlled by both the pH - and temperature - dependent carbonate equilibrium in the surface water, and by physical processes such as wind-caused surface turbulence. Hence the radiocarbon nuclei diffuse into two main reservoirs, the biosphere and the oceans. The oceans contain by far the largest percentage of the world-wide C-14 inventory, but the exchange rate is much slower which results in the surface layer of the ocean having an apparent age which varies from 400 to 700 years for different regions of the world (Mangerud and Gulliksen, 1975).

If the production rate of C-14 remained constant throughout time, a steady state would be achieved in the concentration of C-14 in the atmosphere i.e. the production of C-14 in the atmosphere would be exactly balanced by its loss from the atmosphere, either by radioactive decay or by its transfer to the other carbon-containing reservoirs.

In 1949, W.F. Libby developed a method that used C-14 to determine the age of organic material which is associated with early human occupation sites; for this work Libby was later to be awarded the Nobel Prize. As stated earlier in this Section, all living organisms, both plants and animals, are constantly exchanging carbon with their environment (breathing, food intake, photosynthesis). The fraction of C-14 nuclei present in the material will decay exponentially with a half-life of 5730 years when the organism dies and the interchange of carbon with the environment ceases. By measuring the fraction of C-14 nuclei present in the sample now, N , and knowing the fraction present in the sample when it was formed in the past, N_0 , the age may be determined from the simple exponential decay law,

$$N = N_0 \exp(-t/\tau) \quad (8.3)$$

where τ is the mean lifetime of the C-14 nuclei (=8270 year) and t is the

age in years.

The value of N is determined by measurement of the weak beta particle emitted when the C-14 nuclei decay:



The actual determinations of N for the radiocarbon dating of the Mungo fireplaces were carried out at the ANU Radiocarbon Dating Laboratory by liquid scintillation counting (Barbetti and Polach, 1973). Charcoal from each of the fireplaces was pretreated by boiling in 2N hydrochloric acid to remove any soil carbonate present, after having removed any observed rootlets or other contaminating matter with tweezers (Barbetti, 1973). The charcoal was then converted to benzene using the methods and equipment described by Polach *et al.* (1973). The scintillating material was dissolved in the benzene which was then placed in the counting vial as described by Polach (1969).

The determination of N_0 , the fraction of C-14 present in natural materials at some time in the past, is a more difficult problem to assess due to variations in the atmospheric concentration of C-14. The causes of these variations in atmospheric C-14 concentration are discussed in the next Section.

8.3 Variations in the Concentration of Atmospheric C-14

The problem of calculating the atmospheric concentration of radiocarbon in the past is a difficult one because the C-14 production rate may be influenced by a number of factors:

- (i) The Earth's geomagnetic field determines, for a given latitude, the minimum momentum of a cosmic ray particle that can reach the upper atmosphere and hence give rise to the production of C-14. The production rate will follow variations in the geomagnetic field

approximately as $M^{-0.5}$, where M is the Earth's magnetic moment (Elsasser *et al.*, 1956).

- (ii) The interplanetary magnetic field influences the cosmic ray flux and this field intensifies during periods of high sunspot activity.
- (iii) Solar flare particles which reach the upper atmosphere can produce C-14 and these particles are more abundant during periods of high solar activity.
- (iv) Supernovae explosions can produce short-term variations in the production rate by a possible gamma ray burst associated with the explosion, and a long-term increase then decrease in the cosmic ray flux which is accelerated in the explosion.

The cosmic ray flux arriving at the Earth fluctuates by a few percent over the 11-year solar cycle. This observed variation is thought to result from variations in the inter-planetary magnetic field, caused by variations in the amount of outflowing plasma from the sun (Rossi, 1964). Farmer and Baxter (1973) have observed a correlation between the 11-year solar cycle and the atmospheric concentration of C-14, which can be explained in terms of the variations in the C-14 production rate due to variations in the cosmic ray flux.

The most important causes of changes in the atmospheric C-14 concentration are the variations in the Earth's geomagnetic field. It is appropriate to discuss here the dependence between atmospheric C-14 concentration and geomagnetic field changes and the relevance of the discussion will be seen in the next Section. The effect of the Earth's geomagnetic field on a particular cosmic ray particle is quite complex. Consider a charged particle moving in a plane normal to the lines of force of a uniform magnetic field B . The motion of the particle will describe a circle of radius R and the product BR is equal to the ratio

of the relativistic momentum \underline{P} to the charge \underline{Ze} . The quantity

$$\frac{Pc}{Ze} = cBR \quad (8.5)$$

where c is the velocity of light, is known as the magnetic rigidity of the particle and is measured in volts (Wolfendale, 1963). At a given geomagnetic latitude particles with rigidity less than a certain value cannot reach the Earth. Particles with a slightly greater rigidity may arrive at the Earth's surface from the west (for positively-charged particles), but not from the east. The critical value of rigidity, with which positively-charged particles may arrive at the Earth's surface vertically or from the west (but not the east), is known as the vertical cut-off rigidity, P_λ , given as a function of geomagnetic moment and latitude by Elsasser *et al.* (1956),

$$P_\lambda = \frac{\cos^4 \lambda}{4} \cdot \frac{Mc}{r^2} \quad (V) \quad (8.6)$$

where r is the radius of the Earth.

Several authors have used this model of the modulation of the cosmic ray flux by the Earth's geomagnetic field in calculating the C-14 production rate as a function of the geomagnetic moment - for example, Elsasser *et al.*, (1956); Wada and Inoue (1966); Bucha and Neustupný (1967); Lingenfelter and Ramaty (1970). The calculations of Lingenfelter and Ramaty (1970) are probably the most extensive and they produced the curves shown in Figure 8.1 for the expected variation in C-14 production as a function of the geomagnetic dipole moment and the solar modulation function, η .

Radiocarbon measurements of dendrochronologically-dated wood have provided a direct measurement of variations in the atmospheric C-14 concentration over the past 7,500 years (Ferguson, 1970 and Damon *et al.*, 1972). The difference between the radiocarbon age and the dendrochronological age can be analysed and the trend, a third order polynomial, is

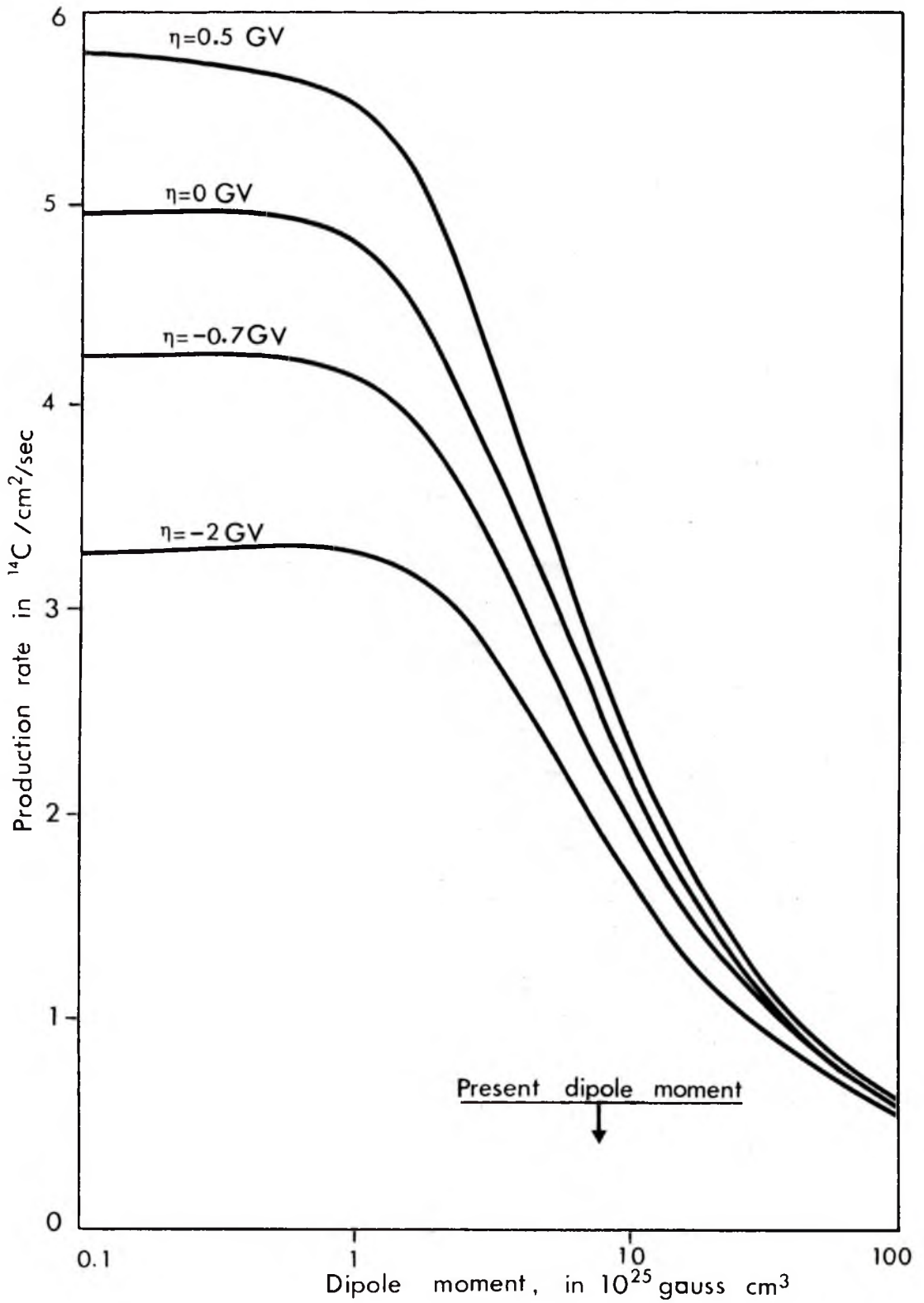


FIGURE 8.1: Production Rate of Carbon-14 as a Function of the Earth's Dipole Moment for Different Values of Solar Activity. The solar modulation function, η , is a measure of the solar activity and is equal to -2GV at a solar maximum.

almost sinusoidal. It is possible, knowing the variations in the geomagnetic dipole moment over the last 7,500 years, to predict the variation in the C-14 concentration and thus to compare the calculated and experimentally determined C-14 fluctuation curves. In order to calculate the variations in the C-14 atmospheric concentration from the predicted fluctuations in the production rate, it is necessary to have a model to describe the mixing of the radiocarbon through the terrestrial system once it has been produced. When considering long-term variations, such as those due to changes in the geomagnetic dipole moment, a two-box model is sufficient and has been adopted by Damon (1970) and Lingenfelter and Ramaty (1970).

The two-box model assumes a source reservoir consisting of the atmosphere, biosphere and possibly the mixed layer of the oceans (the top 100 m or so), with total carbon content N_a and C-14 content n_a , and a sink reservoir, representing the deep oceans, with a total carbon content N_s and C-14 content n_s . The rate of exchange of radiocarbon in the reservoirs is described by the differential equations

$$\frac{dn_a}{dt} = Q - \frac{n_a}{\tau} - \frac{n_a}{T} + \frac{n_s}{vT} \quad (8.7)$$

and

$$\frac{dn_s}{dt} = -S - \frac{n_s}{\tau} + \frac{n_a}{T} - \frac{n_s}{vT} \quad (8.8)$$

where Q is the production rate, S is the loss due to sedimentation, τ is the mean lifetime of a C-14 atom, T is the mean residence time of C-14 atoms in the source reservoir (~ 25 yr according to Wood and Libby, 1964) and v is equal to N_s/N_a .

Damon and Wallick (1971) have solved equations 8.7 and 8.8 and found that the calculated C-14 fluctuations show good agreement with the dendrochronologically measured variations and also that the variations

have a time lag of only 675 yr when compared to the geomagnetic moment curve. Hence for slow variations of M and therefore Q , the total C-14 reservoir is always very nearly in an equilibrium state, with radiocarbon decay nearly balancing the instantaneous production rate. The solution by Lingenfelter and Ramaty (1970) of equations 8.7 and 8.8 also indicates that for slow variations in the production rate, the total reservoir is very nearly in equilibrium.

The various comparisons discussed above, therefore, indicate that most of the atmospheric C-14 fluctuations are due to changes in the geomagnetic dipole moment and hence the production rate (see Figure 8.1). At present, it appears that there may be some residual non-geomagnetic effects (possibly due to climatic change), but the difference between the calculated and experimentally measured fluctuation curves could be accounted for by uncertainties in the geomagnetic variations.

The relevance of this discussion on the dependence between variations of atmospheric C-14 concentration and geomagnetic field changes will be seen in the next Section which examines the results of an archaeomagnetic investigation on the baked sediment of the Mungo fireplaces by Barbetti (1973).

8.4 Geomagnetic Field Variations as Recorded at Lake Mungo

Haematite ($\alpha\text{-Fe}_2\text{O}_3$) is a naturally-occurring magnetic mineral which exhibits the properties of a spin-canted ferromagnet. At grain sizes of less than 0.15 μm (which is more than an order of magnitude larger than the possible grains sizes of haematite in the materials of the Mungo fireplaces) the haematite grains will each be a single magnetic domain. When the material of the fireplaces was heated then allowed to cool under the influence of the Earth's magnetic field, certain of these

single-domain particles would have been coerced to align their magnetic moments with the direction of this field. The number of atoms succumbing to this coercion is proportional to the intensity of the field at that time. Thus a measure of the intensity and direction of the magnetism still retained by the samples, i.e. the thermoremanent magnetization, provides a measure of the geomagnetic field intensity and direction when the samples were last heated.

This forms the basis of the thermoremanent archaeomagnetic studies carried out by Barbetti (1973) on the ovenstones and baked sediment of the Lake Mungo fireplaces. He discovered that a geomagnetic field excursion had taken place probably occurring in two excursion loops, one characterised by a high field intensity and a second during a period of low field intensity. The radiocarbon ages, virtual pole positions and dipole moments recorded by the Mungo fireplaces are given in Table 8.3 which is taken from Barbetti (1973).

In the last Section we saw how the atmospheric C-14 concentration was highly dependent on the geomagnetic field. This led Barbetti (1972) to predict, on the basis of the work of Lingenfelter and Ramaty (1970), that for the fireplaces which indicate a low ancient field intensity (only F6 falls in this category in the present investigation) the radiocarbon ages are likely to be too young by between 2,300 and 5,560 years but that the fireplaces which indicate a high field intensity (F7, F8 and F9) should give apparent radiocarbon ages which are too old by up to 2,000 years. These calculations were based on the assumption that the magnetic field variations measured in the material of the fireplaces took place on a global scale, i.e. they represented variations in the geomagnetic dipole moment.

From Table 8.2, these predictions are seen to be true only for F6 since, by comparison with the TL ages, all the radiocarbon ages are too young. This leads to speculation as to the possible reasons for the

TABLE 8.3

Radiocarbon Ages, Virtual Pole Positions and
Dipole Moments as Recorded by the Mungo
Fireplaces

Fireplace	Conventional C-14 Age (yr BP)	Position of Virtual North Pole		Dipole Moment ($\times 10^{25}$ gauss.cm ³)	
F6	26,270 \pm 470	238 ^o E	3 ^o N	3.8 \pm 0.8	(O,B)
F7	30,780 \pm 520	34 ^o E	28 ^o S	28.1 \pm 4.6 18.8 \pm 0.8	(O) (B)
F8	28,310 \pm 410	230 ^o E	13 ^o N	15.1 \pm 1.8	(B)
F9	27,530 \pm 340	238 ^o E	8 ^o S	40.2 \pm 4.1 21.9 \pm 5.4	(O) (B)

(O) denotes ovenstone; (B) denotes baked sediment.

systematic difference between the TL and C-14 ages. One possible cause is that a systematic error in either or both dating methods, much larger than the quoted errors in Table 7.11 or Table 8.1, has been overlooked. A complete error analysis is given in Section 7.12 for the TL ages and it appears to account for most of the possible systematic errors although other, more subtle errors are discussed in Chapter XI. Thus, although it cannot be completely overruled as a source of the discrepancy, it is not thought likely that an unforeseen systematic error in the TL age determinations can account for the magnitude of the difference between the TL and C-14 ages.

Similarly we should consider the possibility of systematic errors in the C-14 age determinations and this is discussed in the next Section.

8.5 Sources of Error in Radiocarbon Dating

When Libby (1946) established the radiocarbon dating technique he deliberately chose to quote only those errors of age determinations based on the measurement of the residual radioactivity of C-14 in the sample to be dated. Fundamentally this was perfectly valid and still remains so since even today this remains the only error which can be subjected to a strict mathematical and statistical treatment. Thus the errors quoted in Table 8.1 for the radiocarbon ages are simply the precision with which the C-14 activity of each sample was measured. To fully appreciate the accuracy of the radiocarbon age, the various other possible sources of error must be considered. Polach (1975) has conveniently summarized these sources and Table 8.4 is reproduced from his work. Each of these sources will now be considered in relation to the Mungo fireplaces.

TABLE 8.4

Sources of Error in Radiocarbon Dating

Sources of Error		Effect on Age Determination	How to Minimise
1.	Precision of Age Determination	Statistical; Typically $\pm 1\%$ dC^{14} or less	Big samples, optimal counting times
2.	Inherent		
	(i) C-14 Half-life	"Libby" $T_{1/2}$ probably $\sim 3\%$ too low	Multiply ages BP by 1.030
	(ii) C-13/C-12 Fractionation	410 years is common, 550 years is possible	Mass-spectrometry on portion of sample CO_2
	(iii) C-14 Modern Std.	<80 years	International cross-checking of secondary standards
	(iv) Variations in past	Nil to ~ 800 years; beyond 10,000 BP not determined	Tree-ring calibration; otherwise interpret in terms of radiometric time scale
	(v) Distribution of C-14 in nature	Surface ocean, latitudinal dependence -400 to -750 years. Deep ocean -1800 years	Interpretation of results, choice of contemporary standards
	(vi) Changes of C-14 concentration	Industrial effect <i>ca.</i> -2.5% and Atom Bomb effect <i>ca.</i> + 160% in atmosphere	Interpretation of results
3.	Contamination	Nil to 3000 years up to 15,000 BP; >10,000 possible beyond 25,000 BP	Choice of material chemical/physical purification
4.	Age of Material	<10 years to >1000 years	Choice of material and interpretation of results
5.	Association of Sample and Event	Indeterminate	Interpretation of results
6.	Human	Indeterminate	Care in field/lab.
7.	Interpretation of results	Indeterminate	Care in interpretation, interdisciplinary collaboration

1. Precision of Age Determination: This has already been discussed above and is most of the error quoted in the C-14 ages in Table 8.1.

2. Inherent

- (i) C-14 Half-life: the comparison of the TL and C-14 ages was carried out after the C-14 ages had been half-life corrected (see Table 8.2).
- (ii) C-13/C-12 Fractionation: mass-spectrometry was carried out on the samples of interest here (Barbetti, 1973). The ages have been corrected for isotopic fractionation and the error in this measurement is included in the error quoted for the C-14 age in Table 8.1.
- (iii) C-14 Modern Std.: the ANU Radiocarbon Dating Laboratory has been involved in the international cross-checking of primary and secondary standards (Polach, 1976) and no error is thought to arise from this source.
- (iv) Variation in past C-14 production rates: this has been discussed in detail earlier in this Chapter and indeed the inter-comparison of the TL and C-14 ages may be one way of assessing this error, as will be discussed later.
- (v) Distribution of C-14 in nature: the charcoal from the Mungo fireplaces is almost certainly the result of burning bushes and scrub from the near vicinity and hence the C-14 in these plants should have been in equilibrium with the atmospheric concentration. If, however, the burnt material had been aquatic in nature then there would have been a problem. This area has a fairly large amount of geological limestone or calcite and the lake water would certainly have had dissolved

in it large quantities of geological carbon. The carbon from these geological origins is dead, i.e. has no C-14 activity, so that any aquatic plants which absorb it will be depleted in C-14. However, as stated above the burnt material in the fireplaces is almost certainly terrestrial in origin and this source is not thought to introduce any error in the age determination.

{ A striking example of the problems that can arise from the above situation has recently been uncovered by the ANU Radiocarbon Dating Laboratory. Samples of charcoal and shell have been found together in fireplaces at a lake next to Mungo, Lake Arumpo, see Figure 7.1. Radiocarbon dating of these charcoal/shell pairs has produced discrepancies of the order of 10,000 years. The charcoal was dated to about 20,000 years with the shells being 10,000yr older. It is possible that the shell samples were depleted in C-14 through the uptake of dead carbon from the lake waters and a full study of this problem is presently underway at the ANU Radiocarbon Laboratory}.

- (vi) Changes of C-14 concentration in the atmosphere: the Industrial effect (the dilution of the atmospheric C-14 concentration by the burning of "dead" fossil fuels with negligible C-14) and the Atomic Bomb effect (the production of C-14 in the atmosphere by the nuclear radiation produced during atomic bomb testing) are both relatively modern events compared to the ages of the Mungo fireplaces and may only be of consequence when considering modern contamination of the samples.

3. Contamination: Of all the seven sources of error listed in Table 8.4, this one is thought to have the highest probability of introducing an error into the radiocarbon age determination. By contamination we mean a change in the C-14 activity of the sample other than by radioactive decay, which happened after the sample was formed. Every time a sample (no longer living or forming) is deposited in an environment some extraneous material of different origin and age is likely to come into

contact with it. A sample buried in an organically rich soil will be subjected to "cross-talk" with humic and fulvic acids and other soluble soil organic matter which can either form chemical bonds or be deposited within the permeable and often porous structure of the sample. The sample might be penetrated by feeding rootlets which in turn decay and can no longer be isolated from the decay products of the sample itself. Soil carbonate also might deposit or exchange with the sample.

Fortunately the Mungo area has been a fairly arid zone for most of the archaeological life of the fireplaces. Thus contamination, if it has occurred at all, will be reasonably small in the dry Mungo clay. Unfortunately the relatively small sample size did not allow for the application of full contamination checks. These checks usually consist of isolating various fractions of the sample (i.e. acid soluble and acid insoluble; alkali soluble and alkali insoluble) and then dating and inter-comparing the results for each fraction. A full description of just such a contamination study is given by Polach (1972). The pretreatment given to the charcoal from the Mungo fireplaces, as stated earlier, was simply to remove any visible intrusive rootlets with tweezers and then to boil in 2N HCl (Barbetti, 1973).

The removal of any observed rootlets does not, of course, include those which may have penetrated some time ago and had decayed when the pretreatment was taking place. These would no longer be visible and could be much younger than the age of the charcoal. Polach (1975) has shown that only 0.1% "modern" contamination (here "modern" implies material which has the same C-14 activity as 1950 wood) can cause a 100,000 year old sample to be dated at 47,000 years. For the age differences quoted in Table 8.2, a "modern" contamination level of approximately 1% in the radiocarbon samples would be required to account for the discrepancy. A larger percentage of less-than-"modern" contamination would, obviously, be required, and although

this is not entirely impossible, it is quite unlikely that such a large level of contamination has taken place. (This does not preclude the possibility that "modern" or less-than-"modern" contamination has occurred to a limited extent and that the true radiocarbon ages are somewhat older than those given in Table 8.1 but not necessarily as old as the TL ages given in Table 8.2).

The acid bath during pretreatment will hydrolyse any soil carbonate present and in any case this type of contamination with "old" (i.e. minimal or no C-14 activity) material would give apparent C-14 ages which are too old. Also Scharpenseel (1976) has shown that repeated HCl hydrolysis removes younger organic carbon leaving behind the "biologically inert carbon" which is what we require to date.

Contamination as a possible source of error, therefore, is not thought to be responsible for the entire difference in the TL and C-14 ages, although it is not impossible that this difference may be smaller than is indicated in Table 8.2.

4. Age of Material: as mentioned earlier, the charcoal is thought to derive from the burning of small bushes and scrub, none of which would have a significant age before being burnt.

5. Association of Sample and Event: the event is the use of the fireplace which undoubtedly gave rise to the charcoal.

6. Human: the production of many replicate samples (Barbetti, 1973) which were all entirely consistent would appear to negate this as a possible source of error.

7. Interpretation of Results: the interpretation of the results

for the Mungo fireplaces given in this thesis has, hopefully, been made with due care and interdisciplinary collaboration.

In this Section a detailed account of the possible sources of error in the radiocarbon age determinations has been given. Only one of these sources, contamination, is thought to be a possible area where errors may be introduced but it is not thought to be large enough, if it exists at all, to account for the TL/C-14 age difference.

8.6 The Lake Mungo Geomagnetic Excursion - Dipolar or Non-dipolar?

Whenever measurements of ancient field intensity are made they refer to a particular place at a particular time and usually contain a contribution from the non-dipole field, so that many measurements are needed to average out the non-dipole noise. Barbetti (1973) cites the observation in Czechoslovakia (Bucha, 1970) of an excursion at about the same time as the one recorded at Lake Mungo. He proposes that this helps support the hypothesis that the Mungo excursion was a global dipolar, rather than a local, non-dipole field phenomenon, although admitting that the coincidence might be fortuitous.

The effects of geomagnetic dipole variations on the C-14 production rate have been well established (Bucha, 1970; Damon, 1970 and Damon *et al.*, 1972) as was discussed in Section 8.3. The radiocarbon ages of the Mungo fireplaces should, therefore, follow the predictions of Barbetti (1972) i.e. the C-14 age of F6 should be too young because of the low geomagnetic field intensity, and the ages of F7, F8 and F9 should be too old because of the high field intensity. As we have seen earlier in this Chapter, Table 8.2, all of the radiocarbon ages are too young by comparison with the TL ages of Chapter VII. We have been able to find no convincing source of error in either of the two dating methods of

sufficient magnitude to account for the discrepancies in the ages and so this leads to speculation about other possible reasons.

If we accept the TL ages and that the radiocarbon ages are a true representation of the atmospheric C-14 concentration at that time, then we must look to some reason for a higher C-14 production rate than the archaeomagnetic intensity of the fireplaces predicts (except in the case of F6). The most probable explanation would be that the Mungo excursion was not dipolar at all, but was in fact a non-dipole, localised event. Since the C-14 production rate is dependent on the average global dipole field, it would thus not have been influenced by a small non-dipole aberration at Mungo. We can then speculate that the dipole field intensity was lower than the present day level (*ca.* 8×10^{25} gauss. cm³) with an intensity of *ca.* 4×10^{25} gauss. cm³ (similar to that recorded by fireplace F6) being low enough to account for the TL/C-14 age differences.

Bucha (1976) has studied the remanent magnetization of lake sediments, travertines and continental sediments (loesses and soils) covering the period of the last 40,000 years and has shown that it is quite probable that the geomagnetic field intensity was less than half the present day level between 26,000 and 34,000 years ago. These results would tend to support the hypothesis presented here that the Mungo excursion was a localised, non-dipolar event and that the overall dipole field was lower than the present day level, which would result in C-14 ages which are too young.

One further piece of supporting evidence was the TL dating of fired-clay artifacts from Dolni Vestonice by Zimmerman and Huxtable (1971). These authors adopted the fine-grain technique and obtained an average TL date of $33,000 \pm 3000$ years. Two C-14 dates, from the same stratigraphic layer in which the artifacts were found, are $29,150 \pm 300$ and $29,980 \pm 300$ (having been corrected for the 5730 half-life). Accepting the average of

the two C-14 dates, 29,600 years, then the difference between this and the TL date is 3400 years, not unlike the difference between the TL and C-14 ages for Mungo. It should be noted, however, that no fading tests were carried out on these samples which obviously weakens the argument for the validity of the TL dates.

As mentioned in Chapter VII, Huxtable and Aitken (1977) have carried out TL dating on ovenstones (not baked sediment) from six Mungo fireplaces, namely F6, F7, F8, F9, F12, and F14. Because of the "rather poor" measurement precision for their samples (presumably due to the small sample size of the ovenstones), they took a weighted mean for the TL ages of the fireplaces associated with the first polarity excursion, i.e. F7, F8, F9, and F12. This mean TL age is 33,500 years and it has a predicted error (Aitken, 1976) of 4300 years. The average C-14 age for the same fireplaces is 30,400 years (based on the 5730 year half-life). These authors conclude that although the difference of 3100 years is within the TL error limit, their data do not exclude the possibility of a higher atmospheric C-14 concentration than the Modern level.

These last two investigations would appear to rule out the possibility that random errors in either dating method are responsible for the age differences and also greatly diminish the probability that systematic errors are the cause. This is because systematic errors are likely to be laboratory specific, i.e. the calibration of radioactive sources, equipment, standards etc. Thus, although far from being conclusive proof, the results obtained here, and also by the authors mentioned above, do tend to add weight to the hypothesis that around 30,000 years ago the C-14 production rate was higher, probably due to a lower geomagnetic dipole field than at present. Hence C-14 ages from around this time are likely to be too young by approximately three or even four thousand years. In addition, the geomagnetic field

excursion recorded by the thermoremanent magnetization of the material of the fireplaces is therefore likely to have been a non-dipole, localised event of insufficient magnitude to significantly disturb the overall dipole field and hence the C-14 production rate.

8.7 Conclusions

The discussion in this Chapter is not intended to be a comprehensive review of the reasons for secular variations in the atmospheric C-14 concentration. (It would be rather pretentious if it were, since this very problem was the topic of no less than the Twelfth Nobel Symposium held at the Institute of Physics at Uppsala University, Sweden, in August, 1969). It is intended rather as a discussion of some points relevant to the understanding of possible explanations for the systematic differences between the TL and C-14 ages of the Mungo fireplaces.

Hence a brief outline of the radiocarbon dating method has been given together with a short discussion of the various influencing factors on the C-14 production rate. The most predominant of these is the Earth's geomagnetic field and any variations in this will be followed closely by variations in the C-14 production rate.

The discovery of a geomagnetic field excursion as recorded in the thermoremanent archaeomagnetism of the material of the fireplaces, led Barbetti (1972) to predict that the radiocarbon ages of fireplaces indicating a low field strength (i.e. F6) should be too young by between 2300 and 5560 years whilst those indicating a high field strength (i.e. F7, F8 and F9) should be too old by about 2,000 years.

Comparison with the TL ages shows all the C-14 ages to be too young and thus possible explanations were sought. Firstly systematic errors in the actual dating methods themselves were considered. A

detailed error analysis of the TL method was given in Chapter VII and a summary of possible sources of error in the radiocarbon method was given in this Chapter. It was not thought likely that any of these sources would introduce errors of magnitude sufficient to account for the TL/C-14 age differences.

The hypothesis was then put forward that the age differences between the TL and C-14 methods arise from a higher C-14 production rate 30,000 years ago, caused by a geomagnetic dipole field at a level lower than the present day. A value for the field of *ca.* 4×10^{25} gauss. cm³ (compared to the present day value of *ca.* 8×10^{25} gauss. cm³) would have been sufficient to account for the age discrepancies. A dipole field of this magnitude at this time is in keeping with the results of Bucha (1976) who proposed that the geomagnetic field was equal to or less than half its present value between 26,000 and 34,000 years ago.

If the global dipole field was in fact low during the whole lifetime of the fireplaces the high field intensity levels recorded by F7, F8 and F9 must have been due to a localised, non-dipole event. To fully understand these non-dipole events would require a detailed knowledge of the forces giving rise to the magnetism of the Earth. The nature of the geomagnetic dynamo, however, is not well-understood, but on the basis of hydromagnetic theory the Earth's geomagnetic field is defined by movements in the liquid core. Ascending and descending convective fluid motions on the boundary between core and mantle may have a large influence on the non-dipole field and it is possible that just such an event took place near the Mungo region some 30,000 years ago.

The hypothesis presented above is, of course, as yet only speculative and it will not be until many more intercomparisons of radiocarbon ages with either TL ages or some other absolute dating method from other parts

of the world have been made that we shall be able to fully rationalise and subsequently move towards a complete solution of the problem. To this end the results of Zimmerman and Huxtable (1971) and Huxtable and Aitken (1977) are useful and tend to reinforce this hypothesis.

CHAPTER IXTHERMOLUMINESCENCE DATING OF ABORIGINAL FIREPLACESLAKE JINDABYNE9.1 Introduction

The major application of the thermoluminescence dating technique for this thesis has already been described in Chapters VII and VIII. Two further smaller projects were also undertaken and these are described in this Chapter and the next.

The fireplaces investigated in this Chapter have only very recently been unearthed and are situated in and around the shores of Lake Jindabyne which is about 150 km south of Canberra. Very little archaeological information is available about this region but it was thought that the fireplaces were younger than the Pleistocene Age which occurred about 6,000 years ago in this region. No radiocarbon dates are as yet available, although samples of charcoal have been collected and submitted for dating by the archaeologists.

Four samples were tested initially but two of these have since been discovered to be termite mounds and not fireplaces at all! It is interesting to note, however, that preliminary tests on these two sites, JH3 and JH4, using the 'Pre-dose technique' of Fleming (1973) provided both an overestimate of about 1,000 years and an underestimate of about 200 years for both sites (see Chapter X, Section 10.3 for details of this estimating procedure). Traces of charcoal were also found at these sites and it would appear that they had been fired, although whether it was by human intervention or by forest fire still remains an archaeological problem. Because of this uncertainty and in part also because of the necessity to curtail practical work in order to produce this thesis, no further work was carried out on these samples.

Samples from fireplaces JH1 and JH2 were tested thoroughly however, and the results are presented in the following Sections. One of these fireplaces is pictured in Figure 9.1.

9.2 Sample Preparation

The same sample preparation as described in detail in Chapter VII was applied to the Jindabyne fireplaces. X-ray diffraction analysis indicated that this preparation produced 100% quartz for JH2 but that samples from JH1 still contained a small percentage of high sanadine (potassium aluminium silicate) even after the 10 min etching in HF.

This sample was given a further 10 min acid etch and X-ray diffraction indicated only a slight decrease in the amount of high sanadine present. Study of the glow curves from each of the two portions with different etching times showed no apparent difference and so it was assumed that this material contributed negligibly to the TL. Hence both samples were given a 10 min acid etch and equal portions deposited on aluminium discs from the dispenser as illustrated in Chapter VII.

9.3 Archaeological Dose Measurements

Because the Archaeological Dose (AD) received by each of these two fireplaces is much less than that received by the Mungo sites, the growth curve of the quartz is well away from saturation level. Hence the additional laboratory beta doses administered to the quartz grains in the 'additive procedure' (see Chapter I) could be larger.

As is normal with this procedure (Fleming, 1970) additional beta doses of approximately the same as the natural dose were used to evaluate the equivalent dose, ED. The supralinearity correction, I, was determined as before by replotting the TL growth curve after drainage of the



FIGURE 9.1: Fireplace JH2 at Lake Jindabyne.

Note the baked central region with the dark lumps of charcoal surrounding it.

natural TL by heating to 500°C. The slope of the second growth curve was less than 6% different from that of the first for both fireplaces.

A plot of the ratio of the natural TL to the natural plus beta TL versus the temperature was found to exhibit a plateau above about 300°C indicating that the 'plateau test' of Aitken and Fleming (1972) was again satisfied.

The values of ED, I and AD are given in Table 9.1.

9.4 Dose-Rate Measurements

The measurement of the dose-rate from the uranium and thorium series was carried out by alpha-counting then applying the conversion factors developed in Chapter VI. The potassium-40 dose-rate was calculated from the X-ray fluorescence measurements of the K_2O content (see Chapter V, Table 5.2) and again applying the conversion factors of Chapter VI.

Unfortunately insufficient time was available to have trace element X-ray fluorescence analysis carried out on these samples and so the uranium to thorium ratio was assumed to be 1 part uranium for every 4 parts thorium. The actual value for this ratio is not critical since, as before in Chapter VII, the majority of the beta and gamma doses come from the material of the fireplaces themselves. Also, no overlying clay layer is present here to complicate matters.

A check for the possibility of radon emanation was made by measuring 'sealed' and 'unsealed' alpha-counts following the method of Zimmerman (1971) but no such emanation could be detected. The effects of ground water were taken into account as described in Chapter VII (Section 7.7) but here a value of 50% ($\pm 25\%$) was used for the average fraction of the saturation level the fireplaces have experienced since this is a much wetter region than Mungo.

TABLE 9.1

The Equivalent Dose, Supralinearity Correction
and Archaeological Dose of the Lake Jindabyne Fireplaces

<u>Fireplace</u>	<u>Equivalent Dose (Rad)</u>	<u>Supralinearity Correction(rad)</u>	<u>Archaeological Dose (rad)</u>
JH1	2,050	190	2,240
JH2	1,220	175	1,395

The residual alpha dose, the beta dose attenuation and the contribution from cosmic rays were all evaluated as in Chapter VII and used to give the dose-rates quoted in Table 9.2. This Table gives the AD's and the ages with the errors quoted being derived in the next Section.

9.5 Error Analysis

The error analysis formalism developed by Aitken and Alldred (1972) and Aitken (1976) which was modified in Chapter VII, Section 7.8, in order to be applicable to the present studies was used to evaluate the errors quoted in Table 9.2.

One small additional term was added to the error terms quoted in Chapter VII and that is to account for the uncertainty in the uranium to thorium ratio. Because of the similarity in the values of the beta plus gamma doses for each of the two series (see Table 6.6) an error of only 3% is introduced by allowing the ratio to lie between one and seven parts thorium to every one part uranium.

It should be noted that the results of the archaeological dose measurements were slightly less reproducible than for the Mungo samples. This results in larger values of $\delta ED/ED$ and $\delta I/ED + I$ than before and hence a fractionally larger overall percentage error. This overall error is the one given in Table 9.2.

9.6 Summary and Conclusions

The archaeological sites at Lake Jindabyne have only very recently been discovered and thus only limited knowledge is available regarding the human occupation of the area. This TL investigation represents only a pilot study of the feasibility of applying the techniques developed for the study of the Mungo fireplaces to other sites from a different area

TABLE 9.2

Annual Dose-Rates, Archaeological Doses and TL Ages
of the Lake Jindabyne Fireplaces

<u>Fireplace</u>	<u>Annual Dose-Rate (rad/yr)</u>	<u>Archaeological Dose (rad)</u>	<u>TL Age (yr)</u>
JH1	0.748	2,240	2,995 \pm 270
JH2	0.698	1,395	1,998 \pm 180

and a different time period. This preliminary work appears to be successful.

The TL ages of about, 3,000 years and 2,000 years were measured for fireplaces JH1 and JH2 respectively. Two other sites, which have subsequently been discovered to be termite mounds, gave preliminary estimates of between 200 and 1,000 years using the 'p' and 'q' values of the Pre-dose technique (Fleming, 1973) to be described in the next Chapter. It is not certain whether these sites have been fired by human intervention or by natural causes such as forest fires.

The techniques developed for the dating work of Chapter VII have thus been successfully applied to samples from an entirely different context and there is no apparent reason why they should not be applicable to the many fireplaces from different sites scattered over the entire continent of Australia. It is to be hoped that work along these lines will continue.

CHAPTER XTHERMOLUMINESCENCE DATING OF COOKING STONES FROM NEW GUINEA10.1 Introduction

The Kuk Tea Research Station was established in New Guinea by the Australian Department of Agriculture, Stock and Fisheries in 1969 and it is a 700 acre property (mostly swampland) about 15 km northeast of the township of Mount Hagen. The long and complex history of the Kuk swamp extends back into the late Pleistocene as recorded in layers of volcanic ash from up to a dozen different eruptions.

This investigation is concerned mainly with the period from about 300 years ago when widespread use was made of the drained swampland in a system of sweet potato agriculture. A grid of wide, deep barets (ditches or drains cut for water control) subdivided by a close grid of small, shallow, flat-bottomed barets characterises the drainage of the swampland for cultivation of the sweet potato. Several house sites associated with this culture have been excavated and cooking stones from the fires and cooking pits of each house collected.

These stones were heated to a high temperature in the fires and then placed in a cooking pit together with the food to be cooked. From a comparison with the present-day cooking methods used by the natives, which are essentially the same as described above, the stones would have been heated to 'red-heat', i.e. about 450°C , which is sufficient to empty the traps of geologically-accrued TL. It could thus be anticipated that the stones would lend themselves to the technique of thermoluminescence dating.

Cooking stones from eight houses unearthed in one block, A9g, of the close grid baret system (see Fig. 10.1) were submitted for testing

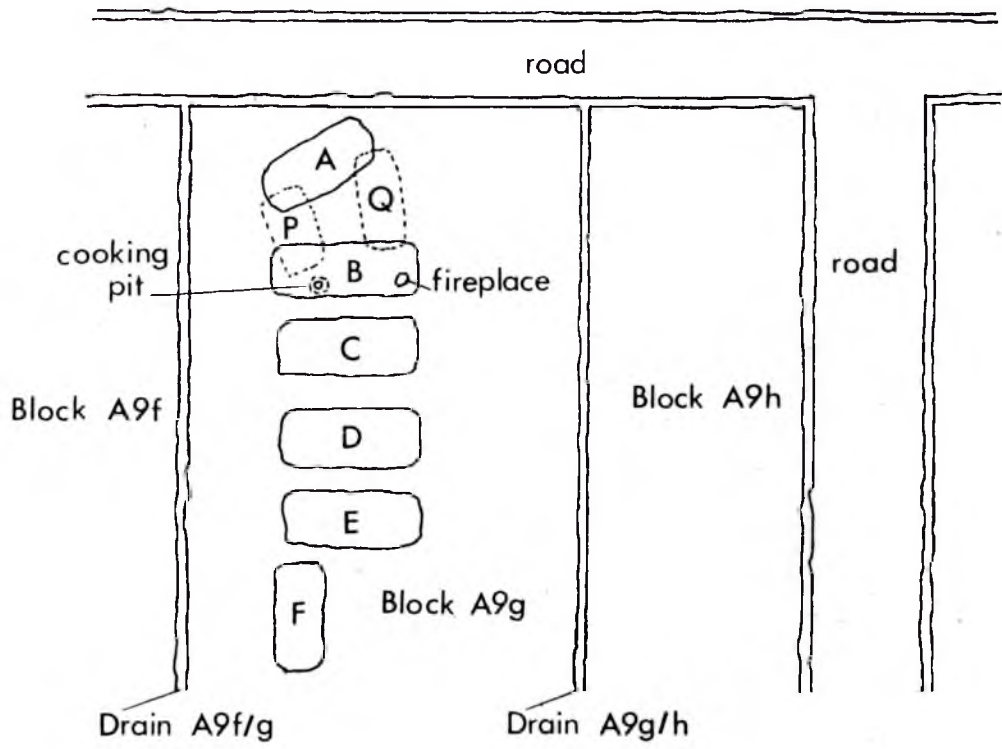


FIGURE 10.1: Houses Unearthed at the Kuk Tea Research Station, Block A9g. Houses P and Q lie stratigraphically below A and B and should be older. The positions of a fireplace and a cooking pit are shown for House B.

and initially the problem was to date and thus chronologically order the houses in order that a picture of the living habits of the natives could be built up.

All the houses were expected to be less than 300 years old, being younger than a volcanic ash layer dated by radiocarbon to around 300 years. The stones themselves were predominantly of the metavolcanic type and were, on average, approximately 5 to 10 cm in diameter. In view of their relatively recent heating in the cooking fires, the Archaeological Dose they will have subsequently received will be very small and thus likewise the TL output.

The Pre-dose Technique developed by Fleming (1973) however, is much more sensitive to small doses than the conventional high temperature techniques and it has thus been adopted for the dating of the cooking stones. This technique is described in the following Sections.

10.2 The Pre-dose Technique: Theory

The Pre-dose technique was first investigated by Fleming (1969) and a proposed mechanism of operation was put forward by Zimmerman (1971b). Fleming (1973) then applied the technique to a group of sherds from British sites and found the accuracy of the dating method to be close to 7% per sherd. The following model, as proposed by Zimmerman (1971b) and Fleming (1973), offers a satisfactory explanation of the phenomenon.

Two electron traps, T_1 and T_2 , and two hole traps, L and K, are postulated (see Fig. 10.2). T_1 is shallow and together with L, a luminescent centre, is responsible for the 110°C peak. Trap T_2 is deep enough not to be emptied by heating to 500°C and is necessary to maintain charge balance with level K in the crystal.

During the TL process, electrons are thermally released from T_1 and

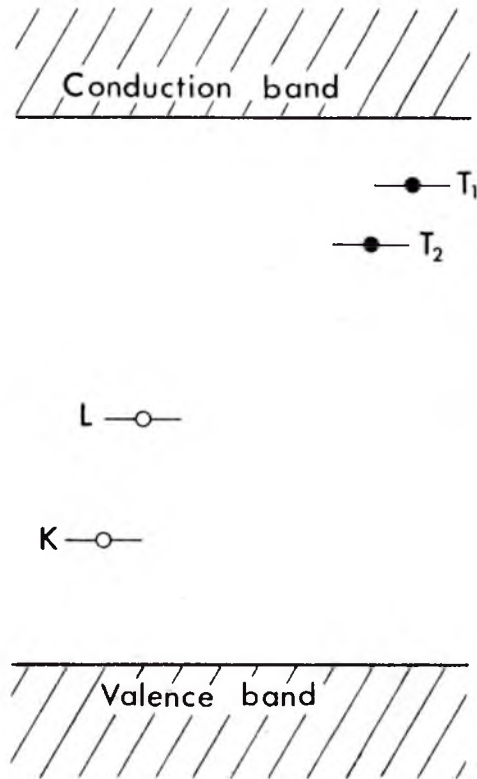


FIGURE 10.2: The Trapping Levels Postulated to Explain the Pre-Dose Phenomenon.

some are captured by TL centres, L, with the consequent emission of light. Such capture only occurs for centres which are charged with a hole and so the TL sensitivity is proportional to the number of electrons in T_1 and the number of holes in L.

During irradiation, electrons are trapped at T_2 and at T_1 but since this latter trap is very shallow the number of electrons will decrease exponentially with a half-life of 55 min at 25°C. (see Chapter I, Table 1.1). In addition, holes are captured at centres K which have a much higher capture cross-section than L so that during archaeological times, the number of holes trapped at K will build up. This phenomenon can be used for dating a sample as described below.

Since the traps T_1 are empty (due to the very short half-life), the sample is given a small laboratory beta test dose (typically about 2 rad) which puts a few electrons into T_1 and a small number of holes into K. On heating through 110°C, the electrons are released and some find those luminescent centres L which are charged with holes. Because there has been no increase in the number of holes at L the observed sensitivity, S_0 , is the same as if the measurement had been made immediately after the sample had been last heated.

The sample is now heated to 500°C which causes the thermal release of holes from K and these are then captured at L. If the sample is now given the same laboratory test dose as before, then the sensitivity, S_N , measured on heating to 110°C will be greater than S_0 because the number of luminescent centres, L, now charged with holes is greater. The difference, $S_N - S_0$, is proportional to the number of holes accumulated at K during antiquity and hence is proportional to the radiation dose received. Two methods of determining the proportionality constants are described in the next section.

10.3 The Pre-dose Technique: Application

As described in the last Section, the TL response to a small test dose before heating to 500°C is S_0 and the response to the same test dose after heating to 500°C is S_N . $S_N - S_0$ is thus a measure of the archaeological dose received by the sample and to quantify this growth in sensitivity from S_0 to S_N in terms of actual rads a further laboratory beta pre-dose is administered. This pre-dose increases the sensitivity to $S_N + \beta$ and two procedures are used based on this in the evaluation of the archaeological dose.

(a) p-value

At least two equal portions of quartz grains are required in this method. The first portion is given a small beta test dose and the value of S_0 is measured by heating through 110°C . A laboratory beta pre-dose, β , is then given to the sample and a 500°C heating carried out. On cooling, a second test dose, equal to the first, is administered to the sample which provides a value of $S_N + \beta$.

The second portion is heated to 500°C and when cool, a test dose measures the value of S_N . The sensitivity enhancement rate is defined by (Fleming, 1973)

$$p = \frac{S_N + \beta - S_N}{S_0} \times \frac{1000}{\beta} \text{ per krad} \quad (10.1)$$

where β is the laboratory pre-dose in rads.

(b) q-value

Only one portion of quartz grains is required in this procedure although it would be repeated on several different portions. A test dose measures the value of S_0 and the sample is then heated to 500°C . A subsequent test dose on cooling measures S_N . A pre-dose, β , is then applied, the sample heated to 500°C and, on cooling, a test dose finally yields a sensitivity $S'_N + \beta$.

The sensitivity enhancement rate for this procedure is defined by

$$q = \frac{S'_N + \beta - S_N}{S_0} \times \frac{1000}{\beta} \text{ per krad} \quad (10.2)$$

It is apparent that both methods should yield the same sensitivity enhancement rate i.e. $p = q$. This will not be the case, however, near the onset of saturation of the pre-dose effect, as follows.

Fleming (1973) has shown that the estimate of the archaeological dose is only valid if the rate of growth of sensitivity stimulated by laboratory pre-dose is the same as that applicable over the archaeological age of the sample. For quartz this will be true up to a pre-dose of about 500 rads after which saturation begins to occur (see Fig. 10.3). The effects of saturation on the p- and q-values will be different as illustrated in Figure 10.4 a and b.

In Figure 10.4a the measurement of the p-value is shown. Even if S_N lies on the linear portion of the sensitivity enhancement curve, $S_N + \beta$ may lie in the region where pre-dose saturation has set in. An assessment of the archaeological dose using S_0 , S_N and $S_N + \beta$ would yield an overestimate.

In Figure 10.4b the q-value measurement is depicted. If the archaeological dose has placed S_N beyond the linear region, then after

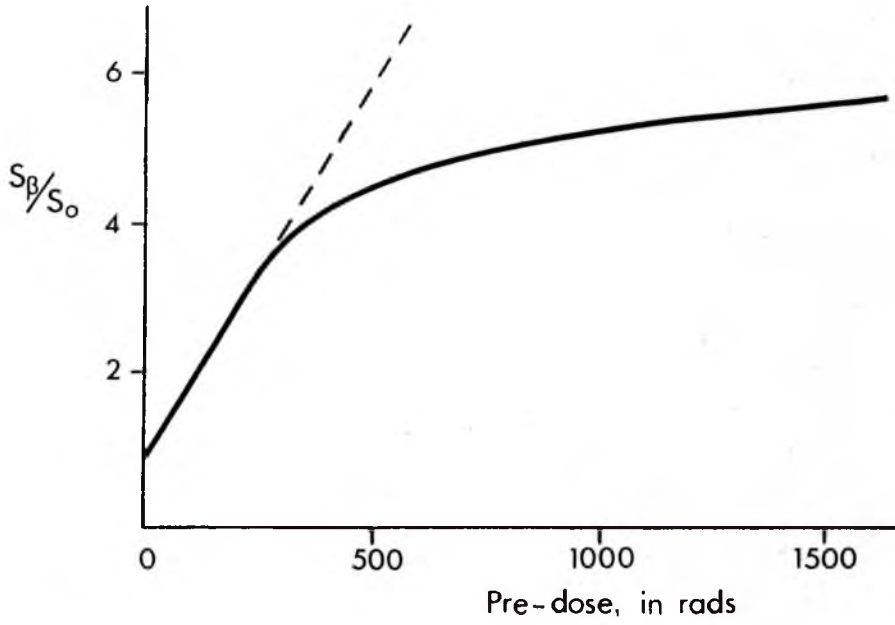


FIGURE 10.3: Saturation of the Pre-Dose Phenomenon.
 S_0 is the sensitivity to a test dose for zero pre-dose and S_β is the sensitivity to the same test dose after the given pre-dose has been administered.

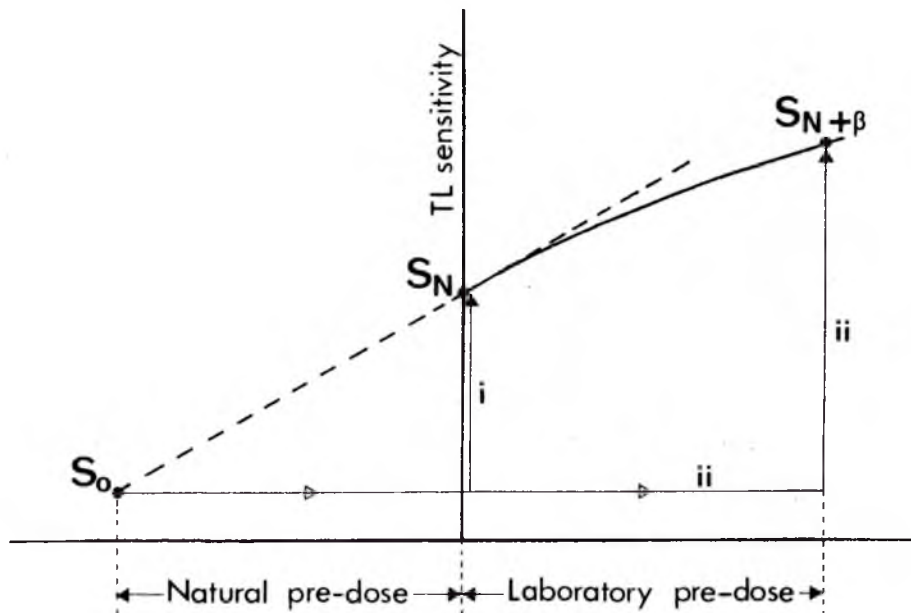


FIGURE 10.4a: Saturation Effects on the p-value Determination. Path (i) is a natural pre-dose plus heating to 500°C to give S_N . Path (ii) is a natural pre-dose plus laboratory pre-dose, β , followed by heating to 500°C to give $S_{N+\beta}$.

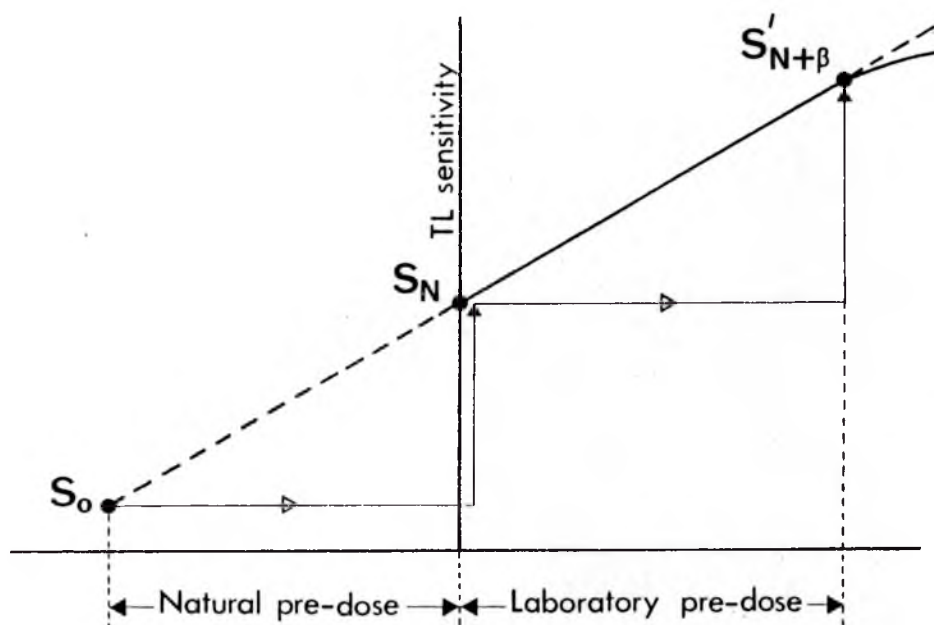


FIGURE 10.4b: Saturation Effects on the q-value Determination. The natural pre-dose plus heating to 500°C gives S_N . A laboratory pre-dose, β , to the same portion followed by heating to 500°C gives $S'_N + \beta$.

heating to 500°C the sensitivity enhancement curve will have an initial linear portion that repeats the original growth from S_0 to S_N . The assessment of the archaeological dose using the values of S_0 , S_N and $S_N + \beta$ obtained by this procedure would yield an underestimate.

(It was this p- and q-value estimating procedure which was used to determine the age ranges for fireplaces JH3 and JH4 in the last Chapter).

10.4 Sample Preparation

The cooking stones were first crushed as gently as possible in a vice and then sieved and prepared as before (see Chapter VII). Great difficulty was experienced in obtaining a non-magnetic fraction using the magnetic separator. Most of the crystals are very discoloured and appear to be heavily diffused with impurities, some of which are obviously magnetic.

Fleming (1973) has recommended that no HF acid treatment should be used as such treatment seems to totally upset the pre-dose data. The resultant fraction obtained for dating does, therefore, contain feldspars as well as quartz as is indicated by X-ray diffraction (see Fig. 10.5).

Each cooking stone yielded a very small number of crystalline grains which could be used for dating and this paucity of sample is probably a cause, in part, for the lack of reproducibility of the archaeological dose measurements described in the next Section since large numbers of discs could not be tested.

10.5 Archaeological Dose Measurements

Of interest in the measurement of the Archaeological Dose (AD) is an increase in sensitivity to a small beta test dose after heating the

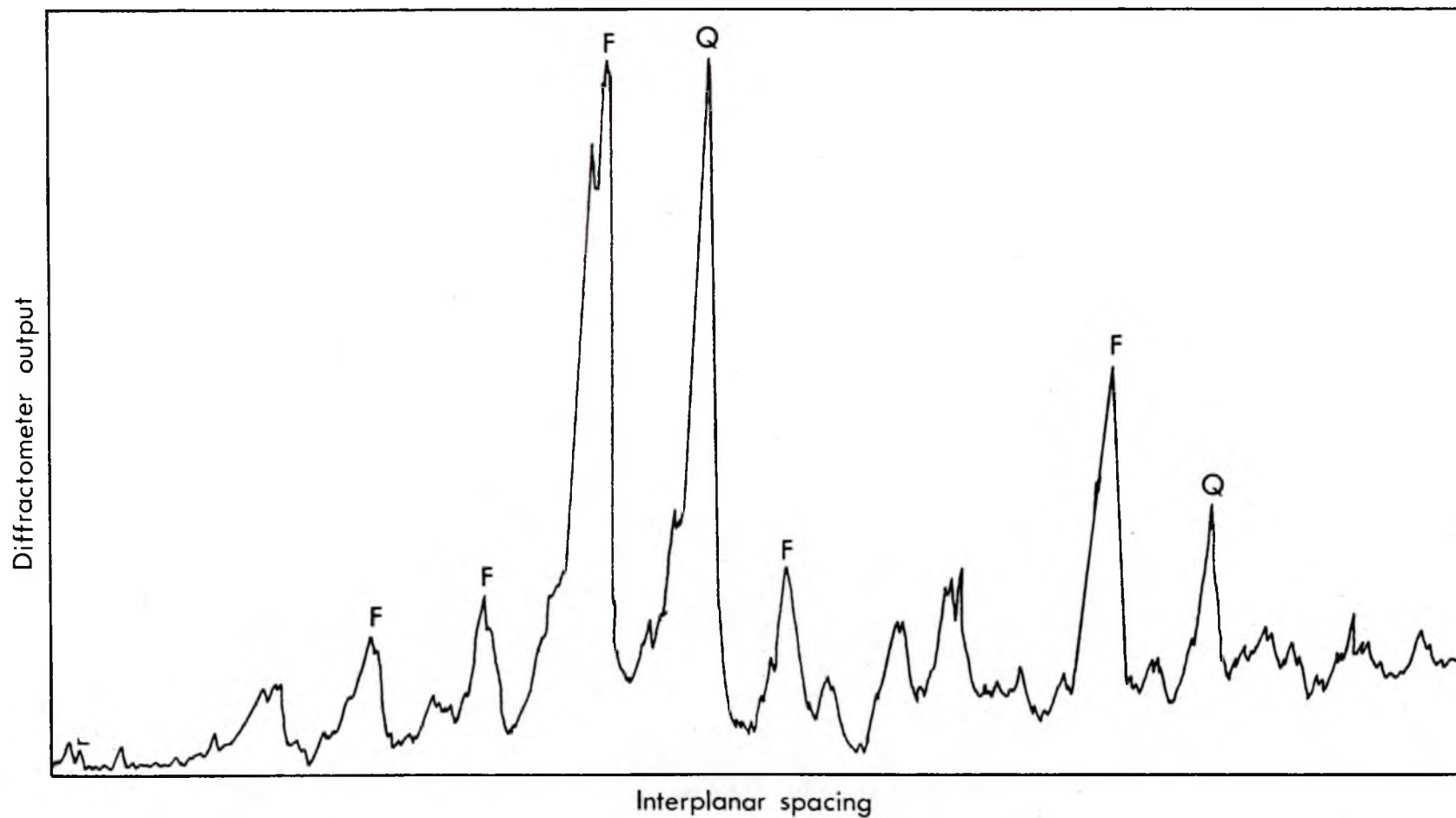


FIGURE 10.5: Typical X-ray Diffraction Pattern of the Non-Magnetic Fraction obtained from the Cooking Stones. Peaks marked 'F' are feldspar peaks; those marked 'Q' are quartz peaks.

sample to 500°C. Broadly speaking the results of the TL dating programme carried out on the cooking stones could be divided into two groups:

- (a) those which exhibited a sensitivity increase
- and (b) those which did not exhibit a sensitivity increase.

Typical glow curves from each of these two groups are shown in Figure 10.6a and b.

The results of the latter group gave no meaningful answers and had to be discarded but even the former group gave answers which were not reproducible within normal error limits. As an example, a series of tests on samples from the cooking pit of House B (A9g 5F40) gave AD's of 26.5, 62.0, 57.0 and 15.2 rads. These values have a mean of 40.2 rads which is subject to a standard error of 11.4 rads or nearly 30%.

All the samples tested had similar large error terms associated with them and these are given in Table 10.1 together with the mean AD for each House. Most of the AD's quoted in this Table were measured using the q-value technique. Some p-value measurements were carried out but due to the poor reproducibility of the samples it was impossible to assert whether the p- and q-values were equivalent. The samples have all received an AD of less than 100 rads so that saturation is not a problem. As a result of this and because of the sample paucity, the q-value procedure for the determination of the AD's which requires only one disc for the measurement of S_0 , S_N and $S_N + \beta$, was used for most of the AD's given in Table 10.1.

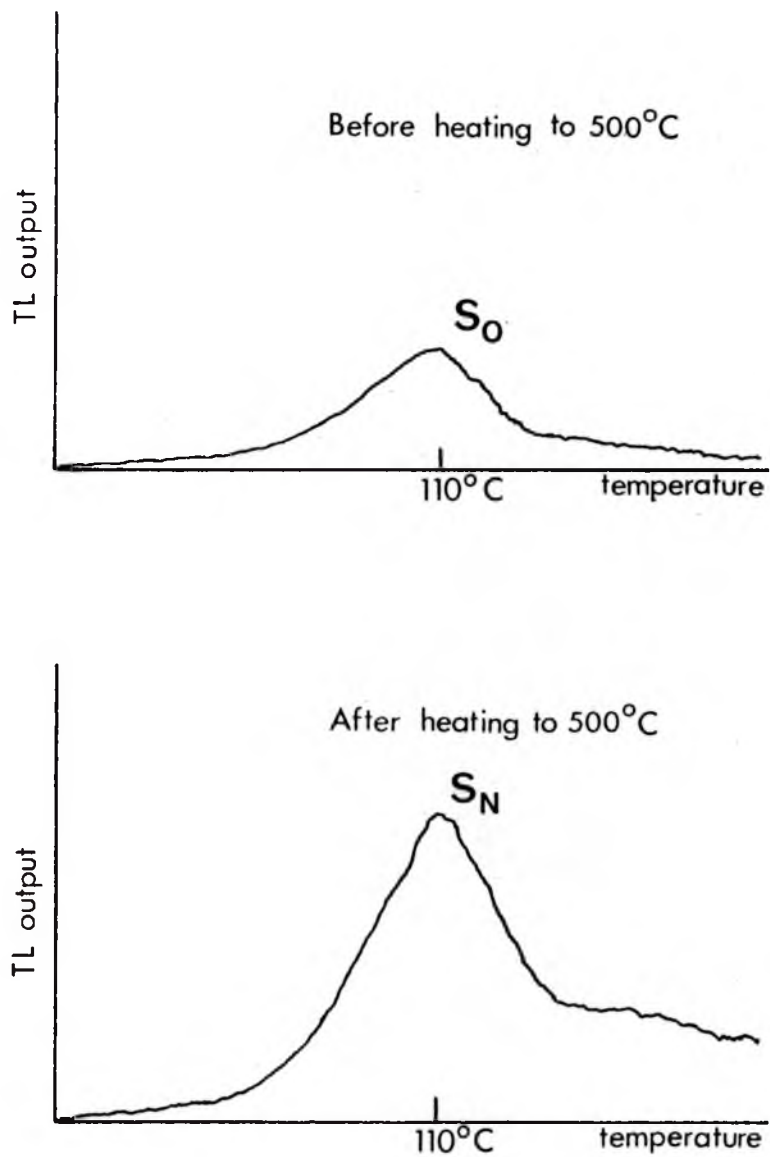


FIGURE 10.6a: Glow Curves from Samples which Exhibited a Sensitivity Increase. S_0 is the response to a test dose before heating to 500°C and S_N is the response after heating.

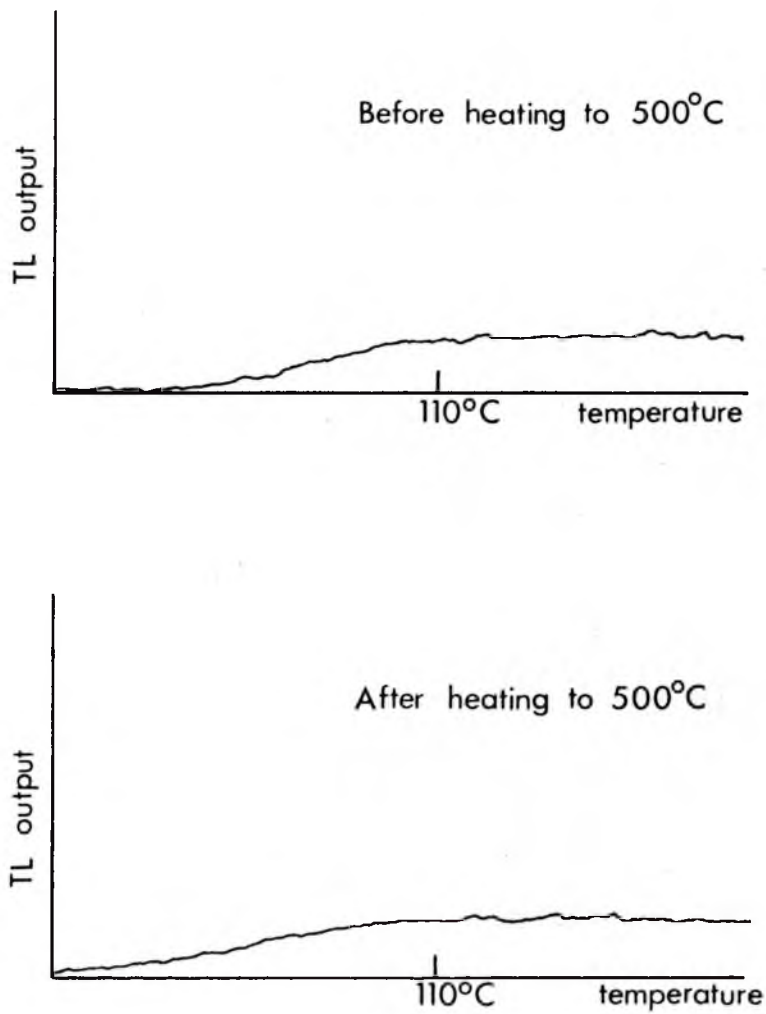


FIGURE 10.6b: Glow Curves from Samples which did not Exhibit a Sensitivity Increase. The response to a test dose before and after heating to 500°C is unchanged.

TABLE 10.1

The Archaeological Doses of the New Guinean Cooking Stones

<u>House</u>	<u>Archaeological Dose (rad)</u>		
B	40.2	±	11.4
A	36.1	±	12.4
Q	37.5	±	14.5
P	63.1	±	19.4

10.6 Dose-Rate Measurements

The dose-rate measurements were carried out in the normal way i.e. alpha-counting for the uranium and thorium series and X-ray fluorescence for the potassium-40 content. The problem does arise here of the environmental gamma dose since the stones themselves are only 5 to 10 cm in diameter and the gamma dose is delivered from a sphere of radius about 30 cm.

The stones were, however, usually found in fairly large piles and in addition the radioactive content does not vary appreciably between different stones. These two factors were taken into account when making the assumption that the dose-rate to each stone was essentially its own self-dose. This will certainly introduce an error in the age but this will hardly be comparable to the error found in the measurement of the AD.

The AD, dose-rate and age of each House site are given in Table 10.2.

10.7 Significance of the TL Ages

As mentioned in Section 10.1 the initial archaeological problem was to date and thus chronologically order the House sites which were all anticipated to be less than 300 years old. The TL ages given in Table 10.2 appear to confirm that the sites are younger than 300 years but the error terms make a chronological ordering impossible.

The errors given in Table 10.2 were evaluated as described in Chapter VII with an additional error of 5% being added to cover the possible error introduced by neglecting the environmental dose. By far the predominant term in the error analysis is the error associated with the AD, this being of the order of 30% for most samples.

The statistical 'z' ratio test was applied to Houses A and P (the extreme ages) and this gave a value of $z = 1.2$. This is not significantly

TABLE 10.2

The Archaeological Dose, Annual Dose-Rate and TL Age
of the New Guinean Cooking Stones

<u>House</u>	<u>Archaeological Dose (rad)</u>	<u>Annual Dose-Rate (rad/yr)</u>	<u>TL Age (yr)</u>
B	40.2	0.25	160 ± 50
A	36.1	0.25	145 ± 50
Q	37.5	0.24	155 ± 60
P	63.1	0.24	260 ± 80

large enough to reject the hypothesis that the difference in the ages is simply due to sampling variations and that the two ages are distributed about some mean value. All that can be asserted is that the four Houses dated appear to be between 100 and 300 years old, which is consistent with radiocarbon dating, but that no chronological ordering could be carried out because of the large errors associated with each age.

10.8 Analysis of the Samples

In an attempt to find out why the TL samples from the cooking stones exhibited such a lack of reproducibility they were all subjected to X-ray diffraction and optical emission spectography.

The X-ray diffraction analysis provided a very good correlation between those samples which did not exhibit a sensitivity increase and those which had a high feldspar content compared to quartz. A typical X-ray diffraction pattern for one of these samples has already been illustrated in Figure 10.5 and it was deduced that for these samples the stronger TL signal from the feldspars is masking the quartz signal and hence no meaningful results could be obtained. This was demonstrated by giving one of these samples a very large pre-dose (~ 10 krad) and then heating to 500°C . The results, as shown in Figure 10.7, indicate that the response to a test dose before heating to 500°C shows no apparent 110°C quartz peak but that after heating to 500°C the response shows a small quartz peak beginning to emerge from the feldspar signal.

Optical emission spectography analysis showed that the samples which did exhibit a sensitivity increase and which had a high quartz content, also had a high impurity level. Table 10.3 shows the results of this analysis for a typical sample from this group compared to the same analysis on relatively pure quartz crystals. The high impurity level

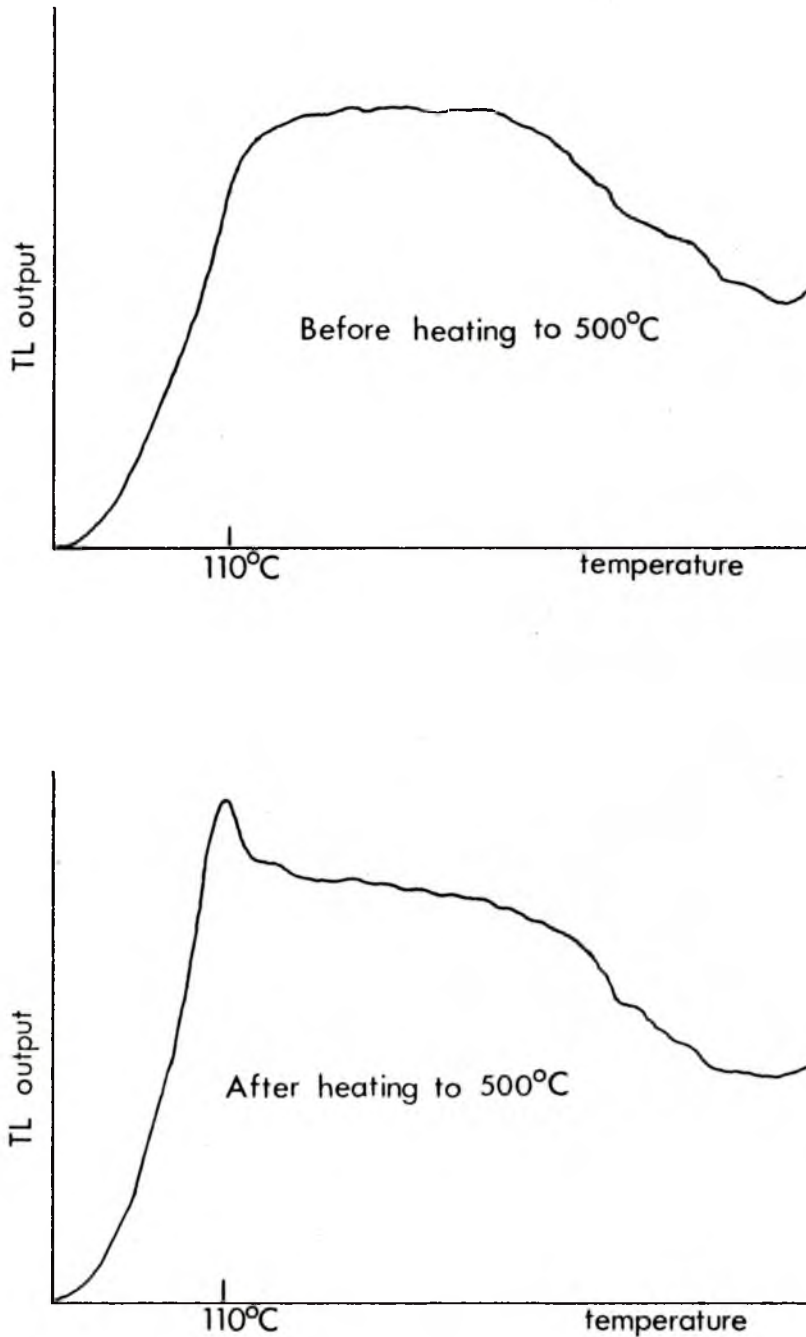


FIGURE 10.7: Glow Curves from a Sample given a Very Large Pre-Dose ($\sim 10\text{krad}$). After heating to 500°C the response to a test dose shows a small 110°C quartz peak beginning to emerge from the feldspar signal.

TABLE 10.3

Optical Emission Spectrography Results
for the New Guinean Cooking Stones

	<u>Impurities (ppm)</u>					
	<u>Al</u>	<u>Ca</u>	<u>Ti</u>	<u>Na</u>	<u>Mn</u>	<u>Fe</u>
Quartz Crystals	< 10	< 5	-	-	< 10	< 10
Cooking Stones	~ 100	~ 100	~ 100	~ 100	~ 50	~ 100

is immediately obvious (the actual numbers given in Table 10.3 should, however, be taken as an order of magnitude figure only).

10.9 Summary and Conclusions

Cooking stones from houses unearthed at the Kuk Tea Research Station in New Guinea have been tested using the Pre-dose technique of Fleming (1973). The results have proven to be extremely unreproducible with consequent large standard errors in the measurement of the mean Archaeological Dose. The dose-rates have been measured as before but no account has been taken of the possible environmental gamma dose. (Radon emanation and ground water effects have also been neglected).

The ages thus evaluated all lie between 100 years and 300 years which is consistent with a radiocarbon age of 300 years on a volcanic ash layer expected to be older than the houses. The initial archaeological problem of chronologically ordering the houses has proved unsuccessful due to the large errors in the ages.

The samples which do not respond to the pre-dose effect (see Fig. 10.6b) have been shown by X-ray diffraction to contain a large percentage of feldspars whose stronger signal masks that of quartz (see Fig. 10.7). Those samples which do exhibit a sensitivity increase (see Fig. 10.6a) have been shown to also contain a high level of impurities which have diffused into the quartz grains over geological times. These impurities are present in the quartz lattice structure to such a high extent that they may destroy or greatly modify the existing TL trapping centres or it may be that the TL centres emit photons in the normal way but that they are absorbed by optical absorption centres created by the high impurity levels. The variation in type and amount of impurities present in each of the grains is thought responsible for the lack of reproducibility exhibited by the TL samples.

This illustrates some of the problems associated with dating of certain geological samples by thermoluminescence due to the wide variation of physical and chemical environment on formation and the wide range of impurities which can diffuse into the quartz during its history. It is encouraging to note, however, that the ages did fall within the expected range and this demonstrates the large time span covered by the technique of thermoluminescence dating as indicated by the practical work of this thesis.

CHAPTER XI

CONCLUSIONS AND SUGGESTIONS FOR FURTHER WORK

11.1 Conclusions

The aim of the research leading to the production of this thesis was to develop the TL dating method so that it could be applied at sites of archaeological interest in the Australian region. This aim has been successfully fulfilled through the TL dating of Aboriginal fireplaces from Lake Mungo and Lake Jindabyne and of cooking stones from New Guinea. In the process of carrying out these dating programmes, a large amount of time and effort has been put into researching the theoretical aspects of the radiation dosimetry of quartz grains embedded in a radioactive matrix. The results of the investigations into the alpha and beta radiation dosimetry provide a thorough and up-to-date description of the absorbed dose from these particles in quartz inclusions and no further work in these areas is immediately obvious.

The gamma dosimetry results, however, are far from complete and the work of this thesis has shown up areas where much more research is needed. This is particularly so in the case of the dependence of the TL response on photon energy and on grain size.

The radiation data on the decay characteristics of the naturally-occurring radioactive series and the resultant dose-rate conversion factors given in this thesis should be taken as the most accurate presently available. The only further work required in this area is the updating of the radiation data as it becomes available from the research of the nuclear physicists.

The TL dating of the Lake Mungo fireplaces confirms the extreme antiquity of the sites and places the lakeside dwellers at Mungo in an era of Australian prehistory more than 30,000 years ago. The comparison of these TL ages with previous radiocarbon ages shows a systematic difference of between 10 and 15% with the TL ages being the elder in each case. This small difference, if real, may be accounted for in terms of variations in the C-14 concentration in the atmosphere due to changes in the Earth's geomagnetic dipole field at this period of time. If this was indeed so, then a geomagnetic dipole field of about half the present day level would have been necessary at this time, a level in keeping with the predictions of Bucha (1976). However, sight must not be lost of the fact that other, more subtle errors than those discussed in relation to the TL dating presented in this thesis may exist. Aitken (1976a) has indicated that the TL of certain quartz samples appears to fade if they are stored in darkness for some time after etching in HF acid. He also suggests that the TL growth of certain quartz samples may not have a linear region but may follow an exponential shape even while the sample has received well short of a saturation dose. This would result in a TL age which is too old if linearity were assumed.

These problems, together with the many corrections and possible errors detailed in Chapter VII, raise the question as to whether the TL ages are accurate enough to draw the conclusions about the behaviour of the Earth's magnetic field made in Chapter VIII. It will only be after much further work in the problem areas mentioned above has been carried out and many more intercomparisons of TL and C-14 ages become available that this question will be answered.

The results of the dating of the fireplaces from Lake Jindabyne and the cooking stones from New Guinea serve to exemplify the wide time span over which TL dating may be applied.

11.2 Suggestions for Further Work

The main areas where the research of this thesis has shown up the need for further work have already been outlined in this Chapter and they are: (i) the gamma ray dosimetry of quartz inclusions embedded in a radioactive clay matrix; and (ii) further intercomparisons between radiocarbon and TL ages (or any other absolute age determination method).

For the gamma ray dosimetry, a method of determining the photon spectrum from the natural radioactive series is necessary. The use of a sophisticated computer technique known as the 'Monte Carlo' method is one possible approach. Then, having determined the photon spectrum, the theory of Chan and Burlin (1970), which was formulated for monoenergetic photons, can be integrated over the entire natural photon spectrum of each series in order to assess the absorbed dose from the gamma rays.

The results of the intercomparison between the TL and C-14 ages for the Lake Mungo fireplaces are in good agreement with the intercomparisons of Huxtable and Aitken (1977) and Zimmerman and Huxtable (1971). Many more such intercomparisons from this and other parts of the world ranging over a much wider time span are necessary, however, before the speculative predictions made in this thesis regarding the behaviour of the Earth's magnetic field can either be verified or negated. This is strongly recommended as an area for immediate further research.

APPENDIX A

ALPHA SOURCE CALIBRATION

The Cm-242 alpha source, designated ANU α -2, was calibrated using two TLD phosphors, $\text{CaF}_2:\text{Dy}$ and MBLE flourite super S, which were kindly supplied by Dr M.J. Aitken of the Research Laboratory for Archaeology, Oxford. Each phosphor had been deposited on two aluminium discs and the alpha efficiency factors for each had been measured by the Oxford laboratory.

Each of the discs was given known doses from α -2 and the laboratory beta source, β -2, which had been calibrated previously (Appendix C). Knowing the alpha efficiency factors and the beta dose delivered to each disc, the alpha dose and hence the dose-rate of α -2 may be calculated. Before detailing the results of this calibration, it is necessary to define the various parameters required in the calculations.

Zimmerman (1971, 1972) has shown that the alpha efficiency factors for thermoluminescent phosphors are energy dependent. Aitken and Bowman (1975) have defined an a-value which is energy independent but which is equal to the ϵ -value quoted by Zimmerman (1971) for irradiation with 3.7 MeV alpha particles (i.e. approximately the average alpha energy for a polonium-210 source). This value, $\epsilon(3.7 \text{ MeV})$, is related to the effective alpha efficiency factors for the natural series, $\epsilon(\text{eff})$, by

$$\epsilon(\text{eff}) = 0.80 \times \epsilon(3.7 \text{ MeV}) \text{ for uranium}$$

and

$$\epsilon(\text{eff}) = 0.86 \times \epsilon(3.7 \text{ MeV}) \text{ for thorium.}$$

For a Th/U ratio of 6/1 this gives

$$\epsilon(\text{eff}) = 0.85 \times \epsilon(3.7 \text{ MeV}).$$

The curium-242 source, α -2, which was used throughout this present

work has a different energy to the polonium-210 source and hence a different alpha efficiency factor. As most of the alpha particles from the Cm-242 source lie within the range 4 to 5 MeV, an average energy of 4.5 MeV is assumed. From the graphs given by Zimmerman (1972), the alpha efficiency factor for α -2, $\epsilon(4.5 \text{ MeV})$, is related to $\epsilon(3.7 \text{ MeV})$ by

$$\epsilon(4.5 \text{ MeV}) = 1.13 \times \epsilon(3.7 \text{ MeV}) \quad (\text{A1})$$

hence

$$\epsilon(4.5 \text{ MeV}) = 1.13 \times a$$

Also, since $\epsilon(\text{eff})$ is equivalent to the k-value quoted throughout this thesis, it is useful to set down the relation for $\epsilon(\text{eff})$ i.e.

$$\epsilon(\text{eff}) = 0.75 \times \epsilon(4.5 \text{ MeV})$$

therefore,

$$k = 0.75 \times \frac{(\text{TL/rad})_{\alpha}}{(\text{TL/rad})_{\beta}} \quad (\text{A2})$$

where $(\text{TL/rad})_{\alpha}$ in equation (A2) refers to the TL induced by the Cm-242 alpha source, α -2.

We can now detail the calibration experiment.

1) $\text{CaF}_2:\text{Dy}$

The two discs with $\text{CaF}_2:\text{Dy}$ deposited on them were given several alpha and beta doses until the TL output from 10 seconds of α -2 was exactly matched by the TL output from a given dose of β -2. This was found to be 105 ± 2 seconds of β -2, or 247 ± 5 rads. $\epsilon(4.5 \text{ MeV})$ is given by

$$\epsilon(4.5 \text{ MeV}) = \frac{(\text{TL/rad})_{\alpha}}{(\text{TL/rad})_{\beta}}$$

Since the TL output is the same, then

$$\epsilon(4.5 \text{ MeV}) = \frac{(\text{rad})_{\beta}}{(\text{rad})_{\alpha}} = \frac{247}{(\text{rad})_{\alpha}}$$

The a-value given by the Oxford laboratory for $\text{CaF}_2:\text{Dy}$ is 0.48 and hence $\epsilon(4.5 \text{ MeV})$ has a value of 0.54. As a result of this

$$(\text{rad})_{\alpha} = \frac{247}{0.54} = 457 \pm 12 \text{ rads}$$

This alpha dose was delivered in 10 secs therefore the dose-rate of α -2 is found to be,

$$\alpha\text{-2} = 45.7 \pm 1.2 \text{ rads/sec.}$$

2) MBLE fluorite super S.

The same procedure was used for the two discs with the MBL fluorite deposited on them. The TL output from 60 seconds of α -2 was matched by the TL output from 115 ± 5 seconds of β -2 i.e. 270 ± 12 rads. Hence,

$$\epsilon(4.5 \text{ MeV}) = \frac{270}{(\text{rad})_{\alpha}}$$

The a-value quoted for MBL fluorite super S is 0.082. This implies

$$(\text{rad})_{\alpha} = \frac{270}{0.093} = 2900 \pm 130 \text{ rads.}$$

This dose was delivered in 60 secs and therefore the dose-rate of α -2 is found to be,

$$\alpha\text{-2} = 48.3 \pm 2.1 \text{ rads/sec.}$$

The two values, 45.7 and 48.3 rads/sec, are in fairly good agreement. The second determination has a larger error associated with it

because of poorer reproducibility in the TL outputs. This is thought to be due to pre-dose effects in peak III of the glow-curve of MBLE fluorite super S.

A value of 46 ± 1.5 rads/sec was used throughout these studies together with a factor to account for the radioactive decay of the source. Also, the k-values quoted in Chapter VII were determined according to equation (A2).

APPENDIX B

ALPHA-COUNTER CALIBRATION

The method adopted to calibrate the alpha-counter was to count a sample with a known uranium and thorium content. The anticipated dose-rates from these concentrations may be calculated from Table 6.5 and then converted through the equations on page 175 to anticipated alpha-count rates assuming maximum theoretical efficiency. The effective or practical efficiency is then calculated by taking the ratio of these two alpha-count rates.

Two geological "standards" were used for the alpha-counter calibration both of which were supplied by the Geology Department, A.N.U. The first was a thorium rich material diluted by the addition of silica (quartz) to have 25 ppm thorium and 1 ppm uranium. The second was the U.S. Geological Survey standard (U.S.G.S.) GSP-1 which has 104 ppm thorium and 1.96 ppm uranium. Both of these standards gave results which were in excellent agreement with each other and provided threshold fractions (or effective efficiencies) of 0.76 for the uranium series and 0.79 for the thorium series. These values were adopted throughout this present work and the former standard (because of its greater quantity) was used regularly to check the constancy of the apparatus. The accuracy of this calibration is estimated to be 5% at one standard deviation.

It is worth noting here that care must be exercised in the preparation of the samples for alpha-counting as Zimmerman (1971) has shown that for samples in which a sizeable fraction of the uranium and thorium is contained in inclusions having an appreciable self-dose (such as zircon and apatite grains), the alpha-count rate will increase when the material is

crushed to a fine grain size. Exactly the opposite effect was found with samples from the Lake Mungo fireplaces i.e. the alpha-count decreased when the material was crushed to a fine grain size. The following explanation is thought to be the cause of this phenomenon.

The Mungo clay is relatively low in radioactivity and also contains many inclusions of radioactivity-free material i.e. the quartz grains. When any sample is crushed to a fine grain size the surface to volume ratio of the grains increases, so that a given mass of material will increase in volume. The distribution of uranium and thorium in the Mungo clay is assumed to be reasonably homogeneous so that when the grains are crushed, the quartz (radioactivity-free) inclusions have the effect of diluting alpha activity and hence the sample gives a lower count rate.

In recognition of this problem, all of the alpha-counting samples were prepared by gently segregating the material in a mortar and pestle with as little crushing as possible. The alpha-counts thus obtained are then representative of the natural radiation environment of the samples over archaeological time.

APPENDIX CBETA SOURCE CALIBRATION

Two quite independent beta source calibration experiments were carried out and the excellent agreement between the results of the two would indicate a high degree of accuracy in the calibration.

Method 1

The laboratory $^{90}\text{Sr} - ^{90}\text{Y}$ beta source, designated ANU β -2, was intercompared with a well-calibrated $^{90}\text{Sr} - ^{90}\text{Y}$ source from the centre for Archaeometry, Washington University, St. Louis, U.S.A. through the kind efforts of Dr. David Zimmerman. The calibration was carried out using the thermoluminescent phosphor lithium fluoride, LiF (TLD-100).

About 100 mg of LiF grains were given a known beta dose at St. Louis and were forwarded, along with a monitor sample which had received exactly the same pre-treatment but no beta dose, to this laboratory. The dosed LiF grains were sprinkled on several aluminium discs and the TL output measured. A second normalising beta dose was administered after the first glow-out and the TL from this was used to normalise each disc for differences in weight.

The monitor grains were then placed on several discs with one disc being glowed out to check that negligible radiation dose had been received by all the grains during their travels. The remaining discs were given various beta doses from ANU β -2 until the TL was exactly equal to that from the grains which had been given the known dose (again using the normalising procedure). It is then possible to say that the dose delivered by ANU β -2 is the same as that delivered at St. Louis.

The results are as follows.

$$\text{Dose to LiF grains at St. Louis} = 571 \pm 10 \text{ rads}$$

Irradiation time for ANU β -2 to give equivalent

$$\text{TL output} = 249 \pm 5 \text{ secs}$$

$$\text{Dose-Rate to LiF from ANU } \beta\text{-2} = \frac{571}{249}$$

$$= 2.29 \pm 0.09 \text{ rad/sec}$$

This can be converted to a dose-rate to quartz by multiplying by the ratio of the mass stopping powers for quartz and LiF.

Hence,

$$\text{Dose rate to SiO}_2 \text{ from ANU } \beta\text{-2} = 2.29 \times 1.06$$

$$= \underline{2.43 \pm 0.09 \text{ rad/sec.}}$$

Method 2

The beta source was also calibrated against a Co-60 gamma source which is situated in the Division of Plant Industry, C.S.I.R.O., Black Mountain, Canberra. This Co-60 source has been calibrated by the 'Fricke Dosimeter' method and has a quoted accuracy of $\pm 2\%$.

The same procedures as described in Method 1 were applied again with two samples being used. One is given a known dose from the calibrated source and the second irradiated by ANU β -2 until it gives an equal TL output. The main problem here is to evaluate the known dose

from the Co-60 source.

The dose-rate from the Co-60 source for the specified geometry is quoted in rads to water. The dose-rate to quartz is then given by the ratio of the mass energy absorption coefficients i.e.

$$D_{\text{SiO}_2} = D_{\text{H}_2\text{O}} \frac{(\mu_a/\rho)_{\text{SiO}_2}}{(\mu_a/\rho)_{\text{H}_2\text{O}}} \quad (\text{C1})$$

LiF (TLD 100) grains were dispersed amongst a volume of quartz grains and thus they were effectively isolated phosphor grains surrounded by quartz. The mixing was accomplished by carefully sprinkling the LiF grains about the central region of the volume of quartz grains and the separation was carried out by sieving. This method of separation was possible because the quartz grains were chosen to be $\sim 200 \mu\text{m}$ in diameter whereas the LiF grains were only $\sim 50 \mu\text{m}$ in diameter.

A very small percentage of the LiF grains were probably within the Compton electron range of other LiF grains but it is extremely unlikely that this would influence the Compton electron flux sufficiently to invalidate the source calibration. It can be assumed, therefore, that the dose absorbed by the LiF grains from the Compton electrons is the same as the dose that would be received by quartz grains if they occupied the same position.

The quartz containing the LiF grains was placed in the same geometry situation in which the Fricke calibration was carried out and irradiated by the Co-60 source. The TL from the LiF grains was measured as was the TL from a second portion of LiF grains which had been irradiated by ANU β -2. When the TL from each of the two portions was equal, we can say that the dose from ANU β -2 was the same as that delivered by the Co-60 source, i.e.

$$D_{\text{H}_2\text{O}} = 624.4 \text{ rads}$$

hence

$$D_{\text{SiO}_2} = 562 \pm 10 \text{ rads}$$

$$\text{Time for ANU } \beta\text{-2 to give equal TL output} = 236 \pm 5 \text{ secs}$$

$$\text{Dose-rate to SiO}_2 \text{ from ANU } \beta\text{-2} = \frac{562}{236}$$

$$= \underline{2.38 \pm 0.09 \text{ rads/sec.}}$$

The two methods give results of 2.43 rad/sec and 2.38 rad/sec to quartz which are in exceptionally good agreement. The average of these two values, 2.41 rad/sec, was the one used throughout these studies together with a factor to account for the radioactive decay of the source.

APPENDIX D

BETA DOSE INFLUENCE FUNCTIONS

The use of influence functions corresponding to the average beta energy of each transition in the natural radioactive series has been used in Chapter IV to calculate the beta dose attenuation in quartz grains of diameter 105 microns. To justify this approach, integration of the influence functions over the complete energy spectra of a high energy (1.0 MeV) and a low energy (0.1 MeV) transition are presented here.

The absorbed beta dose is dependent on both the energy of the beta particles and on their number density $n(E).dE$, that is the number of beta particles per unit energy in the interval E to $E+dE$. Hence the value of \bar{S}_β , the influence function averaged over the beta spectrum, should be calculated as follows:

$$\bar{S}_\beta = \frac{\int_0^{E_{\max}} S(E) \cdot n(E) \cdot E \cdot dE}{\int_0^{E_{\max}} n(E) \cdot E \cdot dE} \quad (D1)$$

where $S_\beta(E)$ is the value of the influence function at energy E and E_{\max} is the maximum beta energy in the transition.

We shall assume an allowed transition and that $Z/(D/2) = 0$. Murthy (1971) gives

$$n(E).dE = k(A_0 + A_1 + A_2 E^2) \times (E_{\max} - E)^2 \cdot dE \quad (D2)$$

where A_0 , A_1 and A_2 are fixed values for each atomic number (here taken to be 90) and k is a constant, each of which are given by Murthy (*op. cit.*). Equation (D2) is utilised in the evaluation of equation (D1) which was carried out by numerical integration.

$$\underline{E_{\max} = 1.0 \text{ MeV}}$$

Taking values of r_0 from Berger and Seltzer (1964) and hence values of $S_\beta(E)$ from Charlton (1970), equation (D1) is evaluated numerically to give

$$\bar{S}_\beta = \frac{0.894}{0.950} = 0.941$$

The average beta energy for this transition, \bar{E}_β , is given by

$$\bar{E}_\beta = \frac{\int_0^{E_{\max}} E \cdot n(E) \cdot dE}{\int_0^{E_{\max}} n(E) \cdot dE} \quad (D3)$$

Again using equation (D2), equation (D3) is evaluated to give

$$\bar{E}_\beta = \frac{0.95}{2.88} = 0.33 \text{ MeV}$$

Using this value of \bar{E}_β , Berger and Seltzer (1964) give the corresponding range $r_0 = 0.044 \text{ cm}$. With $D = 105 \text{ } \mu\text{m}$ this implies $D/r_0 = 0.24$ and hence from Charlton (1970) the value of \bar{S}'_β corresponding to the average energy \bar{E}_β is

$$\bar{S}'_\beta = 0.946$$

Hence, the value calculated by integrating over the complete beta spectrum, 0.941, is in excellent agreement with the value obtained by using the average beta energy, 0.946, for $E_{\max} = 1.0 \text{ MeV}$.

$$\underline{E_{\max} = 0.1 \text{ MeV}}$$

Using equation (D1) with $E_{\max} = 0.1 \text{ MeV}$ gives

$$\bar{S}_{\beta} = \frac{0.219}{0.413} = 0.530$$

The average beta energy is given by equation (D3) which yields

$$\bar{E}_{\beta} = 0.026 \text{ MeV}$$

This results in a value of $r_0 = 7.06 \times 10^{-4} \text{ cm}$ and thus $D/r_0 = 14.9$. The value of \bar{S}'_{β} corresponding to the average beta energy is

$$\bar{S}'_{\beta} = 0.518$$

Again the two values, 0.530 and 0.518, are in very good agreement with each other.

It can be assumed that the use of the value of the influence function corresponding to the average beta energy is an excellent approximation to the value obtained by integrating the influence function over the beta spectrum of each transition of the natural radioactive series.

APPENDIX E
STATISTICAL FORMULAE

The statistical formulae used in this thesis are all based on standard statistical techniques and therefore only the formulae themselves are presented below. Full details of their derivations may be found in almost any introductory text on statistics, e.g. Mood and Graybill (1963).

Mean Value

The mean value, \bar{x} , of the n variables x_1, x_2, \dots, x_n is given by

$$\bar{x} = \frac{1}{n} \sum_{i=1}^n x_i$$

Standard Deviation

The standard deviation, S_x , of a set of n variables x_1, x_2, \dots, x_n is approximated by the relation

$$S_x^2 = \frac{1}{n-1} \sum_{i=1}^n (x_i - \bar{x})^2$$

The standard deviation of the mean value, $S_{\bar{x}}$, is approximated by

$$S_{\bar{x}}^2 = \frac{1}{n(n-1)} \sum_{i=1}^n (x_i - \bar{x})^2$$

Linear Least Squares Fit

The linear least squares method fits a straight line

$$y = a_0 + a_1 x$$

to a set of data points $(x_1, y_1), (x_2, y_2), (x_3, y_3), \dots, (x_n, y_n)$.

The coefficients a_0 and a_1 are given by

$$a_1 = \frac{\sum x_i y_i - \frac{\sum x_i \sum y_i}{n}}{\sum x_i^2 - \frac{(\sum x_i)^2}{n}}$$

and

$$a_0 = \frac{1}{n} \sum y_i - a_1 \times \frac{1}{n} \sum x_i$$

Standard Error of the Estimate

Let y_i^e be the estimated value of y_i corresponding to the data point (x_i, y_i) , i.e.

$$y_i^e = a_0 + a_1 x_i$$

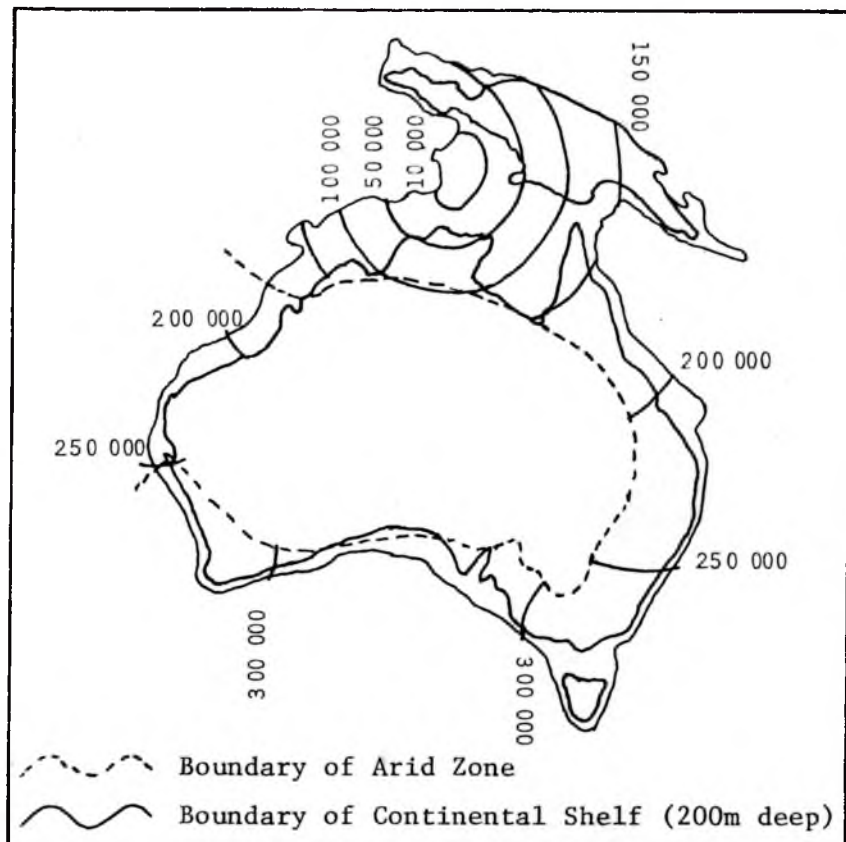
The standard error of the estimate, SE, is then given by

$$(SE)^2 = \frac{1}{n} \sum_{i=1}^n (y_i - y_i^e)^2$$

APPENDIX FA POPULATION EXPANSION MODEL

In Chapter VII the ages of the Lake Mungo finds were argued as being evidence for the much earlier presence of fully sapient populations on the south-east Asian mainland, this region being assumed to be the migrational source for modern Australians. The quantification of this migrational process is extremely difficult because of the large number of unknown parameters, but some light may be thrown on the problem by constructing a simple geographical model, following an idea originally put forward by Professor J.B. Birdsell (see for example; Birdsell, J.B., 1957, *Some population problems involving Pleistocene man, Cold Springs Harbor Symposium on Quantitative Biology*, 22, p47). This model is presently being developed at this University by Dr G. Harrison of the Department of Prehistory and the figures presented in the following paragraphs are his more recent data.

The model is based on the physical analogy of a gas expanding into a region of lower pressure. We will assume, as in Chapter VII, that migration took place from south-east Asia across the Indonesian archipelago at a time of low sea levels. If the new population started from this point with a viable group of one hundred people expanding at the conservative rate of 0.5% per year, and applying the constraint that these hunter-gatherers settled only relatively well-watered country at a population density of one per fifteen square km, then the population would expand across the Arfura and Carpentaria shelf into New Guinea and at the same time divide into two streams expanding along the western and eastern coastal plains of Australia. This population expansion is shown in the diagram below by a series of isoclines of successive increases of fifty thousand people.



The earliest migrants may have populated Australia gradually, starting from the lower end of the Indonesian archipelago and being constrained to the well-watered western and eastern coastal plains.

Assuming that the Willandra Lakes were settled by people moving up from the south via the Murray and Darling and even allowing for conservative input figures, this model predicts that Mungo would probably have been settled by the time the population had reached just over 300,000 total people and that this would have taken place only 7500 years after the original settlement of the Arafura shelf.

As in all such models, it must be remembered that however plausible the analogy may seem, it is not a statement of reality. The simple model discussed here is merely an illustration and should not be taken as an accurate description since all of the input parameters may be significantly different. Nevertheless, the more recent example of the expansion of the population of the U.S.A. to 207 million people effectively within two centuries serves to demonstrate how this expansive migration may have happened.

BIBLIOGRAPHY

- ADAMS, G. and MORTLOCK, A.J., 1974. Thermoluminescent dating of baked sand from fire hearths at Lake Mungo, New South Wales, *Arch. and Phys. Anthropol. in Oceania*, 9 , p236.
- AITKEN, M.J., 1976. Thermoluminescent age evaluation and assessment of error limits: revised system, *Archaeometry*, 18(2) , p233.
- AITKEN, M.J., 1976a. Private communication.
- AITKEN, M.J., ALLDRED, J.C. and THOMPSON, J., 1968. A photon-ratemeter system for low-level thermoluminescence measurements, *Proc. Int. Con. Lumin. Dosim. 2nd, Gatlinburg, Tenn.*, U.S. Atomic Energy Commission CONF-680920, p248.
- AITKEN, M.J., FLEMING, S.J., REID, J. and TITE, M.S., 1968. Elimination of spurious thermoluminescence. In "Thermoluminescence of Geological Materials", ed. D.J. McDougal, Academic Press, London, p133.
- AITKEN, M.J. and ALLDRED, J.C., 1972. The assessment of error limits in thermoluminescence dating, *Archaeometry*, 14(2) , p257.
- AITKEN, M.J. and FLEMING, S.J., 1972. Thermoluminescence dosimetry in archaeological dating. In "Topics in Radiation Dosimetry Supplement 1", ed. F.H. Attix, Academic Press, London, pl.
- AITKEN, M.J. and BOWMAN, S.G.E., 1975. Thermoluminescent dating: assessment of alpha particle contribution, *Archaeometry*, 17(1), p132.
- ALLEN, H., 1972. "Where the crow flies backwards: man and land in the Darling Basin", Unpublished Ph.D. thesis, Australian National University.
- BAMBYNEK, W., CRASEMEN, B., FINK, R.W., FREUND, H.U., MARK, H., SWIFT, C.D., PRICE, R.E. and RAO, P.V., 1972. X-ray fluorescence yields, Auger and Coster-Kronig probabilities, *Rev. Mod. Phys.*, 44 , p716.
- BARBETTI, M.F., 1972. Geomagnetic field behaviour between 25,000 and

- 35,000 yr B.P. and its effect on atmospheric radiocarbon concentration: a current report, *Proc. Eighth International Radiocarbon Dating Conference, Wellington, New Zealand*, pA104.
- BARBETTI, M.F., 1973. "Archaeomagnetic and radiocarbon studies of Aboriginal fireplaces", Unpublished Ph.D. thesis, Australian National University.
- BARBETTI, M.F., 1976. Private communication.
- BARBETTI, M.F. and POLACH, H.A., 1973. A.N.U. radiocarbon date list V, *Radiocarbon*, 15, p241.
- BARBETTI, M.F. and McELHINNY, M.W., 1976. The Lake Mungo geomagnetic excursion, *Phil. Trans. Royal Soc. London*, A281, p515.
- BARKAS, W.H. and BERGER, M.J., 1964. Tables of energy losses and ranges of heavy charged particles, *NASA Report*, No. SP-3013.
- BELL, W.T. and ZIMMERMAN, D.W., 1978. The effect of HF acid etching on the morphology of quartz inclusions for thermoluminescence dating, *Archaeometry*, (in press).
- BERGER, M.J., 1968. Energy deposition in water by photons from point isotropic sources, *MIRD Pamphlet No. 2*, J. of Nuclear Medicine Supplement No. 1.
- BERGER, M.J. and SELTZER, S.M., 1964. Tables of energy losses and ranges of electrons and positrons, *NASA Report*, No. SP-3012.
- BICHSEL, H., 1968. Charged-particle interactions. In "Radiation Dosimetry, Vol. 1", eds. F.H. Attix and W.C. Roesch, 2nd edition, Academic Press, New York, p157.
- BONFIGLIOLI, G., BROVETTO, P. and CORTESE, C., 1959. Thermoluminescence and F-centres. I Theory and II Experimental, *Phys. Rev.*, 114, p951.
- BOWLER, J.M., 1976. Private communication.
- BOWLER, J.M., JONES, R., ALLEN, H. and THORNE, A.G., 1970. Pleistocene human remains from Australia: a living site and human cremation from

- Lake Mungo, western New South Wales, *World Archaeology*, 2 , p39.
- BOWLER, J.M., THORNE, A.G. and POLACH, H.A., 1972. Pleistocene man in Australia: age and significance of the Mungo skeleton, *Nature*, 240 , p48.
- BOWLER, J.M. and THORNE, A.G., 1976. Human remains from Lake Mungo. In "The Origin of the Australians", eds. R.L. Kirk and A.G. Thorne, Australian Institute of Aboriginal Studies, Canberra, p127.
- BOYLE, R., 1663. "Experiments and Considerations upon Colours with Observations on a Diamond that Shines in the Dark", Henry Herringham, London (publ. 1664).
- BROTHWELL, D.R., 1960. Upper Pleistocene human skull from Niah Caves, *Sarawak Mus. J.*, 9 , p323.
- BUBE, R.H., DUSSEL, G.A., HO, C. and MILLER, L.D., 1966. Determination of electron trapping parameters, *J. Appl. Phys.*, 37 , p21.
- BUCHA, V., 1970. Geomagnetic reversals in Quaternary revealed from a paleomagnetic investigation of sedimentary rocks, *J. Geomag. Geoelectr.*, 22 , p253.
- BUCHA, V., 1976. Variations of the geomagnetic field, the climate and weather, *Studia Geoph. et Geod.*, 20 , p149.
- BUCHA, V. and NEUSTUPNY, I., 1967. Changes of the Earth's magnetic field and radiocarbon dating, *Nature*, 215 , p261.
- BURLIN, T.E., 1966. A general theory of cavity ionization, *Brit. J. Radiol.*, 39 , p727.
- CHAN, F.K. and BURLIN, T.E., 1970. The energy-size dependence of the response of thermoluminescent dosimeters to photon irradiation, *Health Physics*, 18 , p325.
- CHARLTON, D.E., 1970. Energy dissipation near an interface: a more realistic approach to electron range and stopping power, *Radiation Research*, 44 , p575.

- CHARLTON, D.E. and CORMACK, D.V., 1962. A method for calculating the alpha-ray dosage to soft tissue-filled cavities in bone, *Brit. J. Radiol.*, 35 , p473.
- CHARLTON, D.E. and CORMACK, D.V., 1962a. Energy dissipation in finite cavities, *Radiation Research*, 17 , p34.
- CHARLTON, D.E. and CORMACK, D.V., 1967. A comparison of models of electron liberation and passage through matter used in calculating absorbed dose near an irradiated interface, *Proc. Euratom Symp. "Microdosimetry", Ispra, Italy*.
- CROSS, W.G., 1967. The distribution of absorbed energy from a point beta source, *Canadian J. Physics*, 45 , p2021.
- CROSS, W.G., 1968. Variation of beta dose attenuation in different media, *Phys. Med. Biol.*, 13 , p611.
- DAMON, P.E., 1970. Climatic vs. magnetic perturbation of the carbon-14 reservoir. In "Radiocarbon Variations and Absolute Chronology", ed. I.U. Olsson, Almqvist and Wiksell, Stockholm, p571.
- DAMON, P.E. and WALLICK, E., 1971. Changes in atmospheric radiocarbon concentration during the last eight millenia. In "The A.P. Vinogradov Jubilee Volume of the U.S.S.R. Academy of Sciences".
- DAMON, P.E., LONG, A. and WALLICK, E.I., 1972. Dendrochronologic calibration of the C-14 time scale, *Proc. Eighth International Radiocarbon Dating Conference, Wellington, New Zealand*, p44.
- DANIELS, F., BOYD, C.A. and SAUNDERS, D.F., 1953. Thermoluminescence as a research tool, *Science*, 117 , p343.
- DAVISSON, C.M., 1968. Interaction of γ -radiation with matter. In "Alpha-, Beta- and Gamma-ray Spectroscopy, Vol. 1", ed. K. Siegbahn, 2nd edition, North-Holland Publishing Company, Amsterdam, p37.
- DITTFELD, H.J. and VOIGT, J., 1963. Comparative studies of thermally stimulated conductivity curves of CdS single crystals, *Phys. Status*

Solids, 3 , p1941.

DRAGOUN, O., PLAJNER, Z. and SCHMUTZLER, F., 1971. Contribution of outer atomic shells to total internal conversion coefficients, *Nuclear Data Tables*, A9 , No. 2, p119.

ELLETT, W.H., BROWNELL, G.L. and REDDY, A.R., 1968. An assessment of Monte Carlo calculations to determine gamma ray dose from internal emitters, *Phys. Med. Biol.*, 13 , p219.

ELSASSER, W., NEY, E.P. and WINCKLER, J.R., 1956. Cosmic ray intensity and geomagnetism, *Nature*, 178 , p1226.

ELSHOLTZ, J.S., 1676. "De Phosphoris Quatuor observationes", Berolini.

EVANS, R.D., 1955. "The Atomic Nucleus", McGraw-Hill, New York, p739.

EVANS, R.D., 1958. Compton effect. In "Handbuch der Physik", 34 , ed. S. Flügge, p218.

EVANS, R.D., 1968. X-ray and γ -ray interactions. In "Radiation Dosimetry, Vol. 1", eds. F.H. Attix and W.C. Roesch, 2nd edition, Academic Press, New York, p93.

EYRE, E.J., 1845. "Journal of Expedition of Discovery into Central Australia", Volumes I and II, T. and W. Boone, London.

FANO, U., SPENCER, L.V. and BERGER, M.J., 1959. Penetration and diffusion of X-rays. In "Handbuch der Physik", 38 , ed. S. Flügge, p660.

FARMER, J.G. and BAXTER, M.S., 1973. Short-term trends in natural radiocarbon, *Proc. Eighth International Radiocarbon Dating Conference*, Wellington, New Zealand.

FERGUSON, C.W., 1970. Dendrochronology of bristlecone pine, *Pinus aristata*; establishment of a 7484-year chronology in the White Mountains of eastern-central California, U.S.A.. In "Radiocarbon Variations and Absolute Chronology", ed. I.U. Olsson, Almqvist and Wiksell, Stockholm, p237.

FLEMING, S.J., 1966. Study of thermoluminescence of crystalline extracts

- from pottery, *Archaeometry*, 9 , p170.
- FLEMING, S.J., 1969. "The acquisition of radiothermoluminescence by ancient ceramics", Unpublished D. Phil. thesis, Oxford University.
- FLEMING, S.J., 1970. Thermoluminescence dating: refinement of the quartz inclusion method, *Archaeometry*, 12 , p135.
- FLEMING, S.J., 1973. The pre-dose technique: a new thermoluminescent dating method, *Archaeometry*, 15(1) , p13.
- GARLICK, G.F.J. and GIBSON, A.F., 1948. The electron trap mechanism of luminescence in sulphide and silicate phosphors, *Proc. Phys. Soc.*, A60 , p574.
- HAGER, R.S. and SELTZER, E.C., 1968. Internal conversion tables. Part 1: K-, L-, M-shell conversion coefficients for $Z = 30$ to $Z = 103$, *Nuclear Data Tables*, A4 , Nos. 1 and 2, p1.
- HALPERIN, A., BRANER, A.A., BEN-ZVI, A. and KRISTIANPOLLER, N., 1960. Thermal activation energies in NaCl and KCl crystals, *Phys. Rev.*, 117 , p416.
- HILL, J.J. and SCHWED, P.J., 1955. Experimental study of the mechanism of thermoluminescence in irradiated sodium chloride, *J. Chem. Phys.*, 23 , p652.
- HOWARTH, J.L., 1965. Calculation of the alpha-ray absorbed dose to soft tissue cavities in bone, *Brit. J. Radiol.*, 38 , p51.
- HOWARTH, J.L., 1965a. Calculation of the absorbed dose in soft-tissue cavities in bone irradiated by X-rays, *Radiation Research*, 24 , p158.
- HUBBELL, J.H., 1969. Photon cross sections, attenuation coefficients, and energy absorption coefficients from 10 KeV to 100 GeV, *NSRDS-NBS 29*.
- HUXTABLE, J. and AITKEN, M.J., 1977. Thermoluminescent dating of Lake Mungo geomagnetic polarity excursion, *Nature*, 265 , p40.
- KELLY, P. and BRAUNLICH, P., 1970. Phenomenological theory of thermoluminescence, *Phys. Rev.*, B1 , p1587.

- KEMMY, P.J., TOWNSEND, P.D. and LEVY, P.W., 1967. Numerical analyses of charge-redistribution processes involving trapping centres, *Phys. Rev.*, 155 , p917.
- KONONENKO, A.M., 1957. Calculation of the intensity of the alpha-radiation dose arising from a radioactive substance distributed inside the organism, *Biophysics*, 2 , p98.
- LANG, A.R. and MIUSCOV, V.F., 1967. Dislocation and fault surfaces in synthetic quartz, *J. Appl. Phys.*, 38 , p2477.
- LIBBY, W.F., 1949. Atmospheric helium three and radiocarbon from cosmic radiation, *Phys. Rev.*, 69X , p671.
- LINGENFELTER, R.E. and RAMATY, R., 1970. Astrophysical and geophysical variations in C-14 production. In "Radiocarbon Variations and Absolute Chronology", ed. I.U. Olsson, Almqvist and Wiksell, Stockholm, p513.
- MANGERUD, J. and GULLIKSEN, S., 1975. Apparent radiocarbon ages of recent marine shells from Norway, Spitsbergen, and Arctic Canada, *Quaternary Research*, 5 , p263.
- MARTIN, M.J., 1975. Private communication.
- MARTIN, M.J. and BLICHERT-TOFT, P.H., 1970. Radioactive atoms, α -, β -, γ -, and X-ray data, *Nuclear Data Tables*, A8 , Nos. 1 and 2.
- MEJDAHL, V., 1969. Thermoluminescence dating of ancient Danish ceramics, *Archaeometry*, 11 , p99.
- MEJDAHL, V., 1970. Measurement of environmental radiation at archaeological excavation sites, *Archaeometry*, 12 , p147.
- MEJDAHL, V., 1972. Progress in TL dating at Risø, *Archaeometry*, 14 , p245.
- MOOD, A.M. and GRAYBILL, F.A., 1963. "Introduction to the Theory of Statistics", McGraw-Hill, New York.
- MULVANEY, D.J., 1975. "The Prehistory of Australia", 2nd edition, The Dominion Press, Victoria.

- MURTHY, M.S.S., 1971. Shape and average energy of beta-particle spectra, *Int. J. of Applied Radiation and Isotopes*, 22 , p111.
- NBS, 1961. Stopping powers for use with cavity chambers, *National Bureau of Standards Handbook*, 79 , U.S. Department of Commerce, Washington.
- NICHOLAS, K.H. and WOODS, J., 1964. Photochemical effects in CdS crystals, *Brit. J. Appl. Phys.*, 15 , p783.
- OLDENBERG, H., 1676. Four sorts of facititious shining substances, *Phil. Trans.*, 11 , p867.
- POLACH, H.A., 1969. Optimisation of liquid scintillation radiocarbon age determinations and reporting of ages, *Atomic Energy in Australia*, 12(3), p21.
- POLACH, H.A., 1972. Cross checking of NBS oxalic acid and secondary laboratory radiocarbon dating standards, *Proc. Eighth International Radiocarbon Dating Conference, Wellington, New Zealand*, p688.
- POLACH, H.A., 1975. Radiocarbon dating as a research tool in archaeology: hopes and limitations, *Proc. Symposium on Scientific Methods of Research in the Study of Ancient Chinese Bronzes and Southeast Asian Metal and other Archaeological Artifacts*, ed. N. Barnard, National Gallery of Victoria, Melbourne, p255.
- POLACH, H.A., 1976. Arizona 1850 wood and ANU sucrose radiocarbon dating standards: progress report on international cross-calibration with NBS oxalic. Preprint, *Proc. 9th (Libby) International Conference on Radiocarbon Dating*, La Jolla, U.S.A.
- POLACH, H.A., KRUEGER, H.A., BANNISTER, B., DAMON, P.E. and RAFTER, A.T., 1972. Correlation of C-14 activity of NBS oxalic with Arizona-1850 wood and ANU-sucrose radiocarbon dating standards: a preliminary report of investigations and results, *Proc. Eighth International Radiocarbon Dating Conference, Wellington, New Zealand*, p190.
- POLACH, H.A., GOWER, J. and FRASER, I., 1973. Synthesis of high purity

- benzene for radiocarbon dating by the liquid scintillation method,
*Proc. Eighth International Radiocarbon Dating Conference, Wellington,
New Zealand*, p144.
- RANDALL, J.T. and WILKINS, M.H.F., 1945. Phosphorescence and electron traps,
Proc. Roy. Soc., A184 , p366.
- ROSSI, B., 1964. "Cosmic Rays", McGraw-Hill, New York, U.S.A.
- SCHARPENSEEL, H.W., 1976. Soil fraction dating. Preprint, *Proc. 9th
(Libby) International Conference on Radiocarbon Dating, La Jolla,
U.S.A.*
- SPENCER, L.V., 1959. Energy dissipation by fast electrons, *Nat. Bur. Stand.
Monograph No. 1*.
- SPIERS, F.W., 1949. The influence of energy absorption and electron range
on dosage in irradiated bone, *Brit. J. Radiol.*, 12 , p521.
- SPIERS, F.W., 1953. Alpha-ray dosage in bone containing radium, *Brit. J.
Radiol.*, 26 , p296.
- SUTTON, S.R. and ZIMMERMAN, D.W., 1976. Thermoluminescent dating using
zircon grains from archaeological ceramics, *Archaeometry*, 18(2) , p125.
- SUTTON, S.R. and ZIMMERMAN, D.W., 1977. Radioactivity of quartz extracts,
*International Symposium on Archaeometry and Archaeological Prospection,
Philadelphia, U.S.A.*
- TANNER, A.B., 1964. Radon migration in the ground: a review. In "The
Natural Radiation Environment", eds. J.A.S. Adams and W.M. Lowder,
University of Chicago Press, Chicago, p161.
- THORNE, A.G., 1971. Mungo and Kow Swamp: morphological variation in
Pleistocene Australians, *Mankind*, 8(2) , p85.
- TITE, M.S., 1966. Thermoluminescent dating of ancient ceramics: a
reassessment, *Archaeometry*, 9 , p155.
- TITE, M.S. and WAINE, J., 1962. Thermoluminescent dating: a re-appraisal,
Archaeometry, 5 , p53.

- TURNER, R.E., RADLEY, J.M. and MAYNEORD, W.V., 1958. The alpha-ray activity of human tissues, *Brit. J. Radiol.*, 31 , p397.
- WADA, M. and INOUE, A., 1966. Relation between the carbon-14 production rate and the geomagnetic moment, *J. Geomag. Geoelectr.*, 18 , p485.
- WHALING, W., 1958. The energy loss of charged particles in matter. In "Handbuch der Physik", 34 , ed. S. Flügge, p193.
- WILLIAMS, E.J., 1930. The rate of loss of energy of beta rays in matter, *Proc. Roy. Soc.*, A130 , p310.
- WINTLE, A.G., 1973. Anomalous fading of thermoluminescence in mineral samples, *Nature*, 245 , p143.
- WINTLE, A.G., 1975. Thermal quenching of thermoluminescence in quartz, *Geophys. J. R. Astr. Soc.*, 41 , p107.
- WOLFENDALE, A.W., 1963. "Cosmic Rays", George Newnes Ltd., London.
- WOOD, L. and LIBBY, W.F., 1964. Geophysical implications of radiocarbon date discrepancies. In "Isotope and Cosmic Chemistry", eds. H. Craig, S.L. Miller and G.J. Wasserburg, North-Holland, Amsterdam, p205.
- WOODLEY, R.G. and JOHNSON, N.M., 1967. Luminescence Dosimetry, *Proc. Int. Conf., Stanford, CONF-650637*, NBS, Springfield, Virginia, p502.
- ZIMMERMAN, D.W., 1967. Thermoluminescence from fine grains from ancient pottery, *Archaeometry*, 10 , p26.
- ZIMMERMAN, D.W., 1971. Thermoluminescent dating using fine grains from pottery, *Archaeometry*, 13 , p29.
- ZIMMERMAN, D.W., 1971a. Uranium distributions in archaeological ceramics: dating of radioactive inclusions, *Science*, 174 , p818.
- ZIMMERMAN, J., 1971b. The radiation-induced increase of the 100°C thermoluminescence sensitivity of fired quartz, *J. Phys. C: Solid State Physics*, 4 , p3265.
- ZIMMERMAN, D.W., 1972. Relative thermoluminescence effects of alpha- and beta-radiation, *Radiation Effects*, 14 , p81.

ZIMMERMAN, D.W., 1976. Private communication.

ZIMMERMAN, D.W., 1977. Radiative recombination and anomalous fading,
International Symposium on Archaeometry and Archaeological Prospection,
Philadelphia, U.S.A.

ZIMMERMAN, D.W., 1977a. Private communication.

ZIMMERMAN, D.W. and HUXTABLE, J., 1971. Thermoluminescent Dating of upper
Palaeolithic fired clay from Dolní Věstonice, *Archaeometry*, 13(1) , p53.

THERMOLUMINESCENCE DATING: REVISED
DOSE-RATE DATA

W. T. BELL*

*Department of Physics, Australian National University, Box 4 P.O., Canberra, A.C.T. 2600,
Australia*

The radiation dose-rate data given earlier (Bell 1976) need slight revision in the light of new figures which have become available for the decay characteristics of certain of the contributing radioisotopes. These figures were obtained from the Nuclear Data Project of the Oak Ridge National Laboratory. Some have been published in Nuclear Data Sheets, Vol. 17, No. 3 while the others were obtained as computer print-out from their Evaluated Nuclear Structure Data File. In most cases the new values agree well with the earlier results, the only notable exception being in the case of ^{214}Bi . The figure for the γ energy of this radioisotope was previously 1.6597 MeV whereas the new figure based on the most recent data comes out as 1.5088 MeV.

Incorporating this and various other smaller changes in the energies of the various radioisotopes, new dose-rate data tables can be calculated. These are given in tables 1 and 2 and these tables should now replace tables 4 and 5 respectively of Bell (op. cit.).

Table 1 *Dose-rate (mrad/yr) for 1 ppm by weight of parent*

	α	β	γ
<i>Thorium series</i>			
no thoron loss	73.8	2.86	5.14
100% thoron loss	30.9	1.03	2.08
<i>Uranium series</i>			
no radon loss	278.3	14.62	11.48
100% radon loss	126.2	6.09	0.56
<i>Natural potassium</i>			
1% K_2O	—	68.2	20.5

Table 2 *Dose-rate (mrad/yr) per alpha particle counted per $\text{cm}^2 \text{ ksec}^{-1}$*

	α	β	γ
Uranium series	2274	119.4	93.8
Thorium series	2055	79.7	143.2

An alpha range and threshold fraction of 6.94 mg/cm^2 and 0.85 respectively for the thorium series and 5.84 mg/cm^2 and 0.82 respectively for the uranium series were assumed (Aitken and Bowman 1975).

* Present address: Radiocarbon Dating Laboratory, Dept. of Prehistory, Research School of Pacific Studies, Australian National University, Box 4 P.O., Canberra, A.C.T. 2600, Australia.

Using the tables for a typical pottery sample which has the activity of the parent ^{232}Th equal to the combined activities of the parents ^{238}U and ^{235}U (which corresponds to 3.167 ppm of thorium for every 1 ppm uranium) then the conversion factors from alpha-counts per ksec to mrad per year (for a thick source 42 mm in diameter and with the threshold set as in table 2) are 157, 7.24 and 8.49 for alpha, beta and gamma doses respectively assuming no gas loss.

REFERENCES

- Aitken, M. J. and Bowman, S. G. E., 1975, Thermoluminescent dating: assessment of alpha particle contribution, *Archaeometry* 17 (1), 132–138.
Bell, W. T., 1976, The assessment of the radiation dose-rate for thermoluminescence dating, *Archaeometry* 18 (1), 107–111.

THERMOLUMINESCENCE DATING OF CALCITE AND BURNT FLINT: THE AGE RELATION FOR SLICES

M. J. AITKEN and A. G. WINTLE

Research Laboratory for Archaeology, 6 Keble Road, Oxford OX1 3QJ, England

Introduction

In early work on the dating of burnt flint Göksu and Fremlin (1972) found that measurements on crushed samples were invalidated by regeneration TL—a form of spurious TL that manifested itself after storage, even though the storage was in darkness. To avoid this they developed a technique in which the flint was prepared for measurement in thin slices. Similarly in work on depositional calcite, travertine and stalagmites, Wintle (1975) found severe interference from surface effects if the material was crushed into grains and therefore adopted the slice technique too. It seems likely that measurements on slices will also be necessary for glassy materials such as obsidian.

The cutting of these materials into thin slices presents no difficulty as long as a wire saw is available, as has been described by Seeley and Burleigh (1975). The main problem occurs in the determination of the TL sensitivity to irradiation by alpha particles. The use of an alpha-thin layer of fine grains is ruled out by the surface effects mentioned above. The difficulty in using slices for measurement of alpha response is in interpretation and this arises because the depth of penetration by alpha particles from an external radioisotope source is less than one-tenth of the thickness of the slice whereas the dosage by beta particles from a ^{90}Sr – ^{90}Y source is nearly uniform for slices about 0.5 mm thick. This does not present any difficulty if the transparency is so poor that TL is collected only from a layer that is thinner than the alpha irradiated layer, or if the transparency is so good that there is no optical attenuation even for TL from the far surface of the slice. Unfortunately, however, measurements of transparency indicate that the intermediate situation pertains. These

THE ASSESSMENT OF THE RADIATION DOSE-RATE FOR THERMOLUMINESCENCE DATING

W. T. BELL

*Dept. of Physics, Australian National University, Box 4, P.O., Canberra, A.C.T. 2600,
Australia*

Introduction

The technique of thermoluminescence (TL) dating relies upon the ability to measure accurately both the archaeologically accrued radiation dose and the rate at which this dose has been delivered to the material under study. The origins of the radiation lie with three main groups of naturally-occurring radioactive elements: (a) the uranium series, (b) the thorium series and (c) potassium-40. One method employed to determine the annual dose-rate from the uranium and thorium series is to measure the alpha activity of the sample by conventional counting methods (Turner *et al.* 1958) and then calculate the radiation dose-rate.

After measurement of the α -activity, the calculation of the annual dose-rate requires an exact knowledge of the decay characteristics of all the contributing radioisotopes. The purpose of this paper is to survey the recently tabulated data on the energies and intensities of the alpha, beta and gamma radiation emitted by the two series and to compare the dose-rate contributions based on these new data with the tabulated dose-rates given by Aitken and Bowman (1975). (Note that ^{40}K emits no alpha particles and hence the dose-rate from this radioisotope must be calculated independently. This is described later.)

Radiation data tables

In order to assess accurately the dose-rate conversion factors for TL dating the energies and abundances of the alpha, beta and gamma radiation released during each transition in the relevant series have been compiled. The uranium series comprises not only the ^{238}U series but also the ^{235}U series at a natural abundance of 0.72%. Tables 1, 2 and 3 give the various forms of energy released for every transition in the ^{232}Th , ^{238}U and ^{235}U series respectively. All energies quoted in the above tables are a summation of the energy times intensity for many individual contributions. For example each gamma energy is the summation over in some cases up to 50 separate γ -rays released during the one transition. β_{max} is the maximum energy a beta particle may have in a certain transition. When a large number of beta transitions are considered, however, it is found that the energy released is divided between the beta particle and a neutrino in a statistical manner so that both the neutrinos and beta particles have energy distributions extending from zero to the maximum value. The beta particles have an average energy, β_{av} , and it is this value which is used in calculating the dose-rates. The internal conversion-electron (IC) contribution derives from atomic electrons which can be ejected from the atom as an alternative to γ -ray emission in the transition of a nucleus from a higher to a lower energy state. When this process results in the production of a vacancy in an inner electron shell of an atom, the filling of this vacancy will produce either X-ray or Auger-electron emission. Vacancies created by the filling of the

Table 1 *Radiation data for the thorium-232 series*

Radioisotope	Half-life	α (MeV)	β_{\max} (MeV)	β_{av} (MeV)	γ (MeV)	IC (MeV)	References*
Th-232	1.40×10^{10} yr	4.006	—	—	—	0.0099	1,3,7,8
Ra-228	5.75 yr	—	0.055	0.0141	—	0.0015	1,2,7,8
Ac-228	6.13 h	—	1.2051	0.4044	0.8750	0.0589	1,2,7,8
Th-228	1.913 yr	5.382	—	—	0.0024	0.0190	1,2,7,8
Ra-224	3.64 d	5.674	—	—	0.0099	0.0021	1,2,7,8
Rn-220	55.3 s	6.288	—	—	0.0002	—	1,2,7,8
Po-216	0.15 s	6.7785	—	—	—	—	1,2,7,8
Pb-212	10.64 h	—	0.3713	0.1067	0.1055	0.0652	1,6,7,8
Bi-212 \rightarrow Po-212	60.60 min	—	1.3360	0.4901	0.1013	0.0015	1,6,7,8
\rightarrow Tl-208		2.1799	—	—	0.0039	0.0074	1,6,7,8
Po-212 (64.07%)	0.30 μ s	5.6295	—	—	—	—	1,6,7,8
Tl-208 (35.93%)	3.07 min	—	0.5804	0.2055	1.2070	0.0098	1,7,8
Positions not shown in decay schemes					0.0021	0.0006	1
X-rays					0.1197		1
Auger-Electrons						0.0094	1
Total		35.9379	3.5478	1.2208	2.4270	0.1853	

*Details of the references are given at the end of this article.

Table 2 *Radiation data for the uranium-238 series*

Radioisotope	Half-life	α (MeV)	β_{\max} (MeV)	β_{av} (MeV)	γ (MeV)	IC (MeV)	References*
U-238	4.49×10^9 yr	4.185	—	—	0.0111	—	3,7,8
Th-234	24.10 d	—	0.1625	0.0456	0.0305	—	3,7,8
Pa-234m	1.17 min	—	2.2647	0.8372	0.0154	—	3,7,8
Pa-234 (0.13%)	6.70 h	—	0.0009	0.0003	0.0023	—	3,7,8
U-234	2.48×10^5 yr	4.759	—	—	0.0150	—	3,7,8
Th-230	7.7×10^4 yr	4.658	—	—	0.0006	0.0119	3,7,8
Ra-226	1.6×10^3 yr	4.775	—	—	0.0090	0.0033	1,2,7,8
Rn-222	3.824 d	5.490	—	—	0.0004	—	1,2,7,8
Po-218	3.05 min	6.004	—	—	0.0001	—	1,2,7,8
Pb-214	26.8 min	—	0.7237	0.2280	0.2430	0.0698	1,2,7,8
Bi-214	19.8 min	—	1.7829	0.6606	1.6597	0.0112	1,2,7,8
Po-214	162 μ s	7.689	—	—	0.0001	—	1,2,7,8
Pb-210	21.3 yr	—	0.0243	0.0062	0.0019	0.0253	1,7,8
Bi-210	5.012 d	—	1.1610	0.3945	—	—	1,7,8
Po-210	138.4 d	5.306	—	—	0.00001	—	1,7,8
X-rays					0.0252		1
Auger-Electrons						0.0074	1
	Total	42.866	6.1201	2.1724	2.0143	0.1289	

*Details of the references are given at the end of this article.

Table 3 Radiation data for the uranium-235 series

Radioisotope	Half-life	α (MeV)	β_{\max} (MeV)	β_{av} (MeV)	γ (MeV)	IC (MeV)	References*
U-235	7.1×10^8 yr	4.3897	—	—	0.1485	0.0131	5,7,8
Th-231	25.52 h	—	0.2193	0.0627	0.0151	0.0503	5,7,8
Pa-231	3.25×10^4 yr	4.9225	—	—	0.0287	0.0888	5,7,8
Ac-227	21.77 yr	0.0689	0.0398	0.0102	0.0099	—	5,7,8
Th-227	18.2 d	5.8379	—	—	0.0988	0.0002	7,8,9
Fr-223 (1.4%)	22 min	—	0.0159	0.0040	0.0007	—	7,8,9
Ra-223	11.43 d	5.8224	—	—	0.0865	—	7,8,9
Rn-219	3.96 s	6.7590	—	—	0.0576	—	7,8,9
Po-215	1.78 ms	7.3864	—	—	0.0003	—	7,8,9
Pb-211	36.1 min	—	1.3234	0.4564	0.0764	0.0025	4,7,8
Bi-211	2.15 min	6.5680	0.0017	0.0004	0.0491	0.0071	4,7,8
Po-211 (0.28%)	0.52 s	0.0209	—	—	0.00002	—	4,7,8
Tl-207	4.79 min	—	1.4340	0.5054	0.0024	—	4,7,8
Total		41.7757	3.0341	1.0391	0.5740	0.1620	

*Details of the references are given at the end of this article.

initial vacancy will in turn give rise to further X-rays or Auger-electrons. Both the X-ray and Auger-electron contributions are, where possible, given in tables 1, 2, and 3.

An estimate of the accuracy of the values obtained is extremely difficult. In most cases the most recent references have been used and these usually agree well with established data. There are, however, a few values which vary significantly (e.g. of the order of 10% in the case of Bi-214) even from contemporary references. In these cases average values are taken.

Revised dose-rate data

It is necessary in evaluating the dose-rate data to assume that the decay series have reached radioactive equilibrium. This implies that the activity (rate of decay) of each member of the series is precisely the same as that of any other member. It is then possible to calculate the

Table 4 Dose-rate (mrad/yr) for 1 ppm by weight of parent

	α	β	γ
<i>thorium series</i>			
no thoron loss	74.0	2.90	5.00
100% thoron loss	31.0	1.05	1.83
<i>uranium series</i>			
no radon loss	278.3	14.64	12.68
100% radon loss	126.2	5.93	0.69
<i>natural potassium</i>			
For 1% K ₂ O	—	68.2	20.5

dose-rates for a given concentration of the parent nuclei from the data of tables 1, 2 and 3. In calculating the dose-rates both the IC and Auger-electron contributions are added to the β -particle contribution since once ejected from the atom these electrons are in every way identical to β -particles. Similarly, the X-rays are added to the γ -ray contribution. Account is also taken of the relative contributions from the ^{238}U and ^{235}U series. The resultant dose-rates for the uranium and thorium series are given in table 4.

Potassium-40

The natural abundance of ^{40}K is well established at 0.0118% of the total potassium content. This total content may be determined by either flame photometry or X-ray fluorescence and it is usual to express the results as a percentage K_2O .

Now ^{40}K decays in 89.3% of cases by emission of a β -particle with an average energy of 0.583 MeV (Martin 1975) and in the other 10.7% of cases by electron capture then γ -ray emission with an energy of 1.4608 MeV. Summing the contributions from β -particles and electrons and also γ -rays and X-rays gives the resultant ^{40}K dose-rate contributions given in table 4. The gamma dose-rate is in agreement with that of Aitken and Bowman (1975) but the beta dose-rate is some 5% lower due to the use here of more up-to-date values for the average beta energy and the half-life (1.28×10^9 yr instead of 1.26×10^9).

Dose-rate based on alpha activity

The alpha count-rate from a thick sample may be measured following the method of Tite and Waine (1962). The alpha activity thus obtained gives a measure of the total concentration of the uranium and thorium series present in the sample. Table 5 gives the dose-rates corresponding to an observed alpha count from a thick sample of 1 particle per cm^2 per ksec for a sample containing only the two uranium series and for a sample containing only the thorium series. Both alpha dose-rates and the thorium gamma dose-rate agree well with the data of Aitken and Bowman (1975), but the beta dose-rates of the uranium and thorium series are 16% and 19% higher respectively and the gamma dose-rate of the uranium series some 5% higher than the earlier data. It is important to note that the earlier values included the internal conversion-electron component in the gamma dose whereas the new values given here have it included in the beta dose.

Table 5 *Dose-rate per alpha particle counted per cm^2 per ksec*

	<i>Dose-rate (mrad/yr)</i>		
	α	β	γ
uranium series	2273	119.6	103.5
thorium series	2053	80.3	138.7

Note: The dose-rates quoted correspond to an alpha range of 6.94 mg/cm^2 for the thorium series and 5.84 mg/cm^2 for the uranium series. In addition, a threshold fraction of 0.85 for thorium and 0.82 for uranium was assumed (Aitken and Bowman 1975).

Since actual samples contain both the thorium and uranium series, table 5 requires a knowledge of their ratio by weight in order to convert from alpha count-rate to dose-rate.

If this ratio is not actually measured by some means, it is then necessary to assume a value. For a typical pottery sample which has the activity of the parent ^{232}Th approximately equal to the combined activities of the parents ^{235}U and ^{238}U (corresponding to 3.16 ppm by weight of thorium for every 1 ppm of uranium) the conversion factors from alpha-counts per ksec (from a thick source of diameter 42 mm and with the threshold set as for table 5) to mrad per yr are 156, 7.27 and 8.70 for alpha, beta and gamma doses respectively.

ACKNOWLEDGEMENTS

I am gratefully indebted to Dr M. J. Aitken for his helpful advice and to Miss Sheridan Bowman and Mr Ian Bailiff for their help in checking the data for errors. I thank also Dr A. J. Mortlock for his assistance during this work.

REFERENCES

- Aitken, M. J. and Bowman, S. G. E., 1975, Thermoluminescent dating: Assessment of alpha particle contribution, *Archaeometry* **17** (1), 132–138.
Martin, M. J., 1975, Private communication.
Tite, M. S. and Waine, J., 1962, Thermoluminescent dating: A re-appraisal, *Archaeometry* **5**, 53–79.
Turner, R. E., Radley, J. M. and Mayneord, W. V., 1958, The alpha-ray activity of human tissues, *Brit. J. Radiology* **31**, 397–406.

The references quoted in the three tables and others which have been of use are given below:

1. *Nuclear data tables A8*, 1–198 (1970).
2. *Nuclear data sheets B1*, No. 5, 1–125 (1966)
3. *Nuclear data sheets B4*, 543–697 (1970)
4. *Nuclear data sheets B5*, 207–388 (1971)
5. *Nuclear data sheets B6*, 209–318 (1971)
6. *Nuclear data sheets B8*, 77–191 (1972)
7. *Atomic data and nuclear data tables 12*, 479–498 (1973)
8. *Atomic data and nuclear data tables 13*, 89–292 (1974)
9. *Table of isotopes*; Lederer, Hollander and Perlman, sixth edition (1967)

POTTERY FIRING TEMPERATURES

H. H. M. PIKE

Department of History, University of Reading, Whiteknights, Reading RG6 2AA, England

It was suggested by Frierman (1969) that pottery could be heated to above 1000°C in kilns available to the Gumelnitza culture of south-east Europe. That suggestion has now been withdrawn (Kingery and Frierman 1974), but it is of some interest to use simple heat balance calculations to show what temperatures are feasible.

For simplicity assume the fuel to be graphite, i.e. fully carbonized charcoal; then the combustion products will be gaseous CO, CO₂, N₂ and O₂. Hot gases react very quickly and hence in calculating temperatures we may assume that thermodynamic equilibrium is

reached instantaneously. Air contains 21% by volume of O_2 and for simplicity we assume all the rest to be N_2 . Specific heats and equilibrium constants are given in the table. Equilibrium constants are given as ratios of partial pressures expressed in atmospheres,

$$K_1 = (P(CO))^2/P(CO_2) \text{ atm}$$

in the presence of excess graphite, and

$$K_2 = P(CO)/(P(O_2))^{\frac{1}{2}} (\text{atm})^{\frac{1}{2}}.$$

We take the total gas pressure to be one atmosphere.

We first assume that all the air passes through the fuel so that combustion takes place in the presence of excess graphite. For an assumed gas temperature of $1500^\circ K$ we calculate* the following partial pressures:

$$\begin{aligned} P(CO) &= 0.347 & \text{atm} \\ P(N_2) &= 0.653 & \text{atm} \\ P(CO_2) &= 0.00007 & \text{atm} \\ P(O_2) &= 5 \times 10^{-10} & \text{atm.} \end{aligned}$$

These values of P also give the number of moles of each constituent in one mole of gas. The heat of reaction is $0.347 \times 26\,620 + 0.00007 \times 94\,240 = 9244 \text{ cal/mol}$.

We assume an initial temperature of $300^\circ K$ ($= 80^\circ F$). In the table C_1 , C_2 and C_3 are the mean specific heats at constant pressure between $300^\circ K$ and T for CO , N_2 and CO_2 , respectively. For the mixture we calculate a mean specific heat of $7.674 \text{ cal/mol } ^\circ K$ and hence we need 9209 cal/mol to heat the gas to $1500^\circ K$. The surplus 35 cal/mol would raise the temperature another 4° , i.e. to $1231^\circ C$. This is the maximum temperature attainable, with no heat losses whatever, close to the burning fuel in a simple furnace.

We can estimate the rate of heat loss if we choose a particular example, say a hemispherical dome 1.5 m in diameter, built of clay 10 cm thick reinforced by wooden twigs and branches. When firing begins the clay is converted to fireclay and the wood to graphite, whose thermal conductivity is so high that we assume it to halve the effective thickness of the dome. Fireclay has a thermal conductivity of $0.003 \text{ cal/cm deg sec}$ and the calculated heat loss

Table 1 *Thermodynamic data*

T $^\circ K$	K_1 <i>atm</i>	K_2 $(\text{atm})^{1/2}$	C_1	C_2 <i>cal/mol } ^\circ K</i>	C_3
900	0.195	1.48×10^{11}	7.311	7.240	11.153
1000	1.91	3.29×10^{10}	7.390	7.313	11.396
1100	12.3	9.55×10^9	7.466	7.382	11.614
1200	57.3	3.39×10^9	7.539	7.451	11.811
1300	209	1.40×10^9	7.608	7.518	11.990
1400	628	6.56×10^8	7.673	7.583	12.153
1500	1630	3.38×10^8	7.731	7.643	12.301
2000	42100	3.19×10^7	7.974	7.893	12.884
2500	272000	7.40×10^6	8.149	8.073	13.293

* Balancing atoms, using K_1 but ignoring K_2 gives us a quadratic to solve; we can then adjust to allow for K_2 .

A
8CC 78
'B4
1978.

Thermoluminescence Dating of Cooking Stones

By W. T. BELL

THERMOLUMINESCENCE DATING OF COOKING STONES

FROM THE KUK TEA RESEARCH STATION SITE, NEW GUINEA

By W. T. BELL

THE Kuk Tea Research Station, established by the Department of Agriculture, Stock and Fisheries in 1969, is a 700 acre property (mostly swampland) about 15 km northeast of the township of Mount Hagen. The long and complex history of the Kuk swamp extends back into the late Pleistocene as recorded in layers of volcanic ash from up to a dozen different eruptions. This investigation is concerned mainly with the period from about 300 years ago when widespread use was made of the drained swampland in a system of sweet potato agriculture. A grid of wide, deep barets (ditches or drains cut for water control) subdivided by a close grid of small, shallow, flat-bottomed barets characterises the drainage of the swampland for cultivation of the sweet potato. Several house sites associated with this culture have been excavated and cooking stones from the fires and cooking pits of each house collected. Research into the possibility of dating these cooking stones by thermoluminescence (TL) was instigated after discussion with Professor J. Golson, Department of Prehistory, Research School of Pacific Studies, A.N.U.

Initially the problem was to date and thus chronologically order eight houses unearthed in one block, A9g, of the close grid baret system (see fig. 1). All the houses were expected to be less than 300 years old, being younger than a volcanic ash layer dated by C-14 to around 300 years. The stones themselves were predominantly of the metavolcanic type and were, on average, approximately 5 to 10cm in diameter. In view of their relatively recent heating in the cooking fires and since TL dating measures time elapsed since last heating, the TL Pre-dose Technique developed by Fleming (1973) was adopted for this investigation.

Dating Procedure

Thermoluminescence dating relies upon the ability of certain crystalline materials to absorb the energy released by naturally occurring radioactive elements during their decay. This release of energy takes place at a very constant rate and is usually measured in rads per year. The energy stored by the crystal can be released in the form of light when the material is heated to a sufficiently

* Department of Physics, Australian National University.

high temperature and the light output can be taken as proportional to the radiation dose (in rads) absorbed by the crystal. Although many materials including most of the feldspars exhibit TL, the one which has proved most propitious for dating purposes is quartz. So in the attempt to date the cooking stones, efforts were made to extract the quartz grains from each stone after it had been gently crushed in a vice. Full details of the TL method are given by Aitken (1974) and of the extraction techniques by Fleming (1973).

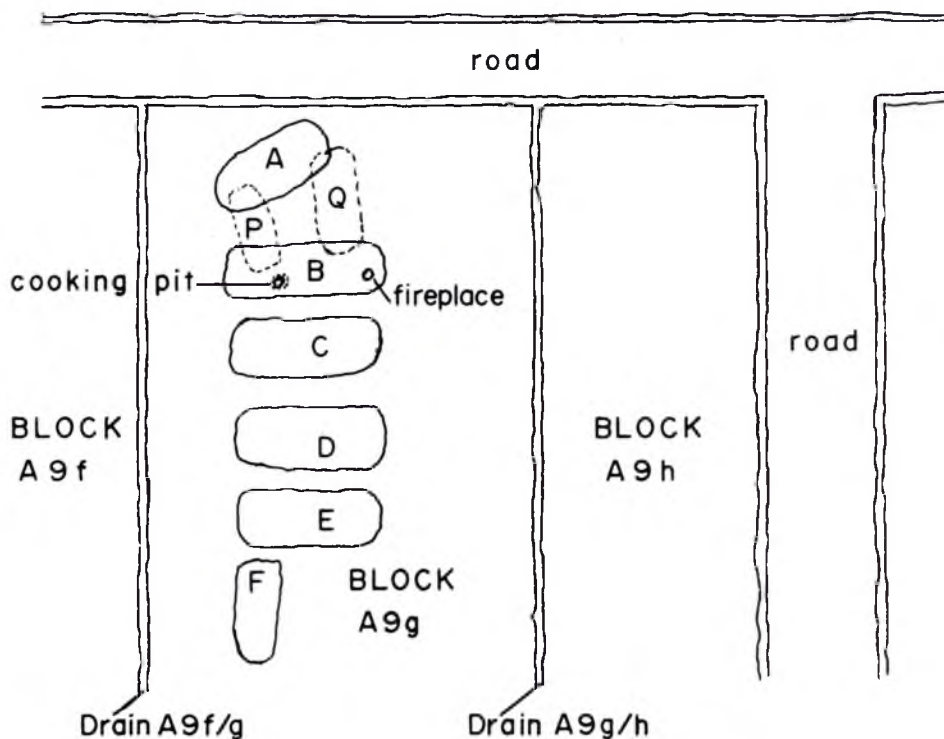


Figure 1—Houses unearthed at the Kuk Tea Research Station, Block A9g. Houses P & Q lie stratigraphically below A & B and should be older. The position of a fireplace and cooking pit are shown for House B.

Results of the TL Dating

Broadly speaking the results of the TL dating programme could be divided into two groups

- (a) those which gave meaningful answers and
- (b) those which did not respond to the Pre-dose Technique.

The results of this latter group had to be discarded but even the former group gave answers which were not reproducible within normal error limits. It was established that each of the houses shown in Fig. 1 which provided sufficient

samples belonging to group (a) were less than 300 years old according to the dates of the cooking stones. Any attempt, however, to chronologically order the houses was impossible due to uncertainties in the ages of around 30%.

For example, a series of tests on stones from the cooking pit of House B (A9g 5F40) gave archaeological radiation doses of 26.5, 62.0, 57.0 and 15.2 rads. These values have a mean of 40.2 rads subject to a standard error of $\pm 28\%$. The dose rate was measured to be 0.25 ± 0.02 rads per year and hence an age of 160 ± 50 years was obtained for House B. Results obtained for other houses are given in Table I.

TABLE 1

House	TL Age (in years)
B	160 ± 50
A	145 ± 50
Q	155 ± 60
P	260 ± 80

Applying the statistical 't' test to Houses A and P (the extreme ages) gives a value of $t = 1.2$ which is not significantly large enough to reject the hypothesis that the difference in the ages is due to sampling variations. All one can say, therefore, is that all four houses dated appear to be between 100 and 300 years old.

Analysis of TL Samples

In an attempt to find out why the TL samples from the cooking stones exhibited such a lack of reproducibility, they were subjected to X-ray diffraction and optical emission spectrography. The X-ray diffraction analysis provided a very good correlation between samples from group (b), those which did not respond to the Pre-dose Technique, and those which had a high feldspar content in addition to quartz. A typical X-ray diffraction pattern is shown in Fig. 2. It was deduced that for these samples, the TL signal from the feldspars is masking the quartz signal and hence no meaningful results could be obtained.

The optical emission spectrography analysis showed that the group (a) samples, which had a high quartz content, also had a high impurity level. It is thought that the lack of reproducibility is due mainly to the variations in type and amount of impurities present in each of the grains.

CONCLUSION

Thus, although it has been possible to date cooking stones to a period less than 300 years ago, the chronological ordering of the houses has proved impossible due to large errors in the individual ages. These errors illustrate some of the problems associated with the dating of certain geological samples by thermoluminescence due to the wide variation of physical and chemical environment

on formation and the wide range of impurities which can diffuse into the quartz grains during their history.

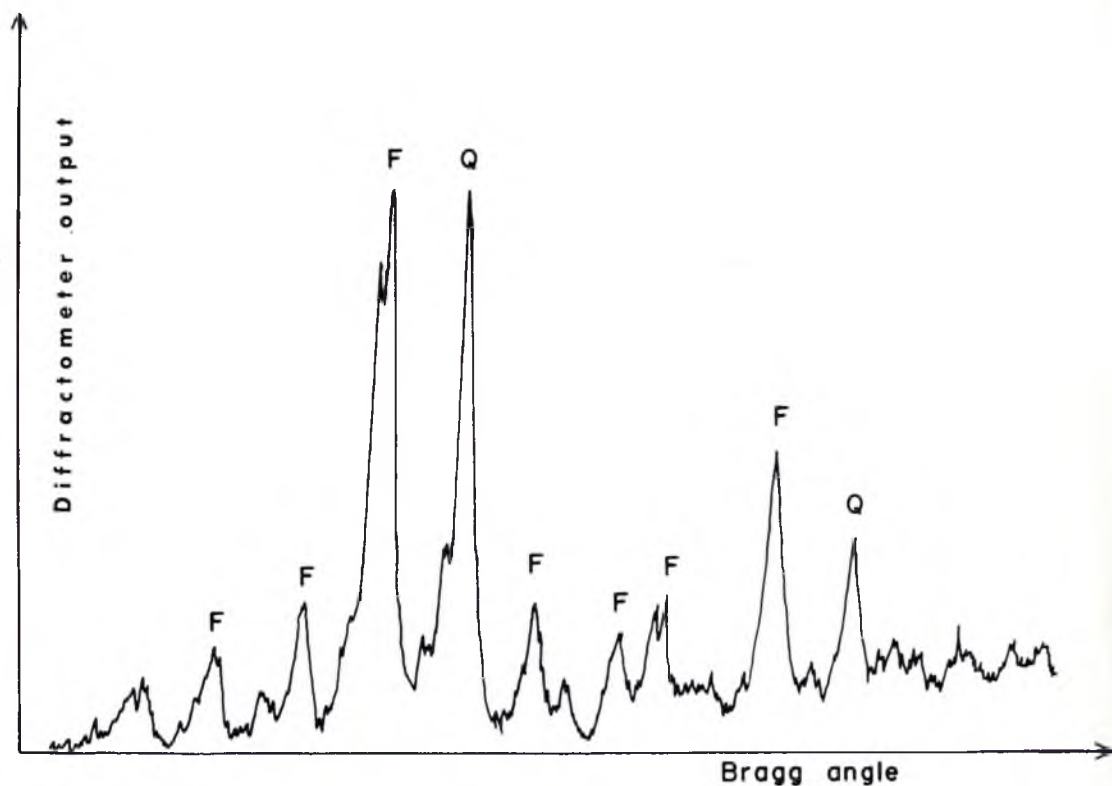


Figure 2—Typical X-ray diffraction pattern of samples which did not respond to the TL Pre-dose technique. Peaks marked 'F' are feldspar peaks; those marked 'Q' are quartz peaks.

ACKNOWLEDGEMENTS

I thank Dr. A. J. Mortlock of the Physics Department, A.N.U. for the use of the technical facilities which allowed the thermoluminescence dating measurements to be made and for guidance during the experiments. The Physics Department, A.N.U. also met the cost of the illustrations. Professor J. Golson of the Department of Prehistory, Research School of Pacific Studies, A.N.U. originated the archaeological problem and supplied the cooking stones from his field site in New Guinea.

Thanks are due also to Mr. J. Pennington of the Geology Department, A.N.U. for the X-ray diffraction measurements and to Mr. W. Nance of the Research School of Earth Sciences, A.N.U. for the optical emission spectrography.

REFERENCES

- Aitken, M. J. (1974): *Physics and Archaeology*, Clarendon Press, Oxford.
Fleming, S. J. (1973): "The Pre-Dose Technique: A new thermoluminescent dating method." *Archaeometry*, Vol. 15, No. 1, pp. 13-30.

W. T. BELL